2013

Minding the P's and Q's: Real and reactive power assessment of hybrid energy conversion systems with wind and solar resources

Subhadarshi Sarkar
Iowa State University

Minding the P's and Q's:

Real and reactive power assessment of hybrid energy conversion systems with wind and solar resources

by

Subhadarshi Sarkar

A dissertation submitted to the graduate faculty

in partial fulfillment of the requirements for the degree of

DOCTOR OF PHILOSOPHY

Major: Electrical Engineering

Program of Study Committee:

Venkataramana Ajjarapu, Major Professor

James D. McCalley

Dionysios C. Aliprantis

Umesh G. Vaidya

Peter J. Sherman

Iowa State University

Ames, Iowa

2013

DEDICATION

This thesis is dedicated to the Almighty God and my family, without whose blessings and unconditional love and support I would not have been able to complete this work. Thank you.

TABLE OF CONTENTS

LIST OF TABLES

LIST OF FIGURES

ACKNOWLEDGEMENTS

I would like to take this opportunity to first and foremost thank God for being my strength and guide in the writing of this dissertation. Without Him, I would not have had the wisdom or the physical ability to do so.

I would like to take this opportunity to express my sincere gratitude to my advisor, Dr. Venkataramana Ajjarapu. I deeply appreciate his guidance, invaluable advice, and continuous support throughout my Ph.D. study at Iowa State University. His leadership, professional accomplishments and dedication to education have motivated and inspired me to pursue excellence in my future career.

I am also grateful to my committee members, Dr. James D. McCalley, Dr. Dionysios C. Aliprantis, Dr. Umesh G. Vaidya and Dr. Peter J. Sherman for their valuable suggestions, comments and support.

I would like to show my gratitude towards all the ISU faculties, especially in the Electric Power and Energy Systems group who have made this stay at ISU a great learning experience. I am indebted to my many fellow graduate students, who have constantly contributed to both my professional career and personal life at Iowa State University.

Finally, I am grateful for funding support from the National Science Foundation's Electrical, Communications and Cyber Systems (ECCS) Research program under grant # 0829025.

ABSTRACT

The growing concern over environmental degradation resulting from combustion of fossil fuels and fluctuating oil prices has raised awareness about alternative energy options and has encouraged many countries to provide new policies promoting renewable energy. Such variable renewable energy sources like wind and solar are environment friendly and have potential to be more widely used. Combining these renewable energy sources with back-up units to form a Hybrid Energy Conversion System (HECS) can provide a more economic and reliable supply of electricity under different load demand conditions compared to single use of such systems.

A major limitation of the wind and solar options is their inherent variability and dependence on weather conditions. Their power outputs are not dispatchable by system operators as conventional generation. However, it may be possible to avoid the emergency circumstances surrounding fluctuations in renewable energy production like sudden drops or surges by evaluating complementary characteristics of some renewables. Because, different alternative energy sources can complement each other to some extent, multi-source hybrid energy systems have greater potential to provide higher quality and more reliable power to customers than a system based on a single resource. This project proposes a comprehensive planning approach to tackling the issues of wind and solar integration into the power grid and develops a procedural tool that will facilitate hybrid generation.

The scope of this dissertation addresses the development of optimal planning procedures for power generation from non-dispatchable wind, solar and other dispatchable facilities. Several tools have been developed with focus ranging from resource identification to optimal sizing determination and grid connection. Historical meteorological data for solar irradiance and wind speed and power transmission information have been analyzed to provide suitable hybrid locations and optimal sizing. Models for wind, solar and reserves for power system simulation studies have been developed. Long term voltage stability has been evaluated iteratively through

system studies and contingency analysis. Based on the application of the developed methodologies on a sample PSSE 23-bus system and the Western Electricity Coordinating Council (WECC) system, several conclusions and performance indicators for HECS have been drawn.

CHAPTER 1. OVERVIEW

1.1 Introduction

The growing concern over environmental degradation resulting from combustion of fossil fuels and fluctuating oil prices has raised awareness about alternative energy options [1], [2]. Public concern related to reduce global warming and the significant increase in the prices of conventional energy sources have encouraged many countries to provide new energy policies that promote renewable energy applications. Such renewable energy sources like wind, solar, hydro based energies, etc. are environment friendly and have potential to be more widely used. Combining these renewable energy sources with back-up units to form a Hybrid Energy Conversion System (HECS) can provide a more economic, environment friendly and reliable supply of electricity under different load demand conditions compared to single-use of such systems [3, 4]. Hybrid power systems combine two or more energy conversion devices, or two or more fuels for the same device, that when integrated, can overcome limitations inherent in either.

Traditionally renewable energy sources have suffered from certain common limitations such as low energy density, periodic power production, and economic viability. While many problems have been identified and some remedial actions have been suggested, problems still remain that hinder the induction of renewable energy systems as a major contributor to the power grid. This project proposes a comprehensive approach to tackling the problem of renewable energy, mainly wind and solar energy integration into the power grid.

Both solar power and wind power are intermittent power sources. Solar power follows annual and diurnal irradiance patterns, caused by the earth's movement around the sun and disturbed by cloud movements, while wind power follows local wind speed variations caused

by moving weather fronts. Despite the advancements in power generation techniques from renewable energies, grid integration has always been of concern. The electric power network is an immensely complex system with its stability depending on many external and internal factors. One of the most basic requirements for power system stability is resource adequacy such that the supplied power must equal the demand at all times. It should be of no surprise that renewable energy sources such as wind and solar have difficulties contributing to system stability due to variations in energy density. As a result, energy systems such as wind and solar are yet not considered secure forms of generation.

Therefore, the majority of power system reliability is still maintained through fossil fuel burning plants. This work provides a framework that addresses this concern with the introduction of a wind and solar based HECS that may be an active substitute for conventional generation. The proposed approach includes methods for determining the proper plant and energy reserve capacity which considers not only feasible energy capture locations, but additionally grid integration studies that are typically neglected [5]. Since the scope of this work is focused towards the integration of reliable renewable hybrid generation, its results can be extended to other hybrid renewable technology combinations.

1.1.1 Background

Federal policy in the form of production tax credits and state regulations in the form of renewable portfolio standards (RPS) have contributed to the development of renewable energy like wind and solar in the United States [6]. Over 25 states have accepted RPS by requiring a substantial contribution from renewables to their power generation portfolio [7] by 2030. Judging from current developments, wind power is the power source most likely to reach substantial penetration levels within this time frame. As of 2010, the cumulative installed capacity of wind power was 43461 MW in USA and contributed to approximately 2.3% of the total electricity generation [8]. Solar power generation is also increasing worldwide, although it currently provides only a minor proportion of the total generation mix even at the locations with the highest penetration levels. As of 2010, the cumulative installed capacity of solar power was 431 MW (solar thermal) and 2153 MW (PV) in USA [9]. However, if the current trends for

grid-connected concentrated solar and PV continue, combined with decreasing system costs, a future expansion of solar power generation is not unlikely.

Solar and wind energy are non-depletable, site-dependent, non-polluting sources of alternative energy. The nation increasingly will rely on these energy resources to meet its growing demand for electricity. Renewable resources can provide a clean, plentiful supply of electricity, but the integration of such resources on a large scale challenges system planners and regulators because of their remote location relative to load and because their output is intermittent and cannot be controlled. These characteristics differentiate variable energy resources from traditional generation resources (e.g., fossil and nuclear) and create regulatory, physical and economic challenges. Electric systems with energy increasingly supplied from variable energy resources require increased generation reserves to ensure electricity remains available when, for example, the sun does not shine or the wind does not blow. Moreover, because wind is most plentiful during off-peak hours when demand is lowest, electric systems with large wind supplies might require additional capacity to meet peak daytime loads. These reserve and capacity requirements impose physical and financial restrictions that limit variable energy resources' ability to cost-effectively replace non-intermittent resources.

A major limitation of wind and solar power options is their inherent variability and dependence on weather conditions. Their power outputs are not dispatchable by system operators as conventional generation; they depend on a number of external natural factors which vary over a wide range. However, it may be possible to avoid the emergency circumstances surrounding fluctuations in renewable energy production like sudden drops or surges by evaluating complementary characteristics of some renewables. Because, different alternative energy sources can complement each other to some extent, multi-source hybrid alternative energy systems (with proper control) have great potential to provide higher quality and more reliable power to customers than a system based on a single resource [10]. Hybrid wind and solar ECSs use two renewable energy sources thus improving the system efficiency and power reliability and reducing the reserve requirements (for grid connected applications) or storage requirements (for stand-alone systems).

The complementary nature of the wind and solar resource in North America was examined

in [11, 12]. The weather patterns dictated by wind and solar resources appear to possess such traits and therefore may help alleviate not only the dominance of convention fossil fuel plants, but also motivate reliable power system operation from renewables. Fortunately, the problems caused by the variable nature of these resources can be partially or wholly overcome by integrating these two energy resources in a proper combination, using the strengths of one source to overcome the weakness of the other. This is apparent by realizing the fact that in many areas more irradiance and less wind are available during the summer months; and similarly more wind and less irradiance are available during the winter months [13]. A mixture of solar and wind energy into a HECS could mitigate their individual fluctuations and increase overall energy output, thus reducing the energy storage or reserve requirements significantly [14] compared to systems comprising of only one single renewable energy source. With the complementary characteristics between solar energy and wind energy for certain locations, the hybrid solar-wind power generation systems offer a highly reliable source of power [15].

The example in Figure 1.1 illustrates this phenomenon of complementary wind-solar profile and compares the average demand with the aggregate wind and solar plant output in California [16]. The left part shows an average July day for 2003 with the load scaled to 2010 levels. The total CAISO (California Independent System Operator) load shape is that of a typical summer diurnal pattern, including relatively high loads at mid-day and an evening load knuckle. The wind power shows a typical summer diurnal pattern, with relatively lower generation mid-day, picking up in the afternoon. As expected, the solar production peaks at mid-day. This net load (i.e., load minus the wind and solar generation) must be served by other generating sources. Note that the wind and solar tend to complement each other, with the result of largely maintaining the load alone shape at a reduced MW level. The right part shows the average load, wind, solar and net load profiles for January 2002. The daily peak load is significantly less than that observed in July, and the evening peak load may be the largest load of the day. Note that the average wind characteristic is flatter than in the summer, and is somewhat more coincident with the daily load shape. This demonstrates the inherent variability and seasonal dependence of the wind and solar resources. The variability around these average demand values, especially for individual wind and solar resources, can fluctuate significantly on a daily

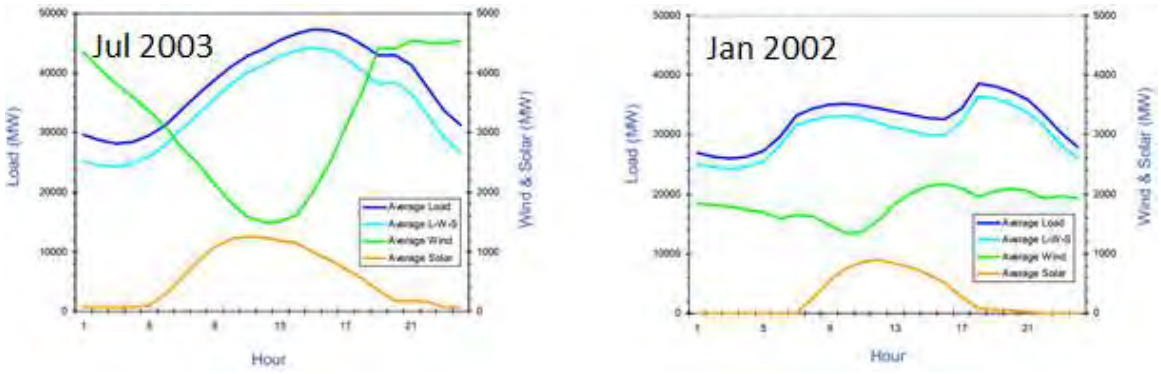

Figure 1.1 Average System-wide Daily Load, Wind, Solar, and Net Load Profiles of July 2003 and January 2002

basis. However, the solar and wind plant profiles when considered in aggregate can be a good match to the load profile and hence improve the resulting composite capacity value for variable generation.

Because of this feature, HECSs involving wind and solar resources have caught worldwide research attention [17–20]. Many alternative energy sources including wind, solar, fuel cells, diesel system, gas turbine, and micro-turbine can be used to build a hybrid energy system. Nevertheless, the major renewable energy sources used and reported are wind and solar power. In [21], correlation among wind and solar data against the electricity load demand for an entire year for the same geographical location was analyzed which concluded that a combined resource can effectively deliver energy to the electricity grid when load demand experiences peaks, hence furthering the cause of combined integration of wind and solar sources with the electricity grid. In the past, the hybrid systems have been considered as preferred for remote systems like radio telecommunication, satellite earth stations, or at sites far away from a conventional power system. Today, there is a trend to update the existing one source system (PV, wind or hydro) into hybrid system for grid-connection applications [22].

1.1.2 Motivation

The growing concern over environmental degradation resulting from the combustion of fossil fuels has generated much controversy within the electric power sector and has increased the focus on renewable energy. There are a vast number of advocates who claim that greenhouse gas

production from conventional electric power plants is a major contributor to global warming. This concept is not only a matter which has been strictly defined within the United States, but involves a global population. The initiative taken on behalf of the United Nations with the ratification of the Kyoto Protocol in 1997 demonstrates the world's awareness towards greenhouse gas emissions [23]. Since the signing of the protocol began, drastic increases in global energy consumption have had researchers scrambling to find both clean and sustainable sources of energy. Over the last decade, renewable and clean sources of electric energy such as wind and solar generation have increased immensely in an attempt to mitigate the consumption of fossil fuels. Despite the overwhelming interest to stimulate renewable and clean energy production, there are inherent drawbacks within both wind and solar generation.

Recently, on February 26, 2008, the Electric Reliability Council of Texas (ERCOT) experienced a 1400 MW drop in wind energy production that was a contributing factor to implementing emergency power grid procedures [24]. As an attempt to mitigate the urgent situation, over 1100 MW of customer electric load was curtailed. Given the conditions of this recent report it is quite apparent that developers of grid connected renewable energy still lack sufficient integration schemes. Therefore, when interconnecting large amounts of renewables into the power grid, the security of the system must be taken as one of the utmost priorities. Avoiding the circumstances surrounding ERCOT's emergency may have been possible when evaluating complementary characteristics of some renewables. The weather patterns dictated by wind and solar resources appear to possess such traits and therefore may help alleviate not only the dominance of convention fossil fuel plants, but also motivate reliable power system operation from renewables. North American Electric Reliability Corporation (NERC) recently mentioned the need to develop a reference manual to educate and guide the electric industry as the integration of large-scale variable resources continues.

In [25], North American Electric Reliability Corporation came up with the following conclusion,

"Deploying different types of variable resources (such as solar and wind generation) to take advantage of complementary patterns of production, locating variable resources across a large geographical region to leverage any fuel diversity that may exist, and advanced control

technology designed to address ramping, supply surplus conditions, and voltage control show significant promise in managing variable generation characteristics."

Also, in [26], a study conducted by Massachusetts Institute of Technology (MIT) commented that

"The interconnection standard provisions for conventional generators are designed to ensure that generators do not harm the grid and that they will contribute to the stability and reliability of the grid when required. Due to their very low penetrations, so far VERs in the U.S. have been required to meet few standards. As a result, their expected impact on the system has not yet been properly formalized, and they generally have not played an active role in maintaining system stability and reliability."

This work aims to answer the above two issues, namely

- Can a solar-wind hybrid energy conversion system be designed where the strength of one resource can negate the weakness of the other and vice versa?
- If a HECS like this is developed, how can it be deployed and properly interconnected with the grid without causing performance issues, or maybe even enhance the system security?

1.1.3 In Summary

Although renewables, with the exception of hydro power, currently play a minor role in the U.S. electricity supply, supporters have long argued that the United States can and should make a rapid transition to greater use of renewables. This work on HECSs focuses on wind and solar technologies as they have a very large remaining resource potential, are commercially available and technically proven, and are the focus of considerable policy attention. They offer several benefits compared to fossil-fueled electricity generation:

- Zero-Carbon Electricity and other Environmental Benefits: Wind and solar, in contrast to fossil fuels, produce no direct GHG (green house gas) emissions and, thus, offer the promise of zero-carbon electricity generation and a significant role in reducing GHG

emissions to avoid climate change. They have no direct air emissions and do not require environmentally degrading fuel extraction.

- Fuel Diversification and Energy Security: Renewable electricity generation makes the electricity generation system less reliant on coal and fossil fuel and thus less exposed to volatility in domestic and global fuel markets.
- Economic Development: Many supporters of renewable energy highlight the potential for job creation from investing in more renewable electricity generation.

The current barriers to increased wind and solar electricity usage include:

- High costs: Solar power generating plants (PV and CSP) currently produce electricity at costs significantly higher than for electricity produced from wind or fossil-fueled power plants.
- Transmission: Transmission lines carry electricity from power plants to cities, industry, and other load centers where it is needed. Large wind and solar power plants are often located more remotely than fossil-fueled plants. Therefore, they require construction of new, expensive, and controversial transmission lines.
- Variability and intermittency: The wind and the sun irradiance are variable resources, meaning that their availability as an energy source fluctuates due to weather patterns, clouds, and cycles of day and night. The electricity output from power plants dependent on these variable resources varies accordingly. The demand for electricity, however, does not follow the same pattern. In the case of wind electricity, electricity generation is sometimes greatest at night when electricity demand is lowest.

The potential advantages by interconnecting combined wind and solar forms of generation include:

- Increased Reliability and Efficiency: Wind and solar generation have inherent variability on different time scales, the chances of both of them going down together is generally

going to be lesser than that when each one is operating independently. Using the same transmission lines for transferring different amounts of power at different times of the day is much more efficient than that of either single operating alone.

- Reduced Reserve Requirements: CSP plants need thermal storage, wind farms need backup reserves in nearly 1:1 ratio; interconnected solar and wind plants can reduce the necessity of reserves.

- Improved load following: Only wind farm output has a diurnal mismatch to the typical electrical loading, combining solar thermal power with wind farms will result is a good match to the loading; the seasonal mismatch for wind farms (i.e. peak load occurs in summer when wind energy is at a minimum) will also be improved by combining solar with wind.

- Economic Benefit: The wind and solar generation rely purely on weather conditions; the highest level of energy injected into the electricity grid can occur at times when the cost of the electricity is also high. This will help in early recovery of the high capital intensive installation cost required for such renewable energy generation systems and thus improve future investment opportunities.

The potential benefits of co-locating wind and concentrating solar power plants are discussed in Appendix A.

1.2 Problem Statement

The fundamental goal of this work is to assess the resource and technical feasibility of the development and deployment of a HECS with wind and solar resources. The target is to result in a methodology for calculating suitable hybrid plant locations and an optimized plant sizing and reserve strategy. Factors such as physical location, grid interconnection point, and the characteristics of existing grid infrastructure are considered while determining the effect of renewables such as wind and solar on the grid. It is expected to integrate renewables smartly in a variety of scenarios and enable to maximize the benefit from each installation. The objective

of this strategy will allow for reliable power injection that is capable of meeting the demand of a variable load and increased system stability.

CHAPTER 2. REVIEW OF LITERATURE

2.1 Current State of Art

Since the 1980's, there has been much discussion over the feasibility of hybrid solar-wind plants, but the emphasis was generally directed toward small stand - alone systems [18]. The authors in [3, 27] present an overview of the methods directed towards stand - alone systems. Although the separate interconnection of both wind and solar based generation has become common place, the integration of a large scale hybrid generation facility is yet to be achieved. The idea that a hybrid plant may supplement conventional generation is a relatively new concept [28] and would require solutions for such issues as resource variability, energy storage/reserve management and power system reliability. Therefore, such considerations demand the development of comprehensive methods which test the feasibility of large hybrid systems.

The independent output power delivery of wind and solar energy systems on any given day generally do not match a typical electric power demand curve. In general, the capture of wind energy is more prominent during evening hours while the abundance of sunlight is conversely a daytime phenomenon. However, the local combination of wind and solar may help offset the unfavorable energy distribution of the individual sources which would provide a supply curve that better matches the daily demand [14]. The merging of the two technologies would then appear to function in a synergistic manner. Even though the synergy exists, there are relatively high cut-in speed (i.e. 3.5 to 4.5 m/s) requirements of a wind generator [29] and a limited number of sunlight hours available for solar plants [5]. This makes selection of appropriate sites with sufficiently high wind and solar irradiation essential for grid integration. The authors in [30], [31] and [32] demonstrated that the peak electrical load during the year is critical to a utility and a wind-solar hybrid was shown to be much better to the utility than

a wind alone system. A major barrier for the acceptance and further integration of wind and solar resources with the electricity grid is the lack of reliable wind data in combination with the solar availability as well as forecasting of such resources [21]. It is therefore crucial to assess the resource availability of the combined solar and wind energy for the same location and contribute to the understanding of the correlation between the solar and wind energy availability against the electricity load demand for a particular location and its local grid. Since the main focus of this work is to study the performance of a wind-solar HECS, both the wind and solar setups need large physical areas for their installations. Thus the maximum distance between the wind and solar facilities having complementary resource profiles need to be determined. This shall be done considering actual locational wind and solar resource data and the use of a GIS tool. Compared with wind, solar radiation has the ability to provide more energy during peak demand hours of the mid-day, i.e., as load increases or decreases throughout a day, the output of solar generation follows that profile. A number of research groups have analyzed the impact of large-scale wind integration on power system operation, including reserve requirements [33]. Some research has also been extended to large-scale solar setups [34].

The potential benefits of co-locating wind and concentrating solar power (CSP) plants have been analyzed and discussed in [35]. Using a location in western Texas as a case study, the authors demonstrated that such a deployment strategy can improve the capacity factor of the combined plant and the associated transmission investment. However, adding transmission constraints reduces performance and the ability of CSP to provide maximum output during periods with high demand and wind. Even with thermal energy storage option, there could be extended periods of high wind and solar resource, resulting in curtailment. Despite these limitations, the authors determined cases in which a mix of CSP and wind were justified by market revenues. It was shown that if the plants were flexibly configured, deployments with up to 67% CSP on a capacity basis yielded a positive net ROI. However, these findings depended on a reduction in CSP costs and deployment economics which were sensitive to transmission costs, which have varied in the past. Although the authors focused only on Texas, there are many parts of the world that have co-located solar and wind resources for the type of combined deployments - other parts of the southwestern U.S., northern Africa, the Arabian peninsula, the

Tibetan plateau, northern Chile, and Australia. The analysis in [35] represented a snapshot of deployments in historic market conditions. Escalation in conventional generation costs, carbon restrictions, and other factors would increase the value of these deployments. While some of the value of dispatchable CSP is captured by the capacity payment, additional values of dispatchable energy, such as the provision of ancillary services, could increase revenues.

A lot of research efforts have been made towards modeling of renewable energy resources - wind standalone, solar standalone or hybrid wind-solar PV energy systems for reliability assessment and economic viability [36–38]. In [39], two probability models for wind energy systems, i.e. Markov model and capacity outage probability model were proposed. In [40] and [41], wind generators were modeled as multi-state units using wind turbine power curves and wind speed profile. In [42] and [43], renewable energy sources were modeled as energy limited units using some form of load modification techniques. In [44], the correlation between load and renewable resources was used to model renewable energy resources. Chronological time series simulation was used to determine reliability indexes like Loss of Load Probability (LOLP) and Loss of Power Supply Probability (LPSP) for stand-alone solar-photovoltaic systems in [45] and [46]. Monte Carlo simulations were used to assess the performance of grid-connected wind energy systems in [47] and [48]. The performance assessment of a stand-alone wind energy system with diesel generator backup was studied in [49] and [50] while with a battery storage was explored in [51]. In [52], the authors employed statistical models for optimal selection of solar modules for a site based on capacity factors. In [53] and [54], a closed-form solution approach was developed for evaluating LPSP of stand-alone renewable energy systems. The load was assumed to be uniformly distributed, the load and renewable energy resources were considered independent. This approach was extended by the authors to utility-interactive renewable energy generation system in [55] and [56]. In [57], closed form analytical expressions to determine energy index of reliability (EIR) for a hybrid wind/solar generation system were developed. In [58], a numerical probabilistic model using convolution was developed for HECS; capacity levels due to hardware failures of the wind turbines and solar modules were also considered. The method of convolution introduces some errors due to the assumption of independence between wind and solar power random variables. Also, it is mathematically tedious to account

for multiple wind farms or solar parks with this method. In [59], the authors demonstrated that various characteristics of wind, wave and solar generation allowed a greater combined penetration rate than using only one predominant type of renewable energy source. By utilizing an equal mix of wind, solar and wave power generation, the overall reserve requirements were reduced compared to those of wind alone. In [60], the authors presented controller design that monitors the operation of the stand-alone or grid-connected systems. The controller determined the energy available from each of the system components, environmental credit of the system and also gave production cost, unmet and spilled energies, and battery charged and discharged losses.

The sizing of the individual components in a HECS is very crucial so as to meet the demand in a reliable and economic way. The independent sizing of both energy sources would result in considerable over sizing, which in turn makes the facility very expensive. With increased complexity as compared to single energy systems, the optimum design of a HECS gets more complicated. This is caused by uncertain renewable profiles, load demand, non-linear characteristics of components, the high number of parameters and variables to be considered. Also, the optimum configuration and optimum control strategy of the system are interdependent. There are several approaches to address this optimum configuration issue:

- Graphic construction approach: Uses long term meteorological data, only two parameters can be included [61, 62].
- Probabilistic approach: Eliminates the need for time series data for assessing the long-term performance, cannot represent the dynamic nature changing performance [57, 58, 63].
- Iterative approach: Utilizes iterative optimization technique according to certain reliability criteria, cost minimization is generally implemented either by linearly changing the values of corresponding decision variables or through linear programming, requires increased computational effort [15, 18].
- Artificial intelligence approach: Includes various methods like genetic algorithms, artificial neural networks, fuzzy logic etc. It finds the global optimum system configuration with less computational burden [64, 65].

- Multi-objective design approach: Several objectives are simultaneously optimized, some of which might be conflicting (for e.g., costs and reliability) [66, 67].

Previous works dealing with optimal sizing of a HECS include [13,17,18,60,68]. Historically, the determination of the size of a HECS used techniques such as the least square method [69], loss of power supply probability (LPSP) [54] method, or the trade off method [70]. A major limitation of these processes is that they are devised for stand alone systems which imply that the effects of power system grid integration were not investigated. There also exists a number of computer simulation programs for evaluating performance of hybrid renewable energy systems. A detailed literature survey on such commercially available software tools can be found in [71]. Most of them have "Black Box" code utilization, each of them has its own advantages and disadvantages. For e.g. in HOMER, first degree linear equations based models are used for hybrid system components that do not represent the source characteristics exactly.

The growing scale of the renewables infrastructure has resulted in a complex patchwork quilt of interconnection requirements. There are existing interconnection standards like for large conventional generators - FERC Order No. 2003 [72], large wind - FERC Order No. 661 [73], Distributed Resources - IEEE 1547 [74], etc. While there are no explicit standards for large scale concentrated solar power yet, it is likely that the solar industry will follow a similar path as wind, adopting similar technical and performance standards.

Adequate reactive power or Var reserve is crucial to maintain system integrity during post-contingency operation when considering random failures of reactive power sources. Most of the existing work has examined reactive power as an ancillary service mainly in the context of large conventional generators [75], [76], and not much work has been reported that examines how new forms of renewable generation such as wind or solar or a combination of both could contribute to system reactive power requirements. Proper technology selection and generation unit sizing are essential in the design of such systems for improved operational performance [4, 17–19, 61]. Most of the existing work on wind/solar ECSs planning have considered them as mainly active power resources. The lack of attention to reactive capability exhibited by a HECS unit, which can help improve the voltage profile and reduce energy loss, at the planning stage may lead to potential increase in investment cost and improper allocation. It is thus of critical importance

that the reactive capability limits of HECS components are accounted to quantify the associated benefits. The reactive capability limits of different renewable distribution generation systems covering wind, solar photovoltaic, and biomass-based generation units were explored in the planning model [77]. The potential benefits of extended reactive capability of DFIG wind parks for enhanced system performance was explored in [78]. The power electronics has a crucial role in interfacing between the variable-speed wind power generator or a changeable supply from solar generator units to the power system [79], [80]. They match the characteristics of the HECS output to the grid operation requirements regarding voltage, active and reactive power, frequency, power quality, etc. [81].

When the penetration of wind or solar generators on any particular network is low, the impact is quite small and utility systems are generally unaffected. However, several utilities in USA are now confronted with high Renewable Portfolio Standards (RPS) ($15-30\%$ by 2020) proposed by most of the states. As these variable resources constitute a larger proportion of the total generation on a system, they may and probably should provide voltage regulation and reactive power control capabilities comparable to that of conventional generation by tapping into the latent excess inverter capacity to generate or consume reactive power to control voltage. Although not permitted by current interconnection standards [74], changes to these standards to allow for injecting or consuming reactive power appear eminent. This opportunity for utilities to leverage the latent capacity of these generators to enhance its own performance however should be accomplished without placing undue burdens on the generators by either excessive dispatch of reactive power or by limiting active power generation. In a competitive framework, these units should receive suitable economic signals to encourage them to control reactive power [82].

A large wind ECS comprised of doubly fed induction generators (DFIGs) and power electronic interface is the most popular option to harness wind energy due to varying nature and unpredictability of the wind speeds [83]. It provides for reduced converter rating, costs and losses, improved efficiency, easy implementation of power factor correction and four quadrant control of active and reactive power control capabilities [84]. In addition to providing active power to the grid, the DFIG based WECS with power electronic converters can also provide reactive power to the system by incorporating minor modifications to their design and/or con-

trol architecture [85], [86]. Large capacity concentrated solar thermal power plants need to meet strict interconnection requirements to be a significant generating part of the grid, unlike small distributed generation (DG) systems. This involves power factor correction, over-voltage protection, and low-voltage ride-through and associated voltage recovery processes. Large synchronous generators typically control their output voltage within the prescribed bounds by manipulating (usually injecting) reactive power. Control is realized via an excitation system that consists of an AC or DC exciter, controller and voltage measurement components [87]. In [88], a voltage stability assessment tool was developed which incorporated wind variability. A similar process was extended here to include both solar and wind variability.

2.2 Intellectual Merit

This work provides with a framework for the development and deployment of a HECS with wind and solar resources. It addresses the issue from both resource and systems point of view. It deals with the real (MW) and reactive (MVar) power assessment of the HECS and the impact of it on grid security. Some of the highlights of the framework include:

- Location Based Variability and Correlation Analysis: Quantification of site specific resource interdependence is generally neglected. The proposed work utilizes site specific resource information which is analyzed to identify complementarity and cite potential locations.

- Renewable Portfolio Combinations: Most studies are static in nature, with fixed assumptions about the size and mix of renewable resources. This work accommodates portfolios of mixed resources, accounting for geographical and technological diversities.

- Incremental Analysis: Instead of focusing on just certain load and renewable levels, this work can provide "incremental" or "aggregate" analyses to better estimate the effects of adding certain resources onto an existing system. This benefits when dealing with retrofitting existing power plants.

- Multi-criteria Optimization: The optimal configuration of the individual components

inside the HECS is carried out using genetic algorithms. Cost function and system performance including energy capacity optimization are considered.

- System Stability: Most studies consider the HECSs as purely active power sources. But with increasing wind and solar penetration in the future power grid, these power plants can and should participate in providing voltage support. This work explores the possibility of enhancing power system voltage security by tapping into reactive power reserves at different generation profiles.

- Incorporation of Wind and Solar resource variability - This work provides a novel tool to include the resource variability into steady state voltage security assessment and provides the power transfer margin. Voltage control areas and different redispatch strategies are determined to increase the system security.

2.3 Framework Formulation

This work constructs a methodology that gives a solution to some of the problems associated with the integration of large scale hybrid plants into the power grid. The solution includes locating multiple feasible interconnection points that will optimize the size of the hybrid plant and reserves. Figure 2.1 shows a general schematic of the proposed HECS. A wind energy conversion system (WECS) and solar thermal energy conversion system (STECS) are connected in parallel through proper electrical interface with a control unit. This combined HECS meets a local load. This control unit may be connected (for grid-connected ECS) or not connected (for standalone ECS) with the rest of the electrical grid. The interaction with the grid may be considered as bi-directional which means that excess of energy generated by the HECS is conditionally supplied to the grid or deficit of energy will be drawn from the grid in time of low generation in order to cater to the local demand. As long as both of the units are under the purview of the same control center, the operators can utilize the synergy of the two energy resources to maintain energy balance and optimally allocate energy reserves.

For Figure 2.1, it can be seen that there are three situations which might rise:

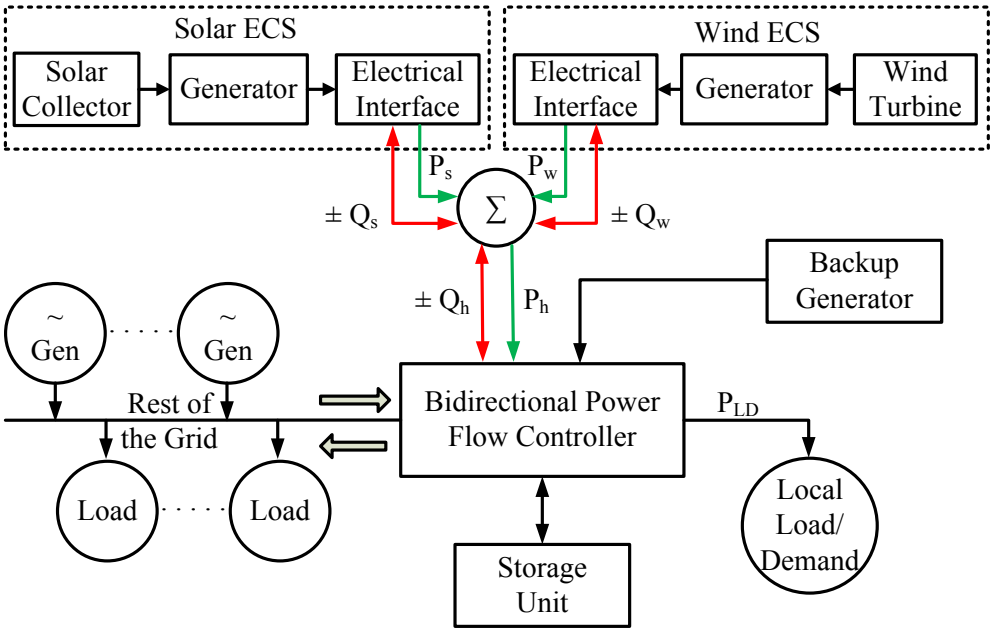

Figure 2.1 General Layout of Hybrid Energy Conversion System

1. When the local load is absent - This represents a situation where the HECS is not meeting a specific load, it is far off from the load center and is feeding into the grid only. In this case, the HECS is supplying all its generated power to the grid and it acts as must-take energy source.

2. When there is a local load and the ECS is grid connected - In this situation, the HECS is connected to the local load through a control unit which supports bidirectional flow of power. This means that excess of energy generated by the HECS is conditionally supplied to the grid or deficit of energy will be drawn from the grid in time of low generation in order to cater to the local demand.

3. When there is a local load and the ECS is standalone - In this situation, the ECS needs to have some sort of energy reserves or backup in the form of battery storage (for small scale systems) or fast acting backup generators.

The different chapters is this dissertation are arranged as follows. Chapter 3 deals with the processing of bulk resource data and identification of candidate wind-solar hybrid locations. Chapter 4 deals with the modeling of locational resource characteristics and computing per-

formance indices which will help in selection and ranking of several sites. It also involves a multi-objective optimization routine which further refines the sizing issue for each individual location. Post site selection and sizing determination, Chapter 5 deals with the grid interconnection and focuses on the steady state voltage security of the grid. It also deals with development of a wind-solar resource variability assessment tool. Chapter 6 deals with large system implementation of the developed methodologies on a reduced WECC (Western Electricity Coordinating Council) system and provides further insights into HECSs. Chapter 7 finally summarizes the entire work and highlights the significant contributions and future scope of the work.

CHAPTER 3. IDENTIFICATION OF CANDIDATE WIND-SOLAR SITES (HECS ID Tool)

Identification of suitable locations that will support both wind and solar integration into the electric power grid require the utilization of several information resources. The Hybrid Energy Conversion System Identification (HECS ID) tool assesses the viability of the locations of these two resources and then forms complementary areas within the United States that meet minimum suitable energy production characteristics. These sites were then filtered based on their relative vicinity to high power transmission lines which have the potential to export energy to a load center. Candidate areas within the United States were identified which provide the most suitable locations for the establishment of a hybrid generation facility.

3.1 Wind-Solar Resource Data Source

Wind resource evaluation is the most crucial element in projecting wind turbine performance at a given site. The energy available in a wind stream can be considered to be proportional to the cube of its speed. Also, the wind resource is very rarely a steady, consistent flow. It varies with the time of day, season, height above ground and type of terrain. The classes of wind power density for two standard wind measurement heights - 10 m and 50 m are shown in [89]. In general, sites with a wind power class rating of 4 (400 - 500 W/m^2) or higher are preferred for large scale wind plants.

A solar thermal power plant consists of a conventional power block and a solar receiver system which acts as the fuel source and substitutes the conventional steam generator. Solar thermal is inherently a utility-scale technology whose near term cost estimates are much lower than those for solar PV [90]. Most solar thermal systems are built around modules of 50 - 250

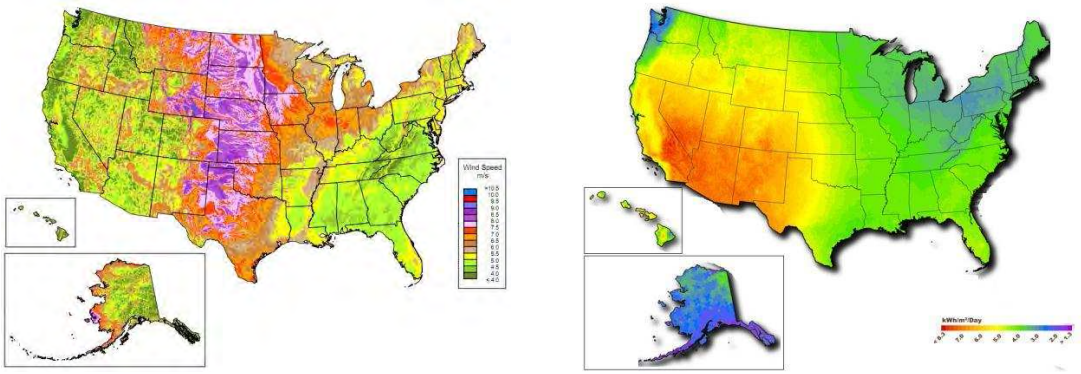

Figure 3.1 Wind and Concentrated Solar Resource of USA [Source: NREL]

MW. Solar thermal power plants use the solar Direct Normal Irradiance (DNI) to convert solar energy into heat with the help of focusing receivers, which is then used to drive a thermodynamic cycle and produce electricity. In order to reach economic competitiveness, they are constructed in regions of solar resources of more than 2000 kWh/m^2 per year [91].

Figure 3.1 shows the wind resource at 80 m height and the concentrated solar power potential in USA. Since the primary factors behind the power output of a solar-wind hybrid power plant are wind speed and solar irradiance information, getting access to reliable meteorological data is of critical importance in their resource modeling and citing considerations.

The solar DNI and wind speed data used in this work are from the following sources:

- The Solar Prospector tool (SP) [92]. It is a mapping tool which provides access to solar resource data-sets and other data relevant to utility-scale solar power projects [93].
- National Solar Radiation Database (NSRDB) [94]. It holds solar and meteorological data for several locations in the United States and its territories.
- Western Wind Resources Dataset (WWSIS) [95]. The Western Wind and Solar Integration Study (WWSIS) was initiated in 2007 to examine the operational impact of up to 35% energy penetration of wind, photovoltaics (PV), and concentrating solar power (CSP) on the power system operated by the WestConnect group of utilities.
- Eastern Wind Resources Dataset (EWITS) [96]. The Eastern Wind Integration and Transmission Study (EWITS) was initiated in 2008 to examine the operational impact of

up to 20-30% energy penetration of wind on the power system in the Eastern Interconnect of the United States.

3.2 HECS ID Tool

The HECS ID tool involves the following steps in the initial selection of potential hybrid locations:

- select areas having wind and solar resources above certain threshold values - for e.g. wind $\geq$ 450 W/m^2 at 50 m hub height), solar $\geq$ 2000 kWh/m^2/year.
- find common overlapping areas, excluding protected lands, excessive slope, wildlife sanctuaries, etc.
- gather the network information - i) transmission grid layout - existing and proposed from various sources and create space bands of pre-determined miles width along the lines, ii) load pockets, iii) other forms of generation - existing and future, iv) local RPS targets (Figure 3.2, [97]).
- gather data in the reduced areas from the sources [92, 94–96].

In this work, 24 locations made up of 12 good wind and 12 good solar resources were selected in US south-western states. These sites were selected based on their vicinity to existing and proposed transmission lines (Figure 3.3, [98]). The individual location details are given in Table 3.1 (see Figure 3.4).

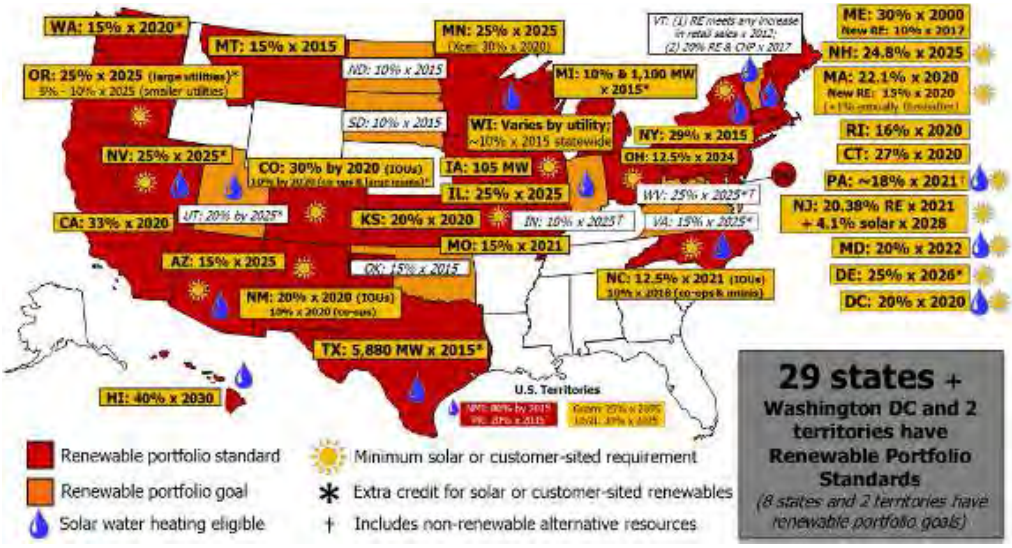

Figure 3.2 Renewable Portfolio Standards Policies (RPS)

Table 3.1 Solar and Wind Location Details

Solar DNI Data				Wind Speed Data			
Serial #	ID	Latitude	Longitude	Serial #	ID	Latitude	Longitude
S1	117053505*	35.05	-117.05	W1	3579◇	35.08	-116.96
S2	116053545*	35.45	-116.05	W2	709◇	32.71	-116.27
S3	117853605*	36.05	-117.85	W3	1169◇	33.94	-116.76
S4	120153995*	39.95	-120.15	W4	1481◇	34.11	-101.17
S5	118553775*	37.75	-118.55	W5	1551◇	34.16	-116.37
S6	116253275*	32.75	-116.25	W6	5606◇	35.56	-116.61
S7	120653985*	39.85	-120.65	W7	2832◇	34.86	-116.74
S8	116753395*	33.95	-116.75	W8	2935◇	34.92	-118.99
S9	116353445*	34.45	-116.35	W9	6172◇	35.89	-117.87
S10	723815+	34.85	-116.80	W10	9039◇	37.66	-118.99
S11	723840+	35.43	-119.05	W11	11819◇	39.78	-120.69
S12	722670+	33.67	-101.82	W12	12514◇	40.17	-120.39
** - SP Source; + - NSRDB Source; ◇ - WWSIS Source*							

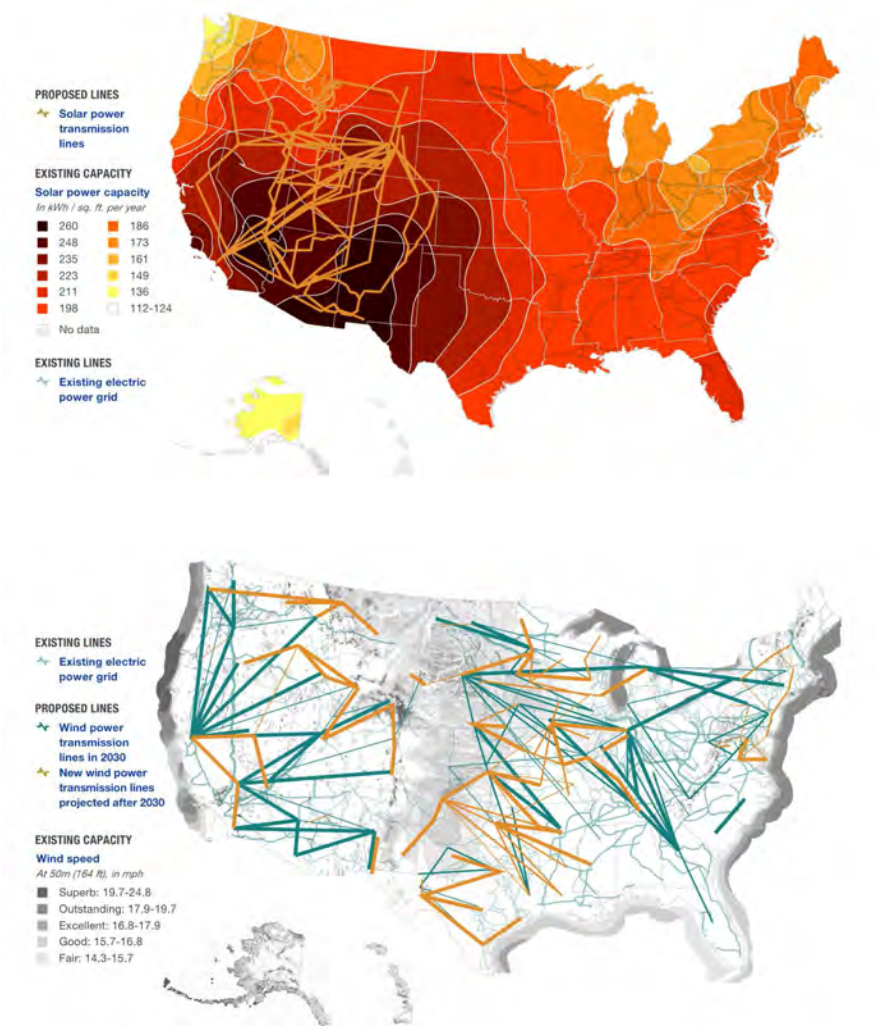

Figure 3.3 Concentrated Solar and Wind Resource Overlay with Existing and Proposed Transmission Grid of USA

3.3 Modeling of Resource Data using Time Series

Understanding the time series dynamics of wind speed and solar irradiance is an essential element. Time series analysis comprises methods for analyzing time series data in order to extract meaningful statistics and other characteristics of the data. The time domain approach is generally motivated by the presumption that correlation between adjacent points in time is best explained in terms of a dependence of the current value on past values. The time domain approach focuses on modeling some future value of a time series as a parametric function of the current and past values. In this scenario, linear regressions of the present value of a time

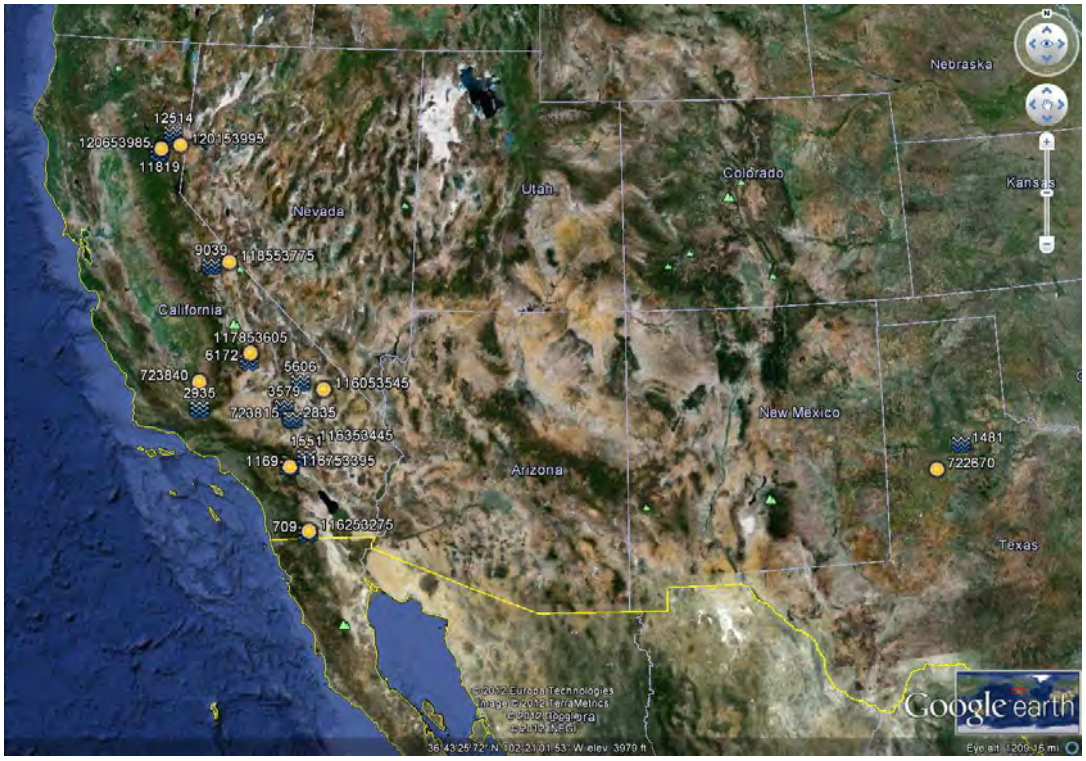

Figure 3.4 Location of the each of the 12 wind and 12 solar sites before pairing [Google Earth]

series on its own past values and on the past values of other series were considered. One approach, advocated in the landmark work of Box and Jenkins [99, 100], develops a systematic class of models called autoregressive integrated moving average (ARIMA) models to handle time-correlated modeling and forecasting. The approach includes a provision for treating more than one input series through multivariate ARIMA or through transfer function modeling. The defining feature of these models is that they are multiplicative models, meaning that the observed data are assumed to result from products of factors involving differential or difference equation operators responding to a white noise input.

Some terms need to be defined [101] before the application of time series is explained. The ***backshift operator*** B can be defined as

$$Bx_t = x_{t-1} \tag{3.1}$$

and can be extended to powers $B^2 x_t = B(Bx_t) = Bx_{t-2}$, and so on. Thus,

$$B^k x_t = x_{t-k} \tag{3.2}$$

Differences of order d are defined as

$$\nabla^d = (1 - B)^d \tag{3.3}$$

where one may expand the operator $(1 - B)^d$ algebraically to evaluate for higher integer values of d.

An ***autoregressive model of order*** p, abbreviated $AR(p)$, is of the form

$$x_t = \phi_1 x_{t-1} + \phi_2 x_{t-2} + \ldots + \phi_p x_{t-p} + \epsilon_t \tag{3.4}$$

where x_t is stationary, $\phi_1, \phi_2, \ldots, \phi_p$ are constants ($\phi_p \neq 0$). Unless otherwise stated, it is assumed that ϵ_t is a Gaussian white noise series with mean zero and variance σ_ϵ^2. The mean of x_t in (3.4) is zero. If the mean, μ of x_t is not zero, x_t is replaced by $x_t - \mu$ in (3.4), i.e.,

$$x_t - \mu = \phi_1(x_{t-1} - \mu) + \phi_2(x_{t-2} - \mu) + \ldots + \phi_p(x_{t-p} - \mu) + \epsilon_t \tag{3.5}$$

or,

$$x_t = \alpha + \phi_1 x_{t-1} + \phi_2 x_{t-2} + \ldots + \phi_p x_{t-p} + \epsilon_t \tag{3.6}$$

where $\alpha = \mu(1 - \phi_1 - \ldots - \phi_p)$.

The ***autoregressive operator*** is defined to be

$$\phi(B) = 1 - \phi_1 B - \phi_2 B^2 - \ldots - \phi_p B^p \tag{3.7}$$

The ***moving average model of order*** q,or $MA(q)$ model, is defined to be

$$x_t = \epsilon_t + \theta_1 \epsilon_{t-1} + \theta_2 \epsilon_{t-2} + \ldots + \theta_q \epsilon_{t-q} \tag{3.8}$$

where there are q lags in the moving average and $\theta_1, \theta_2, \ldots, \theta_q$ are constants ($\theta_q \neq 0$) are parameters.

The ***moving average operator*** is

$$\theta(B) = 1 + \theta_1 B + \theta_2 B^2 + \ldots + \theta_q B^q \tag{3.9}$$

A time series $x_t; t = 0, 1, 2, \ldots$ is **ARMA(p,q)** if it is stationary and

$$x_t = \phi_1 x_{t-1} + \ldots + \phi_p x_{t-p} + \epsilon_t + \theta_1 \epsilon_{t-1} + \ldots + \theta_q \epsilon_{t-q} \tag{3.10}$$

The parameters p and q are called autoregressive and the moving average orders, respectively.

The integrated ARMA, or ***ARIMA model***, is a broadening of the class of ARMA models to include differencing. A process x_t is said to be **ARIMA(p,d,q)** if

$$\nabla^d x_t = (1-B)^d x_t \tag{3.11}$$

is *ARMA(p,q)*. In general, the model can be written as

$$\phi(B)(1-B)^d x_t = \theta(B)\epsilon_t \tag{3.12}$$

If $E(\nabla^d x_t) = \mu$, the model can be written as

$$\phi(B)(1-B)^d x_t = \alpha + \theta(B)\epsilon_t \tag{3.13}$$

where $\alpha = \mu(1-\phi_1-\phi_2-\ldots-\phi_p)$.

The operators

$$\Phi_P(B^s) = 1-\Phi_1 B^s - \Phi_2 B^{2s} - \ldots - \Phi_P B^{P_s} \tag{3.14}$$

and

$$\Theta_Q(B^s) = 1-\Theta_1 B^s - \Theta_2 B^{2s} - \ldots - \Theta_Q B^{Q_s} \tag{3.15}$$

are the seasonal autoregressive operator and the seasonal moving average operator of orders P and Q, respectively, with seasonal period s.

The multiplicative ***seasonal autoregressive integrated moving average model***, or ***SARIMA model***, is given by

$$\Phi_P(B^s)\phi(B)\nabla_s^D\nabla^d x_t = \alpha + \Theta_Q(B^s)\theta(B)\epsilon_t \tag{3.16}$$

where ϵ_t is the usual Gaussian white noise process. The general model is denoted as

$$\textbf{ARIMA}(p,d,q) \times (P,D,Q)_s \tag{3.17}$$

The ordinary autoregressive and moving average components are represented by polynomials $\phi(B)$ and $\theta(B)$ of orders p and q respectively [(3.7), (3.9)], and the seasonal autoregressive and moving average components by $\Phi_P(B^s)$ and $\Theta_Q(B^s)$ of orders P and Q [(3.14), (3.15)] and ordinary and seasonal difference components by $\nabla^d = (1-B)^d$ and $\nabla_s^D = (1-B^s)^D$.

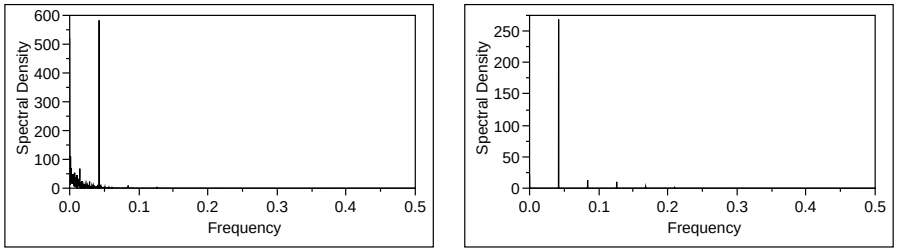

(a) Wind Speed @ W1 (b) Solar DNI @ S1

Figure 3.5 Spectral Densities of Wind and Solar Data

The sequential simulation of a wind energy conversion system (WECS) and solar thermal energy conversion system (STECS) involve the generation of hourly wind speeds and solar irradiance over a sufficiently long period of time for a given site. Time series ARMA wind speed and solar irradiance models can reproduce the high-order auto-correlation, the seasonal and diurnal distribution of the actual wind speed and solar DNI and therefore can be used in resource and performance studies of power systems involving WECS and STECS. Three years of concurrent data was fed as input training data for the time series models. To demonstrate the process, the time series for S1 and W1 have been shown below.

In order to check for the existence of seasonality, the spectral density or the periodogram of the wind and solar data were plotted. In Figure 3.5, it can be seen that in both the spectrum plots, there is a peak at $\omega = 1/24 = 0.0417$ which obviously represents the diurnal cyclical behavior of the energy resources, thus $s = 24$.

Thus, the SARIMA models for wind speed and solar DNI could be written as

$$M_w = \text{ARIMA}(p_w, d_w, q_w) \times (P_w, D_w, Q_w)_{24} \tag{3.18}$$

$$M_s = \text{ARIMA}(p_s, d_s, q_s) \times (P_s, D_s, Q_s)_{24} \tag{3.19}$$

where subscripts w, s denote wind and solar resource respectively.

Different ARIMA models with different values of p, d, q, P, D, Q were tested and the models were ranked according to minimum AIC (Akaike information criterion). The time series models for the wind speed and solar DNI data for location L1 are given as $\mathbf{ARIMA}(2,0,1) \times (2,0,1)_{24}$ and $\mathbf{ARIMA}(2,1,1) \times (2,0,1)_{24}$.

Table 3.2 SARIMA Time Series Model Details for Location L1

Resource	ARIMA Model	(p, q)	(P, Q)	AIC	R^2
wind	$(2,0,1) \times (2,0,1)_{24}$	ϕ_{w_1} =1.069 ϕ_{w_2}=-0.125 θ_{w_1} = -0.305	Φ_{w_1}=1.035 Φ_{w_2} = -0.042 Θ_{w_1} = 0.953	-2960.18	0.958
solar	$(2,1,1) \times (2,0,1)_{24}$	ϕ_{s_1} =0.607 ϕ_{s_2}=0.102 θ_{s_1} = 0.999	Φ_{s_1}=1.103 Φ_{s_2} = -0.108 Θ_{s_1} = 0.798	-2129.49	0.954

The models are validated using the diagnostic plots (Figure 3.6 and Figure 3.7) which consist of the residual plots, ACF, PACF plots and their corresponding p-values.

Let y_{w_t} be the time series value of wind speed which follows M_w (Table 3.2) at time t, ϵ_{w_t} is the normal white noise with zero mean and a variance of $\sigma_{\epsilon_{w^2}}$. The hourly wind speed V_t at hour t can be derived from the mean wind speed μ_{w_t} (=8.07 m/s for W1), its standard deviation σ_{w_t} (=3.18 for W1) and the time series value y_{w_t} as

$$V_t = \mu_{w_t} + \sigma_{w_t} y_{w_t} \tag{3.20}$$

Let y_{s_t} be the time series value of solar DNI which follows M_s (Table 3.2) at time t, ϵ_{s_t} is the normal white noise with zero mean and a variance of $\sigma_{\epsilon_{s^2}}$. The hourly irradiance H_t at hour t can be derived from the mean irradiance μ_{s_t} (=317.54 Wh/m^2 for S1), its standard deviation σ_{s_t} (=358.55 for S1) and the time series value y_{s_t} as

$$H_t = \mu_{s_t} + \sigma_{s_t} y_{s_t} \tag{3.21}$$

Similarly, the wind regimes and solar DNI profiles were simulated for all the 12 sites each, mentioned in Table 3.1. These models are fed as input to the following modules.

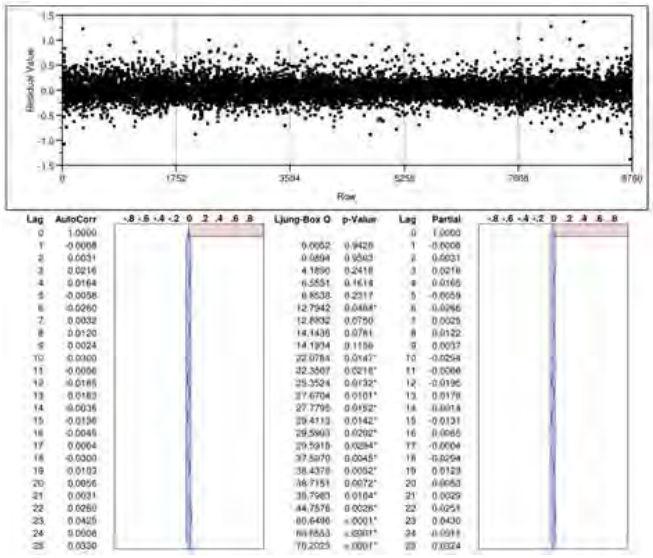

Figure 3.6 Diagnostics of the Residuals for Model M_w

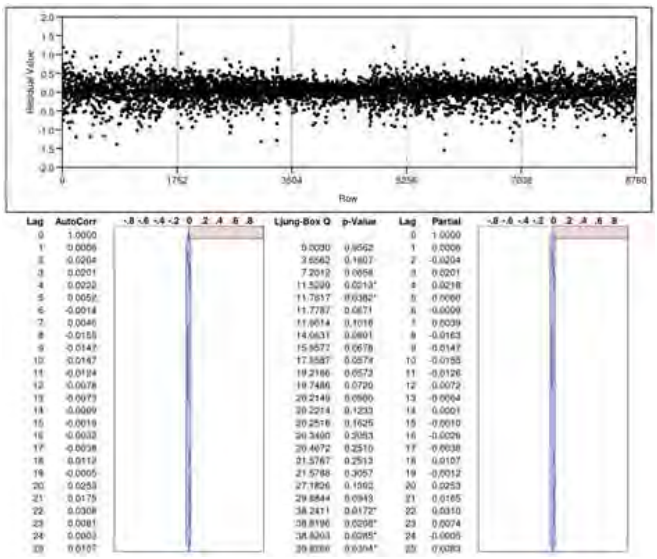

Figure 3.7 Diagnostics of the Residuals for Model M_s

3.4 Correlations between Solar and Wind Power

Most studies of combined solar and wind power systems have been on small-scale hybrid systems. Some studies on higher systems levels that incorporate both wind and solar, have been presented [102, 103], but none that investigate the combined time variability and correlations of these two sources in detail. A fundamental assumption is that wind power will already be integrated in the power system when solar power is introduced on a large scale, which makes it necessary to study them in combination [104].

To compare the characteristics of solar and wind power, the respective amount is set to produce the same amount of electricity annually, say 1 TWh annually. When combined HECS generation is considered, the total production is set to 1 TWh, i.e. either wind or solar is scaled down. Correlations between individual units and variability in the combined output are analyzed statistically. The two statistics that will be used in this section are defined below.

- The correlation coefficient (ρ) is a measure of the correlation between two variables, giving a value between +1 and -1 inclusive and is widely used as a measure of the strength of linear dependence between two variables. The sample correlation coefficient ($\rho_{x,y}$) between any two data series x_i and y_i ($i = 1 \ldots n$) is defined as

$$\rho_{x,y} = \frac{C(x,y)}{\sqrt{C(x,x)C(y,y)}} \tag{3.22}$$

  where

$$C(x,y) = \sum_{i=1}^{n}(x_i - \mu_x)(y_i - \mu_y) \tag{3.23}$$

$$\mu_x = \frac{1}{n}\sum_{i=1}^{n} x_i; \mu_y = \frac{1}{n}\sum_{i=1}^{n} y_i \tag{3.24}$$

  μ_x and μ_y are the mean values and $C(x,x)$ and $C(y,y)$ are the variance of the data series. It should be noted that the higher the value of the correlation coefficient, the higher the similarity between the two data sequences.

- The power ramp function ($\Delta P(k)$) describes how the output changes from hour to hour and is critical for the power system on the hourly operational time scale. Considering,

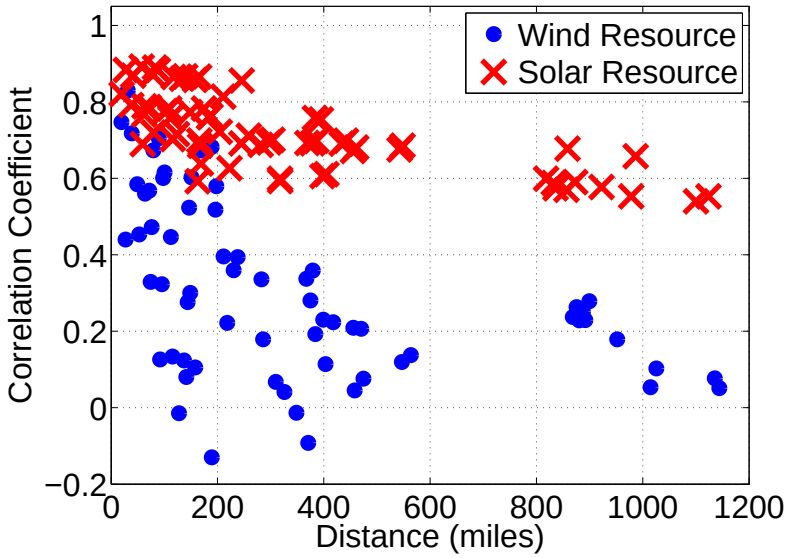

Figure 3.8 Correlations between individual wind farms and solar radiation stations

the hybrid output to be $P(k)$, power ramp ($\Delta P(k)$) can be defined as

$$\Delta P(k) = P(k) - P(k-1) \tag{3.25}$$

3.4.1 Correlations Between Individual Resource Points

Figure 3.8 shows the hourly correlations between individual solar radiation stations and wind farms and the dependence of the correlations on the distance between the locations. The figure shows that the correlation is strong between adjacent wind farms, but decreases with distance. This is in accordance with previous results for wind power and is due to the fact that weather fronts do not affect wide-apart regions at the same time. Contrary to the wind power data, the correlation between radiation stations is consistently stronger and converges to somewhere just around 0.6 for the longest distances. This is because all stations follow very similar seasonal and diurnal irradiance patterns.

3.4.2 Correlations Between Combined Solar and Wind Power

The correlations between total solar power and wind power, on different time scales, are shown in Figure 3.9. The top plots show the mean profiles of wind and solar power, integrated

over different time scales, while the bottom plots show the corresponding correlation plots with the least-square regression line (green) drawn, the slope of which gives an indication of the correlation coefficient or the measure of the strength of linear dependence between the two variables - wind and solar power. A negative correlation is seen between annual totals of solar and wind power. This suggests that more windy years are less sunny, and vice versa. However, only three years of concurrent wind and solar data were used here (2004-2006), a longer sequence of years would be needed to determine if this pattern is consistent. The correlation varies with the integration time and is different for different totals, where there is negative correlation. On the hourly time scale the correlation is weak, and it is also seen in the average daily profile that there is no evident diurnal fluctuation in wind power over the year on the overall scale, whereas for solar power the diurnal pattern is very clear.

These negative correlations suggest that a combination of solar and wind power would even out fluctuations, but it is not clear on which time scales. As there are fluctuations both on seasonal and diurnal time scales, the seasonal correlations could still be visible in the correlation coefficients for hourly and daily series. Although the daily correlations are not particularly strong, they suggest that to some extent less solar power is produced during windy days while the wind power production is lower during sunny days.

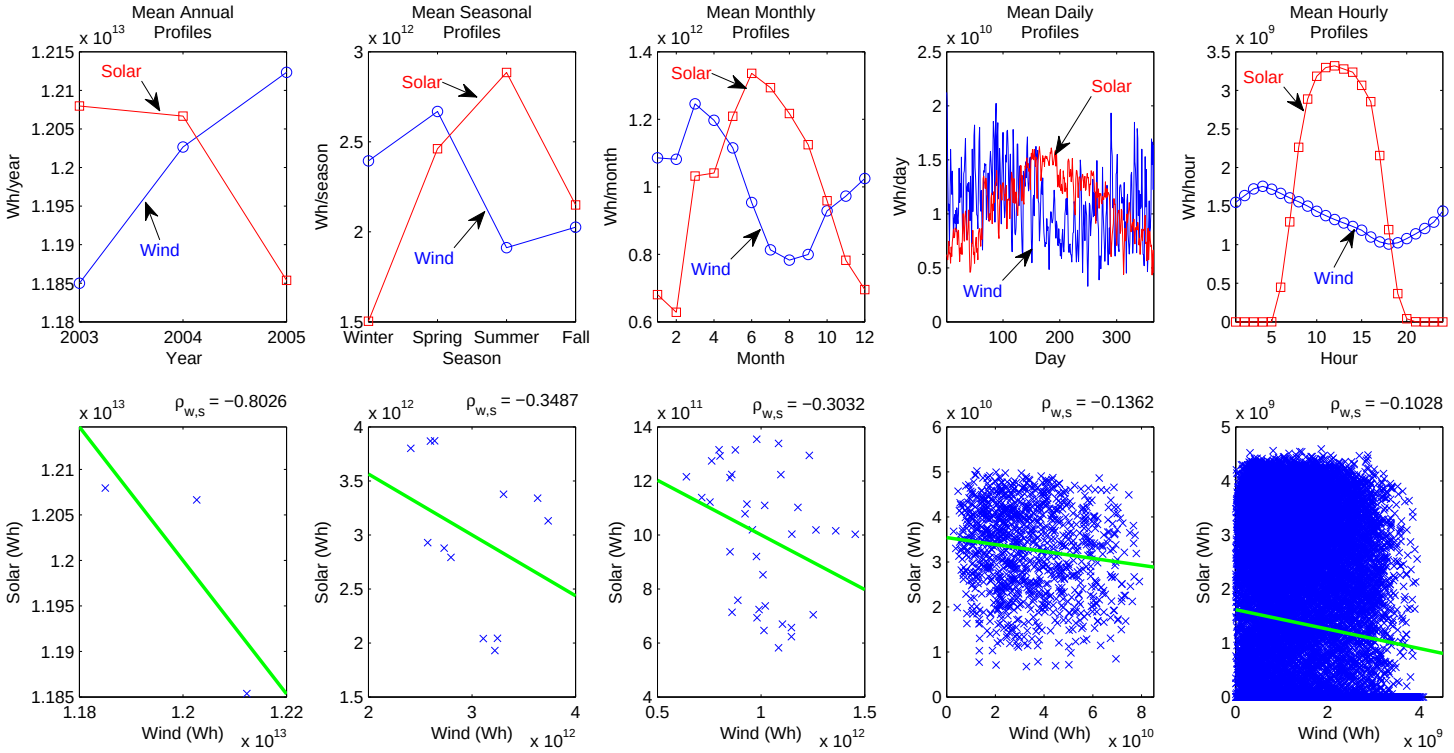

Figure 3.9 Variability and correlations between overall solar and wind power on different time scales - Annual totals; seasonal totals; monthly totals; daily totals; hourly totals

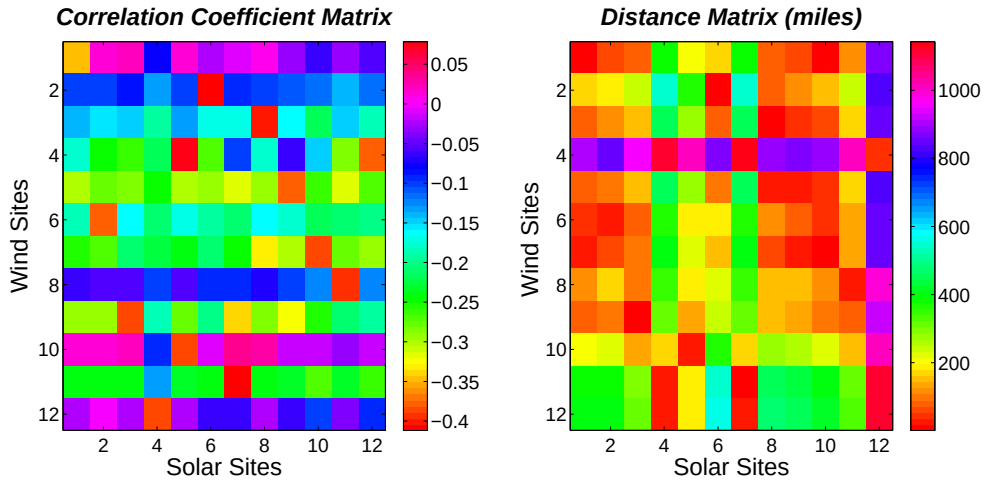

Figure 3.10 Correlation Coefficient Matrix and Distance Matrix

3.4.3 Complementarity Analysis

For a ECS which has both wind and solar units, they need to be under the purview of the same control center or the balancing authority, thus the operators can utilize the synergy of the two energy resources to maintain energy balance and optimally allocate energy reserves. But the geographical distance between the two ECSs also should be under a certain threshold. This limiting distance depends on a bunch of factors, for e.g. the terrain, individual capacities, number of wind turbines, solar collector area, etc. Thus both factors - resource complementarity and distance need to be considered when selecting potential HECS sites. In Figure 3.10, the correlation coefficient matrix and the distance matrix are shown on the left and right respectively, which denote the element-wise relationship between the wind and solar location resources and the distances between them. Those sites which have simultaneously most negative correlation coefficient (highest complementarity) and least distance are most suitable. This model does the pairing for each of the solar site with a single wind site such that they are within a certain fixed distance from each other and possess greatest complementarity. For the 24 sites mentioned in Table 3.1, the possible hybrid combinations can be done from figure 3.10. The pairing details and distance in miles are given in Table 3.3.

Table 3.3 Pairing of the wind/solar sites to form hybrid sites

Hybrid Site	Pairing	Solar ID	Wind ID	Distance (miles)
H1	(S1,W1)	117053505	3579	6
H2	(S2,W6)	116053545	5606	33
H3	(S3,W9)	117853605	6172	12
H4	(S4,W12)	120153995	12514	20
H5	(S5,W10)	118553775	9039	25
H6	(S6,W2)	116253275	709	3
H7	(S7,W11)	120653985	11819	6
H8	(S8,W3)	116753395	1169	1
H9	(S9,W5)	116353445	1551	21
H10	(S10,W7)	723815	2832	4
H11	(S11,W8)	723840	2935	36
H12	(S12,W4)	722670	1481	49

3.4.4 Combinations of Solar and Wind Power

Since the wind and solar resources are intermittent, they are considered as energy replacement rather than capacity-replacement resources [105]. While combining the solar and wind power outputs, the respective amount is set to produce the same amount of electricity annually, say 1 TWh. When combined HECS generation is considered, the total production is set to 1 TWh, i.e. either wind or solar is scaled down.

Table 3.4 and figure 3.11 shows the variations in the total output and the ramp function for combinations of solar and wind power for all the sites. The standard deviation of has a minimum at 30%-70% solar-wind power, but the inter-hour fluctuations are consistently higher with a larger share of solar power. For example, the average change from hour to hour is 2.6 times higher and the maximum change 1.3 times higher with 100% solar power compared to 100% wind power.

But, here the concept of top-down may not translate into bottom-up scaling, i.e. for individual HECSs, the mix between wind and solar would not be necessarily the same as the overall combined situation. The standard deviation of P and ΔP for all the 12 sites in Table 3.1 are shown in Figure 3.12, where the minimum in the standard deviation is clearly seen for different sites. It gives evidence that there is a smoothing effect from combining solar

Table 3.4 Fluctuations in Combined Wind and Solar Generation at all Sites, each producing 1 TWh

Annual Production (Ratio)		Combined Output P (GW)			Hourly Change $\|\Delta P\|$ (GW)		
Wind	Solar	Mean	Max	Std. Dev.	Mean	Max	Std. Dev.
0	1	1369.863	4412.411	1479.854	841.1357	3257.408	901.9334
0.05	0.95	1369.863	4283.489	1401.832	802.0064	3099.082	850.8664
0.1	0.9	1369.863	4154.567	1325.371	763.3575	2940.756	799.9177
0.15	0.85	1369.863	4066.586	1250.756	725.2334	2782.429	749.1427
0.2	0.8	1369.863	3991.32	1178.34	687.6593	2624.103	698.6406
0.25	0.75	1369.863	3916.054	1108.551	650.71	2465.777	648.4956
0.3	0.7	1369.863	3840.788	1041.92	614.3347	2325.293	598.9652
0.35	0.65	1369.863	3765.522	979.0898	578.6095	2214.404	550.2491
0.4	0.6	1369.863	3694.549	920.8397	543.6065	2104.901	502.6451
0.45	0.55	1369.863	3639.795	868.092	509.3672	1995.397	456.6209
0.5	0.5	1369.863	3595.012	821.9067	476.1262	1885.894	412.6247
0.55	0.45	1369.863	3554.751	783.4453	444.0564	1776.391	371.4396
0.6	0.4	1369.863	3528.415	753.8909	413.6091	1666.887	333.8853
0.65	0.35	1369.863	3517.215	734.3197	384.9665	1627.948	301.5818
0.7	0.3	1369.863	3520.736	725.5401	358.6437	1753.175	276.2693
0.75	0.25	1369.863	3524.257	727.9427	335.4655	1878.402	259.6392
0.8	0.2	1369.863	3591.631	741.4186	316.9545	2003.629	252.3673
0.85	0.15	1369.863	3703.884	765.3833	304.7579	2128.856	254.3071
0.9	0.1	1369.863	3816.137	798.8934	300.824	2254.082	263.9216
0.95	0.05	1369.863	3928.39	840.8084	306.4974	2379.309	279.3014
1	0	1369.863	4078.058	889.9415	322.9529	2504.536	297.7442

and wind power. The minimum in the standard deviation of P occur at different values of the ratio of the wind/solar mix depending on the local site resource characteristics. We know that generally solar power production is higher during summer and that of wind is higher in winter months. Thus, combining the two sources means winter capacity will be decreased while summer capacity can be increased. Thus the combination which provides the minimum P deviation will be around the levels at which their individual peak power are close to each other.

3.5 Comments

Here, large-scale solar and wind power in some locations in S-W USA were modeled, the correlations between the two power sources were studied and the effects of geographic dispersion and of combining solar and wind power were determined. It is possible to get a more evenly distributed output with combined solar and wind power generation than with any of the sources alone, due to the negative seasonal correlations, but that the variability on the hourly time scale is lowest with wind power. There is a smoothing effect on the aggregate output resulting from dispersion of generation units for solar power, but lower than that for wind power because of systematic variability in the availability of solar irradiance. A combination of solar and wind power generation for different locations assume a minimum standard deviation at differing values of solar and wind power (annual production) because of the complementarity indicated by the negative correlations. However, the hour-to-hour variability is always higher with a larger share of solar power because of the faster fluctuations in solar power.

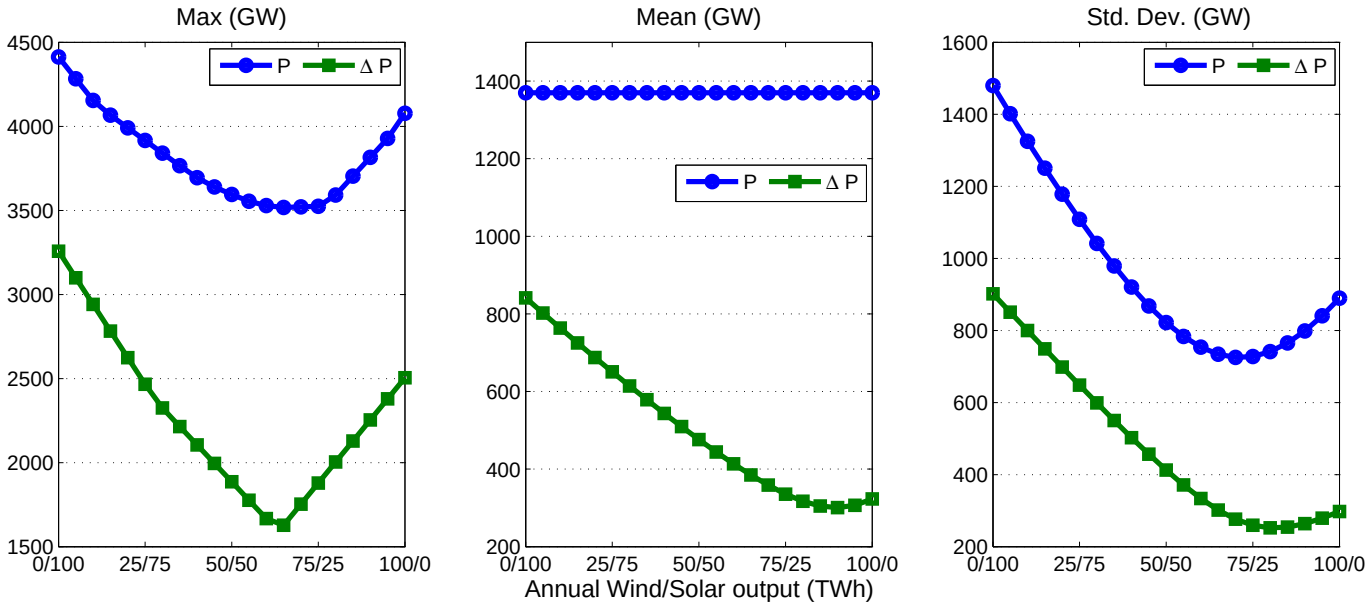

Figure 3.11 Maximum, mean and standard deviation of the combined wind and solar power output (P) and the absolute value of the ramp function ($|\Delta P|$) for all sites. [Here, $\Delta P(k) = P(k) - P(k-1)$]

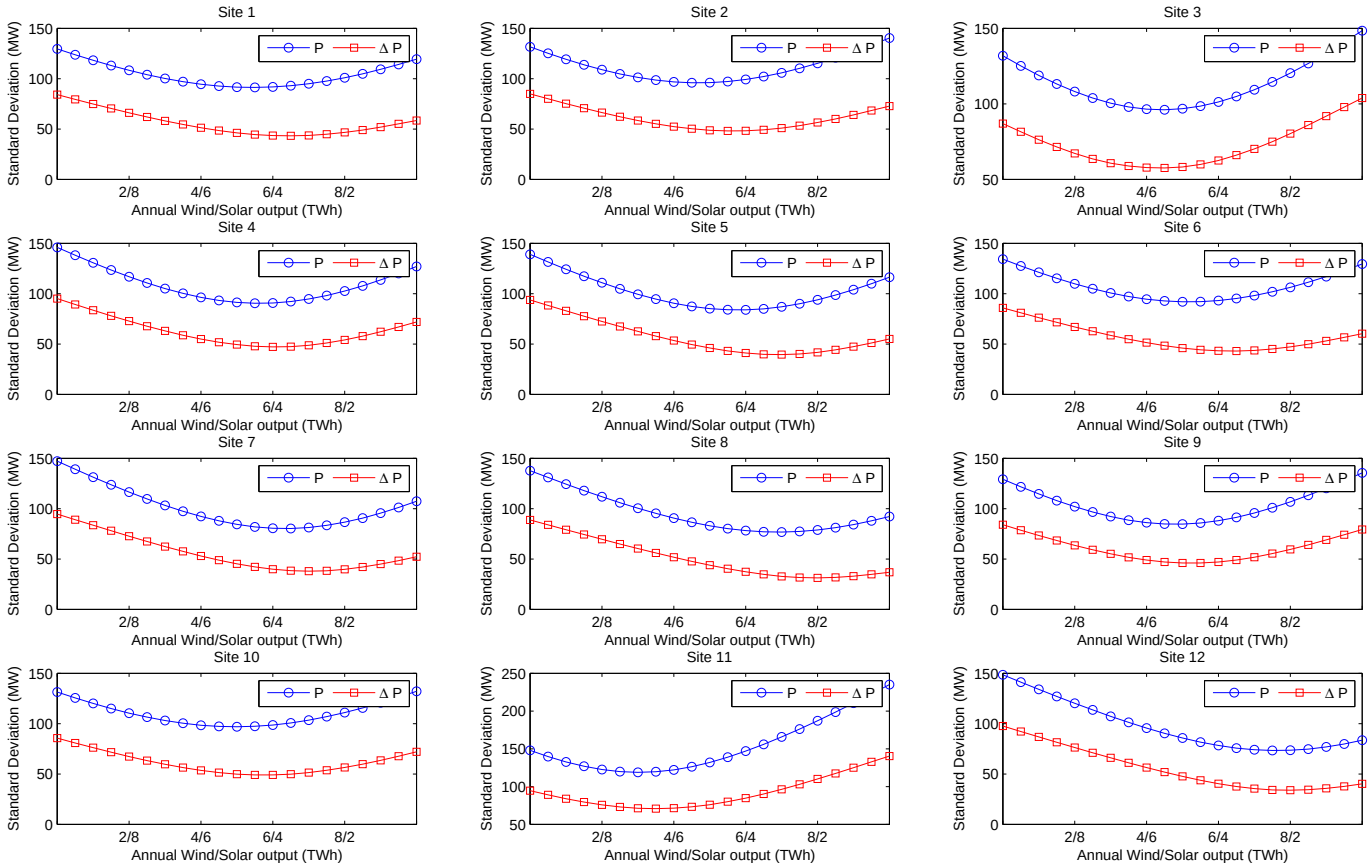

Figure 3.12 Standard Deviation of the combined wind and solar power output (P) and the absolute value of the ramp function ($|\Delta P|$) for each of the 12 sites. [Here, $\Delta P(k) = P(k) - P(k-1)$]

CHAPTER 4. MEGAWATT RESOURCE ASSESSMENT MODEL DEVELOPMENT (MWRAM)

The Megawatt (MW) resource modeling requirements includes two levels of synthesis. The first stage introduces appropriate models which determine the characteristics of wind and solar potential for a given location. The following stage is dedicated to develop appropriate models which determine the potential power extracted from both wind and solar resources. The wind power generation is modeled as turbine with a doubly fed induction generator while the solar conversion system is modeled as a parabolic trough due to the high efficiencies and long operational history of this type of system. A detailed ECS will utilize wind and solar thermal energy models that use wind speed and solar radiance data. To effectively optimize a hybrid facility, accurate models for the various components of the system are crucial.

There have been mainly two classes of approaches - deterministic modeling using chronological time series and stochastic modeling using proper statistical distributions. The issue with the former is that they are time and memory consuming. Also, suppose the year that was selected to characterize a location was a rich year and thus all the indexes would be over optimistic as compared to the actual resource profile. In this case, to capture the inherent variability of the wind speed and solar radiation and also due to their stochastic nature, the proposed HECS modeling is based on probabilistic approach. This work presents a systematic probabilistic planning approach for the integration of wind and solar resources together. The wind and solar MW power output are treated as random variables which are modeled using appropriate probability density functions. The problem of performance assessment is then reduced to working with these models. The HECS may consist of several wind turbines (wind farm) and several concentrating reflectors (solar park). The work presented here aims to quantify the resource potential of a site for a HECS setup for planning purposes; it does not focus

on energy forecasting or operations.

The performance of the HECS under study was assessed by employing suitable probabilistic models. It is well established that wind speed follow Weibull distribution, while the solar cloud cover data follow Beta distribution. Both the distributions are modeled using actual measured data and the model parameters are computed using Maximum Likelihood Estimation (MLE) method. Instead of fitting a single distribution model for the whole year, multiple Weibull and Beta distributions were fitted to the clustered data. This method of 'stratified fitting' captures the seasonal or monthly as well as hourly wind speed and solar irradiance variations.

4.1 Modeling of Renewable Resources at a given location

Figure 4.1 shows the flowchart of the various steps involved in building the HECS MW Resource Assessment Model (MWRAM). For most renewable resources, the energy availability and load distribution are correlated to each other [58]. The study period (i.e., 24 hours in a single day in different seasons) is divided into various segments, each being called a time frame t.

4.1.1 Wind Resource Modeling

Power output of a wind turbine generator at a specific site depends on the wind speed at hub height and speed characteristics of the turbine. The wind speed data collected at any height can be extrapolated to other heights on the basis of the roughness height of the terrain. A simple approach to consider the effects of hub height variation is by using the power-law equation [106], as shown in (4.1).

$$V_Z = V_i\left(\frac{Z}{Z_i}\right)^x \tag{4.1}$$

where V_Z and V_i are the wind speeds at hub and reference heights Z and Z_i (generally 10 m) respectively, and x is the Hellman exponent which depends upon location and shape of the terrain and the stability of the air. However, this extrapolation approach has some flaws [107]. This technique is much less reliable for hub heights of 80 m and higher. The decreasing influence of surface roughness on wind shear and increasing influence of lower atmospheric features such

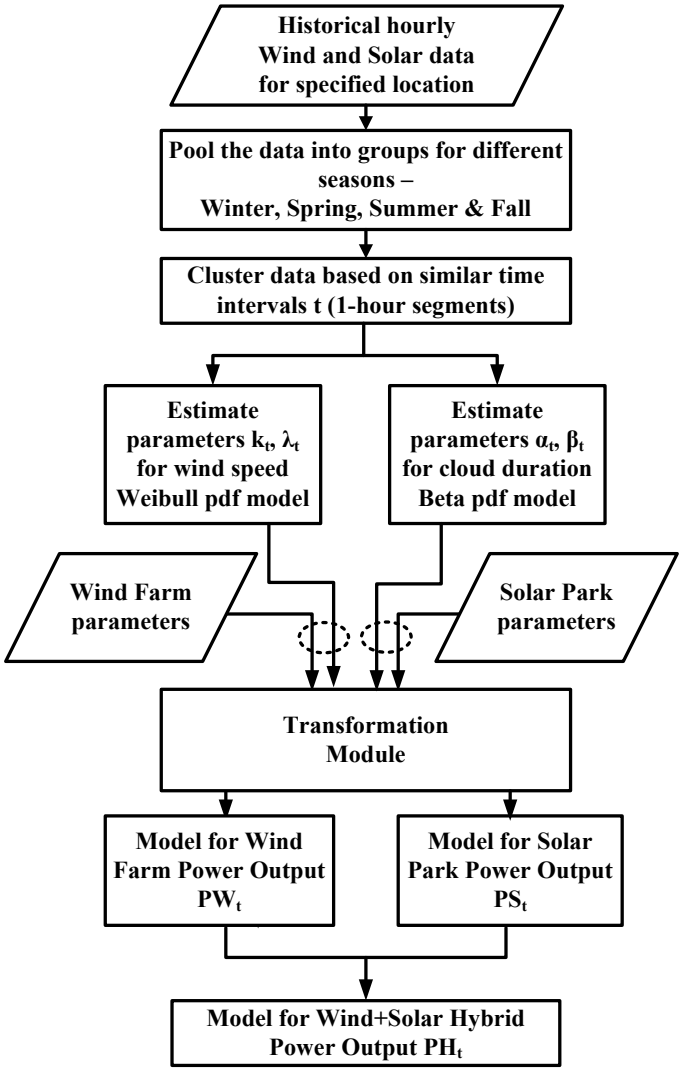

Figure 4.1 MW Resource Assessment Model (MWRAM) Steps for a Hybrid Energy Conversion System (ECS)

as low-level jets and thermal circulations makes simple extrapolation prone to large errors. Thus, the diurnal behavior at most locations is very different when comparing 10 m to hub height (say, 80 m or 100 m), as a consequence of the turbulent transport of momentum being very different between night and day in response to the radiative heating/cooling of the surface. Using the power law shearing up assumption does nothing to remove this behavior. Thus the wind speed data should come from a reliable source which considers hub heights of 80 or 100

m [1].

Wind speed is uncertain and stochastic in nature. Since the wind speed v_i is a random variable, long-term historical and meteorological data is required to determine the wind energy potential of a site. Prior research [108] has shown that the wind speed profile at a given location most closely follows a Weibull Distribution over time. During the time frame t, the wind speed random variable v_t can be assumed to be characterized by a Weibull distribution with a scale parameter λ_t (> 0) and shape parameter k_t (> 0). The probability distribution f_{v_t} and cumulative distribution F_{v_t} are given by (4.2), (4.3).

$$f_{v_t}(v_t; \lambda_t, k_t) = \frac{k_t}{\lambda_t}\left(\frac{v_t}{\lambda_t}\right)^{k_t-1} e^{-(v_t/\lambda_t)^{k_t}} \tag{4.2}$$

$$F_{v_t}(v_t; \lambda_t, k_t) = 1 - e^{-(v_t/\lambda_t)^{k_t}} \tag{4.3}$$

4.1.2 Solar Resource Modeling

The solar irradiance H_t of unit area of solar collector (W/m^2) can be expressed in terms of the maximum possible value for that time interval, H_{max_t} as

$$H_t = H_{max_t}(1 - C_t) \tag{4.4}$$

where C_t is a random variable which accounts for the cloud cover and other irradiance reducing phenomena during the time interval t. From (4.4), we get

$$C_t = 1 - H_t/H_{max_t} \tag{4.5}$$

During the time frame t, the random variable C_t can be assumed to be characterized by a Beta distribution with shape parameters α_t (> 0) and β_t (> 0) [109]. The probability distribution f_{C_t} and cumulative distribution F_{C_t} are given by (4.6), (4.7).

$$f_{C_t}(C_t; \alpha, \beta) = \frac{\Gamma(\alpha+\beta)}{\Gamma(\alpha)\Gamma(\beta)} C_t^{\alpha-1}(1 - C_t)^{\beta-1} \tag{4.6}$$

$$F_{C_t}(C_t; \alpha, \beta) = I_{C_t}(\alpha, \beta) \tag{4.7}$$

[1] Email Communication: Dr. Eugene S. Takle, Professor of Atmospheric Science, Department of Geological and Atmospheric Science, ISU; George Scott, National Wind Technology Center, NREL

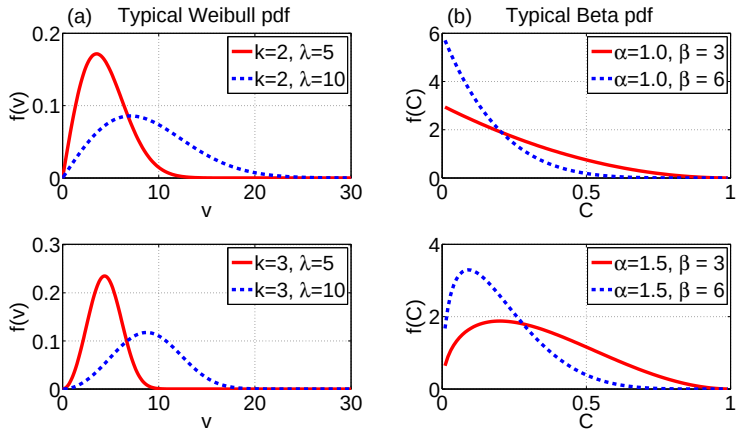

Figure 4.2 (a) Sample Weibull Probability density functions for k factors of 2 (left top) and 3 (left bottom), each with λ factors of 5 and 10 & (b) Sample Beta Probability density functions for α factors of 1 (right top) and 1.5 (right bottom), each with β factors of 3 and 6

where $I_{C_t}(\alpha, \beta)$ is the regularized incomplete beta function.

Figure 4.2 (a) shows the Weibull pdf with shape factors (k) of 2 and 3; within each of these plots, curves of scale factors (λ) 5 and 10 are drawn and Figure 4.2 (b) shows the Beta pdf with shape factors (α) of 1 and 1.5; within each of these plots, curves of shape factors (β) 3 and 6 are drawn.

4.1.3 Estimation of Model Parameters

The influence of correct parameter estimation is demonstrated in [110] for a wind ECS, similar effect can be assumed for solar ECS as well. Most of the existing literature dealing with HECS modeling assumes certain parameters to represent the wind and solar profile. If the parameter assumptions are wrong, then even if the model is correct, the resultant performance assessment might be off the mark. This work considers actual field measured/modeled data and computes hourly parameters for the wind (λ_t, k_t) and solar (α_t, β_t) probability density functions using Maximum Likelihood Estimation (MLE) method. The goal of MLE is to find parameter values such that the theoretical probability of the sample data is maximized [111].

Given a finite set of wind and solar measurements ($l = 1 \cdots n$) for each time interval t, according to MLE theory, likelihood function required to estimate the wind Weibull and solar

Beta distribution parameters is built as following

$$L_1(k_t, \lambda_t) = \prod_{l=1}^{n} f_{v_t}(v_l) = \prod_{l=1}^{n} \frac{k_t}{\lambda_t}\left(\frac{v_l}{\lambda_t}\right)^{k_t-1} e^{-(v_l/\lambda_t)^{k_t}} \tag{4.8}$$

$$L_2(\alpha_t, \beta_t) = \prod_{l=1}^{n} f_{C_t}(C_l) = \prod_{l=1}^{n} \frac{\Gamma(\alpha_t+\beta_t)}{\Gamma(\alpha_t)\Gamma(\beta_t)} C_l^{\alpha_t-1}(1-C_l)^{\beta_t-1} \tag{4.9}$$

In (4.8) and (4.9), the required parameters, namely $\hat{k_t}$, $\hat{\lambda_t}$, $\hat{\alpha_t}$ and $\hat{\beta_t}$ likelihood values can be solved by the likelihood equations (4.11).

$$\mathbf{F} = [F_1(k_t, \lambda_t), F_2(k_t, \lambda_t), F_3(\alpha_t, \beta_t), F_4(\alpha_t, \beta_t)]^T \tag{4.10}$$

$$= \left[\frac{\partial \ln L_1(k_t, \lambda_t)}{\partial k_t}, \frac{\partial \ln L_1(k_t, \lambda_t)}{\partial \lambda_t}, \frac{\partial \ln L_2(\alpha_t, \beta_t)}{\partial \alpha_t}, \frac{\partial \ln L_2(\alpha_t, \beta_t)}{\partial \beta_t}\right]^T \tag{4.11}$$

In order to solve (4.11), we use the Newton-Raphson method as following

$$\mathbf{F} + \frac{\partial \mathbf{F}(\mathbf{x})}{\mathbf{x}} \Delta \mathbf{x} = 0 \tag{4.12}$$

where

$$\mathbf{x} = [k_t, \lambda_t, \alpha_t, \beta_t]^T$$

$$\frac{\partial \mathbf{F}(\mathbf{x})}{\mathbf{x}} = \begin{bmatrix} \frac{\partial F_1(k_t,\lambda_t)}{\partial k_t} & \frac{\partial F_1(k_t,\lambda_t)}{\partial \lambda_t} & 0 & 0 \\ \frac{\partial F_2(k_t,\lambda_t)}{\partial k_t} & \frac{\partial F_2(k_t,\lambda_t)}{\partial \lambda_t} & 0 & 0 \\ 0 & 0 & \frac{\partial F_3(\alpha_t,\beta_t)}{\partial \alpha_t} & \frac{\partial F_3(\alpha_t,\beta_t)}{\partial \beta_t} \\ 0 & 0 & \frac{\partial F_4(\alpha_t,\beta_t)}{\partial \alpha_t} & \frac{\partial F_4(\alpha_t,\beta_t)}{\partial \beta_t} \end{bmatrix}$$

The simulation procedure used to solve the parameters of Weibull and Beta distributions includes the following steps:

1. Take the historical data of v_i and C_i for $i = 1 \cdots n$.
2. Choose the appropriate initial values of $k_t^{(0)}$, $\lambda_t^{(0)}$, $\alpha_t^{(0)}$ and $\beta_t^{(0)}$.
3. Taking $k_t^{(0)}$, $\lambda_t^{(0)}$, $\alpha_t^{(0)}$ and $\beta_t^{(0)}$ in (4.11) to calculate F_1, F_2, F_3 and F_4, then to calculate the Jacobian Matrix $\frac{\partial \mathbf{F}(\mathbf{x})}{\mathbf{x}}$.
4. Using (4.12), solve for Δk_t, $\Delta \lambda_t$, $\Delta \alpha_t$ and $\Delta \beta_t$.

5. From Step 4, check for tolerance error as follows

   $\max |F^{(m)}_{p(p=1,2)}(k_t, \lambda_t), F^{(m)}_{q(q=3,4)}(\alpha_t, \beta_t)| < \epsilon_1$ or

   $\max |\Delta k_t^{(m)}, \Delta\lambda_t^{(m)}, \Delta\alpha_t^{(m)}, \Delta\beta_t^{(m)}| < \epsilon_2$,

   where ϵ_1 and ϵ_2 are maximum error allowed.

6. If Step 5 is not satisfied, then

$$k_t^{(m+1)} = k_t^{(m)} + \Delta k_t^{(m)}$$
$$\lambda_t^{(m+1)} = \lambda_t^{(m)} + \Delta\lambda_t^{(m)}$$
$$\alpha_t^{(m+1)} = \alpha_t^{(m)} + \Delta\alpha_t^{(m)}$$
$$\beta_t^{(m+1)} = \beta_t^{(m)} + \Delta\beta_t^{(m)}$$

   Then go to Step 3.

Thus, the calculated values define the stochastic models and contain in them the information of the terrain, location, wind and solar profiles of the site under consideration relevant to MW generation.

4.2 Modeling of Individual MW Resources

4.2.1 Transformation Theorem

Let x be a random variable following a probability density function $f_x(x)$ and cumulative distribution function $F_x(x)$ such that $f_x(x) = \frac{dF_x(x)}{dx}$. We have another variable y such that $y = g(x)$. Suppose we need to determine the density $f_y(y)$ in terms of the density $f_x(x)$ of x. We assume that x is continuous and $g(x)$ is continuous. To find $f_y(y)$ for a given y, we solve the equation $y = g(x)$ for x in terms of y. Let x_i be all the real roots of $y_i = g(x_i)$, then

$$f_y(y) = \sum_i \frac{f_x(x_i)}{|g'(x_i)|} \tag{4.13}$$

where $g'(x) = \frac{dg(x)}{dx}$.

4.2.2 Wind Power Output Modeling

Once the uncertain nature of the wind is characterized by a random variable, the output power from the wind ECS can also be characterized as a random variable through a transformation from wind speed (m/s, say) to wind power (MW). Ignoring minor non-linearities, for a typical wind ECS, the power output characteristics can be assumed to be such that it starts generating power at the cut-in speed V_{ci}, the power increases with the cubic power as the wind increases from V_{ci} to the rated wind speed V_r [110].The rated power P_R is produced when the speed varies from V_r to the cut-out wind speed V_{co} at which the turbine is shut down for safety reasons. Figure 4.3 shows a typical wind turbine power curve. The parameters V_{ci}, V_r, V_{co} and P_R are fixed for a particular type of wind turbine.

Let there be T number of turbines. Then the maximum possible rated power of the wind farm is given be $PW_{max} = TP_r$. Thus we have the following,

$$PW(v_t) = \begin{cases} PW_{max}(av_t^3 - b) & \text{for } V_{ci} < v_t \leq V_r \\ PW_{max} & \text{for } V_r < v_t \leq V_{co} \\ 0 & \text{otherwise} \end{cases} \tag{4.14}$$

Here $a = 1/(V_r^3 - V_{ci}^3)$ and $b = V_{ci}^3/(V_r^3 - V_{ci}^3)$, which are fixed for a particular kind of turbine with fixed values of V_{ci}, V_r and V_{co}. The probability density function f_{PW_t} for the wind ECS power output during the time interval t can be obtained by the application of the transformation theorem, defined in (4.13) [112]. Thus, we get the following:

$$f_{PW_t}(PW_t) = \begin{cases} W1 & :PW_t = 0 \\ \frac{k_t}{3(PW_t + bPW_{max})} \times \frac{\left(V_{ci}^3 + \frac{PW_t}{aPW_{max}}\right)^{k_t/3}}{\lambda_t^{k_t}} \times & \\ e^{-\frac{\left(V_{ci}^3 + \frac{PW_t}{aPW_{max}}\right)^{k_t/3}}{\lambda_t^{k_t}}} & :PW_t \in (0, PW_{max}) \\ W2 & :PW_t = PW_{max} \end{cases} \tag{4.15}$$

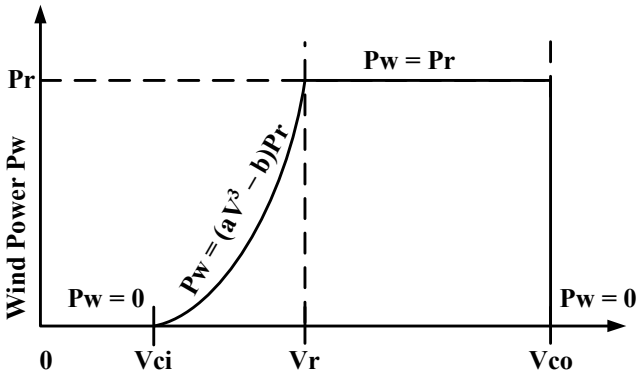

Figure 4.3 Typical Wind Turbine Power Curve

Here

$$\begin{aligned} W1 &= 1 - [F_{v_t}(V_{co}) - F_{v_t}(V_{ci})] \\ &= 1 - e^{-(V_{ci}/\lambda_t)^{k_t}} - e^{-(V_{co}/\lambda_t)^{k_t}} \\ W2 &= [F_{v_t}(V_{co}) - F_{v_t}(V_r)] \\ &= e^{-(V_r/\lambda_t)^{k_t}} - e^{-(V_{co}/\lambda_t)^{k_t}} \end{aligned} \tag{4.16}$$

Thus, (4.15) and (4.16) give the analytical expression of the variation of the MW output of the wind ECS for different time intervals t.

4.2.3 Solar Power Output Modeling

For a typical solar thermal ECS, the power output characteristics can be assumed to be a function of the irradiance, ambient temperature, cloud cover etc. But the main influencing factor is the irradiance [113]. Let the solar collector area be A_c m^2. Then, the power output of a solar collector PS_t (MW) is given by

$$\begin{aligned} PS_t &= H_t \eta_c \eta_{net} A_c \\ &= H_{max_t}(1 - C_t)\eta_c \eta_{net} A_c \\ &= PS_{max_t}(1 - C_t) \end{aligned} \tag{4.17}$$

where $PS_{max_t} = \eta_c \eta_{net} H_{max_t} A_c$ gives the maximum possible value of the solar power output for that time interval. The parameters η_c and η_{net} denote the collector efficiency and the net efficiency of the heat exchanger (η_{he}), steam turbine (η_{tu}) and the electric generator (η_g) respectively as shown in Figure 4.4, i.e. ($\eta_{net} = \eta_{he} \times \eta_{tu} \times \eta_g$).

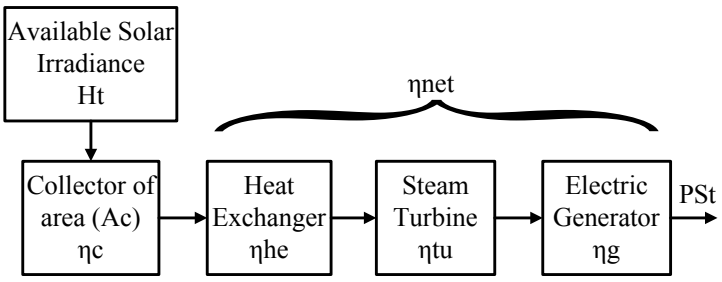

Figure 4.4 Layout of Solar Thermal Energy Conversion System

The probability density function f_{PS_t} for the solar thermal ECS power output during the time interval t (where, t could be either a day-time interval or night-time interval) can be obtained by the application of the transformation theorem defined in (4.13). Thus, for night-time intervals,

$$f_{PS_t}(PS_t) = 0 \tag{4.18}$$

For day-time intervals,

$$f_{PS_t}(PS_t) = \begin{cases} 0 & :PS_t = 0 \\ \frac{1}{PS_{t_{max}}} \frac{\Gamma(\alpha_t+\beta_t)}{\Gamma(\alpha_t)\Gamma(\beta_t)} \times & \\ \left(\frac{PS_t}{PS_{t_{max}}}\right)^{\beta_t-1} \times & \\ \left(1-\frac{PS_t}{PS_{t_{max}}}\right)^{\alpha_t-1} & :PS_t \in (0, PS_{t_{max}}) \\ 0 & :PS_t = PS_{t_{max}} \end{cases} \tag{4.19}$$

Thus (4.18) and (4.19) give the analytical expression of the variation of the MW output of the solar thermal ECS for different time intervals t.

4.3 HECS MWRAM

4.3.1 Expected Value of a Random Variable

In probability theory, the expected value of a random variable is the weighted average of all possible values that this random variable can take on. The weights used in computing this average correspond to the probabilities in case of a discrete random variable, or densities in case of a continuous random variable [112]. If X is a discrete random variable with probability

mass function $p(x)$, then the expected value becomes

$$E(X) = \sum_i x_i p(x_i) \tag{4.20}$$

If X is a continuous random variable with probability density function $f(x)$, then the expected value becomes

$$E(X) = \int_{-\infty}^{\infty} x f(x) dx \tag{4.21}$$

HECS Output Model

The MW generated by the hybrid system at time interval t, i.e. PH_t is equal to the sum of the MW output of wind unit PW_t and solar unit PS_t (see Figure 2.1), i.e.

$$PH_t = PW_t + PS_t \tag{4.22}$$

Without any loss of generality, the time intervals t can be assumed to be of 1 hour duration. Though the wind and solar energy profiles over the course of a day, season or year are dependent on each other, they can be assumed to be independent of each other in time frames of $t = 1$ hour each. From (4.15) and (4.19), we get the probability density functions of the power output from the wind and solar units respectively. In order to get an estimated value of the actual combined MW output, we compute the first moment or the expected value of the hybrid output, defined in (4.20) or (4.21).

$$E(PH_t) = E(PW_t + PS_t) = E(PW_t) + E(PS_t) \tag{4.23}$$

Thus the MW output of a HECS at a given location for a given hour in a given season can be written as some function $g(.)$ of several parameters which are known or can be computed (4.24).

$$PH_t = g(k_t, \lambda_t, P_r, T, V_{ci}, V_r, V_{co}, \alpha_t, \beta_t, H_t, A_c, \eta_c, \eta_{net}) \tag{4.24}$$

For a given wind farm with known number of wind turbines (T) with known parameters (V_{ci}, V_r, V_{co}, P_r) and given solar park with known collector area (A_c) and components with known efficiencies (η_c, η_{net}), the main task lies in the computation of the parameters ($k_t, \lambda_t, \alpha_t, \beta_t$) in order to model the real power output. The performance assessment of the HECS can then be explored using MWRAM as defined in (4.24).

4.4 Analysis and Discussion

4.4.1 Data Collection

- Historical Wind Speed and Solar DNI Data: For this study, three sites from Table 3.3 were selected. For both, the data have been analyzed and divided into four seasons - winter, spring, summer and fall which are represented by any day within that season. The day representing each season is further subdivided into 24 1-hour time segments, each referring to a particular hourly interval for the entire season. Hence, there are $(24 \times 4 = 96)$ time segments. The available wind speed and solar irradiation data are then utilized to generate typical frequency distributions for each hour in each season . From these data, the maximum likelihood estimated parameters for the Weibull and the Beta distribution for each of the 24 1-hour segments for 1 day for each of the 4 seasons were computed; thus forming a (24×16) matrix which contains the vectors λ_t, k_t, α_t and β_t, where $t \equiv (i, j)$ denotes season i $(i = 1 \ldots 4)$ and hour j $(j = 1 \ldots 24)$.

- Test System and Load Data: Three 3 sites (say, A, B and C) were selected from Table 3.1 and the corresponding locational load profile was developed after analyzing concurrent years of actual load data from [114], [115]. The seasonal hourly load profile provided hourly peak load as a percentage of the daily peak load. Various penetration levels at 10, 20 and 30% were simulated to investigate the effects of increasing renewable energy penetration level, defined as the ratio of the total annual energy produced by the HECS and the total annual energy consumed. At each penetration level, the wind and solar units contribute at various ratios as shown in Table 4.1.

Table 4.1 Wind-Solar Mix considered at each penetration level

Case	Wind Level	Solar Level	Comment
I	100%	0%	Wind Standalone
II	75%	25%	Strong Wind; Weak Solar
III	50%	50%	Equal Wind and Solar
IV	25%	75%	Weak Wind; Strong Solar
V	0%	100%	Solar Standalone

The rest of the load demand is considered to be satisfied by the conventional generating systems. A thermal unit is represented by a two-state Markov model [116]. The power output from wind or solar thermal generator unit is determined by the wind speed and solar DNI regime at the candidate location respectively.

4.4.2 Individual and HECS Output

Using the proposed algorithm, the hourly wind speed and solar irradiance data were clustered and the MLE parameters were computed for each hour of the data. For a location, the computed MLE parameters for hour 11-12 for summer are $\lambda_t = 7.97$, $k_t = 1.32$; $\alpha_t = 1.07$, $\beta_t = 5.75$. Using these parameters, the distributions of the wind and solar power, after doing the transformation are shown in Figure 4.5 (the two arrows indicate the two impulses corresponding to W1 and W2 respectively). They show the variability of the power output over the range of the power with the corresponding associated probabilities. It can be observed that the wind power generation has higher probability at lower values of power while the solar generation has higher probability of producing closer to rated capacity. In order to determine the hourly HECS output, it is necessary to determine the ratio of the wind and solar units in the total rated capacity; MWRAM can help in calculating this ratio.

4.4.3 Combined Correlation of Wind-Solar Resource with Electricity Load Demand

A per-unit system was used to present the combined availability of the two resources and it was assumed that the wind generation system and the solar generation system have same rated maximum power output (i.e. Case III). Figure 4.6 gives values for each season for the correlation coefficient between solar, wind, and a combined resource with the electricity load demand and also between wind and solar power profile. For all sites, the wind and load appear somewhat complementary to each other, the solar and load are positively related (this is expected because when solar reaches its peak, the load demand is also high). The combined output has positive correlation throughout. Between wind and solar, Site B shows strongest complementarity among all three sites. The different levels of complementarity indicate the

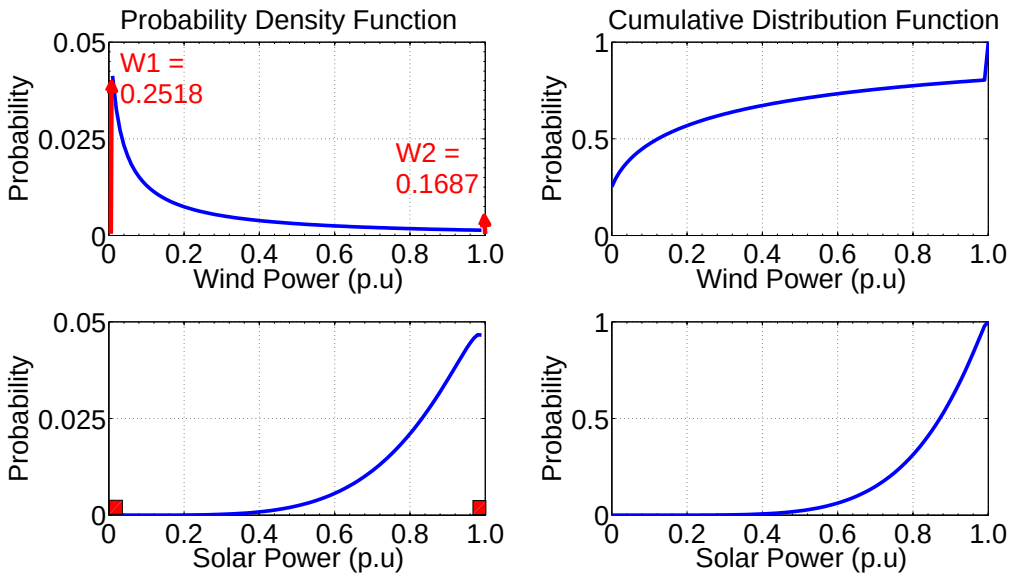

Figure 4.5 Distribution of Wind and Solar Power for Site A for 1100-1200 hours in Summer

profound dependence of location on the siting of wind and solar systems. The two systems must be coordinated to get maximum benefit from their combination as long as they share the point of interconnection and feed the same electricity grid.

4.5 Applications of MWRAM

4.5.1 Capacity Factor Calculation

The capacity factor (CF) can be used as a measure of efficiency/energy output capability of power plants. Renewable energy resources, such as wind and solar, are often considered as energy resources with a residual capacity value. If the capacity were zero or considered as zero then conventional resources (thermal and reservoir-hydro resources) would be needed to guarantee the satisfaction of the power demand. On the other hand, if the capacity were nonzero, then some of those conventional resources would not be needed; hence they would not be required in the expansion plans. Thus, considerable investment costs could be spared [117]. It can be defined as

$$\text{CF} = \frac{\text{Energy Output (MWh)}}{\text{Rated Power of Plant (MW)} \times \text{Hours in interval (h)}} \tag{4.25}$$

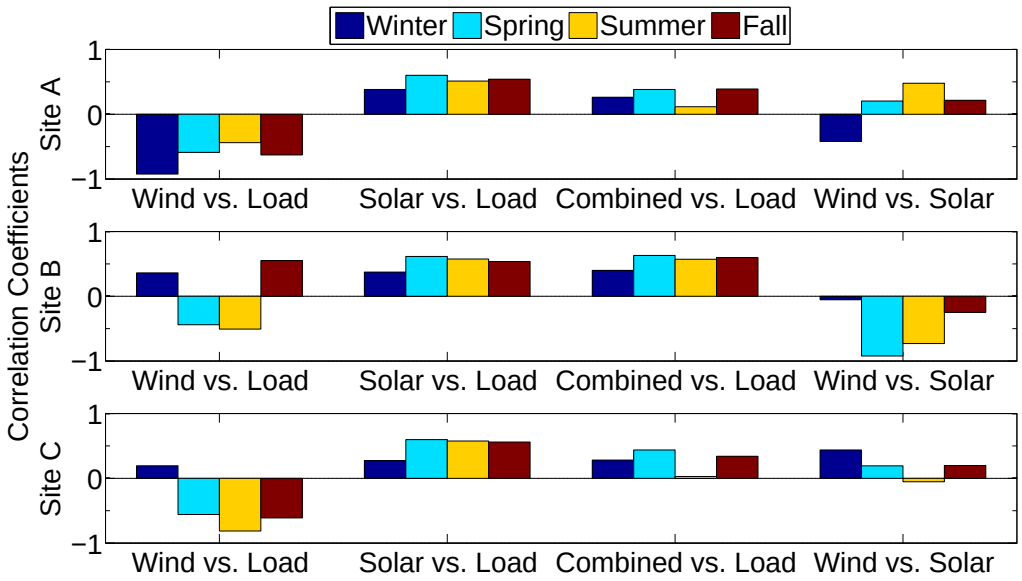

Figure 4.6 Correlation Coefficients among Wind power, Solar power, Combined power and Load for Sites A, B, C

The energy output can be computed using (4.26)

$$EO_{i,j} = \sum_{i=1}^{4} \left[n_i \left(\sum_{j=1}^{24} PH_{i,j} \right) \right] \tag{4.26}$$

where $EO_{i,j}$ denotes the HECS energy output for season i and hour j; n_i denotes the number of days in the season.

Figure 4.7 shows the average annual capacity factors for the three site locations (left one (a) shows grouped over cases, the right one (b) is grouped by sites). Over different scenarios at 20% penetration level, the three sites show different capacity factors. Thus, based on a fixed wind/solar ratio and for a desired penetration level, different candidate locations can be ranked according to capacity factors. This would help in the determination of suitable locations to set up HECS. For Site A, the locational resource profiles are such that a wind-standalone to solar-standalone sweep decreases the capacity factor by 8%, for Site B, the capacity factor is increased by 33% and for site C, it is decreased by nearly 53%. These values demonstrate that each location is unique and not all sites have equal potential for HECS development. The dependence of the locational resource profiles on the performance indices is very important. It can be observed that combining solar thermal power plants with wind farms for sites A and

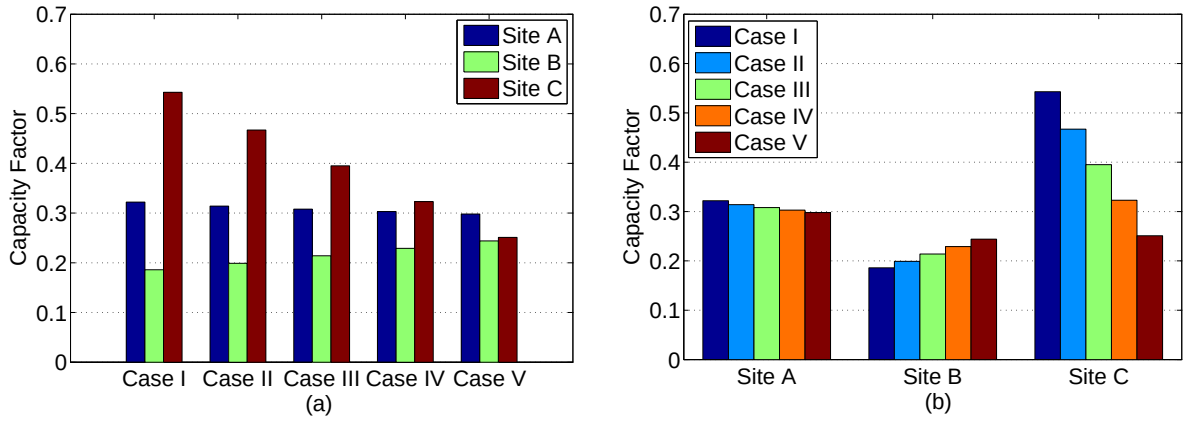

Figure 4.7 Annual Average Capacity Factors for Sites A, B, C ((a) - grouped by Cases; (b) grouped by Sites)

C lowers the overall annual capacity factor as compared to a wind standalone. However the electricity generated will be much more valuable to the utility since it is generated more often during the time periods when the utility needs it most, i.e. during peak electrical load periods.

4.5.2 Load Deviation Variation Analysis

The grid-connected HECS is connected to the local load and the rest of the electrical grid through a control center. It is the responsibility of the control center to maintain energy balance at all times. One is mainly interested in the average amount of MW reserve that needs to be maintained to cater to the demand. The ratio of the wind and solar energy components in the HECS is critical because of varying energy densities and cost factors involved. The described methodology can be used to roughly determine this mix ratio so as to minimize the load deviation and hence ensure better load following.

Figure 4.8 shows the variation of the load deviations for Sites A, B and C for 20% penetration level. It can be defined as

$$\text{Load Deviation} = \frac{(P_H - P_{LD})}{P_{LD}} \times 100\% \tag{4.27}$$

The top half is when $P_H > P_{LD}$, i.e. the HECS is exporting power to the grid and the bottom half is when $P_H < P_{LD}$, i.e. the HECS is importing power from the grid. It can be

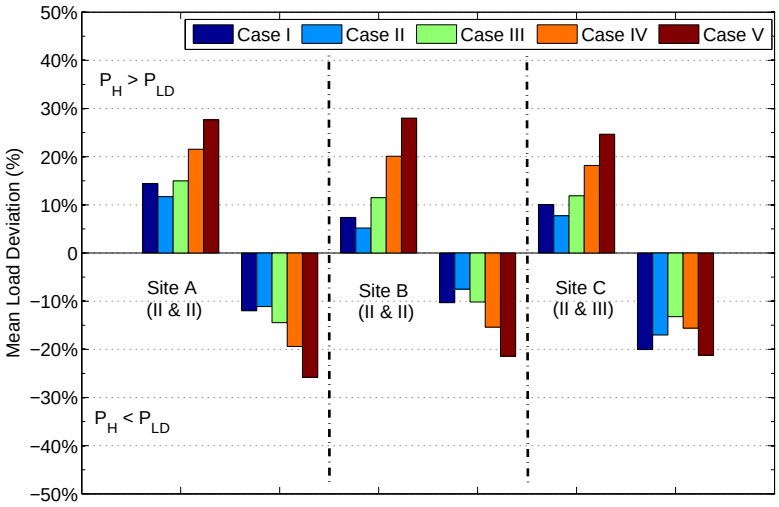

Figure 4.8 Mean Percentage Load Deviations for Sites A, B, C

observed that Case II and Case III give the minimum value of reserve requirements for the different sites.

For all the three sites, there are different combinations which give the optimal mix for wind-solar ratios. It can be seen that on an average, the hybrid mixing gives around 24% and 56% less reserve requirements than their corresponding wind or solar stand alone counterparts.

Also, it was found that the level of renewable energy penetration marginally affects the percentage of MW reserves required; the amount of MW is obviously different. This implies that as the amount of renewable energy in the total generation mix increases, the utility needs to accommodate for similar increase in MW reserves for proper power balance.

4.6 Sizing Optimization

The preferred sizing of the unit components that is available from MWRAM varies from site to site and is one of the five cases (Table 4.1) - actually three cases (II/III/IV), disregarding the two extreme standalone cases (I/V). This is a rough estimate and has been computed only keeping the minimization of reserves in mind. However, in the design of a hybrid ECS, there are myriad of factors that need to be considered - for e.g. the cost factors associated

with the different energy forms, power balance criteria, etc. This can be further refined by formulating the following optimization problem. This routine optimizes the layout of a HECS through systematically testing different combinations of wind and solar generation capacities. This is an iterative process which maximizes the total electric power injected into the grid with constraints that the deviation in load matching must remain within a specific tolerance. The effective sizing of the total hybrid facility will allow for the design criteria to meet conventional generation standards.

4.6.1 Optimization Formulation

The primary concern in the design of a HECS employing renewable energy sources is the accurate selection of system components that can satisfy the load demand in an economic and reliable manner, while being subject to physical and operational constraints.

4.6.1.1 Design Objectives

- **Objective I:** Minimizing Annual Cost Function

  Cost estimation is a crucial factor in decision-making for constructing a HECS. The annualized cost function (AC) ($\$/year$) is generated by dividing the summation of the initial or capital investments, the yearly operation and maintenance costs and subtracting the present worth of all the salvage values of the equipment by the lifetime of the project [118]. In calculation of this cost function, changes in the monetary value due to time must also be taken into consideration. The following formulation of the cost function is based on the work done in [118] which was further adapted into [60] and [68]. The Annual Cost function AC ($ /year) can be defined as:

$$AC = \sum_{i} \frac{1}{N_p}(I_i + OM_{p_i} - S_{p_i}) \tag{4.28}$$

  where I_i is the initial investment ($), S_{p_i} is the present worth of the salvage value of each component, OM_{p_i} is the present worth of the operation and maintenance costs. N_p is

the life-time of the project in years. The index i is made to account for wind farm (w), solar park (s).

To represent changes in the monetary value due to time, two factors, M_1 and M_2 are defined as follows:

$$M_1 = \sum_{n=1}^{N_p} \left(\frac{1+es}{1+r}\right)^n = \\ = \begin{cases} \left(\frac{1+es}{r-es}\right)\left[1-\left(\frac{1+es}{1+r}\right)^{N_p}\right] & \text{for } r \neq es \\ N_p & \text{for } r = es \end{cases} \tag{4.29}$$

$$M_2 = \left(\frac{1+j}{1+r}\right)^{N_p} \tag{4.30}$$

In (4.29) and (4.30), j is the inflation rate, r is the interest rate, es is the escalation rate.

- ***Wind Farm Cost:*** The design variable in the wind component is the total rotor area of the wind turbine A_w (m^2). The initial investment cost of the wind farm becomes

$$I_w = \alpha_w A_w \tag{4.31}$$

where α_w is the initial cost of the turbine ($\$/m^2$).

The total yearly operation and maintenance (O&M) cost would be

$$OM_w = \alpha_{OMw} A_w \tag{4.32}$$

where α_{OM_w} is the yearly operation and maintenance cost ($\$/m^2/year$). The present worth of the O&M value is

$$OM_{p_w} = M_1 \alpha_{OMw} A_w \tag{4.33}$$

The total salvage value would be

$$S_w = S_w A_w \tag{4.34}$$

where S_w is the salvage value ($\$/m^2$). The present worth of the salvage value is

$$S_{p_w} = M_2 S_w A_w \tag{4.35}$$

– ***Solar Park Cost:*** The design variable in the solar thermal component is the total surface area of the solar collector A_s (m^2). The initial investment cost of the solar park becomes

$$I_s = \alpha_s A_s \tag{4.36}$$

where α_s is the initial cost of the collector $(\$/m^2)$.

The total yearly STECS O&M cost would be

$$OM_s = \alpha_{OMs} A_s \tag{4.37}$$

where α_{OM_s} is the yearly operation and maintenance cost $(\$/m^2/year)$. The present worth of the O&M value is

$$OM_{p_s} = M_1 \alpha_{OMs} A_w \tag{4.38}$$

The total salvage value of STECS would be

$$S_s = S_s A_s \tag{4.39}$$

where S_w is the salvage value $(\$/m^2)$. The present worth of the salvage value is

$$S_{p_s} = M_2 S_s A_s \tag{4.40}$$

- **Objective II:** Maximizing Capacity Factor

The net capacity factor of a power plant is the ratio of the actual output of a power plant over a period of time and its potential output if it had operated at full nameplate capacity the entire time. To calculate the capacity factor, take the total amount of energy the plant produced during a period of time and divide by the amount of energy the plant would have produced at full capacity. Capacity factors vary greatly depending on the type of fuel that is used and the design of the plant.

The capacity factor (CF) can be used as a measure of efficiency/energy output capability of power plants. Renewable energy resources, such as wind and solar, are often considered as energy resources with a residual capacity value. If the capacity were zero or considered

as zero then conventional resources (thermal and reservoir-hydro resources) would be needed to guarantee the satisfaction of the power demand. On the other hand, if the capacity were nonzero, then some of those conventional resources would not be needed; hence they would not be required in the expansion plans. Thus, considerable investment costs could be spared [117]. It can be defined as

$$\text{CF} = \frac{\text{Energy Output (MWh)}}{\text{Rated Power of Plant (MW)} \times \text{Hours in interval (h)}} \tag{4.41}$$

Thus, we have,

$$CF = \frac{\sum_{t=1}^{T} [P_w(t) + P_s(t)]}{T * (P_{w,max} + P_{s,max})} \tag{4.42}$$

$$= \frac{\sum_{t=1}^{T} [\eta_w P_{WTG}(t) A_w + \eta_s H_s(t) A_s]}{T * [(\frac{P_r}{A_{WTG}} A_w) + (H_{s,max} \eta_{total} A_s)]} \tag{4.43}$$

where $P_w(t)$, $P_s(t)$ are the wind power, solar power.

4.6.1.2 Design Constraints

There is a set of constraints that should be satisfied throughout system operations for any feasible solution.

- **Constraint 1:** Power Balance constraint

  For any time interval t, the sum of the total power from the HECS must supply the total demand with a certain reliability criterion. This relation can be represented as

$$P_w(t) + P_s(t) \geq (1 - R) P_D(t) \tag{4.44}$$

$$P_w(t) + P_s(t) - P_{dump_t} \leq P_D(t) \tag{4.45}$$

  where P_w, P_s, P_D and P_{dump} are the wind power, solar power, total demand and dumped power respectively. R is the ratio of the maximum permissible unmet power with respect to the total load in each hour. This limits the reserve margin requirement to a certain threshold.

The wind turbine generator power output per unit area P_{WTG} (kW/m^2) for wind speed V_t can be computed as:

$$P_{WTG} = \begin{cases} P_r(aV_t^3 - b) & \text{for } V_{ci} < Vv_t \leq V_r \\ P_r & \text{for } V_r < V_t \leq V_{co} \\ 0 & \text{otherwise} \end{cases} \tag{4.46}$$

where $a = 1/(V_r^3 - V_{ci}^3)$ and $b = V_{ci}^3/(V_r^3 - V_{ci}^3)$, which are fixed for a particular kind of turbine with fixed values of V_{ci} (cut-in speed), V_r (rated speed) and V_{co} (cut-out speed), P_r is the rated power (kW/m^2). The real power from the wind ECS can be determined as follows:

$$P_w = P_{WTG} * A_w * \eta_w \tag{4.47}$$

where A_w is the total swept area of WTGs and η_w is the efficiency of the WECS.

The output power of the solar thermal ECS P_w can be determined as follows:

$$P_s = H * A_s * \eta_s \tag{4.48}$$

where H (kW/m^2) is the direct normal irradiance, A_s is the solar collector area (m^2) and η_s is the efficiency of the STECS.

- **Constraint 2:** Bounds on design variables

The swept area of the wind turbines should be within a certain range. This range is dependent on the location or the site chosen, the available land area, keeping in mind the proper layout of the individual wind turbines - leaving appropriate clearance between turbines.

$$A_{w_{min}} \leq A_w \leq A_{w_{max}} \tag{4.49}$$

Similarly, the solar collector surface area should also be within a certain range. This range is also dependent on the location or the site chosen, the available land area with suitable slope.

$$A_{s_{min}} \leq A_s \leq A_{s_{max}} \tag{4.50}$$

4.6.1.3 Problem Statement

Thus, in summary, for the grid connected HECS design, the objective for optimal sizing can be listed as follows:

- minimize annual cost (4.28)
- maximize capacity factor (4.43)

subject to the constraints (4.44) - (4.50).

The design parameters include the WECS swept area A_w (m^2), the STECS solar collector area A_s (m^2). In case of grid linked system, minimization of cost and maximization of capacity factor, while meeting the reserve margin constraint, are both of concern, however these two objectives conflict with each other. Thus, a trade-off curve of cost and capacity factor is required for optimal unit sizing. The choice of an operating point on the trade-off curve depends on the operational characteristics and the discretion of the system planner.

This being a multi-objective optimization problem, there are various solvers that can be used. The results from the previous section will act as initial conditions for the optimization formulation. For nontrivial multi-objective problems, one cannot identify a single solution that simultaneously optimizes each objective. While searching for solutions, one reaches points such that, when attempting to improve an objective further, other objectives suffer as a result. A tentative solution is called non-dominated, Pareto optimal, or Pareto efficient if it cannot be eliminated from consideration by replacing it with another solution which improves an objective without worsening another one. Finding such non-dominated solutions, and quantifying the trade-offs in satisfying the different objectives, is the goal when setting up and solving this multi-objective optimization problem. There are different methods existing that will solve this sizing optimization problem, including Genetic Algorithms, Multi-objective Linear Programming Solvers, Successive Pareto Optimization, etc. Due to more variables and parameters that have to be considered, the sizing of the hybrid solar-wind systems is much more complicated than the single source power generating systems. This type of optimization includes economical objectives, and it requires the assessment of long-term system performance in order to reach the best compromise for both power reliability and cost. The minimization of the cost (objective)

function is implemented employing a genetic algorithm (GA), which dynamically searches for the optimal system configurations [Appendix C].

The initial solution estimate for the GA is the output of the MWRAM routine (Figure 4.9). Here $A_w = T \times \frac{\pi d^2}{4}$ (from Eqn. 4.14) where T is the number of turbines and d is the swept area of one turbine and $A_s = A_c$ (from Eqn. 4.17) where A_c is the solar collector area.

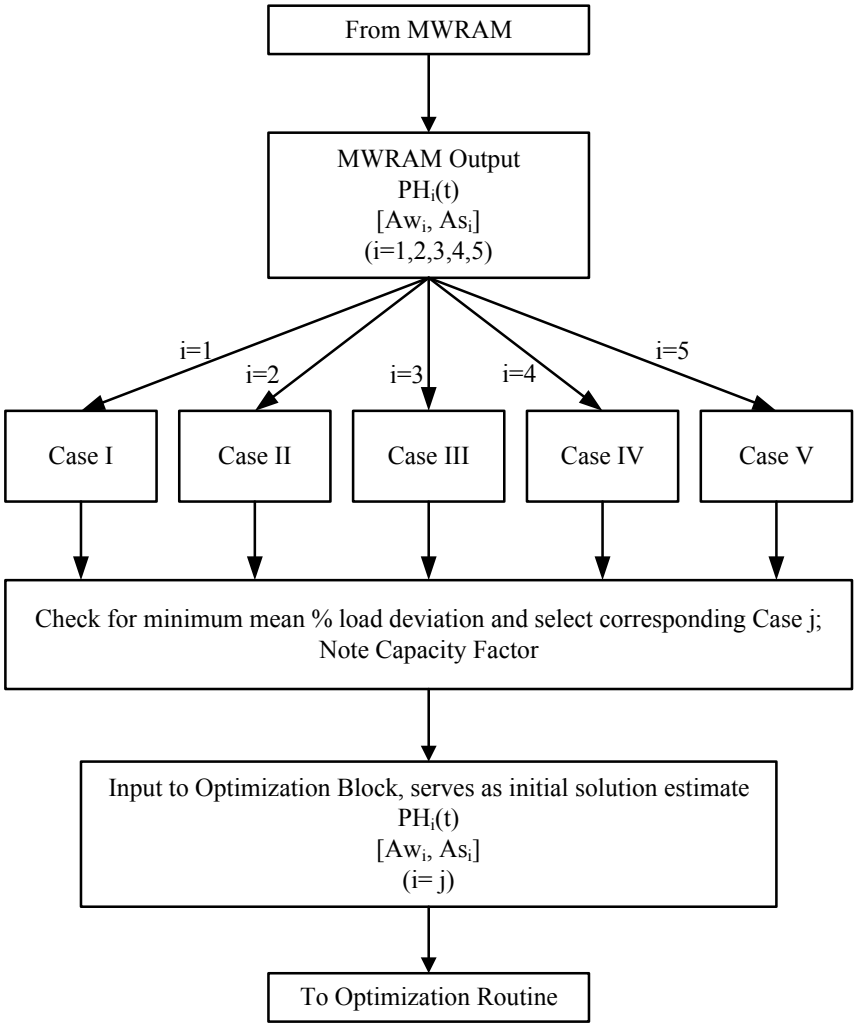

Figure 4.9 Output of MWRAM feeding as input to Optimization

The flowchart of the optimization process is given in Figure 4.10.

The output of this optimization routine will be the wind turbine swept area A_w^* (m^2), solar thermal collector area A_s^* (m^2). The rated capacities of the ECS can be computed as follows:

$$P_{w,max}^* = P_r \times \left\lceil \frac{A_w^*}{A_{WTG}} \right\rceil \tag{4.51}$$

and

$$P_{s,max}^* = H_{t_{max}} \times A_s^* \times \eta_{total} \tag{4.52}$$

where P_r is the rating of a single wind turbine generator, A_{WTG} is the swept area of a single generator, $H_{t_{max}}$ denotes the maximum solar DNI, η_{total} denotes the overall efficiency of the STECS, and $\lceil x \rceil$ denotes the ceiling function of x.

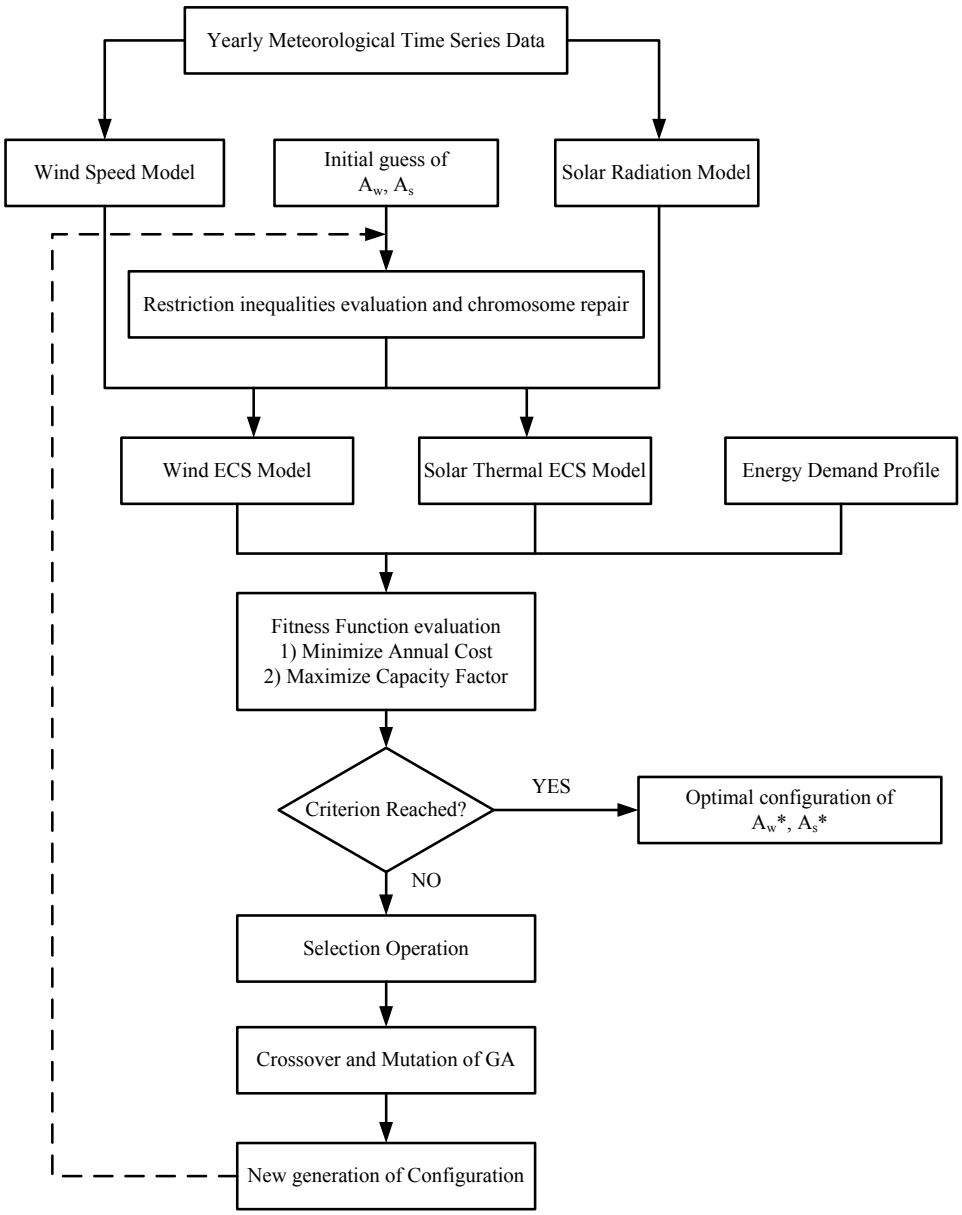

Figure 4.10 Flow chart of the optimal sizing model using GA

4.6.2 Optimization Results

The input data for the optimization routine were gathered from various sources. The cost parameters used here are the same as the ones used in [60] and [68]; however a sensitivity analysis has been included to study the effect of variation in these parameters. The nomenclature details are shown in Table 4.2.

Table 4.2 Optimization Input Data

Parameters	Nomenclature	Value
Inflation Rate	j	9%
Escalation Rate	es	12%
Interest Rate	r	12%
Project Life Span	N_p	20 years
Solar Collector Price	α_s	$450\$/m^2$
Wind Turbine Price	α_w	$100\$/m^2$
Solar Collector OM Costs	α_{OMs}	$4.3\$/m^2/year$
Wind Turbine OM Costs	α_{OMw}	$2.5\$/m^2/year$
Solar Collector Salvage Value	S_s	$45\$/m^2$
Wind Turbine Salvage Value	S_w	$10\$/m^2$
WECS efficiency	η_w	50%
STECS Efficiency	η_s	20%
Cut-in Speed	V_{ci}	$3m/s$
Rated Speed	V_r	$12m/s$
Cut-out Speed	V_{co}	$25m/s$
Rated WTG Power	P_{WTG}	$2500kW$
WTG Rotor Diameter	d_{WTG}	$100m$

The hourly load profile, hourly wind speed patterns and the hourly irradiance conditions are shown in Figure 4.11. These time-series data will be used by the ARMA model to derive forecasted wind speed and solar irradiance, which are then used to calculate the available wind power, solar power, and the insufficient or surplus power at each time instant.

The Pareto-optimal fronts evolved using genetic algorithm approach for bi-objective optimization problem are shown in Figure 4.12 and two illustrative non-dominated solutions are listed in Table 4.3. Since the two objectives are conflicting to each other, it is the task of the designer/planner to choose an option on the trade-off curve, such that the reliability criterion R is not violated (R is set at 10% here) and there is judicious balance between the energy capacity and the annual cost.

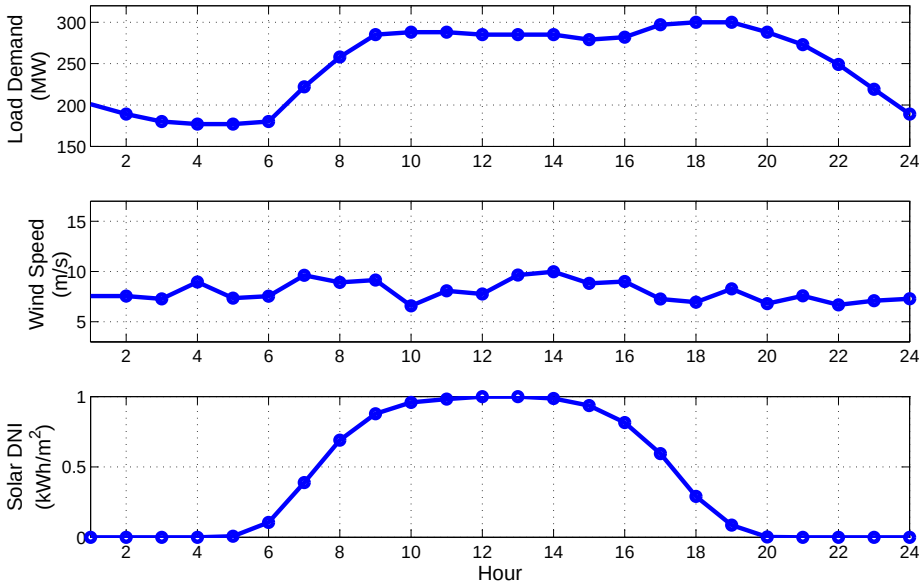

Figure 4.11 Hourly mean wind speed, irradiance, and load profiles

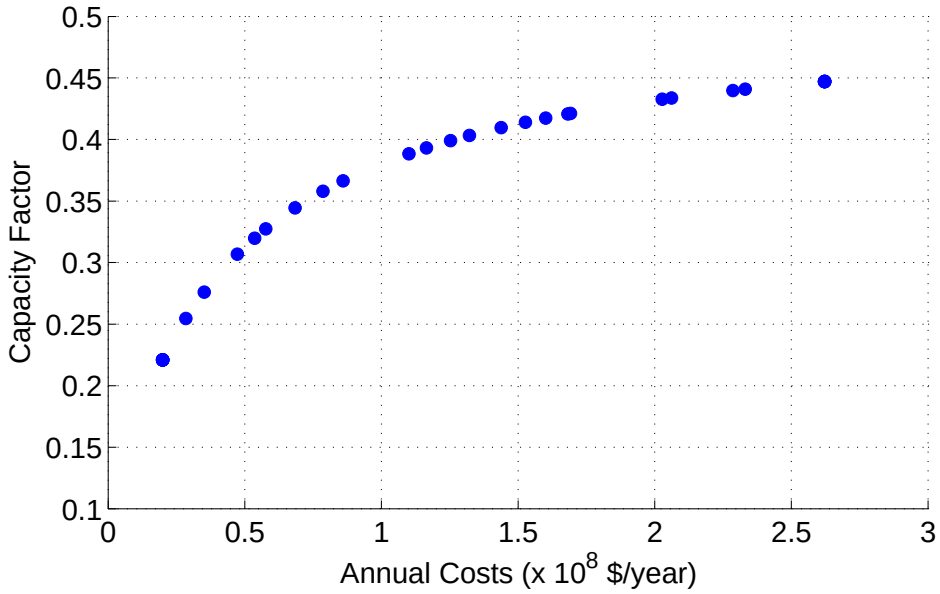

Figure 4.12 Pareto front for optimization scenario

Table 4.3 Two illustrative non-dominated solutions for bi-objective optimization

Variables/Objectives	Design 1	Design 2
A_w (m^2)	1.00E+06	8.60E+05
A_s (m^2)	5.64E+06	8.39E+06
Annual Cost ($/year)	1.51E+08	2.20E+08
Capacity Factor	41.30%	44.40%
$P_{w,max}$ (MW)	325	275
$P_{s,max}$ (MW)	90	135
$P_{h,max}$ (MW)	415	410

4.6.3 Further Sensitivity Analysis

To examine the impacts of different wind speeds and irradiances on the derived Pareto-optimal solutions, sensitivity studies are carried out. Figures 4.13 and 4.14 show the tradeoff surfaces obtained in different scenarios in terms of wind speeds and solar irradiances, respectively. During the simulations, when different wind speeds are examined, the original irradiance value is used. Likewise, when different irradiances are examined, the original wind speed value is used. It can be observed that at the same energy capacity level, the generating systems with the highest speed and irradiance result in the lowest costs as compared to scenarios with lower wind speed and irradiance. Thus, this confirms the previous observation that it is crucial to properly select HECS location when renewable sources of energy are involved. The plant sites with richer renewable sources of energy can cause lower generation costs.

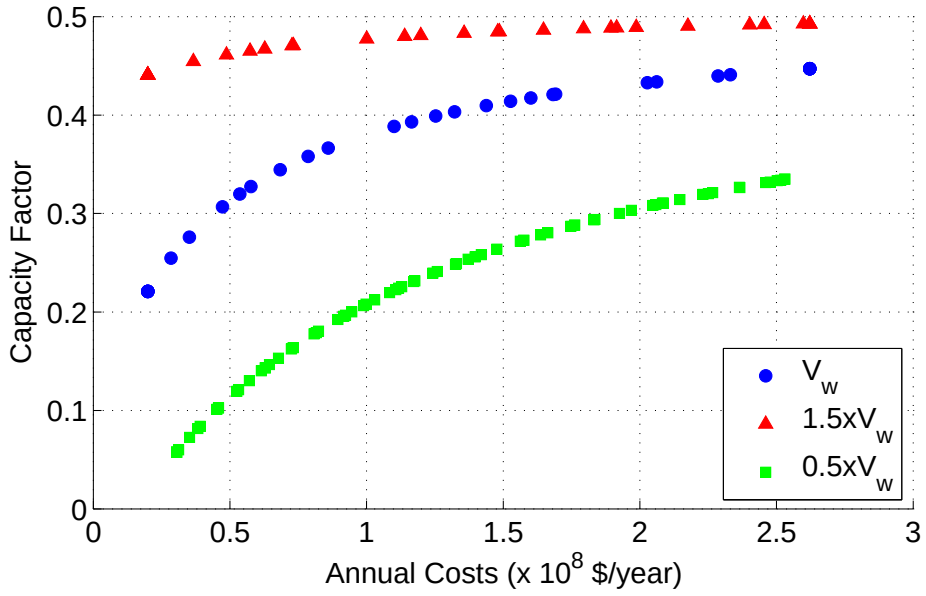

Figure 4.13 Impacts of different wind speeds on Pareto fronts

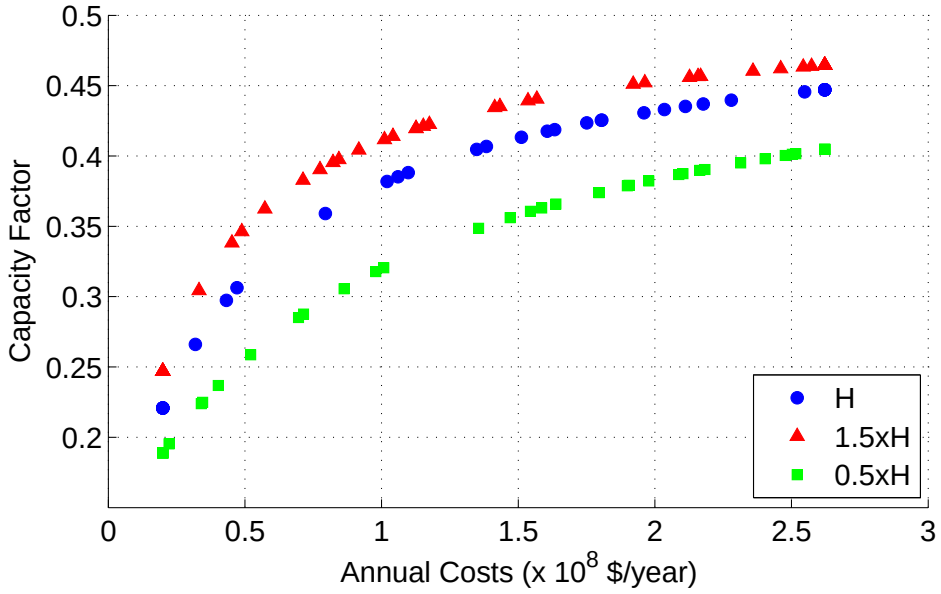

Figure 4.14 Impacts of different irradiances on Pareto fronts

Also, the sensitivity analysis is carried out to examine the effects of changing the values of certain system parameters on the final derived Pareto front. For instance, to see the effect of cost variation, the base values are changed by different multiplication factors (MFs). Figure 4.15 shows the effect of the variation of the cost of the wind turbine. Figure 4.16 shows the effect of the variation of the cost of the solar collector and components. With the help of aggressive RPS targets by the various state governments and also at the federal level, and the effect of PTCs, the cost of wind energy has dramatically reduced over the last several years. The monetary cost per unit of energy produced is similar to the cost for new coal and natural gas installations. Even though the current cost of concentrated solar power units is much higher as compared to the wind power units, it might be reasonable to think that the cost of STECS will go down in the coming future. From Figure 4.16, we see that a 50% reduction of capital and O&M costs for STECS reduces the overall annual cost of the HECS project by nearly 55% while keeping the performance intact. Figure 4.15 shows that considering the current value of WECS, a 50% reduction in cost delivers around 20% reduction in over annual costs. But the potential effect of expiration of PTC's which will increase the capital costs by close to 30-40% can be seen by increasing annual costs and thus the overall lifetime cost of the HECS project.

The potential for renewed cost reductions is good, as supply bottlenecks have been removed and increased competition among suppliers will put downward pressure on prices in the next few years. In the medium-to long-term, reductions in capital costs in the order of 10% to 30% could be achievable from learning-by-doing, improvements in the supply chain, increased manufacturing economies of scale, competition and more investment in R&D.

Figure 4.17 shows the effect of the variation of the assumed value of the efficiency of the wind energy conversion system. Figure 4.18 shows the effect of the variation of the assumed value of the efficiency of the solar thermal energy conversion system. The base values of WECS and STECS efficiencies used in the work were current typical values $\eta_w = 50\%$ and $\eta_s = 20\%$. With a lot of research being invested in improving the efficiency of these energy conversion systems, different Pareto fronts were derived considering different values of the ECS efficiencies.

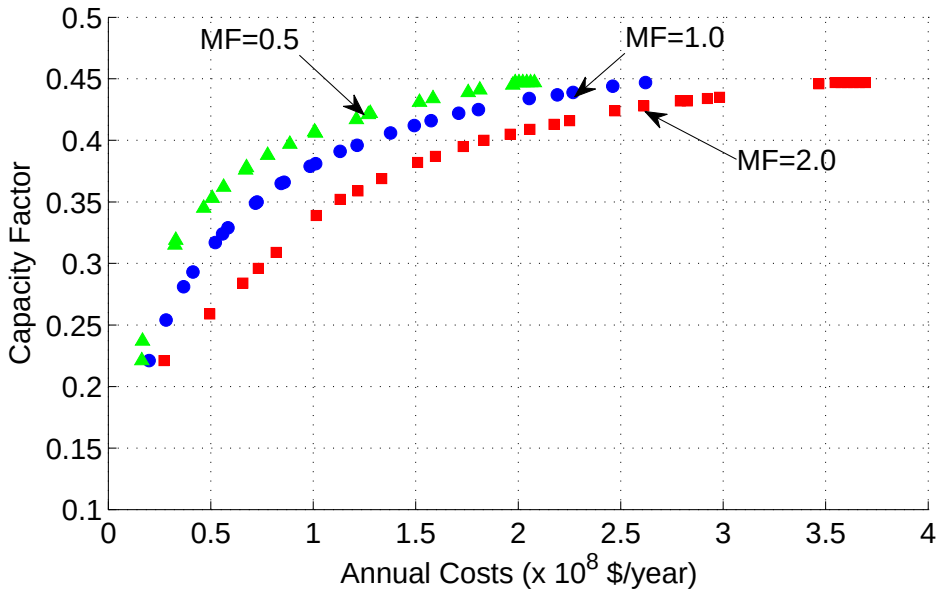

Figure 4.15 Impacts of WECS cost components on Pareto fronts

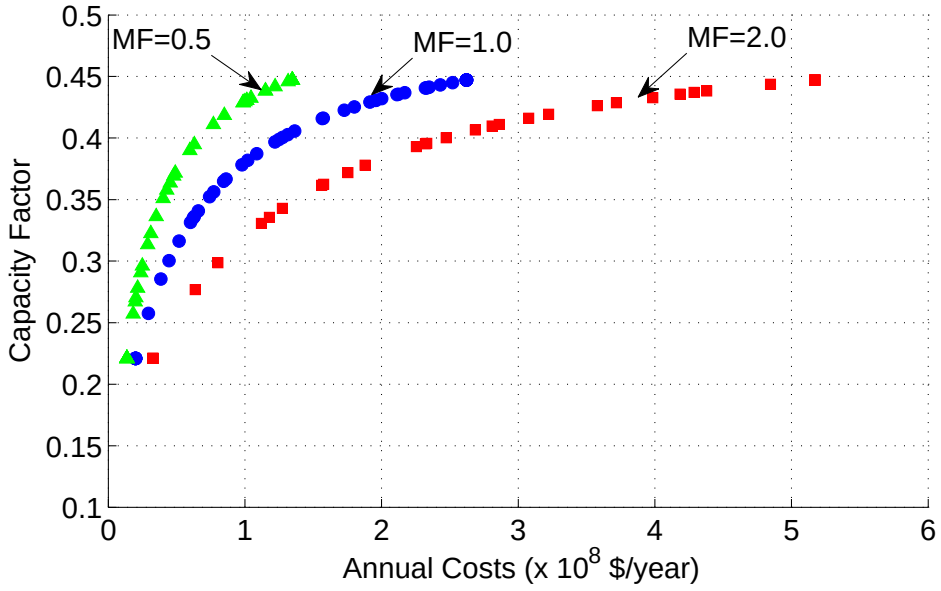

Figure 4.16 Impacts of STECS cost components on Pareto fronts

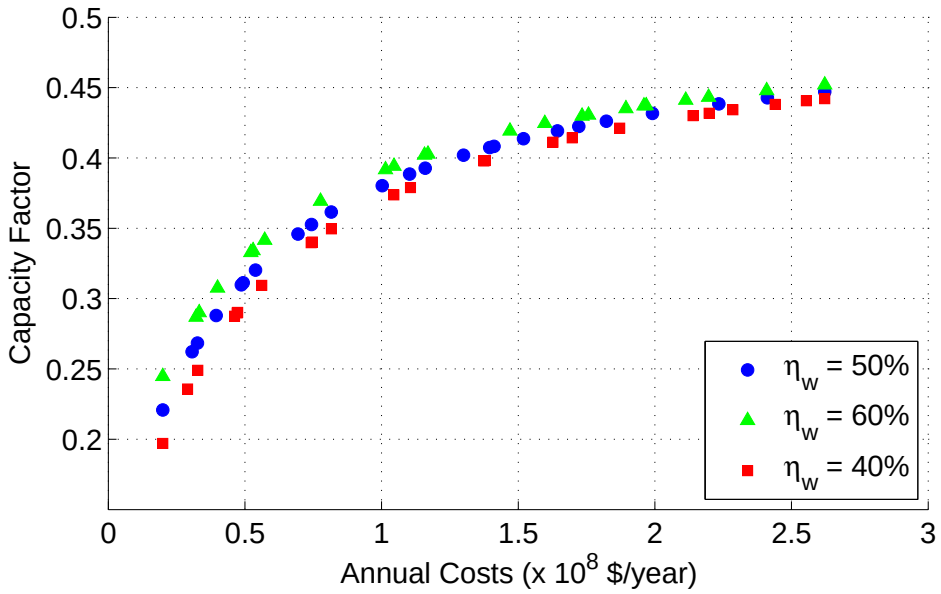

Figure 4.17 Impacts of WECS efficiency components on Pareto fronts

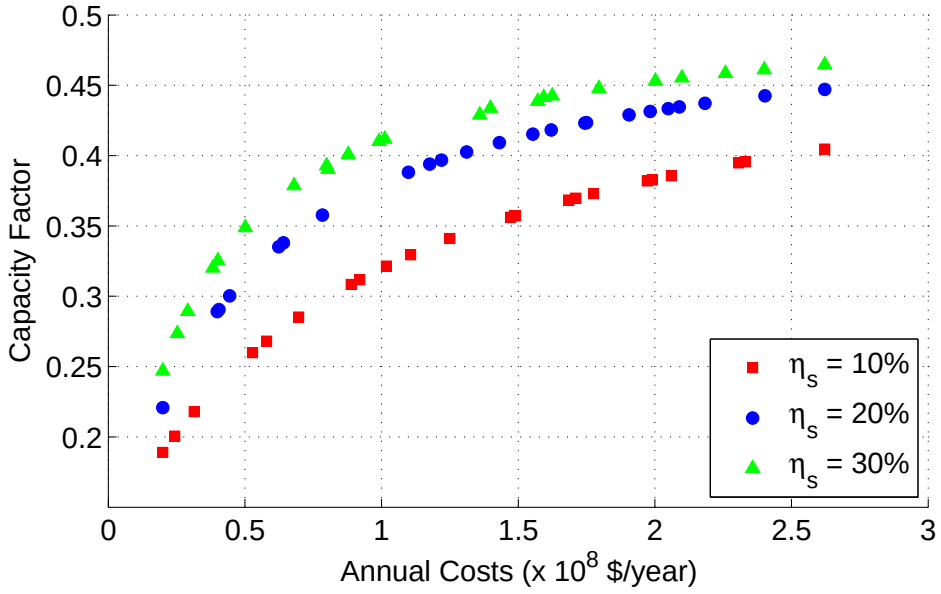

Figure 4.18 Impacts of STECS efficiency components on Pareto fronts

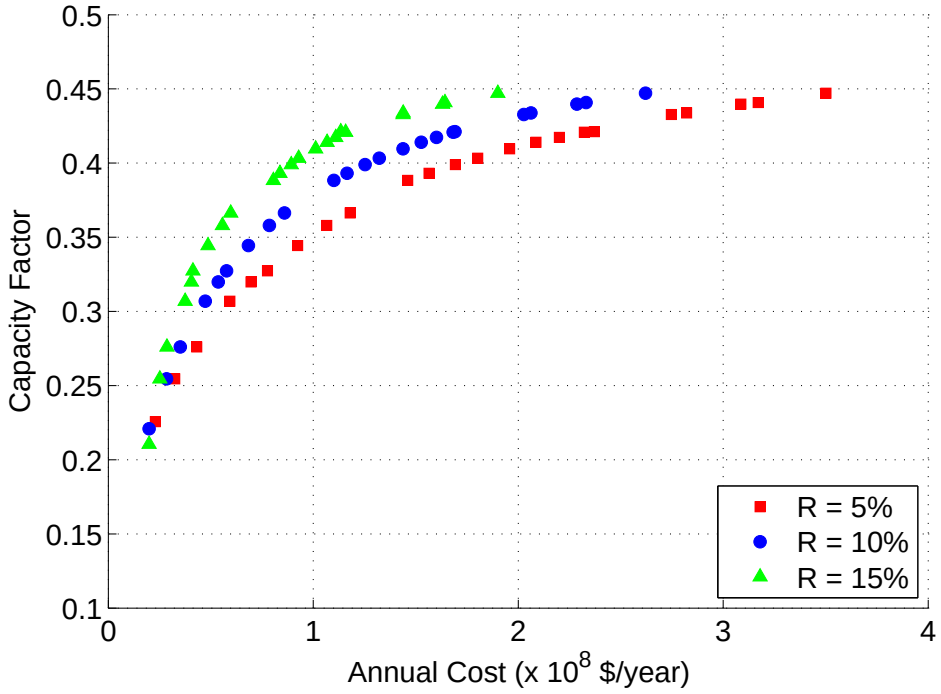

Figure 4.19 Impacts of different R (reserve) factor on Pareto fronts

The factor representing the mean reserve requirements R (Eqn. (4.44)) was taken as 10%. Figure 4.19 shows the different Pareto fronts for varying R. A smaller R increases the portion of the load that should be met by the system during each hour and hence causes larger system components, whereas bigger R relaxes the load criteria that needs to be met by the HECS output, thus the system components required could be of smaller size. However, since the HECS is grid connected, if there is surplus generation available, then it can be supplied to the grid through the bidirectional control unit - provided there is enough transmission bandwidth available to accommodate the excess generation.

4.7 Comments

Here, a systematic stochastic planning approach (MWRAM) was demonstrated for assessing the MW resource availability of a HECS with wind and solar resources for a given location. The study period of one year was divided into four seasons; one day in each season was further divided into 24 1-hour time segments. This "stratified" approach captures the varying nature of the resources over different times of the day as well as the year by explicitly computing the probabilistic model parameters from actual field measurement data using the MLE method. These parameters defined the MW output of the ECS using a transformation theorem. The MWRAM can be used to study the influence of different parameters such as cut-in speed, rated speed, furling speed and power rating of the wind turbines, the efficiencies of the heat exchanger, steam turbine and electric generator, ratio between the HECS rating and maximum load, availability of hardware - all of which have a bearing on the energy potential of the system. Features like hardware failure modes, multiple types of wind turbines or solar collectors, concentrated / distributed representation of ECS, scaling up / down of hybrid energy conversion can be easily incorporated into the model.

A set of tradeoff solutions is obtained using genetic algorithm to solve the multi-objective optimization which minimizes the annual cost and maximizes the energy capacity of the HECS that offers many design alternatives to the system designer/planner.

It should be noted that all the current work assumed the wind and solar power sources to be point sources. It may be true for the solar thermal plants where the solar collector area may be widely distributed but all the solar energy is used to power a single generator. But for the wind farms with multiple DFIG turbines installed, this sort of aggregation may need to be modified to have better resolution to characterize all the individual turbines or cluster of turbines inside the HECS.

CHAPTER 5. MEGAVAR RESOURCE ASSESSMENT MODEL DEVELOPMENT (MVRAM)

The optimized model of the hybrid plant is fed into a Voltage Stability and Reactive Power planning block where the model is integrated into the grid and voltage stability is assessed. This section also examines the possibility of providing reactive power support to the grid from the HECS as a part of the ancillary service provisions. The capability curves of different forms of generation are analyzed and combined to develop an integrated capability curve for the wind/solar HECS. The entire operating trajectory of the available reactive power from the HECS is mapped out for different values of real power outputs, corresponding to the different times of the day. It will help in determining the availability of reactive power from a HECS for all possible operating scenarios, for different time horizons. It will then be utilized in estimating the voltage stability margin of the system, for base case situations and (N-1) contingencies as well. The grid interconnection impact of the hybrid plant needs to be analyzed to ensure that there is no adverse impact on the power system. If necessary, reactive power planning will be implemented to improve the stability margin. This will enable prevention of plant disconnection during major power grid disturbances which enhances overall power system security.

The growing scale of the renewables infrastructure has resulted in a complex patchwork quilt of interconnection requirements. In the USA, there are existing interconnection standards like for large conventional generators - FERC Order No. 2003 [72], large wind - FERC Order No. 661 [73], Distributed Resources - IEEE 1547 [74], etc. While there are no explicit standards for utility scale concentrated solar power yet, it is likely that the solar industry will follow a similar path as wind, adopting similar technical and performance standards. Fulfilling the new grid codes constitutes one of the main challenges for these renewable resources. There are ride through requirements. Enhancing the operation of these units in front of the grid faults

is mandatory requirement, they must stay connected to the grid during grid disturbances and should continuously feed the reactive power in addition to limited active power.

5.1 Reactive Power Assessment

Traditionally, variable energy resources like wind and solar have been considered as not having the capability to control voltages, and therefore, it has been modeled in power flow studies as a negative load, i.e., as a PQ node. However, if it is able to control reactive power, the node where it is connected should be modeled as a PV node. The typical power flow formulation includes box constraints on a generator's real and reactive injections, specified as simple lower and upper bounds on P (P_{min} and P_{max}) and Q (Q_{min} and Q_{max}). However, the true P-Q capability curves of physical generators usually involve some tradeoff between real and reactive capability, so that it is not possible to produce the maximum real output and the maximum (or minimum) reactive output simultaneously. The reactive capability boundary does not represent the locus of points where the generator must operate. It may operate anywhere inside of the boundary. Because generators are the source of the P and (most of) the Q, their interdependency is very important and need to be suitably modeled in power flow analysis.

The capability curve of these wind and solar units with unique machine parameters needs to be defined taking the natural resource variations into account. Different cost components associated with reactive power generation by these units need to be examined as well. A knowledge of these cost components will assist the ISO in formulating appropriate financial compensation mechanisms for their reactive power service provision. When these issues are answered, HECSs with reactive power capability can be treated by the ISOs as reactive power ancillary service providers.

5.1.1 Modeling of Individual MVar Resources

5.1.1.1 Wind Capability Curve Modeling

A Doubly Fed Induction Generator (DFIG) has advantages over the Singly Fed Induction Generator in its inherent capability to handle variable wind speed. The rotor side converter

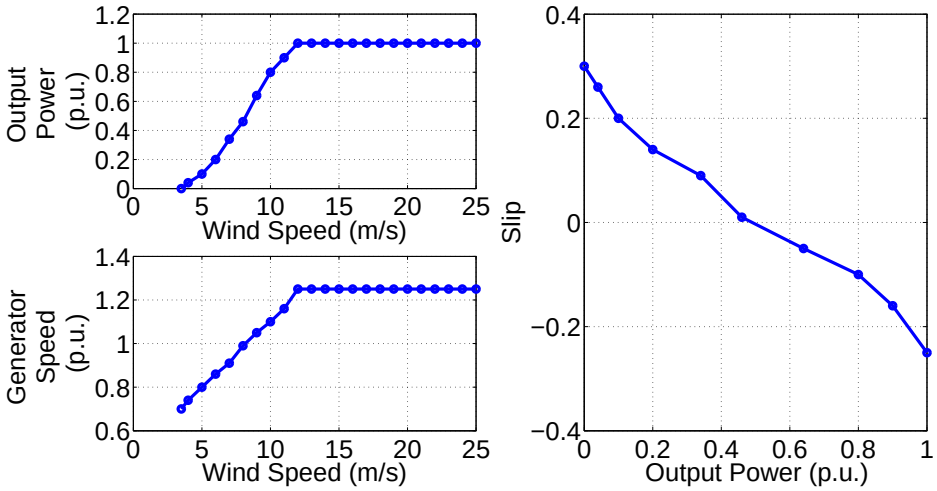

Figure 5.1 DFIG Power and Speed vs. Wind Speed; Maximum Power Tracking Scheme

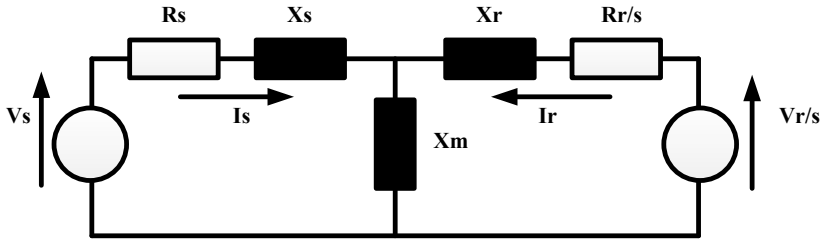

Figure 5.2 T - Equivalent Circuit of DFIG

injects currents and voltages according to various wind speeds. Figure 5.1 indicates the variation in power output and generator speed of a DFIG with respect to the wind velocity and also the values of rotor slip at different power output levels. The DFIG exchanges power through both the rotor and the stator. Majority of the power is passed through the stator, and a fraction of the power is passed through the rotor and the power converter. Since the DFIG is a variable speed machine, the rotor speed and the slip play an important role. Figure 5.2 gives the T-equivalent of a Doubly Fed Induction Generator [119]. All variables in (5.1) - (5.5) are referred to the stator side.

$$(R_s + jX_s)I_s + jX_m(I_S + I_r) = V_s \tag{5.1}$$

$$\left(\frac{R_r}{s} + jX_s\right) I_r + jX_m(I_S + I_r) = \frac{V_r}{s} \tag{5.2}$$

The power exchange in the Figure 5.2 is considered positive coming out of the generator and rotor. Thus, the apparent stator and rotor powers are represented as:

$$S_s = -V_S I_s^*; S_r = -V_r I_r^* \tag{5.3}$$

The power delivered to the grid is given by the sum of the power delivered by the stator and the grid side converter. Hence the total power delivered to the grid can be given as:

$$S_{tot} = S_s + Re\{S_r\} - S_{loss} \tag{5.4}$$

In (5.4), S_{loss} consists of active and reactive losses in the generator and the converters. We have,

$$\begin{bmatrix} V_s \\ I_s \end{bmatrix} = \mathbf{Z} \begin{bmatrix} \frac{V_r}{s} \\ I_r \end{bmatrix} \tag{5.5}$$

where $Z = \begin{bmatrix} Z_s + Z_m & Z_m \\ Z_m & Z_r + Z_m \end{bmatrix}$, $Z_r = \frac{R_r}{s} + jX_r$, $Z_s = R_s + jX_s$, $Z_m = jX_m$.

The three limiting parameters for the reactive power capability of the DFIG are stator current, rotor current and rotor voltage [119].

- Rotor Current Limitation - The rotor current is fixed at its rated value and the angle is varied to determine the reactive limits of a DFIG as a function of the rotor current. Thus,

$$\left(\frac{P_{tot} - Re(c_{s\_Ir})}{(1-s)}\right)^2 + (Q_{tot} - Im(c_{s\_Ir}))^2 = (r_{s\_Ir})^2 \tag{5.6}$$

  which is in the form of a standard ellipse and thus can easily be implemented for different values of slip. In (5.6), $c_{s\_I_r}$ and $r_{s\_I_r}$ can be calculated as

$$c_{s\_I_r} = -|V_s|^2 \left(\frac{1}{Z_s + Z_m}\right)^* \tag{5.7}$$

$$r_{s\_I_r} = |I_r||V_s|\left|\frac{Z_m}{Z_s + Z_m}\right| \approx |I_r||V_s| \tag{5.8}$$

- Rotor Voltage Limitation - The reactive power limits as a function of the rotor voltage can be obtained from (5.9).

$$\left(\frac{P_{tot} - Re(c_{s\_Vr})}{(1-s)}\right)^2 + (Q_{tot} - Im(c_{s\_Vr}))^2 = (r_{s\_Vr})^2 \tag{5.9}$$

In (5.9), $c_{s\_V_r}$ and $r_{s\_V_r}$ can be calculated as

$$c_{s\_Vr} = -|V_s|^2 \left(\frac{(Z_r + Z_m)}{(Z_r + Z_s)Z_m + Z_r Z_s}\right)^* \tag{5.10}$$

$$r_{s\_Vr} = |\frac{V_r}{s}||V_s||\frac{Z_m}{(Z_r + Z_s)Z_m + Z_r Z_s}| \tag{5.11}$$

- Stator Current Limitation - The stator apparent power is directly available as a function of stator current. The center is at the origin. The reactive power limits as a function of the stator current can be calculated as

$$\left(\frac{P_{tot}}{(1-s)}\right)^2 + (Q_{tot})^2 = (r_{s\_Is})^2 \tag{5.12}$$

In (5.12), r_{s_Is} can be obtained from

$$r_{s\_Is} = |I_s||V_s| \tag{5.13}$$

Combination of Limitations - The capability curve is obtained by the most restrictive of the three limitations (5.6), (5.9) and (5.12). For all the analysis, a DFIG is selected with parameters (Table 5.1). The mechanical power limitation is reflected in the slip. The maximum power tracking scheme in Figure 5.1 is used to obtain the slips at 5% (s=0.25, corresponds to cut-in speed), 25% (s=0.12), 50% (s=0.03), 75% (s=-0.08) and 100% (s=-0.25, corresponds to just before cut-out speed) output levels. A capability curve for a DFIG wind park was formulated using the method described above with a maximum power tracking characteristic. This technique is given for only a single machine, but it is assumed that the power capability of one machine can be scaled up to accurately aggregate the behavior of the WECS. The plot in Figure 5.3 displays the capability curve for the DFIG at different wind speeds corresponding to variable levels of power output.

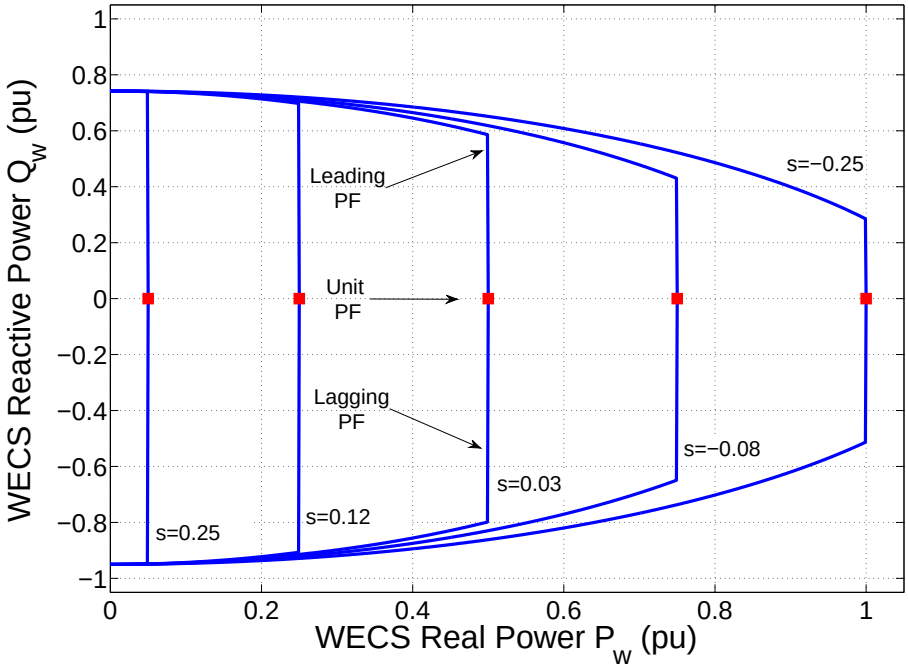

Figure 5.3 WECS P-Q Capability Curve

Table 5.1 WECS DFIG Simulation Parameters

Machine Parameter	Value
Rated Mechanical, Generator Power	1.5 MW, 1.3 MW
Rated Stator Voltage	575 V
Rotor to Stator turns ratio	3
Machine, Rotor Inertia	30 Kgm^2, 610000 Kgm^2
Inductance: mutual , stator, rotor	4.7351, 0.1107, 0.1193 p.u.
Resistance: stator, rotor	0.0059, 0.0066 p.u.
Number of poles	3
Gearbox ratio	1:72
Nominal rotor speed	16.67 rpm
Rotor radius	42 m
Grid frequency	60 Hz
Maximum slip range	±30%

5.1.1.2 Solar Capability Curve Modeling

A solar thermal power plant consists of a conventional power block and a solar receiver system which acts as the fuel source. Most solar thermal systems are built around modules of 50 - 250 MW. Synchronous generators are generally rated in terms of the maximum MVA output at a specified voltage and power factor (usually 0.85 or 0.9 lagging) which they can carry continuously without overheating. The active power output is limited by the prime mover capability to a value within the MVA rating. Figure 5.4 gives the steady state equivalent of a synchronous generator [87].

We have

$$\widetilde{E_q} = \widetilde{E_t} + (R_a + jX_s)\widetilde{I_t} \tag{5.14}$$

Neglecting saliency, we have the magnitude of E_q as

$$E_q = X_{ad} i_{fd} \tag{5.15}$$

E_q represents the excitation voltage due to the field current. The synchronous reactance X_s accounts for the flux produced by the stator currents, i.e. the effect of armature reaction. The continuous reactive power output capability is limited by three considerations: armature current limit, field current limit and end region heating limit.

- Armature Current Limit - The armature current results in I^2R power loss, and the energy associated with this loss must be removed so as to limit the increase in temperature of the conductor and its immediate environment. The reactive power limits as a function of the armature current can be obtained from

$$P^2 + Q^2 = (E_t I_t)^2 \tag{5.16}$$

  which represents a circle with the center at the origin and radius equal to the MVA rating.

- Field Current Limit - The field current imposes a limit on the generator operation due to heat resulting from $R_{fd} i_{fd}^2$ power loss. The reactive power limits as a function of the field current can be obtained from

$$P^2 + \left(Q + \frac{E_t^2}{X_s}\right)^2 = \left(\frac{X_{ad}}{X_s} E_t i_{fd}\right)^2 \tag{5.17}$$

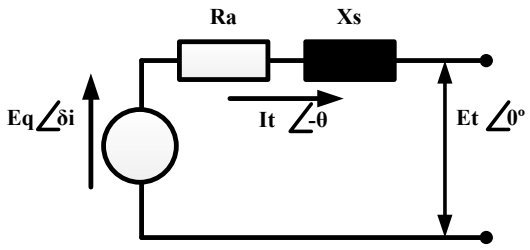

Figure 5.4 Equivalent Circuit (per phase) of Synchronous Generator

The constant field current locus is thus a circle centered at $(0, -\frac{E_t^2}{X_s})$ with $\frac{X_{ad}}{X_s} E_t i_{fd}$ as the radius.

- End Region Heating Limit - The localized heating in the end region of the armature imposes a limit on generator operation which affects the capability of the machine in the under-excited condition. To avoid such heating and also for steady-state stability limit, the machine manufacturers prepare capability curve specific to their own designs and recommend limits within which they operate. Here, we define the end region heating limit as the line segment joining points $(0,-\frac{E_t^2}{X_s})$ and mirror image of the point of intersection between the loci of the armature and the field current limits.

Combination of Limits - The capability curve is obtained by the common area of the most restrictive of the three limitations (5.16), (5.17) and the end region heating limit. For all the analysis, a cylindrical-rotor turbo generator with parameters shown in Table 5.2 is selected. This technique is given for only a single machine, but it is assumed that the power capability of one machine can be scaled up to accurately aggregate the behavior of the STECS. The plot in Figure 5.5 shows the capability curve of the solar thermal synchronous machine.

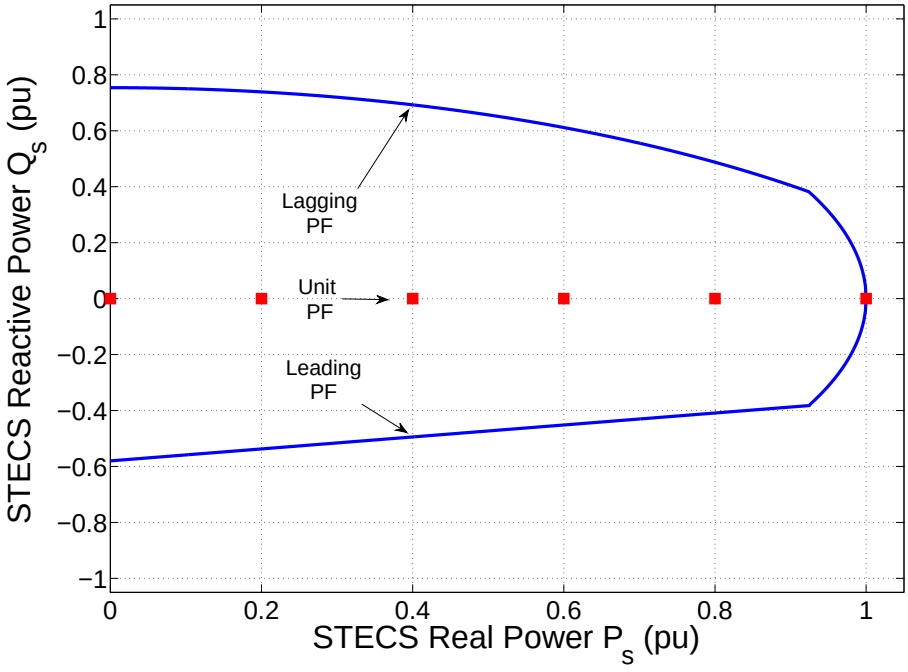

Figure 5.5 STECS P-Q Capability Curve (p.u)

Table 5.2 STECS Synchronous Generator Parameters

Machine Parameter	Value
Rated Megavoltamperes	635 MVA
Maximum Turbine Output	635 MW
Rated Stator Voltage	24 kV
Rated power factor	0.95
Rated Synchronous reactance	172.4%
Grid frequency	60 Hz
Rated rotor speed	3600 rpm

5.1.2 HECS MVRAM

The driving forces behind the wind and solar active power output are wind speed and the solar direct normal irradiance (DNI), both of which are variable in nature. Thus, the corresponding reactive power outputs or availability are also variable. In order to correctly capture and properly represent the time variability over different time scales in the power system load flow analysis, the reactive power from each of the components are expressed as polynomial functions of the real power outputs. The method of Polynomial Least Squares Fitting [120] is used to determine the coefficients of the polynomials of different orders and the final models were selected and validated using the coefficient of determination (R^2) indicating goodness-of-fit of the regression. Thus, we have the HECS real power output as the sum of the outputs from the wind and the solar thermal, i.e.

$$P_H(t) = P_W(t) + P_{ST}(t) \tag{5.18}$$

The reactive power outputs can be expressed as $Q_{W_{o/u}} = f_{W_{o/u}}(P_W)$ (see Figure 5.3) and $Q_{ST_{o/u}} = f_{ST_{o/u}}(P_{ST})$ (see Figure 5.5). Thus,

$$\begin{aligned} Q_{H_{o/u}}(t) &= Q_{W_{o/u}}(t) + Q_{ST_{o/u}}(t) \\ &= f_{W_{o/u}}\left(P_W(t)\right) + f_{ST_{o/u}}\left(P_{ST}(t)\right) \end{aligned} \tag{5.19}$$

Here, o/u refers to the over and under excited conditions respectively.

Once the capability curves of the system specific WECS DFIG and STECS synchronous generator units have been obtained (in p.u), the next step is to properly combine them to represent the wind-solar HECS capability diagram. However, there is a fundamental difference between conventional P-Q diagram and the Hybrid CES P-Q diagram (refer Figure 5.6). When $P_h = k_i$ $(i = 1, 2, 3)$, that k_i could be comprised of a different combination of P_w and P_s: all possible combinations can be found on the line having the equation $P_w + P_s = k_i$ in the (P_w, P_s) plane. Thus the traditional 2-dimensional P-Q diagram would transform into a 3-dimensional region for the HECS. We can call this as the **MV**ar **R**esource *A*ssessment **M**odel (MVRAM). The rated capacities of the individual WECS and STECS also need to be considered while scaling up.

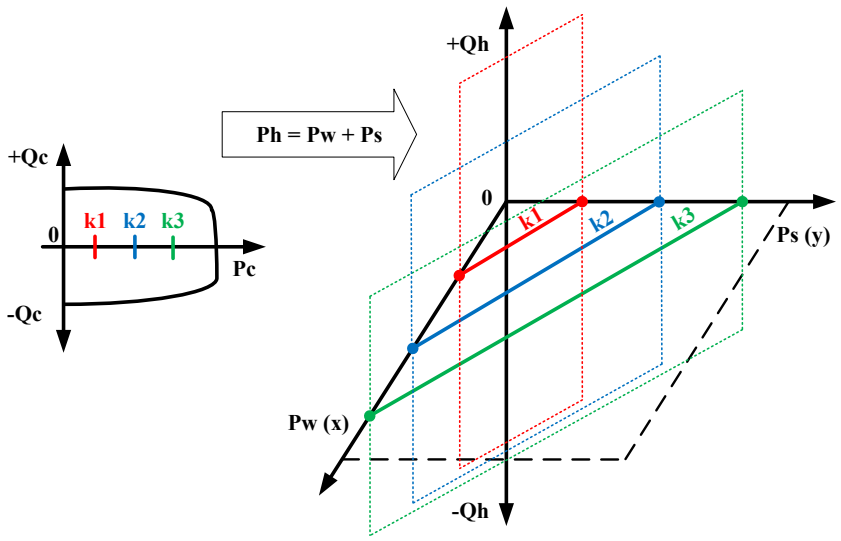

Figure 5.6 Difference between Regular P-Q diagram and Wind-Solar ECS P-Q diagram

5.2 System Impact of HECS

5.2.1 Test System Description

A sample power network available in the PSS/E software [121] was imported into MATPOWER [122] for system analysis. The original network consists of 6 conventional machines and 23 buses (Figure 5.7). The total load was modified to 2345 MW and 661.5 MVAr. Shunt compensation (950 MVAr sum) is located at various buses throughout the system with a large 600 MVAr reactor at bus 151. The transmission voltages range from 230 - 500kV and the line parameters have been modified to reflect appropriate transmission distances [87].

In the base case, the majority of generation is concentrated in the Northern region of the grid. The load centers are located in the South and South-East portion of the system with major concentration at buses 154 and 205. The South-West part of the network contains low load and low transmission capacity. Typical high wind and solar regions have these characteristics and hence it is assumed a potential site for large scale HECS facilities [123]. Unit 3018 has been taken off line, and kept as a non-spinning reserve unit. Installed in place of this unit is one wind-solar HECS facilities strategically placed at bus 3008. To facilitate the transfer of energy from these regions to the load centers the lines (3008−154), (3005−3007) and (3007−3008) are upgraded to have sufficient transmission capacity, but leaving the electrical parameters

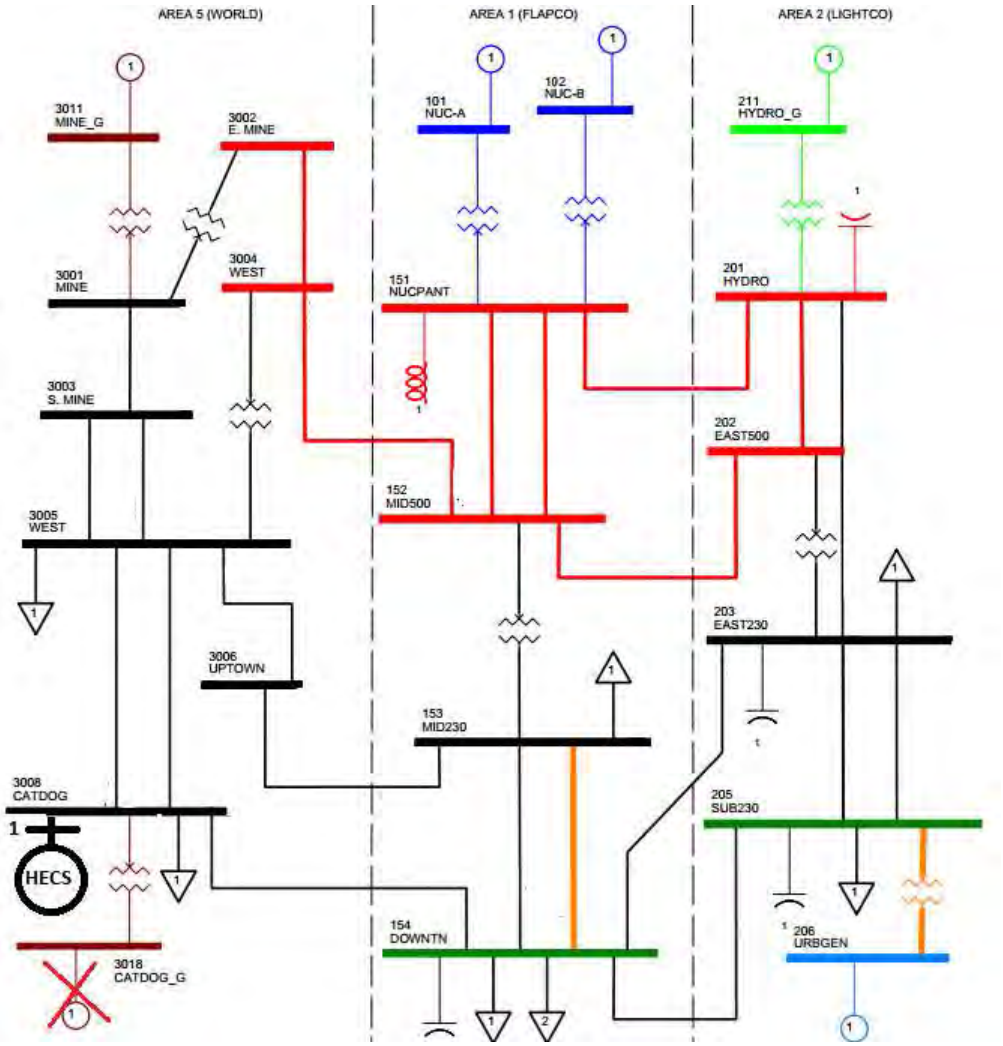

Figure 5.7 Simulated power system with wind-solar HECS interconnection at bus 3008

unchanged.

The total capacity of the other generation in the system is 5020 MW. The initial (base case) dispatch of the generation units including the HECS is done through an optimal power flow [124], [125] whose objective is to minimize system costs while adhering to operation constraints such as line flow, generation, and bus voltage limitations. The formulation is presented:

$$\text{Minimize} \qquad f(P_{gk}) = \sum_{k=1}^{n} C(P_{gk}) \tag{5.20}$$

$$\text{Subject to} \qquad \sum_{k=1}^{n} P_{gk} - \sum_{i=1}^{m} P_{di} - \sum_{j=1}^{p} P_{loss_j} = 0 \tag{5.21}$$

$$\sum_{k=1}^{n} Q_{gk} - \sum_{i=1}^{m} Q_{di} - \sum_{j=1}^{p} Q_{loss_j} = 0 \tag{5.22}$$

$$P_{gk,min} \leq P_{gk} \leq P_{gk,max} \tag{5.23}$$

$$Q_{gk,min} \leq Q_{gk} \leq Q_{gk,max} \tag{5.24}$$

$$V_{u,min} \leq V_u \leq V_{u,max} \tag{5.25}$$

$$-F_{j,lim} \leq F_{j,u} \leq F_{j,max} \tag{5.26}$$

where,

u $\in (1, 2, \ldots q)$, q - total number of buses

j $\in (1, 2, \ldots p)$, p - total number of branches

k $\in (1, 2, \ldots n)$, n - total number of generators

l $\in (1, 2, \ldots m)$, m - total number of load buses

Here, (5.20) indicates the total cost of production of power, where $C(P_{gk})$ is the price for P_{gk} units of power from unit k. Q_{gk} is the reactive injection of unit k. The real and reactive demand at bus i is P_{di} and Q_{di} and the real and reactive loss on line j is given by P_{loss_j} and Q_{loss_j}. Eqns. (5.21) and (5.22) are the power balance equations for real and reactive power. Eqns. (5.23) and (5.24) are the real and reactive power limits on the generators. The bus voltage constraints (0.9 - 1.1) and the line flow limits (< 1.0 p.u.) are given in (5.25) and (5.26).

Since the generators at bus 206 and bus 3011 are assumed to be the fastest acting units, their production cost is set the highest amongst the committed units. The units at buses 101, 102 and 211 are assumed to be base load plants and have the same production cost set. The HECS is modeled to have a fixed production cost and are the least expensive generation. The units are modeled in the way to simulate the current practice of handling intermittent

resources as price taking units, wherein all the available renewable generation is purchased and no market is used to clear these bids [126], [127]. The non-spinning reserve unit 3018 is assumed to have the highest production cost in the system. The contingencies considered are all line outages (N-1). Generation outages are not considered. Bus 154 is heavily loaded in the system and hence its voltage is monitored to obtain the PV curves. MATPOWER is used for the analysis and the different reactive capability limits are incorporated into the load flow data.

5.2.2 Estimation of Voltage Stability Margin

A major aspect of voltage stability analysis is to determine how far the system is operating from the voltage collapse point using consecutive load flow solutions or continuation methods [128] (to determine PV curves), considering a given load increase pattern and generator sharing scheme. The voltage stability margin (VSM) represents the distance (in MW), from the base case operation point to the maximum power transfer capability point of the system (PV curve nose point). For each load increase a load flow problem is solved, and the set of obtained equilibrium points defines the PV curve. In this work, PV curves are obtained by considering load increases for all load buses in a proportional way to the base case loading (keeping constant power factor). System generation level is also increased in order to match the load increases during the PV curve construction process, following the recommendations of WECC [129]. It should be emphasized that all generators or a group of selected generators respond for an increase in demand, and not just the slack bus. Generators reactive power and tap limits are also properly considered. Figure 5.8 demonstrates the typical P-V curves for a system. The three curves correspond to the base case (BC) and two contingencies (C1, C2). The PV margin reduces for contingencies (PV margin BC > PV margin C1 > PV margin C2), and hence including contingencies into voltage stability margin estimation is critical.

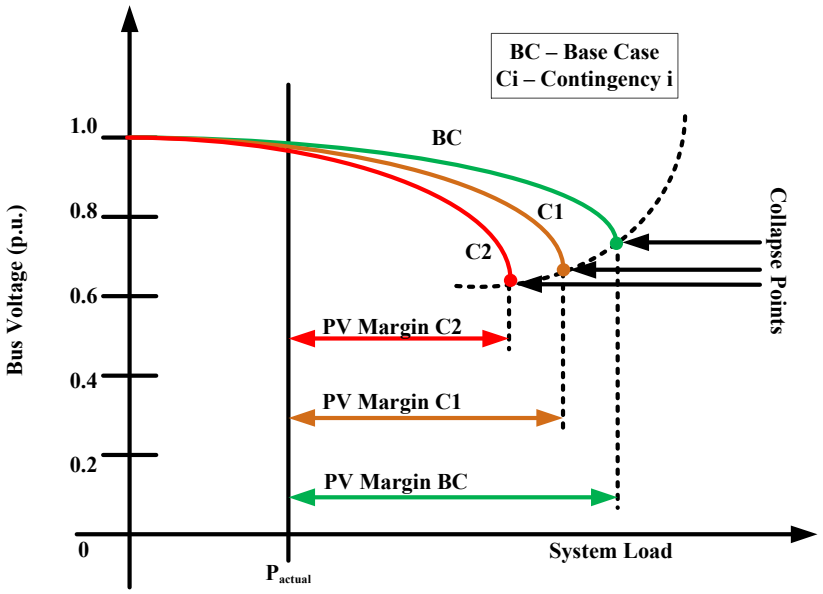

Figure 5.8 P-V Curve: Base case and Contingencies

In the test case studied, the WECS is rated 600 MW ($= P_{w,max}$) and the STECS is rated 400 MW ($= P_{s,max}$), thus making the total HECS rating to be 1000 MW ($= P_{h,max}$). This sizing of the WECS and STECS ratings is based on the work in [130] and was demonstrated to have better capacity credits and less reserve requirements. Using Table 5.3 and Eqn. (5.19), the contour plot showing the distribution of the reactive power of the HECS over different MW output can be derived in Figure 5.9. Figure 5.10 shows the P-Q capability curve of the HECS.

Table 5.3 HECS Varying Power Output Conditions

Range #	Range
Range I	$0 \leq P_h(t) \leq \min(P_{w,max}, P_{s,max})$
Range II	$\min(P_{w,max}, P_{s,max}) < P_h(t) \leq \max(P_{w,max}, P_{s,max})$
Range III	$\max(P_{w,max}, P_{s,max}) < P_h(t) \leq P_{s,max} + P_{w,max}$

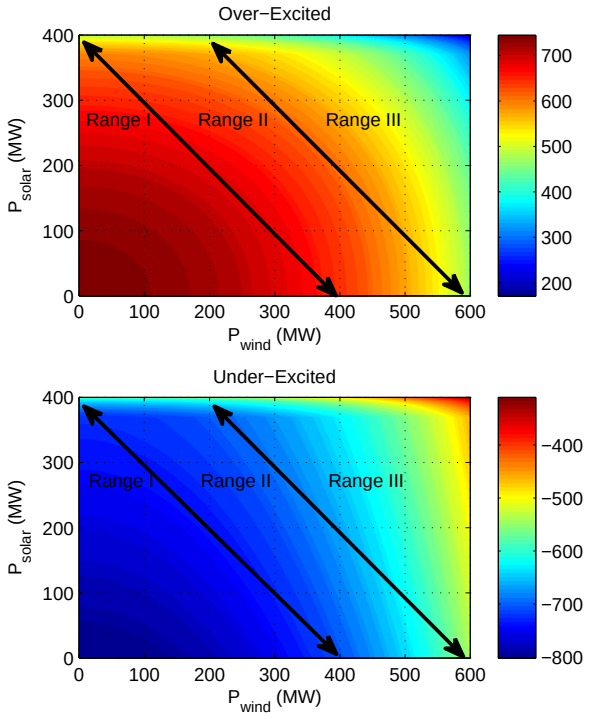

Figure 5.9 Reactive Power Contour Plot (over/under excited) over different P_H range

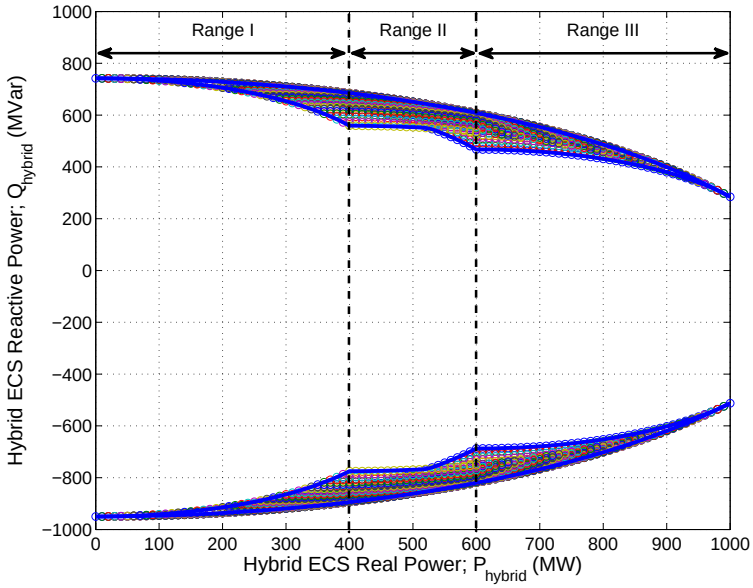

Figure 5.10 HECS P-Q Capability Curve

5.2.3 Applications of MVRAM

The purpose of this analysis is to explore the application of MVRAM for voltage security studies, and suggest new grid connection guidelines for combined variable energy resources facilities. When employing the capability curve, the reactive limits of the machines are the greatest at low output. As wind speeds and solar DNI (direct normal irradiance) increase, the HECS real output increases and consequently the reactive capability reduces.

5.2.3.1 Effect on Voltage Stability Margin (VSM)

Wind and solar resources are not dispatchable and hence they operate under different scenarios at different times of the day depending on the local factors. In order to represent different operating conditions, we study the effect of MVRAM for different scenarios, as defined in Table 5.4. Here, High $\rightarrow (75-100\%)$, Medium $\rightarrow (25-75\%)$, Low $\rightarrow (0-25\%)$ power output range.

For each of the scenarios in Table 5.4, we study the influence of using different reactive power limits (Figure 5.11), namely

- Limit 1 - Zero Reactive Support
- Limit 2 - Triangular Curve (Restricted Power Factor ± 0.95 Operation)
- Limit 3 - Rectangular Curve (Fixed Reactive Power Limits)
- Limit 4 - Full Capability Curve

Table 5.4 Different Wind-Solar Output Scenario Definitions

Scenario Definition		STECS Output (%)		
		High	Medium	Low
WECS Output (%)	High	A	B	C
	Medium	D	E	F
	Low	G	H	I

The Figure 5.12 shows the different values of voltage stability margins obtained using the above defined limits. In all the scenarios, the VSM obtained through using the full capability

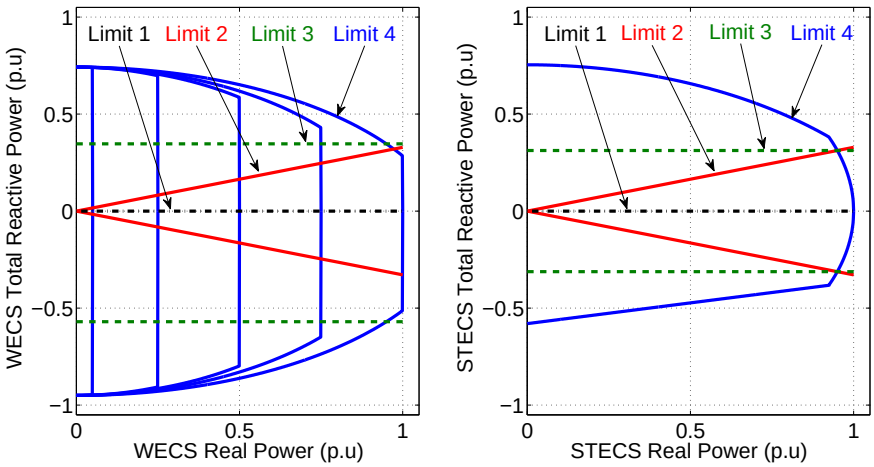

Figure 5.11 Different Reactive Power Limits

curve is the maximum as expected. It is evident that the additional reactive power available by incorporating the capability curve results in a larger power transfer margin available over the entire range of VER output and this can be made available without incurring any additional costs. For Scenario A, the 3 non-unity PF limits are close to each other and hence the VSMs are also close. The important take-away is that during the medium range of operation [Scenarios E, F, H, I], which are generally the most common condition in VER operation, there can be benefit to the system due to increase in the VSM.

5.2.3.2 Effect of Wind/Solar Resource Variability

The scenarios defined in Table 5.4 attempts to capture the different possible operating conditions throughout different time intervals of the day. However, under each of the scenario defined, there is and will be resource variability. Power system operators are not new to the concept of variability, the load profile is a variable quantity and they are equipped with various tools and reserves at their disposal to tackle that issue. Load variability affects power system operations in three different time frames. Figure 5.13 demonstrates the three time frames [131]. Load variability affects voltage and frequency regulation in the power system. This is in the time-frame of a few seconds to a few minutes. The means of maintaining system operations in this time frame is Automatic Generation Control (AGC). The second time-frame of concern

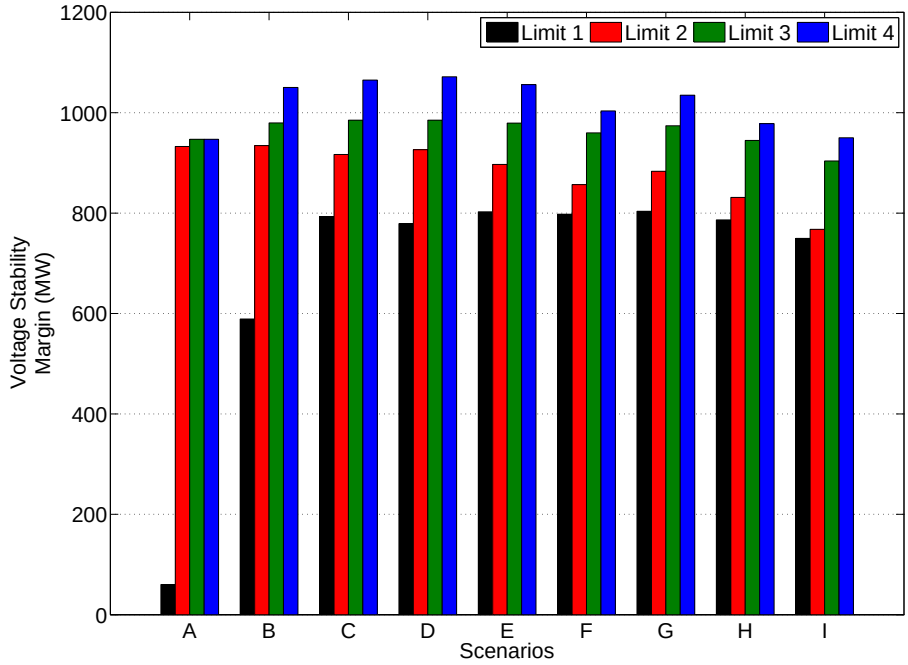

Figure 5.12 Voltage Stability Margin Estimation for varying WECS/STECS Outputs

is the minutes to hours' time frame. This time frame is generally handled by spinning and non-spinning reserves. The final period of concern is the day ahead period and this is handled by committing units in advance to handle the uncertainty. The addition of large scale wind and solar generation in the power system can affect all these time frames. The increasing penetration of wind and solar resources make the complexity of the variability issue even more challenging. There needs to be proper tools which can incorporate this resource variability in the system security assessment.

Traditionally PV curves are drawn to study the nature of the voltage profiles of a particular load bus given an assumed direction of increase of conventional generation. Existing static voltage stability analysis assumes all generation to be dispatchable. But wind and solar generation cannot be considered to be dispatchable [132] and hence a different approach is needed to understand the impact of wind variability on Voltage Stability Margin.

Electricity generated from wind/solar power can be highly variable with several different timescales - hourly, daily, and seasonal periods. Since instantaneous electrical generation and

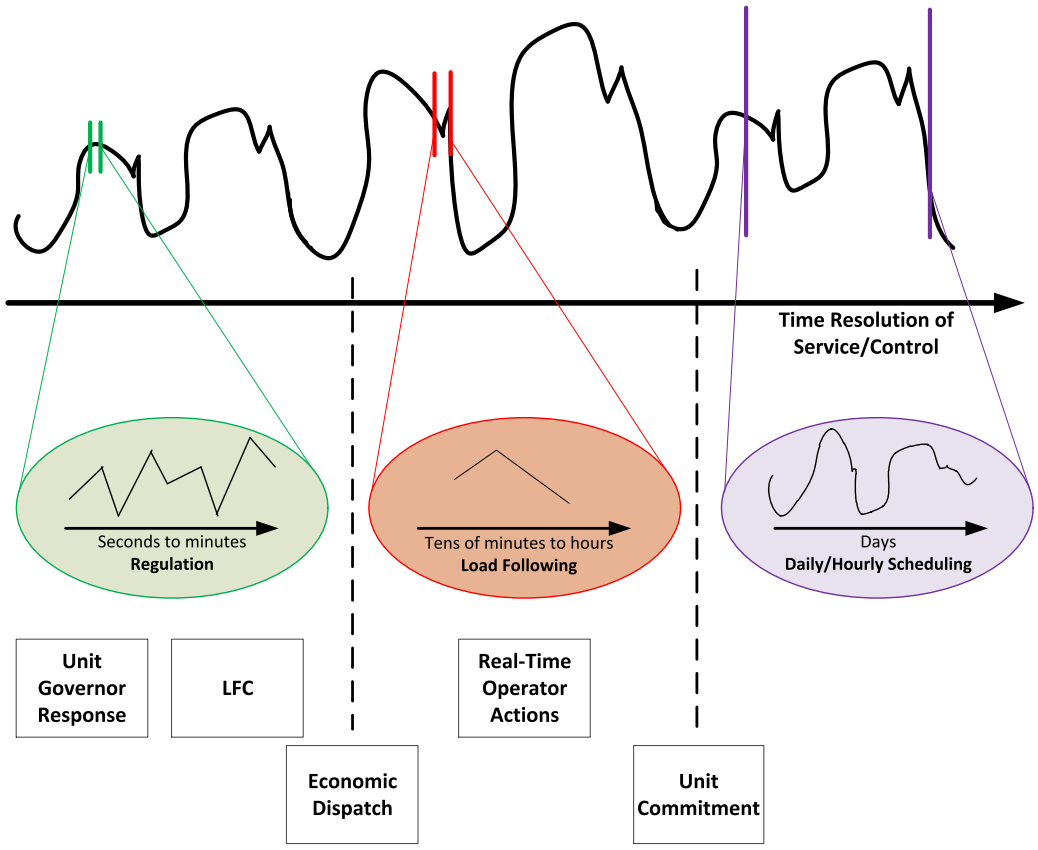

Figure 5.13 System operating time frames and control mechanisms

consumption must remain in balance to maintain grid stability, this variability can present substantial challenges to incorporating large amounts of HECSs into a grid system. With wind and solar power generation being increasingly incorporated into the existing power system, the traditional PV curves are unable to capture the stability margin for an integrated system which has high renewable penetration (around 20%).

In order to include the wind/solar resource variability, a P-V surface for secure operation is proposed. The developed surface is called the Voltage Secure Region of Operation (VSROp). The surface incorporates different levels of wind and solar generation by representing different PV curves at different hybrid generation levels to obtain a three dimensional region of voltage secure operation. In the three dimensional region, the non-dispatchable wind and solar generation (z axis) forms the additional axis along with the existing power generation, including losses of the system (x axis) and the per unit voltage (y axis).

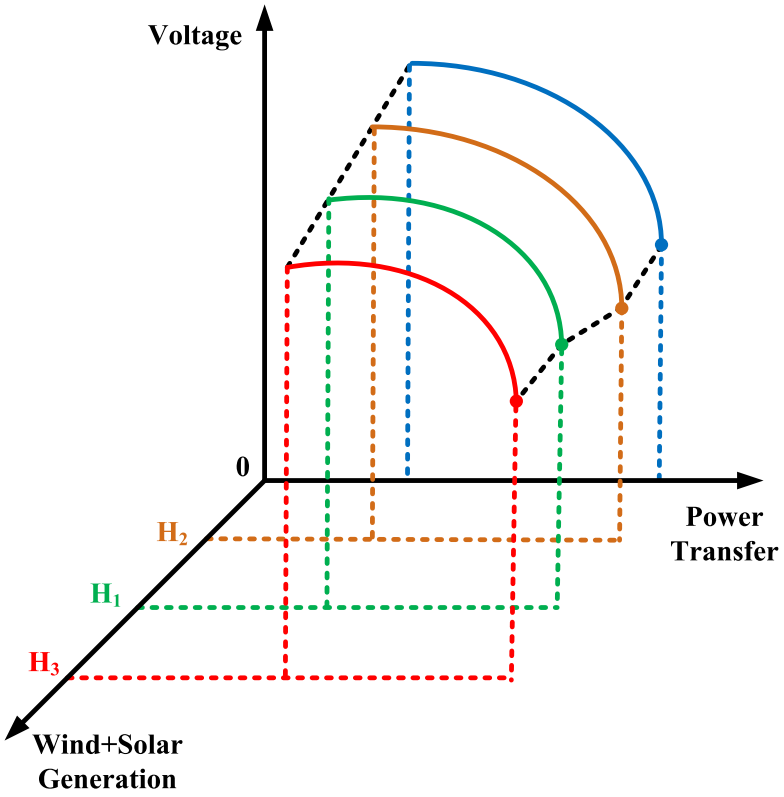

Figure 5.14 Conceptual Voltage Secure Region of Operation (VSROp)

Figure 5.14 demonstrates a sample VSROp. The four PV curves corresponds to no wind and solar and wind and solar generations H_1, H_2 and H_3, where $H_2 < H_1 < H_3$). For each PV curve, the amount of hybrid generation is kept constant and the load and generation is increased according to a set loading and generation increase scenario, which is kept constant for all PV curves. Another input to the PV surface calculation algorithm is the redispatch strategy for increase or decrease in wind generation.

The flowchart in Figure 5.15 shows the steps involved. The proposed methodology includes the following steps:

Step (i) Obtain Input Data

This step basically involves obtaining the three inputs to the Voltage Security Assessment tool: (a) The power flow data for the system under consideration, (b) The assumed level of hybrid generation in the base case and resource variability that is to be studied and (c) The redispatch strategy for increase or decrease in hybrid genera-

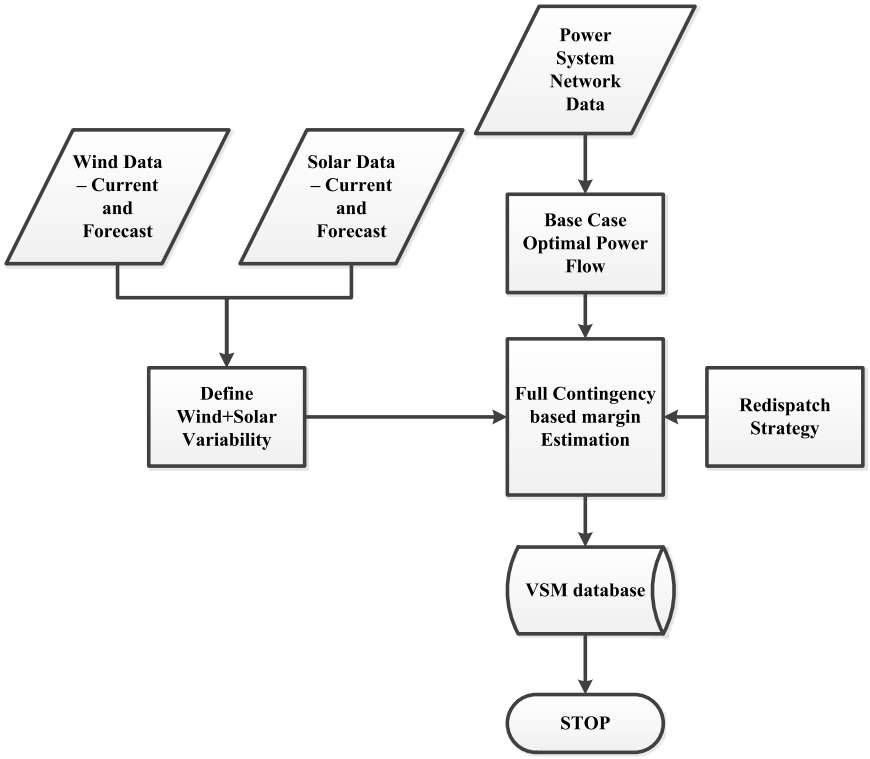

Figure 5.15 Flowchart for Voltage Security Assessment

tion. The power flow data includes the committed generations and their bid curves. It also includes the load increase direction and generation increase direction. The generation increase scenario is provided for all other generations except wind and solar. Historical wind speed, solar DNI data and load data is utilized to decide the amount of wind generation available in base case. The wind speed and solar DNI forecasts for maximum variability is utilized to decide at what values of resource variation PV curves are to be plotted. The resource rate of variation along with the ramp rates of available generation is utilized to develop the generation redispatch strategy to compensate for variation in wind and solar power in the system.

Step (ii) Optimal Power Flow in the base case

The Optimal Power Flow (OPF) methodology as described in (5.20) - (5.26) is utilized. MATPOWER is the software tool used in this OPF analysis.

Step (iii) Full contingency based Margin Estimation

For a fixed HECS energy dispatch, plot the PV curves using powerflow for all (N-1) contingencies. MATPOWER is used to obtain the PV curves. The contingency corresponding to the least power transfer margin is noted and the corresponding PV plot is stored. The redispatch strategy of the remaining generators which account for the variation in wind and solar variability acts as a critical factor and is fed as input. The set of all PV curves is plotted in the previously mentioned three dimensional space to obtain the Voltage secure PV surface. The series of PV curves on different planes corresponding to a particular hybrid generation level will constitute a hyperspace which will represent the stable voltage operating zone. The base case dispatch is then utilized to estimate the least available margin in the PV surface.

Step (iv) Margin Database Buildup

The margin obtained in Step (iii) is verified to meet the power margin requirements and the values are stored in a database which is readily available to the operators. This hyperspace would give the power system operators a given region which might be too conservative, but is the perfectly safe operating zone. Also given current wind and solar dispatch and estimated variability in the next operating time horizon, the operator would be able to quickly determine the amount of the margin that would be available for the system.

Under each of the scenarios defined in Table 5.4, there is inherent variability in the wind and solar resource which needs to be addressed. Let the current WECS and STECS output power levels be $P_w^{'}$ and $P_s^{'}$ respectively, and the corresponding percentage variability in WECS and STECS output be defined as $\pm x\%$ and $\pm y\%$. Then, we have the following,

$$\Delta P_h^{'} = \Delta P_w^{'} + \Delta P_s^{'} \tag{5.27}$$

$$\%\ P_h^{'}\ \text{Variability} = \pm \frac{xP_w^{'} + yP_s^{'}}{P_h^{'}} \tag{5.28}$$

The terms in (5.27) denote absolute values, while those in (5.28) denote percentage variability.

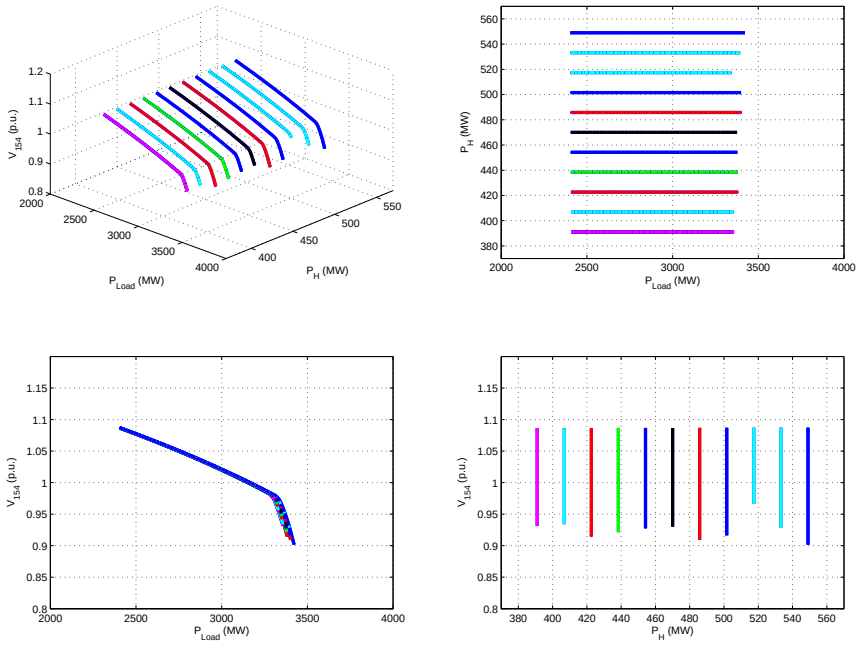

Figure 5.16 Voltage Secure Region of Operation with its 3 projections for given variability in HECS Output; V_{154}: Voltage at Bus 154, P_{Load}: System Demand, P_H: HECS Output

The initial HECS generation is set to 470 MW (WECS: 320 MW; STECS: 150 MW), which is 20% of the base load. The wind and solar output variabilities are assumed to be ±20% and ±10% respectively. Thus the range of variability is then (2×79 MW) or ±16.8% (from (5.28)). The operation conditions are simulated at 11 linearly spaced intervals to obtain the PV hyperspace. The redispatch strategy is such that 50% of the decrease/increase in combined wind and solar generation is compensated by the fast acting unit at bus 206, and the remaining power and additional losses are compensated by the slack bus at 3011. Figure 5.16 shows the VSROp hyperspace using the capability curves. The optimal power flow solution provides the starting point for the PV curve corresponding to 470 MW of HECS generation. The other initial points are obtained using the redispatch strategy. It also shows its 3 projections which clearly demonstrates show the effect of a given profile of wind and solar resource variability on the voltage transfer margin and the voltage profiles. The MVRAM can handle any random profile of resource variability and reassess the security of the system and provide critical information

to the system monitors.

5.3 Comments

A systematic mathematical approach - MVRAM - was demonstrated for assessing the MVar resource availability (maximum and minimum limits) of a HECS with wind and solar resources. The developed MVRAM can be used by system planners and operators as an easy tool to estimate the reactive power availability of the HECS which can be procured during emergency and restorative states of the power system with the help of power electronic interface. Different operating scenarios were modeled and the corresponding voltage security assessment was executed. The MVRAM can help in furthering the cause of grid integration of variable renewable energy sources and will encourage policy makers to amend the current fixed power factor regulation to bolster reactive support from wind-solar HECSs. A novel voltage stability assessment tool that incorporates wind and solar variability was developed. The technique developed is general and is applicable for any type of wind or solar generation technology. The traditional methodology of drawing PV curves to assess static voltage stability margin is modified to address the intermittent nature of wind and solar energy. Given a range of resource variability, the developed tool calculates sets of PV curves plotted along parallel planes, thus giving a three-dimensional VSROp.

CHAPTER 6. LARGE SYSTEM IMPLEMENTATION - WECC SYSTEM

6.1 Motivation

Formed in 2002 by the merger of the Western Systems Coordinating Council (WSCC) and two regional transmission associations, the Western Electricity Coordinating Council (WECC) system encompasses the entire Western Interconnection and covers more than 1.8 million square miles. From the wind and solar energy distribution maps, it is evident that the south-west part of US is rich in both wind and solar resources and thus would be ideal for the development of the HECS. Thus a test bed based on a reduced modified version of the Western Electricity Coordinating Council (WECC) was created to test the developed models and study the grid impact of these HECS. The physical layout of the WECC was overlaid with the resource maps to determine the resource pockets and the load centers. The following grid investigation reflects the effect of siting, sizing and grid integration of the proposed hybrid energy conversion systems.

6.2 System Modeling

The Western Electricity Coordinating Council (WECC) region encompasses the entire Western Interconnection, which comprises the states of Washington, Oregon, California, Idaho, Nevada, Utah, Arizona, Colorado, Wyoming, portions of Montana, South Dakota, New Mexico and Texas in the United States, the Provinces of British Columbia and Alberta in Canada, and a portion of the Mexican state-owned electric utility CFE's system in Baja California in Mexico. WECC is tied to the Eastern Interconnection through six high-voltage direct current transmission facilities, and also has ties to non-NERC systems in Northwestern Canada and the rest of the CFE system in Northwestern Mexico (Figure 6.1).

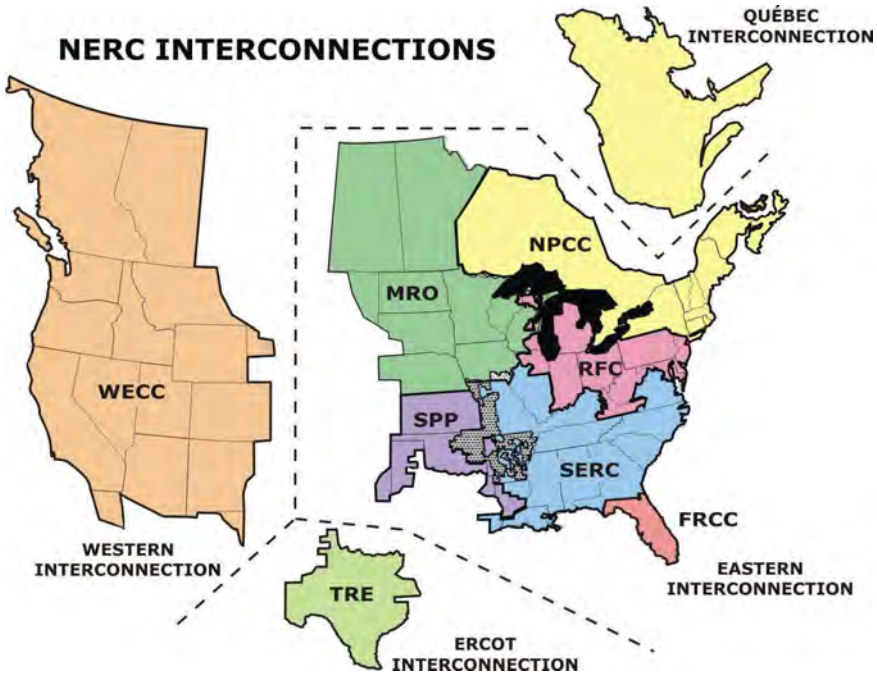

Figure 6.1 NERC Interconnections including WECC

Figure 6.2 Portion of WECC in USA

The US portion of the WECC covers all or part of 14 western US states (shown as shaded Figure 6.2).

The full WECC system model is not available for general research use, and a reduced model was desired for practical reasons such as computing time and software limitations on model size. Researchers at the California ISO (CAISO) developed a 240-bus model from publicly-available data and validated it using the full WECC models [133].

Development of the model began with a 179-bus model [134] used for multi-agent research. The model was extended to 225 buses [135] to conform the models topology to that of models used in CAISO [136] and other organizations [137] transmission planning studies. The 240-bus model adjusted a few aggregated transmission line impedances to produce power flow results that better agree with full planning models [133]. It also includes transmission wheeling charges [133].

The topology of the 240-bus model is shown in Figure 6.3: 240-bus WECC Model Topology [133]. Colored blocks within the diagram are constrained load and generation pockets. The solid red lines signify inter-ties between CAISO and neighboring areas, and significant transmission constraints (e.g. flowgates) within CAISO. Each balancing authority within the WECC has a primary responsibility to maintain reliable conditions within its area, with inter-area transactions typically being secondary to serving native load. The buses in the system were classified under 30 zones as shown in Table 6.1. All the buses are numbered with 4 digits, the 1st two being their corresponding Zone Number. The details of all the buses are given is Appendix D.

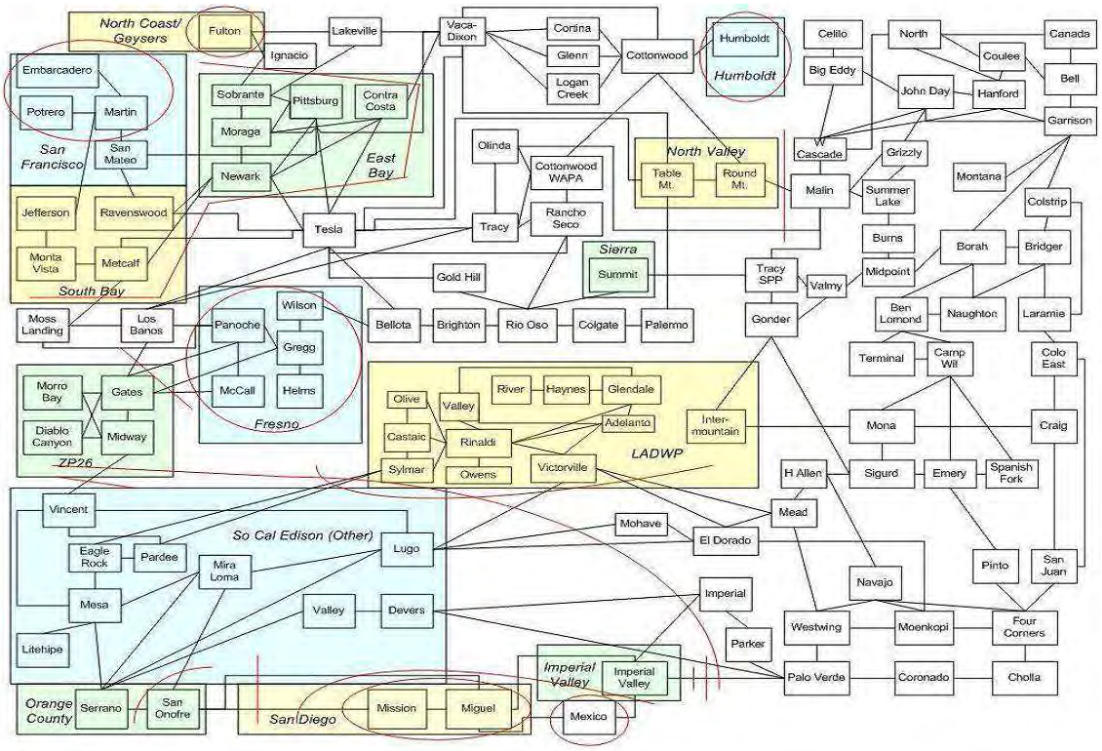

Figure 6.3 Topology Of The 240-Bus WECC Network Model

Table 6.1 WECC System Zone Details

Zone Num	Zone Name	Zone Num	Zone Name	Zone Num	Zone Name
10	SOUTHWST	32	EASTBAY	42	W_CASCAD
20	MEXICO	33	SOUTHBAY	50	CANADA
21	IMPERIAL	34	FRESNO	61	IDAHO
22	SANDIEGO	35	GEYSERS	62	MONTANA
23	SDG_MIV	36	HUMBOLDT	63	WYOMING
24	SCE_OTHR	37	SIERRA	64	N NEVADA
25	LAORANGE	38	CNTCOAST	65	UTAH
26	LADWP	39	PGE_OTHR	70	COLORADO
29	SCE_NV	40	S_JONDAY	80	SMUD
31	SNFRNCSC	41	N_JONDAY	90	DC TIES

The complete data set for the model is available online [138]. Hourly aggregated base-case (2004) and future (2015) data are provided with the model:

- Loads for eleven areas within CAISO and for sub-regions outside CAISO.
- Wind and solar resources for 16 wind resource and 5 solar resource areas.
- Geothermal resources at the North Bay/Geysers area in CAISO. Four geothermal resource areas outside CAISO are assumed to operate at constant 80% of maximum capacity.
- Biomass generation at three buses within CAISO.
- Hydroelectric generation. While hydro should be modeled as dispatchable, the complexities of hydro dispatch will prevent realistic modeling in most research applications, so representative hydro output values are provided.

Other generation resources are modeled as follows:

- Eleven generic renewable resource areas, representing mixed renewables, and including a limited amount of biomass outside CAISO, operate with constant output of 80% of maximum capacity.
- Gas-fired generation is dispatchable. To allow for unit commitment and dispatch within aggregated generators, a minimum output of 5% of capacity is assumed.
- Coal-fired generation is aggregated at 17 sites outside of CAISO and operates at constant load of 85% of capacity.
- Four nuclear generators are operated at 100% capacity, but may be reduced to 90% for congestion management.

Figure 6.4 illustrates two important generation trends between now and 2020 relative to the generation assumptions [139]. First, there are not significant increases in dispatchable generating capacity as most of the gas-fired additions in California merely offset the OTC retirements. Second, there are over 33,000 MW of assumed renewable generation additions. Combined, these developments raise significant questions around having adequate dispatchable

resources to balance the large increase in variable generation (wind and solar). Some integration problems could be resolved by using complementary renewable resources, demand response programs, distributed generation, and energy storage projects. Renewable generation includes such non-variable types such as small hydro, geothermal, or biomass.

Figure 6.5 represents the mix of renewable generation in 2020, which continues to be dominated by wind [139]. However, strong growth in solar is anticipated. Of the solar resources assumed in the 2020 Expected Future, 50% (by capacity) is concentrated solar power type. Finally, over the next ten years, over 20,000 MW of wind and solar capacity is expected to be interconnected (increasing supply volatility), while approximately 18,000 MW of thermal generation will be repowered or retired (increasing uncertainty surrounding thermal resources).

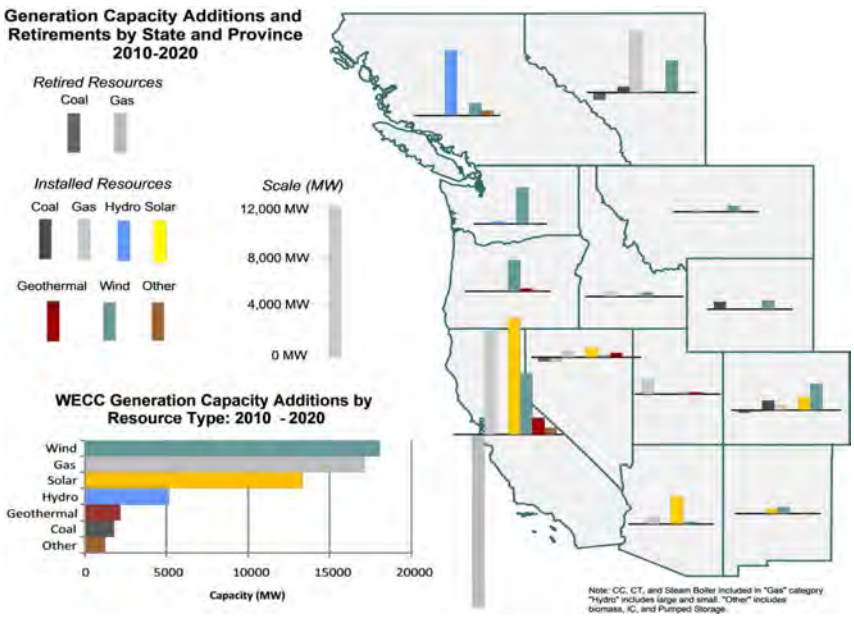

Figure 6.4 Generation Capacity Additions and Retirements by State and Province 2010-2020

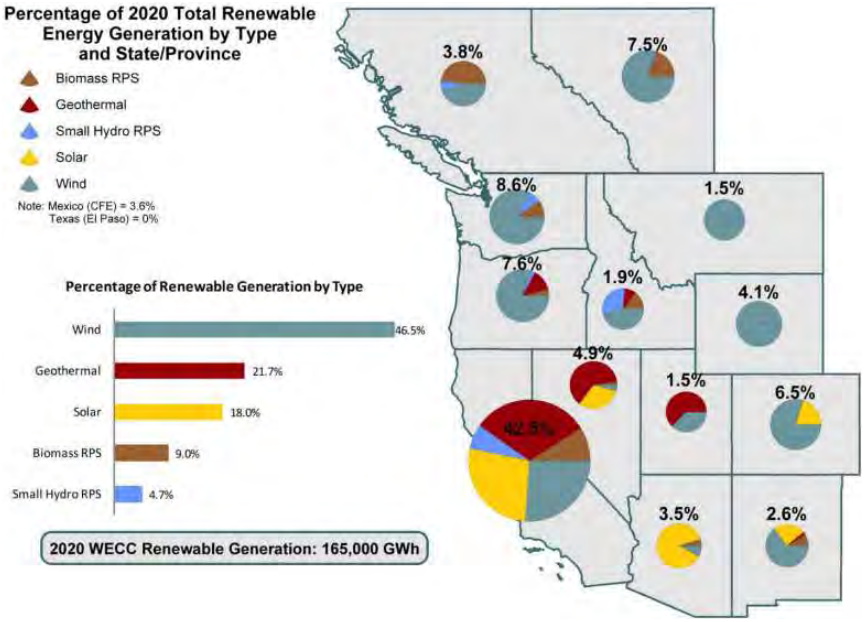

Figure 6.5 Percentage of 2020 Total Renewable Energy Generation by Type and State/Province 2010-2020

6.3 Resource Identification and Sizing

The Renewable Energy Atlas [140] is an interactive application of the renewable energy resources in the contiguous United States, Alaska and Hawaii. It illustrates the geographic distribution of wind, solar, geothermal, and biomass resources.

The CSP data from [140] provides monthly average and annual average daily total solar resource (DNI) averaged over surface cells of 0.1 degrees in both latitude and longitude, or about 10 km in size. The irradiance values represent the resource available to concentrating systems that track the sun throughout the day. The data are averaged from hourly model output over 12 years (1998-2009) [93]. This model uses hourly radiance images from geostationary weather satellites, daily snow cover data, and monthly averages of atmospheric water vapor, trace gases, and the amount of aerosols in the atmosphere to calculate the hourly total irradiance (sun and sky) falling on a horizontal surface. The direct beam radiation is then calculated using the atmospheric water vapor, trace gases, and aerosols, which are derived from a variety of sources. Where possible, existing ground measurement stations are used to validate the data.

The nation has more than 8,000 GW of available land-based wind resources. Potential capacity estimated assuming 5 MW/km^2 [141]. The onshore wind data are based on 50 m height above surface. Areas with annual average wind speeds of 7 m/s and greater at 50 m height are considered to have a wind resource suitable for onshore development. The data only applies to areas of low surface roughness (i.e. grassy plains), and excludes areas with slopes greater than 20%. For areas of high surface roughness (i.e. forests), the values shown may need to be reduced by one or more power classes. There is also around 2,200 GW of offshore wind class 5 and better between 0 and 50 nautical miles from shore, based on NREL's most recent offshore resource estimates. The offshore wind data are based on 90 m height above surface. Areas with annual average wind speeds of 7 m/s and greater at 90 m height are generally considered to have a wind resource suitable for offshore development.

Figures 6.6 and 6.7 shows the spatial energy density of wind power and concentrated solar power respectively [140]. This facilitates the process of locating common overlapping areas which carry both of the energy density criteria.

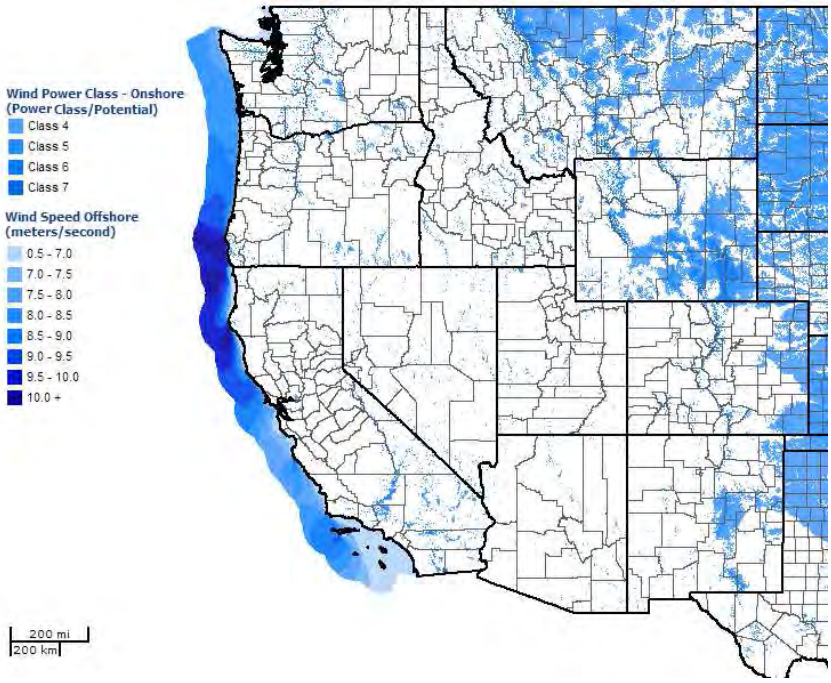

Figure 6.6 Wind Resource in WECC

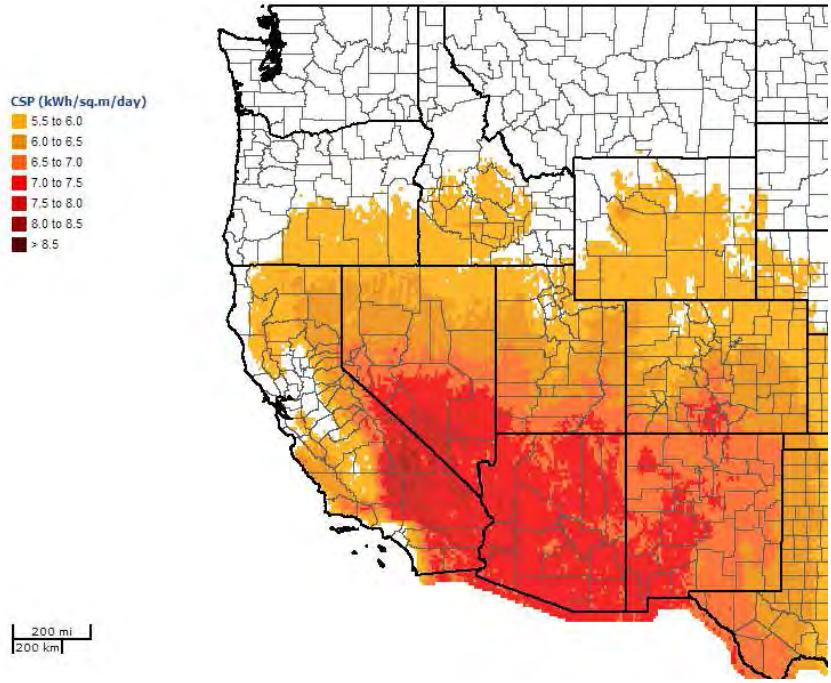

Figure 6.7 CSP Resource in WECC

Electricity must be transmitted from where it is generated to areas of high electricity demand, using the existing transmission system or new transmission lines where necessary. If existing suitable transmission facilities are not available for a proposed renewable energy development, new transmission lines and associated facilities must be constructed. In some cases, existing transmission facilities might require upgrading. The costs associated with construction or upgrading activities may determine whether or not a project is economically feasible. The current existing and future proposed transmission grid information of WECC were referred from two maps (available for sale at WECC website [142]): The WECC Principal Transmission Map that denotes existing transmission lines and other electrical devices and the WECC Planned Facilities Map that illustrates the location of future projects. Figure 6.8 shows a very high level view of the transmission (>100 kV) and distribution (<100 kV) network layout of the WECC [92]. This serves as critical input to the HECS ID tool to determine the proximity of wind-solar resource rich locations to existing and future transmission lines. Figure 6.9 remaps the block diagram shown in Figure 6.3 on the physical map and maintains the transmission connections. Each block in Figure 6.3 is represented by a colored marker in Figure 6.9. The details of all the buses are given is Appendix D. For e.g., the Southern California Edison buses (24XX) and LADWP buses (26XX) are located on their actual physical location in the map (blue cluster towards the bottom left).

The RPS mechanism generally places an obligation on electricity supply companies to produce a specified fraction of their electricity from renewable energy sources. Certified renewable energy generators earn certificates for every unit of electricity they produce and can sell these along with their electricity to supply companies. RPS mechanisms have tended to be most successful in stimulating new renewable energy capacity in the US where they have been used in combination with federal Production Tax Credits (PTC). The participating states in WECC have different RPS goals. For e.g., Arizona - 15% by 2025, California - 33% by 2020, Colorado 30% by 2020, Montana - 15% by 2015, New Mexico - 20% by 2020, Nevada - 25% by 2025, South Dakota - 10% by 2015, Utah - 20% by 2025, Washington - 15% by 2020, etc. [7]

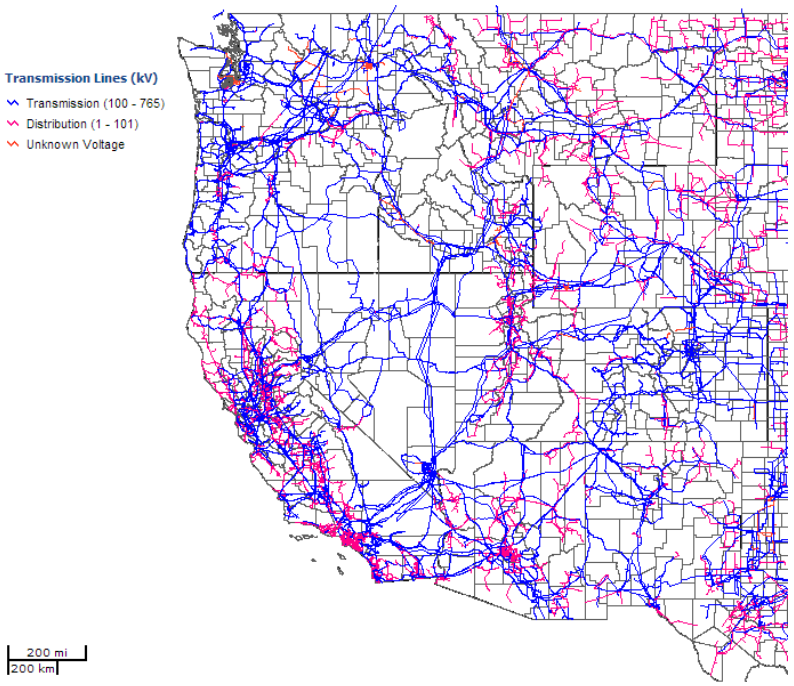

Figure 6.8 Transmission and Distribution Network in WECC (High-Level)

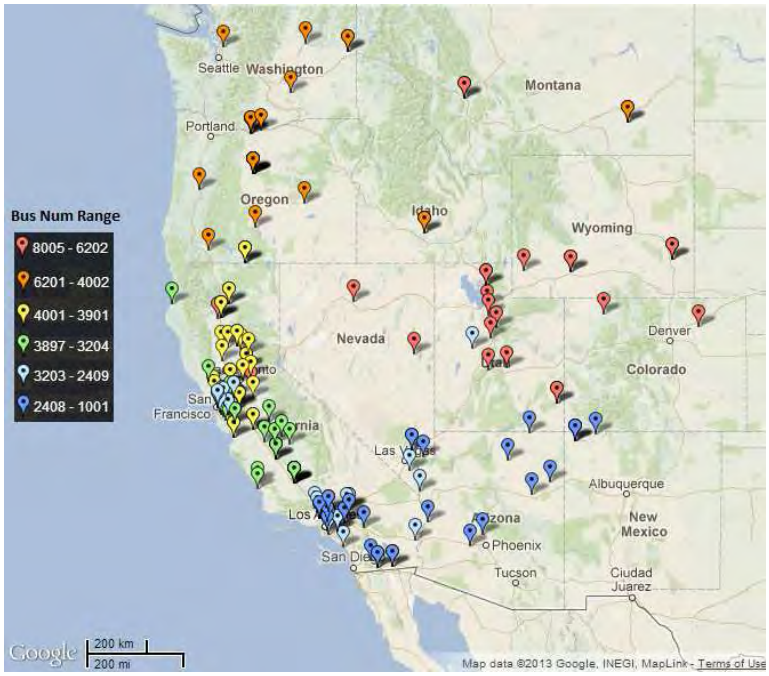

Figure 6.9 Physical Location of the buses in WECC - 240 Bus System

In order to determine potential HECS locations in the WECC system, the HECS ID Tool (Chapter 3) and MWRAM (Chapter 4) were applied to present an integrated visualization approach to assess the resource characteristics and performance. Different tools were used in conjunction to implement this, like ArcGIS [143] and MATLAB [144]. As a widely accepted geo-information system platform, ArcMap (the main component of ESRI's ArcGIS suite of geospatial processing programs) presents geospatial data in an easily understood and customized way. The geospatial resource data of the wind and solar potential are gathered from reliable sources like NREL databases [145] and [146]. ArcMap was used as the visualization platform for the renewable resources and the grid layout and an interface was developed so that it can effectively exchange information and communicate with MATLAB, where the resource characteristics and availability were simulated. This combined approach provides an effective way to understand the power grid behavior with geographical details under different wind solar resource potential scenarios. Furthermore, it could help to develop new siting strategies to improve the resource allocation and adequacy of the emerging grid.

The wind, solar resource data and the location of the buses in the WECC system were forwarded to a MATLAB interface, which computed the proximity of the resource points and also the correlation coefficient between the two renewable resources to check for their complementary nature and updated the database with a new attribute as an identifier. A script was developed to run in ArcGIS to keep track of the database and visualize the status of one interested group of objects in the ArcGIS map in the form of layers, and layers could be overlapped to provide complex visualization. In ArcGIS, a geo-database is stored in a format called shapefiles. A shapefile dataset consists of three mandatory shapefiles for each single layer: a .shp file containing primary geographic reference data, a .dbf file storing all the attribute values, and a .shx file saving the shape index table. It may also contain a projection file (.prj) or a spatial index file (.sbn). The database format is ideal for visualization as they can be categorized into two sets of fields, one fixed set containing the geometry information such as the coordinates and types of object (e.g., polygon, point, link), and another attributes set includes all other specific information of the object, for e.g. wind power class, solar DNI level, substation voltage level, etc. These set attributes could be easily customized and updated, which is ideal for

monitoring and management through a visualization platform. The shapefile database can be imported to MATLAB as structure arrays by using MATLAB mapping toolbox [147]. The mapping toolbox is a set of tools and utilities to process geographic data analysis and map displaying. MATLAB loads the shapefiles from both databases of wind and solar data and substations and transmission lines. The import is done by a function called shaperead from MATLAB's mapping toolbox. This function reads geo-information stored in shapefile format and loads them into an array of geo-structures. The compact geo-structure array is MATLAB-friendly and easy to customize which provides fast calculation as well as good compatibility. The resource characteristics of the wind and solar resource potential and the degree of their complementary nature were computed in MATLAB and an attribute was added to the modified database. The mapping toolbox provides a function called shapewrite to export geostructure arrays to shapefiles which can then be visualized in ArcGIS.

The HECS ID tool involved the following steps in the initial selection of potential hybrid locations:

- select areas having wind and solar resources above certain threshold values - for e.g. wind $\geq$ 400 W/m^2 at 50 m hub height (Figure 6.6), solar $\geq$ 6 kWh/m^2/day (Figure 6.7).
- find common overlapping areas, excluding protected lands, excessive slope, wildlife sanctuaries, etc.
- gather the network information - i) transmission grid layout - existing and proposed from various sources and create space bands width along the lines (Figures 6.8, 6.9), ii) load pockets, iii) other forms of generation - existing and future, iv) local RPS targets (Figure 3.2).
- gather detailed time series resource data in the reduced areas from the sources [92, 94–96].

The different geospatial data layers that are superimposed on top of each other and lead to the determination of locations which are suitable for HECS development are shown in Figure 6.10.

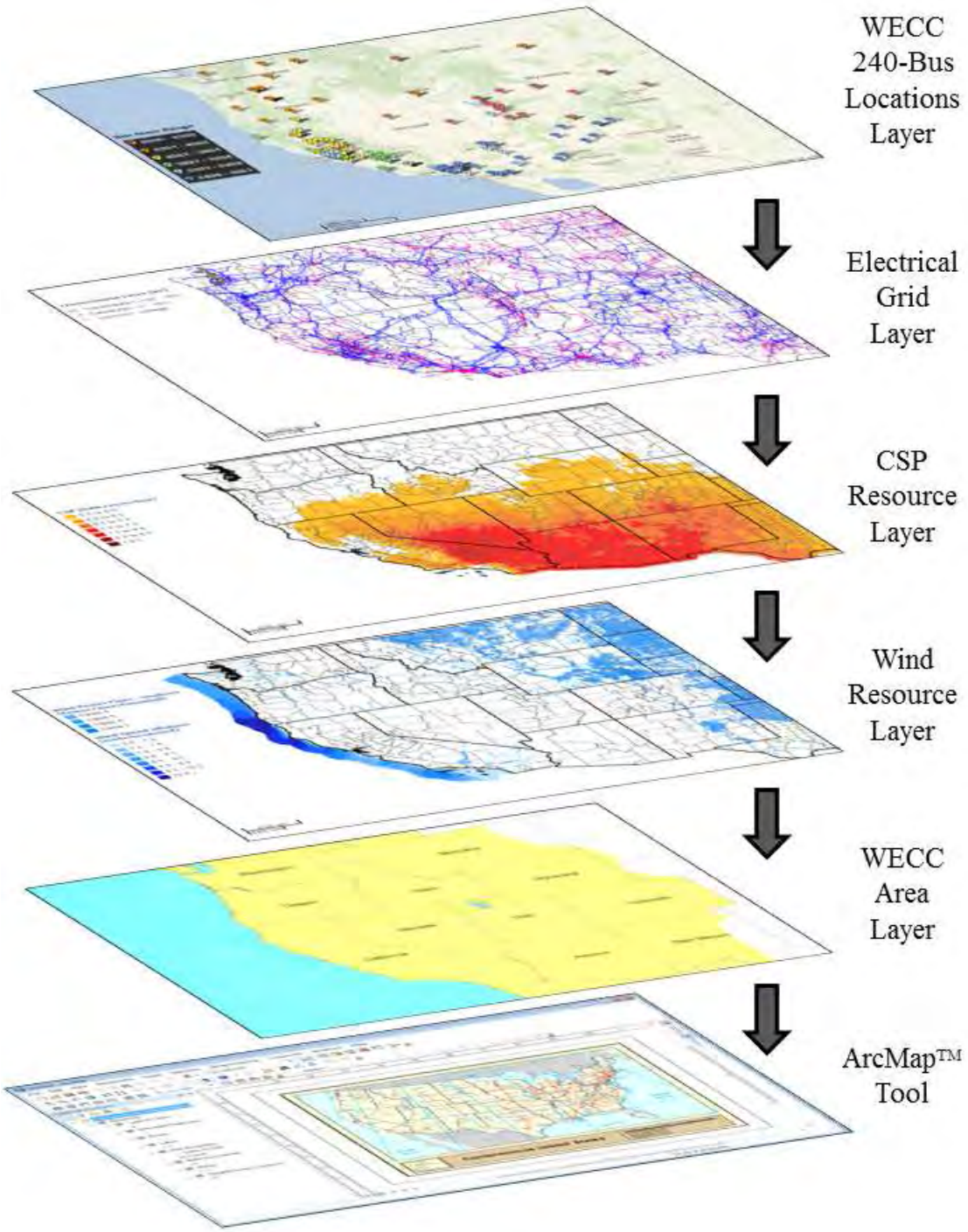

Figure 6.10 Multiple Layers in ESRI ArcGIS

Using the method described above, a resource map of WECC was developed that located the areas that are conducive for the development of wind-solar hybrid energy conversion systems. Figure 6.11 shows the sites that have wind potential (D_W) and solar potential (D_S) above the set thresholds and have complementary nature (determined by correlation coefficient $\rho_{S,W} \leq -0.2$). Table 6.2 shows the logic behind the allocation of different scores ($1-10$) to the different resource potential of solar-wind HECS. It takes into account the individual solar direct normal irradiance and wind power class information and also the correlation between them.

Table 6.2 Explanation of HECS Resource Score Allocation

	Solar DNI Density ($kWh/m^2/Day$) D_S		Wind Power Density (W/m^2) D_W		Correlation Coefficient $\rho_{S,W}$		HECS Score
IF	(6.0,6.5]	AND	(400,500]	AND	≤ -0.2	THEN	1
IF	(6.0,6.5]	AND	(500,600]	AND	≤ -0.2	THEN	2
IF	(6.5,7.0]	AND	(400,500]	AND	≤ -0.2	THEN	2
IF	(6.0,6.5]	AND	(600,800]	AND	≤ -0.2	THEN	3
IF	(7.0,7.5]	AND	(400,500]	AND	≤ -0.2	THEN	3
IF	(6.0,6.5]	AND	>800	AND	≤ -0.2	THEN	4
IF	>7.5	AND	(400,500]	AND	≤ -0.2	THEN	4
IF	(6.5,7.0]	AND	(500,600]	AND	≤ -0.2	THEN	5
IF	(6.5,7.0]	AND	(600,800]	AND	≤ -0.2	THEN	6
IF	(7.0,7.5]	AND	(500,600]	AND	≤ -0.2	THEN	6
IF	(6.5,7.0]	AND	>800	AND	≤ -0.2	THEN	7
IF	>7.5	AND	(500,600]	AND	≤ -0.2	THEN	7
IF	(7.0,7.5]	AND	(600,800]	AND	≤ -0.2	THEN	8
IF	(7.0,7.5]	AND	>800	AND	≤ -0.2	THEN	9
IF	>7.5	AND	(600,800]	AND	≤ -0.2	THEN	9
IF	>7.5	AND	>800	AND	≤ -0.2	THEN	10

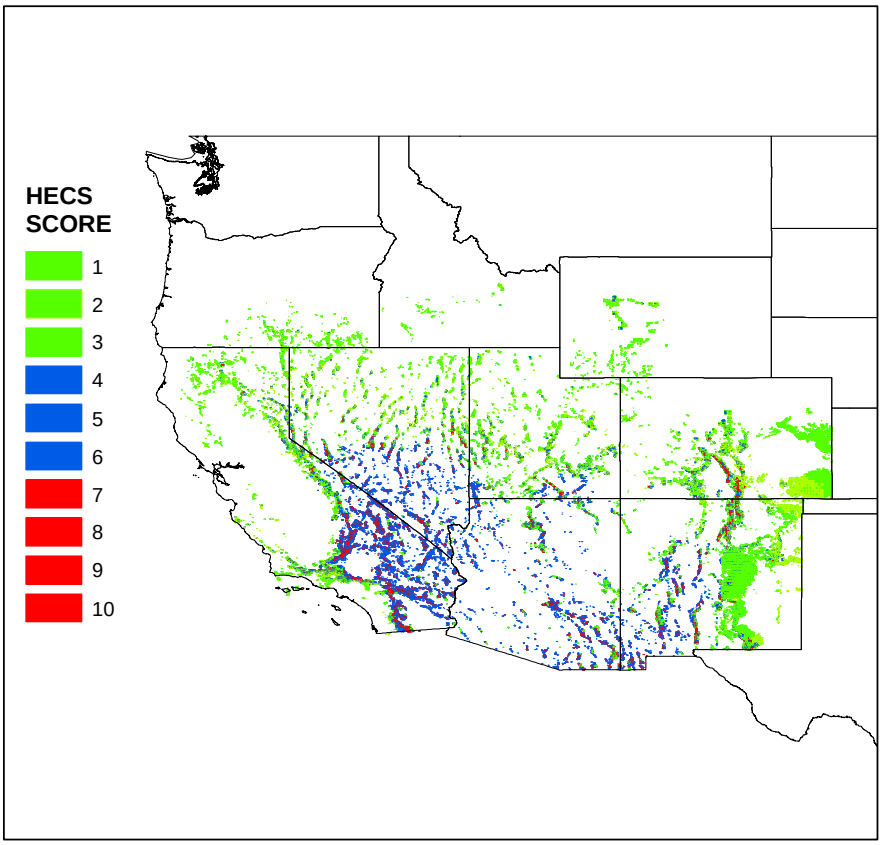

Figure 6.11 WECC Potential Solar-Wind HECS Resource

The HECS score provides the combined resource potential for wind and solar resources for the entire US portion of WECC area averaged over surface cells of 0.1 degrees in both latitude and longitude, or about 10 km in size. Figure 6.12 shows the distribution graph, or histogram, and displays the count of the surface cells that fall within each score bins. For e.g., there are close to 1000 surface cell counts corresponding to Score 10 ($D_S \geq kWh/m^2/Day$ and $D_W \geq 800W/m^2$); this implies that there is approximately (1000×10 km $\times$ 10 km $= 10^5\ km^2$) of land area in entire WECC that have the best co-located wind and solar resources. Also, the surface cells corresponding to Score 4 represent the areas which have either very strong wind; weak solar or strong solar; weak wind potential - these areas are not suitable for hybrid development, but the focus should be on single renewable technology.

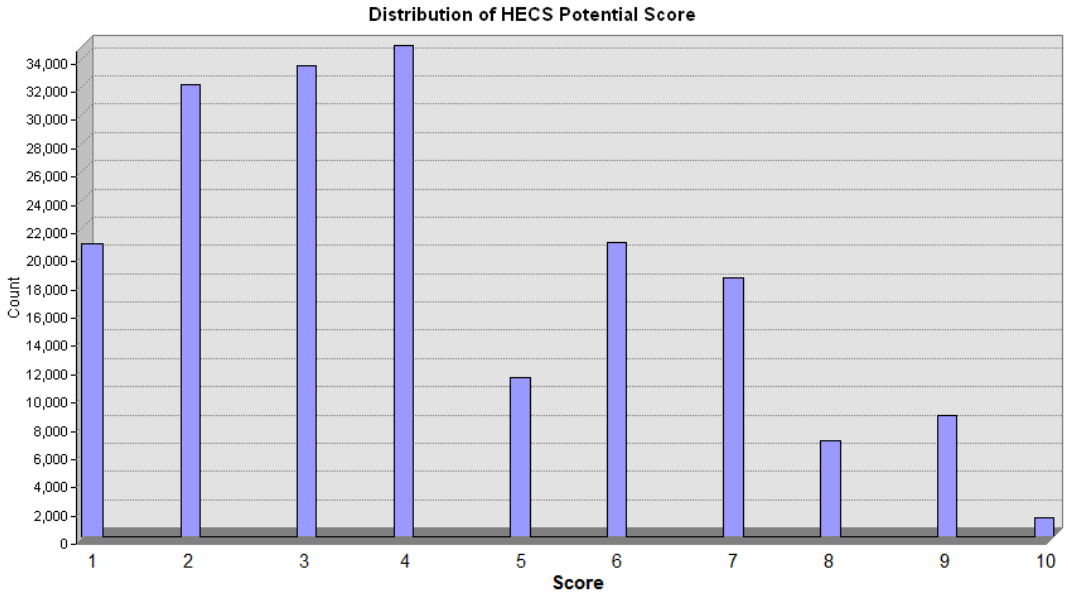

Figure 6.12 Distribution of HECS Potential Resource Scores in WECC

It can been seen that in WECC, the states of California, New Mexico and Colorado have a lot of high-scored cells, followed by Arizona, Utah and Nevada. The states of Oregon, Idaho and Wyoming have some areas which meet the bare threshold criteria, but HECS development might not be suitable option, individual resource development needs to be focused on to meet RPS targets.

Most of the states in the US have set RPS goals of serving a portion of its electric load with renewable energy by 2020; however, transmission is a major barrier to achieving this goal. Renewable resources are location constrained. They are often far from the grid and load centers, requiring extensive and expensive transmission upgrades. In order to achieve cost-savings through economies of scale, and to limit environmental impacts and ultimate build-out time, large transmission projects are needed to access large geographic areas of developable, economic renewable resource potential. There were several areas found which have very good resource potential but not with the defined proximity range of the existing and future transmission grids. It will be very interesting to explore that and do a cost-benefit analysis or comparison between several sites - some close to the transmission but less resource rich, while some far from the transmission, but extremely rich in energy density. It might so happen that even after considering the added cost of building transmission for those locations, in the end they might be more fruitful.

From Figures 6.11 and 6.9, two locations having high HECS potential score were shortlisted to determine their seasonal characteristics and for optimal sizing determination. These two sites are in the CAISO regions of Lugo and Mesa Cal (Bus 2401 and 2408 respectively) (Figure 6.13).

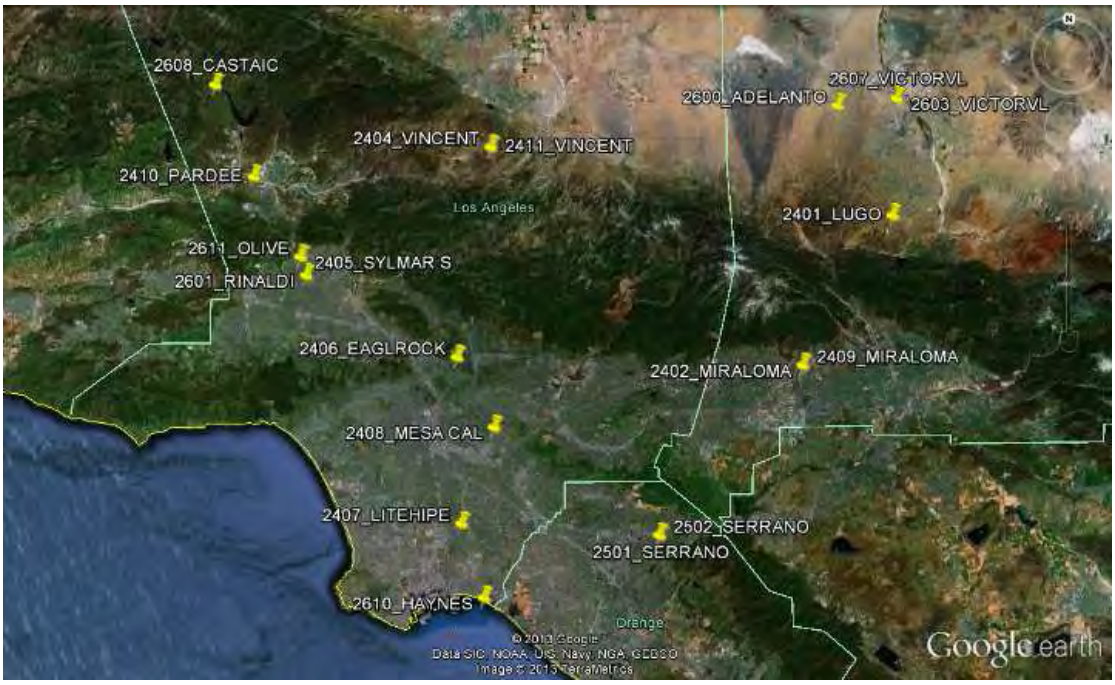

Figure 6.13 Location of Lugo (2401) and Mesa Cal (2408) [Google Earth]

Hourly time series data for these 2 sites were modeled using SARIMA modeling using multiple year raw data input (2007-2009) from [92] and [148]. The wind and solar resource characteristics of the two sites are shown in Figure 6.14 and 6.15. They graphically depict the wind speed and solar DNI data through their five-number summaries: the smallest observation (sample minimum), lower quartile (Q1), median (Q2), upper quartile (Q3), and largest observation (sample maximum); also shown in the figure are the hourly means and modes. These give an idea about the inherent variability of the wind speed and solar DNI resources at a location, thus reinforcing the premise of using stochastic approach to model them.

Using the MLE method of model parameter estimation and MWRAM explained in Chapter 4, the seasonal hourly parameters of wind speed (λ, k) and solar cloud cover (α, β) were determined. The maximum likelihood estimated parameters for the Weibull (wind) and the Beta distribution (solar) were determined for each of the 24 1-hour segments for 1 day for each of the 4 seasons; thus we get a (24×16) matrix which contains the vectors λ_t, k_t, α_t and β_t, where $t \equiv (i, j)$ denotes season i $(i = 1 \ldots 4)$ and hour j $(j = 1 \ldots 24)$ for each site. These parameters are shown in Figures 6.16 and 6.17 for Lugo and Mesa respectively.

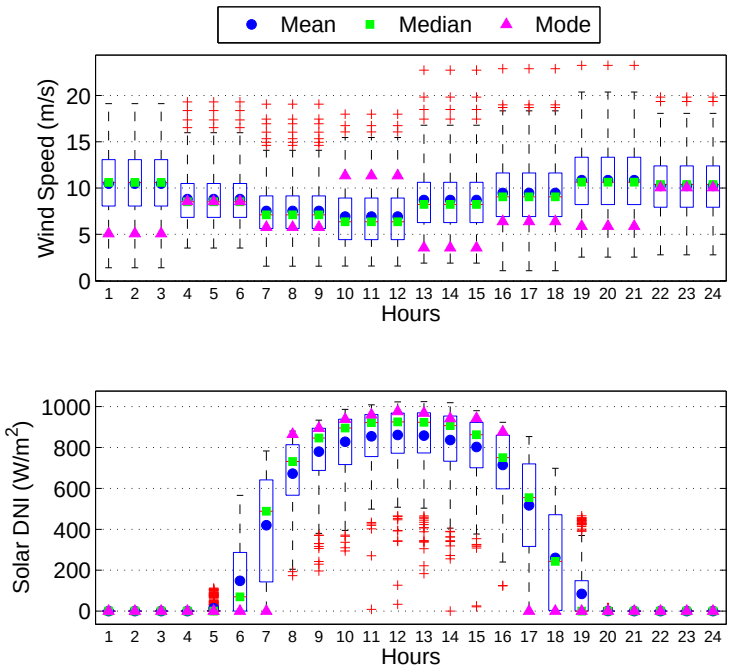

Figure 6.14 Wind/Solar Resource Characteristics for Site Lugo

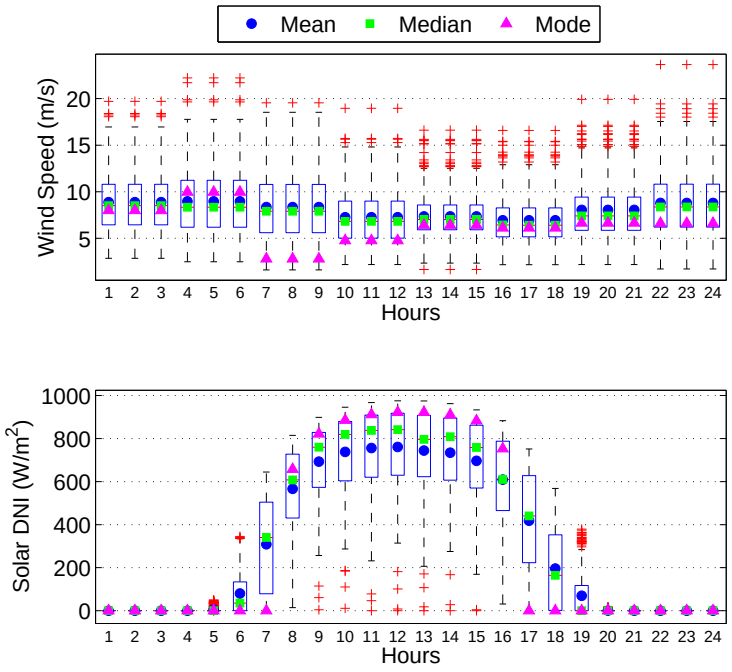

Figure 6.15 Wind/Solar Resource Characteristics for Site Mesa

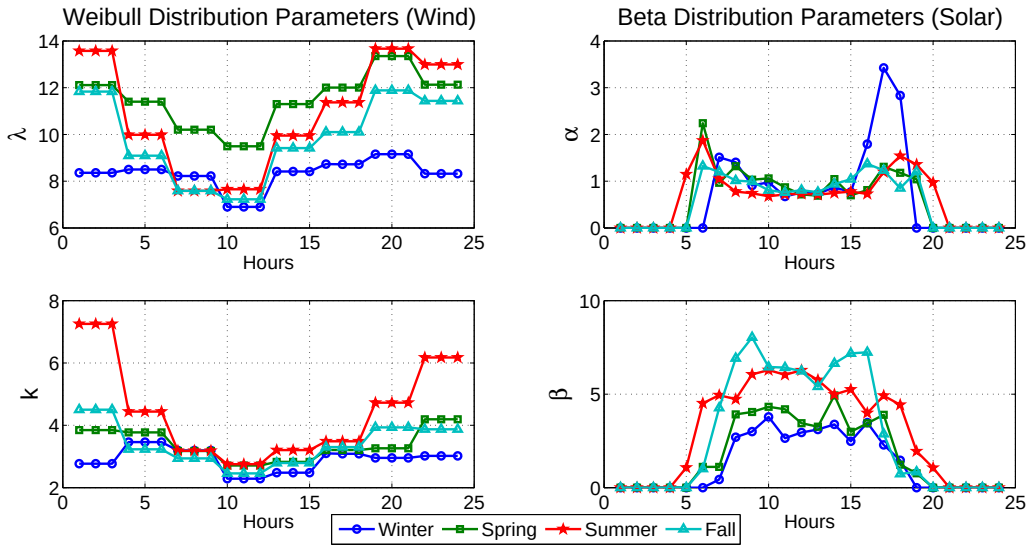

Figure 6.16 MLE Parameters for Site Lugo

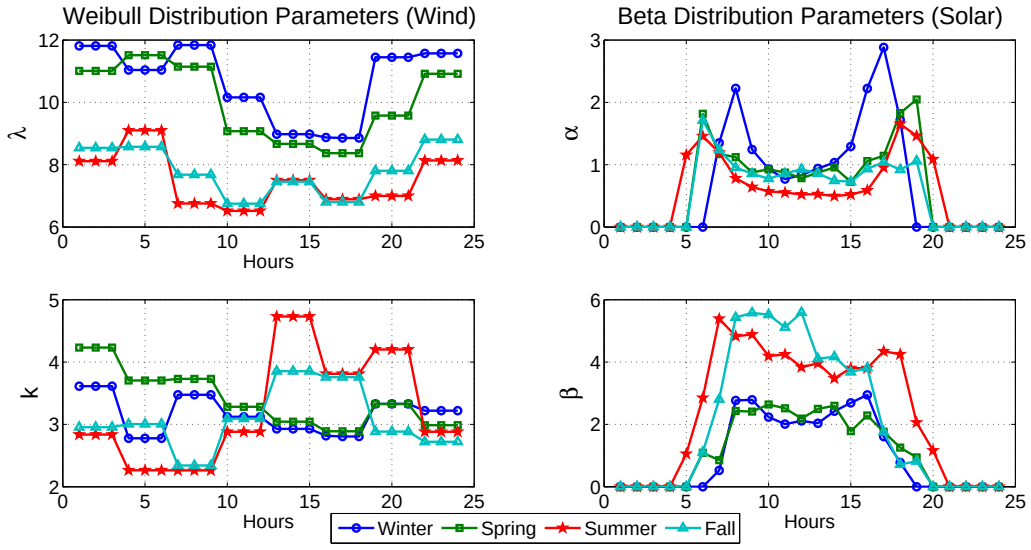

Figure 6.17 MLE Parameters for Site Mesa

The optimization routine explained in Chapter 4 was used here to determine the optimal sizes and ratings of the HECSs at Lugo and Mesa. The input wind speed and solar DNI resource are the mean values as shown in Figures 6.14 and 6.15. The different cost parameters, financial rates etc. are the same as used previously (Table 4.2). The load profile that was fed as input was determined from the load data as given in [138]. It was scaled accordingly to reflect the regional load profile for the 2 locations. The peak values of the load profiles considered to be supplied by Lugo and Mesa were assumed to be 420 MW and 280 MW respectively. The Pareto-optimal fronts evolved using genetic algorithm approach for bi-objective optimization problems for the 2 sites are shown in Figure 6.18. Keeping both the capacity factors fixed at 40%, the different system sizes and corresponding ratings are shown in Table 6.3. These ratings are used in MVRAM for steady state voltage security assessment in the next section.

Table 6.3 Selected Pareto Optimal Solutions for Lugo and Mesa

Variables/Objectives	Site Lugo	Site Mesa
A_w (m^2)	1.10E+06	7.62E+05
A_s (m^2)	14.20E+06	9.01E+06
Annual Cost ($/year)	3.70E+08	2.35E+08
Capacity Factor	40.0%	40.0%
$P_{w,max}$ (MW)	360	240
$P_{s,max}$ (MW)	230	145
$P_{h,max}$ (MW)	590	385
Peak Load (MW)	420	280

6.4 Grid Integration Effect on Voltage Stability

The 240 bus WECC system is used to obtain static data for the region being considered. The study region is restricted to Southern part of California (comprising of Southern California Edison and LADWP areas) region of the system (Figure 6.19). All buses over and above 20 kV are modeled.

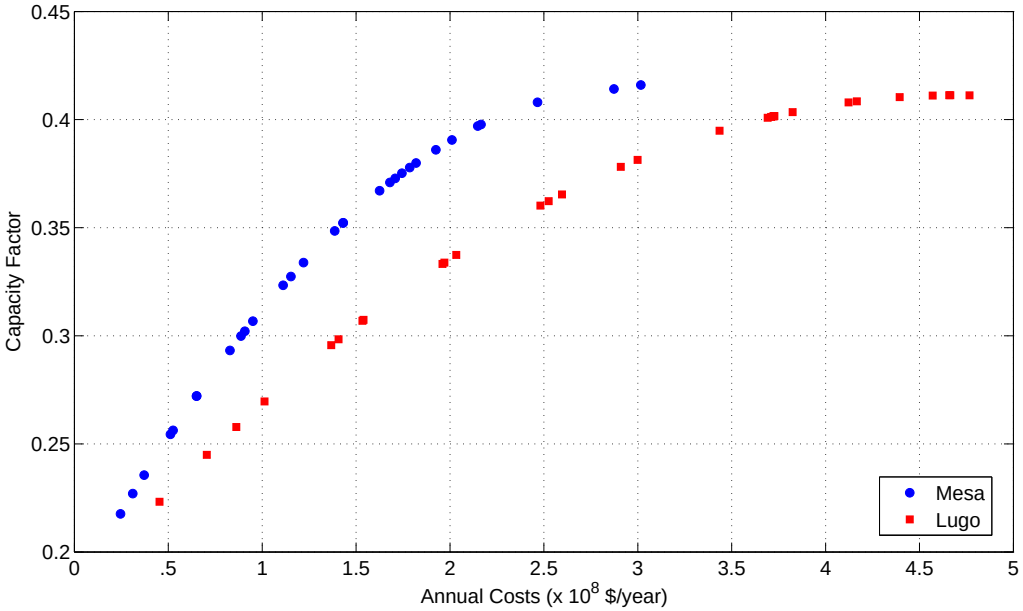

Figure 6.18 Optimal Pareto Fronts for Lugo and Mesa Sites

In the following section, a static analysis of the system is conducted to analyze the impact of the additional reactive capability. The two HECSs are connected to the system at buses 2401 (Lugo) and 2408 (Mesa Cal), with the ratings as derived from the previous section (Table 6.3). The two buses are circled in Figure 6.19 in green. Three load buses in the system are monitored. The monitored buses are 2612 (Rinaldi), 2608 (Castaic) and 2609 (Glendale). The three buses are circled in Figure 6.19 in yellow. The inherent variability of wind and solar resources raise concerns about the effectiveness of a HECS to enhance system reliability. Also, the interaction between the resources and demand - the inverse nature of diurnal load and wind variation and the direct nature with solar profile plays an integral role while examining system reliability.

Five cases are considered in the PV analysis. The base case, with the system as it exists without the two HECSs at Mesa and Lugo. The other four cases correspond each with varying resource conditions with respect to wind-solar power availability as fraction of their rated output, namely high-high, high-low, low-high and low-low.

The system described in Figure 6.19 is utilized to conduct a static transfer analysis. The

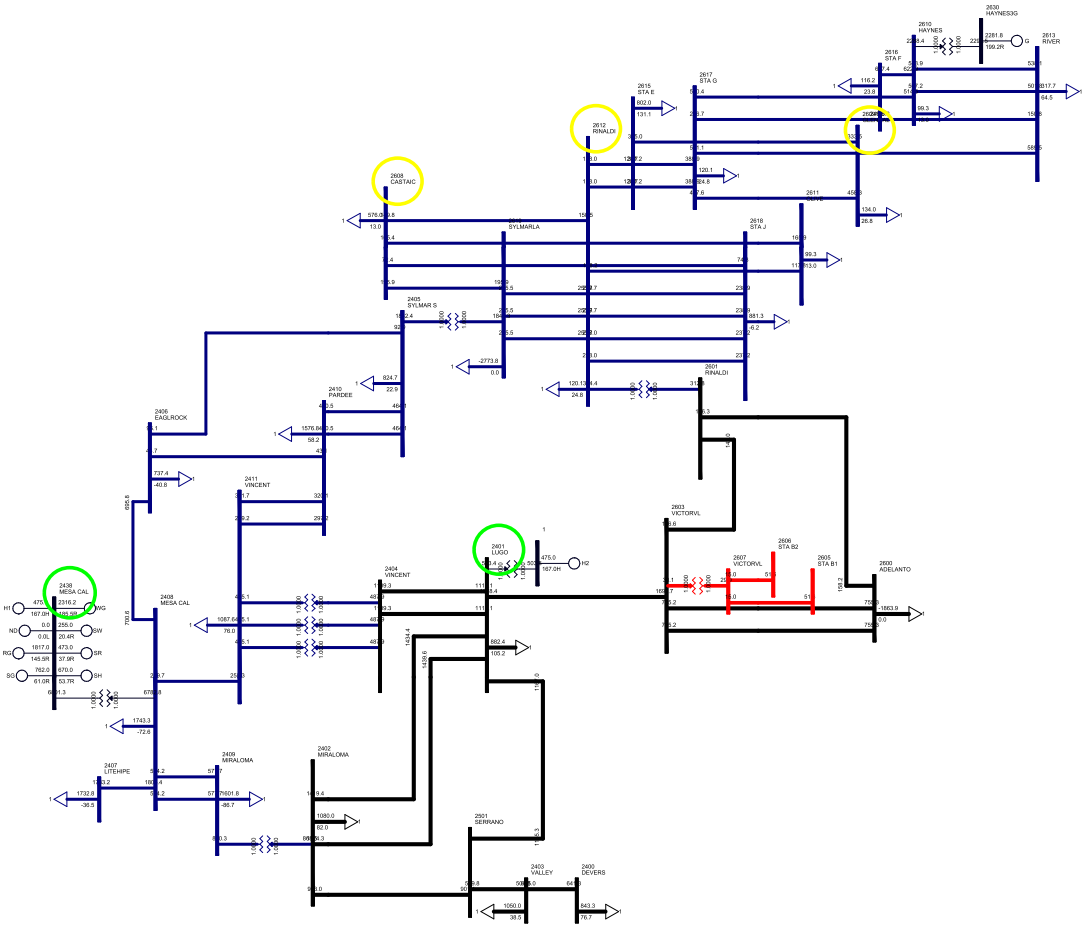

Figure 6.19 SCE and LADWP Area in WECC

initial load level in the area is maintained at 16625 MW. The load is increased while maintaining a constant power factor.

The voltage criteria used for the system is that all pre-contingency voltage should be above 0.95 p.u and below 1.05 p.u. on all buses over 115kV. For post-contingency scenarios, the minimum voltage is extended to 0.9 p.u. and the maximum voltage is increased to 1.1 p.u.

All line out contingencies are considered. PSS/E is the tool used to carry out the PV analysis [149], [150]. The most restricting contingencies are screened and ranked. Of the three buses monitored, bus 2608 (Castaic) is the most susceptible to low voltage violation. Of the contingencies considered, the most restricting contingency is the loss of the line from 2406 (Eagle Rock) to 2408 (Mesa). The PV analysis is done for five cases, namely high wind-high solar (95%-95%), high wind-low solar (95%-5%), low wind-high solar (5%-95%), low wind-low

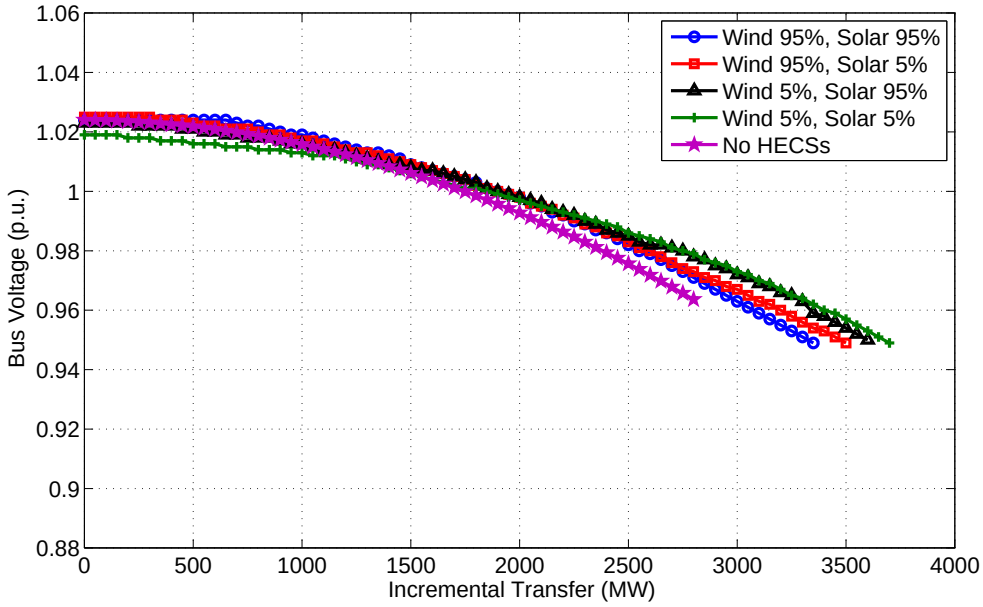

Figure 6.20 Pre Contingency Voltage Variation (Bus: 2608 (Castaic); Contingency: Line 2406-2408)

solar (5%-5%) and no HECSs present.

Figure 6.20 demonstrates the pre-contingency voltage at Bus 2608 bus as the load is increased. The voltage criteria used for the system is that all pre contingency voltage should be above 0.95 p.u and below 1.05 p.u. With no HECSs present, the maximum loading without any voltage criteria is 2800 MW. The maximum incremental transfer between the two zones - the source and the sink with both the wind and solar generation at 95% output is 3350 MW. The maximum incremental transfer possible with the wind and solar generation at their low level, i.e. 5% is 3700 MW.

Figure 6.21 indicates the voltage variation at bus 2608 (Castaic) bus for the five different cases. The voltage criteria used for the system is that all post contingency voltage should be above 0.90 p.u and below 1.10 p.u. The first voltage violation in the post contingency scenario occurs for the case without any HECSs at 2750 MW. The post contingency voltage dips below 0.9 p.u. after this load level. The maximum incremental transfer ranges from 3100 MW (high-high) to 3500 MW (low-low).

Depending on the proximity of the HECS to the load center, it can be seen that the

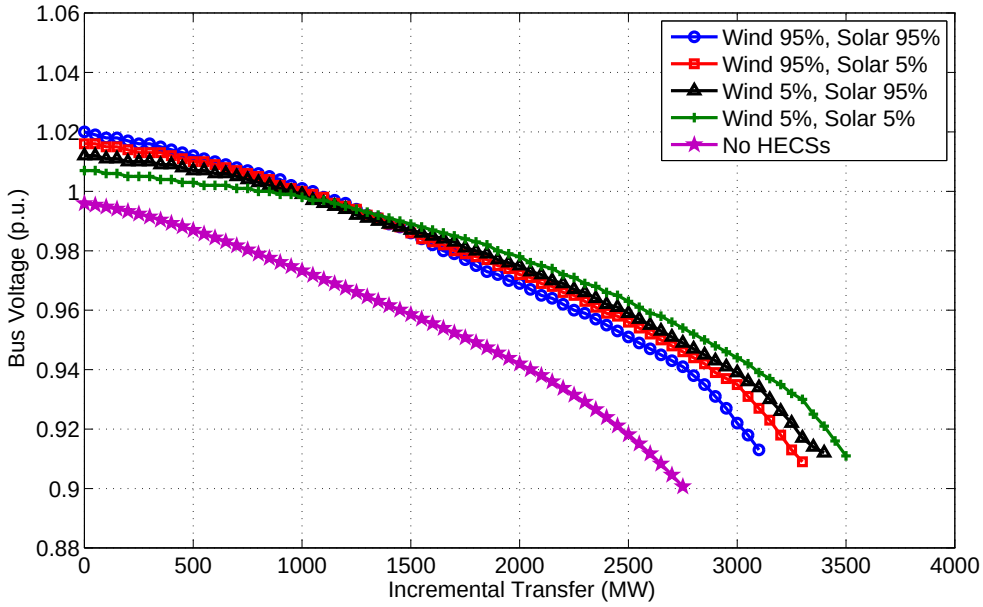

Figure 6.21 Post Contingency Voltage Variation (Bus: 2608 (Castaic); Contingency: Line 2406-2408)

additional reactive power available at low wind speeds and solar irradiance levels allows for more loads to be served. In this example, the additional transfer capability provided by the HECSs at low output in this case is about 400 MW. Thus at low wind and solar levels, the transfer margin is increased by nearly 12.9%. This is especially important because at peak load levels on the system, the wind speeds are generally minimal - in these two cases, the transfer margin is increased by 300 MW and 400 MW respectively.

The above analysis indicates that even though wind power and solar power generally peak at different periods of relatively low and high loads respectively, the incorporation of the capability curve of the HECSs can enable the load areas to meet higher demands of power reliably. If the capability curve were not employed, then to reliably serve the load, additional system modifications in the form of either transmission lines or reactive devices will be required. The use of the capability curve in this analysis thus demonstrates the cost savings for the power system by utilizing the capability curve.

6.5 Summary

Being seasonal, current independent standalone solar and wind systems cannot provide continuous source of energy without having maintaining enough storage or reserves. By integrating and optimizing the complementary solar and wind systems, the reliability of the systems can be improved, reserve requirements reduced and the unit cost of power can be minimized. Selection of areas that have some of the strongest, most consistent on-peak winds and sun resources is very crucial for the successful development and deployment of HECSs. In this chapter, the developed HECS ID Tool, MWRAM and MVRAM methodologies were implemented on a large WECC system and their performance validated. An integrated ArcGIS-MATLAB based visualization platform to facilitate the siting of HECS was developed. The ranking of the locations which had energy resource above the minimum required were based on their different levels as well as their correlation. The MLE parameters which represent the stratified modeling of the wind and solar characteristics of a location were tabulated and the optimal sizing at each location considering the locational energy demand profile and resource assessment were determined. The application of MVRAM was also demonstrated here, and the potential benefits of relaxing the restricted power factor operation on wind and solar generation were shown. However, it should be noted over here that voltage stability being a local issue, and reactive power not being able to travel far, the location of the HECSs will affect the efficacy of the excessive reactive capability. The major reason behind this is the distance of the renewable resources from the load center and transmission bottle necks.

Also, it is worth mentioning that under the purview of a balancing authority (for e.g. an ISO), there will be multiple locations having HECSs connecting to the grid. These are connected to the grid at different locations each having their own local wind and solar resource profiles. The integration of these resources over a wide area leads to a less variable energy output that is fed into the power system. Also, the weather fronts will not be affecting these different HECSs in the same way, i.e. a low wind front will not affect all the WECS, and likewise a cloud cover might affect the solar output of a single or part of STECSs, but overall STECS output will be less affected.

CHAPTER 7. CONCLUSIONS

7.1 Summary of Work

The depletion of fossil fuel reserves makes it an imperative task for future researchers to stimulate new and alternative ways to meet society's growing energy needs. This thesis addresses the integration of hybrid renewable solar and wind energy sources into the power grid.

In recent years, it is becoming clear that between wind and solar, one source most often does not outperform the other. Instead, there exist seasonal benefits to each source. It has been determined that both wind and solar have compelling benefits within their seasonal range. A wind-solar hybrid system is fully integrated and designed to provide improved system efficiency. Throughout the seasons, hybrid systems provide a balance and increased energy production when both wind and solar energy are available.

This work investigates the technical feasibility of the development and deployment of renewable hybrid energy conversion systems using wind and solar resources. Historical solar irradiance and wind energy density information was analyzed to provide suitable hybrid locations. Models were developed for wind, solar, and reserve technologies for power system simulation studies. Meteorological and economic data were used to determine the optimal requirements of thermal, wind, and grid connections. Long term voltage security was evaluated iteratively through system studies and contingency analysis.

Chapter 3 dealt with resource identification and establishing candidate locations from favorable wind and solar resources with an extensive survey of wind flow and solar irradiation data across United States. The survey included overlaying transmission line routes with the identified favorable resources to determine realistic interconnection locations. The correlation

between the wind and solar profiles at a given location were analyzed to give an initial estimate of the wind-solar mix in the ECS.

Chapter 4 dealt with developing the MW Resource Assessment Model or MWRAM. It is a systematic stochastic planning approach for assessing the MW resource availability of a hybrid energy conversion system with wind and solar resources for a given location. The study period of one year was divided into four seasons; one day in each season was further divided into 24 1-hour time segments. This "stratified" approach captures the varying nature of the resources over different times of the day as well as the year by explicitly computing the probabilistic model parameters from actual field measurement data using MLE method. These parameters defined the MW output of the ECS using a transformation theorem. The effect of varying renewable energy penetration on the resource assessment was demonstrated by fixing the penetration ratio level at 10, 20 and 30%. The MWRAM can be used to study the influence of different parameters such as cut-in speed, rated speed, furling speed and power rating of the wind turbines, the efficiencies of the heat exchanger, steam turbine and electric generator, ratio between the HECS rating and maximum load, availability of hardware - all of which have a bearing on the energy potential of the system. It also dealt with the optimal design of a HECS employing renewable energy sources - wind and solar. The primary concern is the accurate selection of system components that can satisfy the load demand in an economic, reliable and environmentally responsible manner, while being subject to physical and operational constraints. A multi-objective optimization problem was formulated, different solvers were explored to solve it and Genetic algorithm was chosen to solve it. The sizing issue adheres to the following objectives - minimizing the cost, maximizing the capacity factor while maintaining resource adequacy. Sensitivity analysis to various input data to the optimization routine was done.

Chapter 5 dealt with the grid connection issue and voltage security of the power system with high HECS penetration. The reactive power capability of the different generation technologies were assessed. The benefits of utilizing the full reactive capability as compared to the existing interconnection requirements was demonstrated. Resource variability was incorporated and remedial actions like redispatch strategies were defined.

Chapter 6 validated the models developed by testing them on a large system, namely the WECC system which has resources conducive for the development of wind/solar hybrid energy conversion systems. An integrated ArcGIS-MATLAB based platform was developed to study where the resource characteristics and availability. This combined approach provides an effective way to understand the power grid behavior with geographical details under different wind solar resource potential scenarios.

This work provides a comprehensive approach to develop and deploy a hybrid energy conversion system with wind and solar energy resources. It tried to address both the resource and system aspects of the HECS and grid connection.

7.2 Significant Contributions

This research has investigated the potential of developing hybrid energy conversion systems by combining the complementary nature of wind and solar energy. This work addresses the issue of increasing the use of renewable energy in the future grid from two aspects, namely (i) the resource point of view where the focus was the siting and sizing of a solar-wind hybrid energy conversion system where the strength of one resource can negate the weakness of the other and vice versa and (ii) the systems point of view where the focus was to interconnect with the grid and support and maybe enhance the voltage security of the system.

The specific contributions of the work in this dissertation are:

- **Hybrid Energy Conversion System Identification Tool (HECS ID-Tool)**
  - The Hybrid Energy Conversion System Identification Tool is a ArcGIS-MATLAB based tool which analyses the geospatial resource characteristics and availability of renewable resources. Analyzed solar irradiance and wind energy information along with electric substations and transmission line placements provided for suitable hybrid locations.
  - This combined approach provides an effective way to understand the power grid behavior with geographical details under different wind solar resource potential sce-

narios. Furthermore, it could help to develop new siting strategies to improve the resource allocation and adequacy of the emerging grid

- **MW Resource Assessment Model (MWRAM)**
  - The MW Resource Assessment Model is a systematic stochastic planning approach for assessing the MW resource availability of a hybrid energy conversion system with wind and solar resources for a given location. The "stratified" modeling approach captures the inherent varying nature of the resources over different times of the day as well as the year by explicitly computing the probabilistic model parameters from actual field measurement data using the MLE method.
  - This also leads to location based optimal HECS sizing and reserve management. Given the ideal hybrid locations identified within the US, optimal power plant sizes were determined from site-specific energy capture information.
- **MVar Resource Assessment Model (MVRAM)**
  - The MVar Resource Assessment Model is a mathematical approach for assessing the MVar resource availability (maximum and minimum limits) of a hybrid energy conversion system with wind and solar resources. An integrated reactive capability curve was developed for the HECS which will be very useful for system planners and operators to determine the available reactive power limits. For specific ECSs employing DFIG units or synchronous generators, the restriction on power factor can be lifted because additional performance may be obtained at no extra cost to the HECS owner. This work also demonstrates the enhanced steady state voltage security by using the capability curve over the current mandates - restricted $\pm$ 0.95 power factor operation or fixed reactive limits.
  - **Voltage Secure Region of Operation (VSROp)** - This voltage stability assessment tool incorporates wind/solar resource variability. It is very helpful in determining the sensitivity of the power system reliability to resource variability and also in assessing proper redispatch strategy for increased voltage stability margins. The

traditional methodology of drawing PV curves to assess static voltage stability margin is modified to address the intermittent nature of wind and solar energy. Given a range of resource variability, the developed tool calculates sets of PV curves plotted along parallel planes, thus giving a three-dimensional VSROp.

- **HECS Resource Map of WECC**
  - Renewable resource maps are among the most valuable tools to initiate state-based communication efforts about renewable energy development. A ranked resource map for HECS potential was compiled for the entire WECC area. The focus is to provide the renewable energy industry, policy makers, and other stakeholders with combined resource data and a quick initial assessment to effectively evaluate and develop HECS.

7.3 Future Scope

There needs to be enhancements to support the growth of renewable generation. Some of the enhancements include wind and solar forecasting tools (output, ramping requirements), more sophisticated grid monitoring systems, over-generation mitigation procedures, coordination with neighboring balancing areas, updating generation interconnection procedures/standards. Some of the market enhancements that need to be investigated include development of new market products and changes to market rules, increased regulation and reserve requirements, and more sophisticated day-ahead unit commitment algorithms.

The availability of accurate and reliable data on the cost and performance of renewable power generation technologies is a significant factor in the initial assessment of these renewable technologies. Without access to reliable information on the relative costs and benefits of renewable energy technologies, it is difficult, if not impossible, to arrive at an accurate assessment of which renewable energy technologies are the most appropriate for their particular circumstances. There is also a significant amount of perceived knowledge about the cost and performance of renewable power generation technologies that needs to be updated regularly considering the rapid growth in installed capacity of renewable energy technologies and the

associated cost reductions. Thus the development and maintenance of a national database of renewable energy resources is very important. Also, in most of the existing databases, only hourly data is provided. It is known that solar power can have large swings on shorter timescales. Therefore, this limitation may have important consequences. This effect is more important for solar PV rather than solar thermal because of the heat inertia.

Most of the states in the US have set RPS goals of serving a portion of its electric load with renewable energy by 2020; however, transmission is a major barrier to achieving this goal. Renewable resources are location constrained. They are often far from the grid and load centers, requiring extensive and expensive transmission upgrades. In order to achieve cost-savings through economies of scale, and to limit environmental impacts and ultimate build-out time, large transmission projects are needed to access large geographic areas of developable, economic renewable resource potential. There were several areas found which have very good resource potential but not with the defined proximity range of the existing and future transmission grids. It will be very interesting to explore that and do a cost-benefit analysis or comparison between several sites - some close to the transmission but less resource rich, while some far from the transmission, but extremely rich in energy density. It might so happen that even after considering the added cost of building transmission for those locations, in the end they might be more fruitful.

The VSROp is a useful tool for large practical systems. But to accurately carry out the analysis detailed information of the reserve generator's location and their capacities must be available. With the deregulated market environment, even though the large system data was available, the details of the generating units on the system, in terms of their fuel type and ramp rates are not available.

The current work deals with large wind and concentrated solar power elements. However, the developed methodologies are flexible and can be easily extended to include solar PV (photovoltaic) which is increasingly being developed now in the utility scale. The three components of irradiance most critical for determining solar installation production values are Global Horizontal (GHI), Direct Normal (DNI), and Diffuse (DIF). Fixed panel photovoltaic installations are dependent on GHI, or the total amount of radiation received by a horizontal surface. Con-

centrated solar power projects and PV tracking systems rely predominantly on DNI, which is the total amount of radiation received by a surface that is always kept perpendicular to the sun's direct rays. Unlike solar thermal which use reflective surface to concentrate sunlight, solar PV use semi-conductor technology to directly convert sunlight into electricity. Over the last few years, PV technology has made some great advances as a result of significant utility commitments. By incorporating the solar GHI characteristics and the inverter modeling for the solar PV, the existing hybrid scheme can be extended to include solar PV also.

APPENDIX A. ASPECTS OF CO-LOCATING CONCENTRATING SOLAR POWER AND WIND

Introduction

In this section, different aspects of co-locating wind and concentrating solar power (CSP) resource plants are discussed. The solar projects need not be on the same property as the wind farms, but they will be close enough, upwards of a weak transmission path to test whether there's a benefit to locating two renewable energy sources near each other. One potential savings of such a layout is that only a single connection might be needed to the power grid; it might be possible to bring on more renewable energy by sharing existing transmission infrastructure or by marginally enhancing the transmission system in the resource rich areas which are generally far from high density population areas.

In certain locations within the United States, two (or more) renewable resources may be co-located to take advantage of temporal synergies, including both daily and seasonal fluctuations [151]. Wind and solar are intermittent resources that can interact synergistically in locations where solar energy peaks during daylight hours and wind energy peaks during late-night hours. Meteorological conditions may also create synergies between solar and wind power, such as in areas of the country where low barometric pressure fronts create more windy and cloudy conditions, and stable, high-pressure conditions create sunny, stagnant conditions. Co-location might also help renewable generation located in remote regions. The California Renewable Energy Transmission Initiative has looked at the use of Competitive Renewable Energy Zones (CREZs) to aggregate projects based on their physical location and shared transmission needs [152]. Significant progress has been made in Texas's CREZs, and recently specific projects have been purposed to take advantage of the new transmission structure. The issue of co-locating

renewables was also the subject of the NREL Western Wind and Solar study looking at the costs and operating impacts due to the variability and uncertainty of wind, PV and concentrating solar power (CSP) on the grid [153].

Unpredictable variations in power output from renewable energy sources such as wind and solar can cause problems for electrical grid operators [154]. Electrical power generation must match load to maintain the stability of the electrical grid. Currently this balancing is typically done by fast-ramping gas turbines distributed throughout the grid. However, reducing those variations at the source has potential benefits in some scenarios. On longer time scales, reducing power variations allows more efficient use of transmission capacity [155]. On shorter time scales, reducing rapid changes in power output helps to maintain the stability of the grid [156]. Some methods for reducing power variations, such as energy storage, can also help the grid recover from faults and other transient events. Finally, variable energy sources in small, isolated grids or locations with weak transmission access must have their variability tightly controlled to match the load, and may require co-located smoothing services.

Over periods of hours or days, large variations in wind and solar power cause the transmission lines connected to them to be under-utilized. Transmission lines are typically built for the maximum power output of a generator, but wind and solar installations output their maximum power less than 30% of the time. There are some ways for a variable resource to more efficiently use transmission line: either store some energy to be transmitted at less-congested times, co-locate the renewable generator with a conventional generator, build a transmission line with a capacity less than the maximum generator output and occasionally curtail some power that cannot be transmitted, or build the wind or solar plant closer to load that would be less optimal from a power generation standpoint.

The primary barrier to implementing the strategies is cost. Some of the strategies have very high capital costs but low operating costs. For example, batteries are very expensive to purchase but cheap to maintain. Similarly, building widely separated solar collectors requires investment in long electrical cables to connect them, but requires very little operating cost. Other strategies have low capital costs but high operating costs. For example, the power output of a wind farm can be curtailed at no cost by changing some settings in the software

that controls the turbines, but the owner loses revenue when the turbines capture less than the available wind. Similarly, a gas turbine is relatively inexpensive to install (compared to other types of power plants), but the natural gas fuel is expensive.

The strategies can be implemented be requiring their adoption through policy mandates or by offering incentives. Grid operators are acknowledging the increasing renewable energy penetration by beginning to write grid-connection rules that address the variability of renewable resources. The existing grid connection rules for wind and solar power were written when the penetration of variable renewable resources in the grid was so small that it did not affect the electrical grid majorly. The level of renewable energy has increased rapidly, fueled mainly by federal and state subsidies and Renewable Portfolio Standards (RPS). Grid operators in areas with significant penetrations of wind power, such as ERCOT (Texas), Germany and Ireland now require that new wind farms be able to limit the rate of power increase and be able to decrease their power output or "spill" wind to regulate the grid frequency and also provide voltage control mode of operation at times when reactive support is required.

Currently, solar and wind resources within certain balancing areas are not responsible for energy market imbalance charges created by their variable output , hence they have no reason to incur the extra cost of minimizing variability. There must be a robust transmission network to allow the benefit of geographic diversity to be realized. Even with this in place, there is a significant effect on voltage control of the interconnection circuit caused by rapid changes in output. Solar and wind must be "good neighbors" and not create voltage flicker or other power quality issues. Market and government incentives can and should encourage power plant operators to reduce the variability of their power output. Markets can reward power producers by offering premium price for more stable power, or fine generators for unexpected variations (beyond a certain predefined tolerance bandwidth) in their power output. Many grid operators that set prices through market mechanisms have penalties for deviations from scheduled power output, but those penalties have not yet been applied to wind or solar power. Current government incentives for renewable resources (like production/investment tax credits for wind and solar respectively) do not address variability.

A lot of renewable energy developers are evaluating their wind projects for where a co-

located and co-interconnected solar project would increase capacity factor and transmission line usage efficiency as well as decrease sub-hourly intermittency. EDF Renewable Energy has dedicated the 143 MW Catalina Solar project in Kern County, California. The project is located near the 140 MW Pacific Wind project, a wind power project. The two renewable energy power plants were developed and contracted independently, but their close geographic proximity to one another enabled the projects to share certain infrastructure and thus evolve into one of the largest wind-solar hybrid projects in the US [157]. The combined generation plant will provide more balanced (and less intermittent) power to the grid. The project is positioned to take advantage of the new Whirlwind substation that Southern California Edison (SCE) is building as part of the Tehachapi Renewable Transmission Project (TRTP) for thousands of new wind and solar megawatts. Both will deliver electricity into the grid for San Diego Gas & Electric Company's (SDG&E) generation portfolio under two separate power purchase agreements. These new projects bring the total renewable energy capacity under long term agreements with SDG&E to 343 MW - all of which are generated in Kern County. Also, Element Power has announced for the Wildflower Renewable Energy Farm in California's Antelope Valley, an area that has some of the strongest, most consistent on-peak winds and sun resources in California. The site is 70 miles north of Los Angeles near transmission lines. The 250 MW farm would deliver 100 MW of solar and 150 MW of wind, enough to power more than 70,000 California homes.

Synergy between Wind and Solar Energy

There is a need to explore the opportunities, the advantages and the synergies between wind and solar.

(1) Solar is peak coincidental and wind is intermittent. Even more interesting is that in many areas, wind rises in both speed and consistency in the late afternoon and evening hours. Electric utilities and other purchasers of wind energy struggle with the dispatch of the electricity because of the intermittency of the resource.

(2) The vacant land in the near vicinity of wind farms is often flat (having low slope) and might also be located in regions with favorable direct normal irradiance (DNI).

(3) In most cases, wind owners and operators got to the power market first and have already done the initial bulk work, which includes securing land, entitlements and environmental clearances. They have negotiated amenable contracts with the surrounding community. Even more important, they have found a market for the power sales (power purchase agreement) and a means to get that power to the market (proximity to transmission and interconnection agreement).

Co-location of wind and solar generation substantially reduces the time and cost of planning and development. Solar developers typically start with land control and often assume that all the other critical details, such as power purchase and interconnection agreements, will work out. Wind asset developers already have these agreements guaranteed. Sure, the power purchase agreement and interconnection agreements are for a specific purpose and a specific plant capacity, but many a times there are a few wind projects out there that are under producing, thereby leaving a bit of latent capacity at the point of interconnection and a less than optimized power purchase agreement. The long list of siting permits [1] can often be re-purposed to accommodate changes. It is less expensive to re-purpose a permit with the agency having jurisdiction than it is to start from scratch. Another benefit is the agency having jurisdiction is familiar with the site conditions and may favor additional development at an existing project than a proponent seeking development of yet another facility. The other potential benefit to co-locating wind and solar generation is the ability to utilize the same point of interconnection for both generating types without increasing or modifying a large generation interconnection agreement (LGIA) or small generation interconnection agreement (SGIA) with an independent system operator or utility. Xcel Energy has recently adopted, and been a big proponent of, this approach through the use of what is called a net zero interconnection [158]. This way to collaborate and co-locate might lead to an optimal arrangement that could accelerate the return on investment (ROI) for the wind developer while reducing the installed cost for the solar developer. Viewing maps and graphs, whether global or that provided for the South Western states in USA, it can be noted that many regions have abundant solar and wind potential.

[1] for e.g., NEPA - National Environmental Policy Act, USACE - United States Army Corps of Engineers, FEMA - Federal Emergency Management Agency, FAA - Federal Aviation Administration, SHPO - State Historic Preservation Office, etc.

The smoother one can make the output, the smaller the storage system needs to be to shave the peaks and fill the valleys in output, turning intermittent into highly valuable base load. Battery and other grid storage techniques are in their infancy and are still very expensive. Using techniques such as co-located sources and geographical distribution to reduce the degree of intermittency means the storage capacity and therefore cost is minimized.

One of the big mitigating factors of renewable intermittency is the variety of technologies and the way they complement each other. It is not that geographical distribution alone can solve the whole issue of intermittency, it is just one of the stronger mitigators of intermittent output. Thus, additional mitigating factors like co-located complementary technologies are being discussed. Wind and solar are a highly complementary pairing, they naturally play off each other in that there tends to be more wind at times with less sun and vice-versa so the size of the battery storage needed and the need to run a generator can be both significantly reduced by combining these two technologies.

Potential benefits of co-locating Wind and Solar

Wind and solar have different power generation profiles that depend on the weather and other factors. Both require backup power or energy storage to smooth out generation peaks and valleys. Wind is more comparable to a base-load power source because it can generate power 24 hours a day. Solar, on the other hand, generates power only during the daytime hours, making it a perfect peak power source. This does not make one better than the other necessarily; it means that they complement each other quite well. Thus the combined generation could play a very crucial role in a more firm output and filling some of the power peaks and valleys.

The potential benefits of co-locating wind and concentrating solar power (CSP) plants have been analyzed and discussed in [35]. Using a location in western Texas as a case study, the authors demonstrated that such a deployment strategy can improve the associated transmission investment. However, adding transmission constraints reduces performance and the ability of CSP to provide maximum output during periods with high demand and wind. Even with thermal energy storage option, there could be extended periods of high wind and solar resource, resulting in curtailment. Despite these limitations, the authors determined cases in which a

mix of CSP and wind were justified by market revenues. It was shown that if the plants were flexibly configured, deployments with up to 67% CSP on a capacity basis yielded a positive net ROI. However, these findings depended on a reduction in CSP costs and deployment economics which were sensitive to transmission costs, which have varied in the past. The analysis in [35] represented a snapshot of deployments in historic market conditions. Escalation in conventional generation costs, carbon restrictions, and other factors would increase the value of these deployments. While some of the value of dispatchable CSP is captured by the capacity payment, additional values of dispatchable energy, such as the provision of ancillary services, could increase revenues. Although the authors focused only on Texas, there are many parts of the world that have co-located solar and wind resources for the type of combined deployments - other parts of the southwestern U.S., northern Africa, the Arabian peninsula, the Tibetan plateau, northern Chile, Australia, etc.

The authors in [159] evaluated the opportunity to load co-located wind and solar generation capacity onto a constrained transmission system while engendering only minimal losses. It also quantified the economic and energy opportunities and costs associated with pursuing this strategy in two Texas locations - one in west Texas and the other in south Texas. It was determined that solar generation can be reasonably accommodated within transmission systems already constrained by existing wind generation while experiencing only minimal energy and economic losses, especially when the solar and wind generation is negatively correlated, such as when solar generation is paired with inland wind generation in south or west Texas.

Renewable energy generation projects are viable when the revenue generated from selling the power is sufficient to cover the initial cost of the project development. Typically, the only place to sell power is to the electric utility that buys the power at their incremental cost of producing power, and then sells it at their standard retail rates. Renewable energy producers could make significantly more revenue by instead selling their power directly to an energy consumer. In a deregulated environment, the energy is transported on the utility's transmission facilities and the producer is required to pay transmission costs. This is possible in a few states where energy is still deregulated. However, in the vast majority of states, this is not possible. As an alternative, one can co-locate the energy consumer with the energy producer. The current

renewable energy credits that are given to new producers of renewable power can be so high that the revenue from selling the power to the utilities is actually greater than the retail utility rates. Clearly in the short term, it is simply better in those cases to simply sell to the utility, however it is generally recognized that this is a short-term phenomenon - having a local retail customer insulates one from the whims of government incentives and provides a long-term revenue stream.

New large wind and solar plants present particular challenges to the transmission system. One is that wind and solar power plants must be located where the renewable resource is sufficient, and this location may be far from any existing transmission lines and far from electricity users. This is in contrast to fossil-fueled power plants, for example, which can be sited near existing transmission and/or electricity users. Variable generation resources such as wind and solar are often located in remote locations with weak transmission connections. It is not uncommon for wind plants and solar sites to have short circuit ratios (i.e., ratios of three-phase short circuit MVA divided by nominal MVA rating of the plant) of 5 or less. Voltage support in systems like this is a vital ancillary service to prevent voltage instability and ensure good power transfer. Transmission system operators consistently express concern about managing wind and solar variability but adjacent projects makes the task somewhat simpler. Studies show that wind and solar generate at different times; wind might feed the transmission system 30% to 40% of the time. When one layers in the solar, that puts more power onto those same lines.

In many areas, wind resources may generate disproportionately at night during load valleys, and may provide relatively little generation on the hottest summer peak days. Solar generation has the opposite patterns. Solar generation closely follows the diurnal cycle, thus allowing solar resources to closely complement changes in load. As wind generation is ramping down during late morning, solar generation ramps to peak at noon and then tails off with load in the late afternoon. Wind output then resumes higher levels of output during evening and early morning hours [34]. Therefore, wind and solar resources together can provide a somewhat constant power source to serve load [160]. In addition, the variations in both solar and wind resources can serve to reduce overall transmission system volatility, much like aggregating

wind resources over wider geographic areas. It should however be noted here that wind and solar resources do not have coincident peaks, and therefore the two resources may not offset variability as substantially as when aggregating just wind resources across a wider geographic region. Consequently, transmission lines that access both robust solar and robust wind areas can tap this diversity to benefit from relatively constant output from intermittent resources and reduced variability across the system.

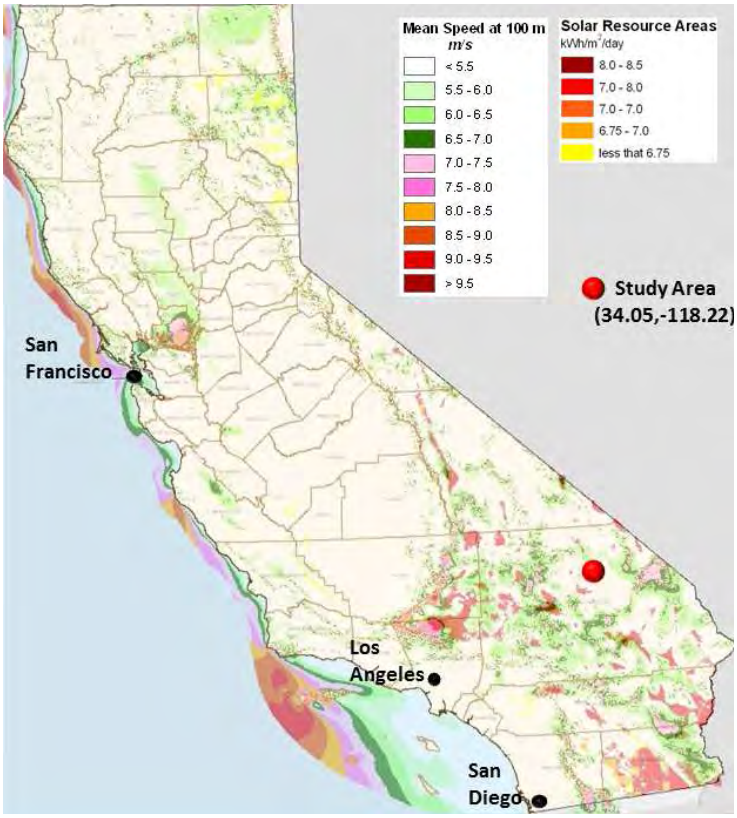

Figure A.1 Average daily DNI of locations in California with good wind resource

Sample Test Location Study

We simulated the wind and solar resource at a location in east CA (Co-ordinates 34.05, -118.22 W; Figure A.1) that is studied over the years 2004-2006. Resource data for several point resources around that location were gathered and analyzed for the following sections. One of the main synergies between wind and solar corresponds to the negative correlation that exists between real-time wind and solar resource availability (Figure A.2).

Substantial transmission capacity has been added to access these resources and further transmission expansion is in the planning stages. However, the capacity of wind exceeds the transmission capacity, resulting in some wind curtailment. Given the variability of the wind and solar resource, and relatively low capacity factor, transmission built for either wind or solar stand-alones will often be underutilized. Figure A.3 illustrates a week of simulated wind and solar data in January 2004 on a transmission line sized at the peak output of the wind or solar

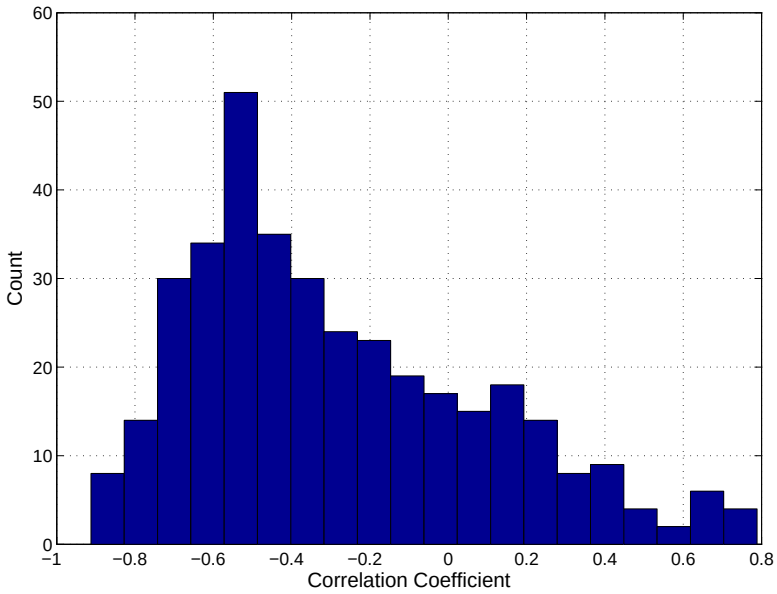

Figure A.2 Histogram of Daily Correlation Coefficient Values

plant. The average generation duration curve for the simulated wind and solar plant in east CA (Figure A.1) that is studied over the years 2004-2006 is illustrated in Figure A.4. It is assumed that the facility feeds into the grid on a radial transmission line and various combinations of wind and CSP are deployed with different amounts of transmission capacity.

In figure A.4, the total rating of the plant is set at 500 MW, for wind and solar standalone, and for the hybrid, 250-250 MW. The utilized transmission capacity in each of the three cases are 41.3%, 30.9% and 44.3% respectively (as marked be the shaded area under the curves). For different combinations of wind and solar ratings, the transmission usage variation is shown in figure A.5. It can be seen that for some deployment configuration, the utilization of the transmission corridor from the HECS to the grid is increased by nearly 20%.

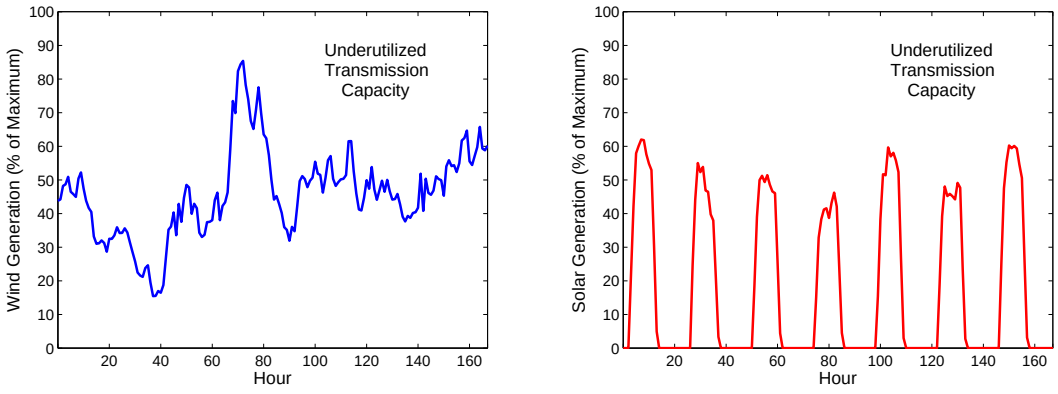

Figure A.3 Example simulated wind and solar output during a week period in January 2004 and opportunities to fill underutilized transmission capacity with other generation sources

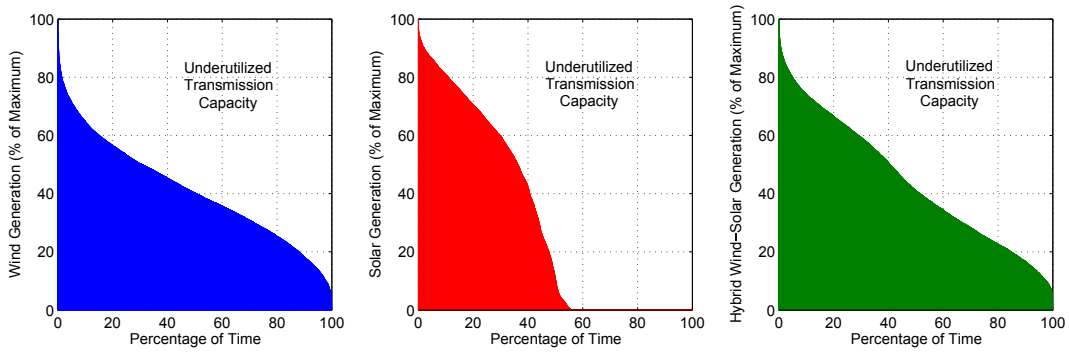

Figure A.4 Average wind, solar and combined generation duration curve during the years 2004-2006 at the location modeled; (Wind 500 MW; Solar 500 MW; Wind+Solar Combined 250 MW each)

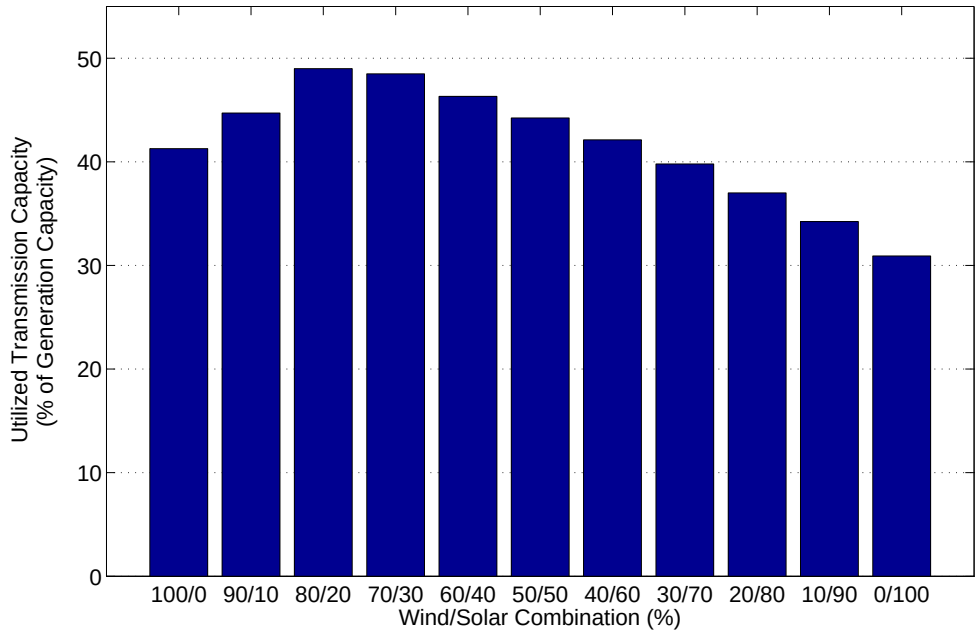

Figure A.5 Transmission Capacity (% of Generation Capacity) Variation for different wind/solar deployments; Transmission Limit 500 MW

We evaluate the opportunity to load co-located wind and solar generation capacity onto a constrained transmission system while engendering only minimal losses. For the purposes of this study, solar/wind co-located generation refers to the presence of solar and wind generating capacity upstream from a transmission constraint. It does not necessarily mean the solar and wind capacity is co-located on the same property or is operated jointly by a single project owner.

We developed a base case scenario which assumed the following parameters: Wind Capacity - 375 MW; Transmission Limit - 375 MW; Solar Capacity - 125 MW. The base case scenario assumes that when fully utilized, wind generation capacity alone reaches but does not exceed the transmission capacity limit in the study location. The additional solar capacity in the same location results in a combined wind and solar capacity which sometimes exceeds the assumed transmission capacity limit. However, because wind and solar generation have relatively low capacity factors and are not highly correlated, the amount of energy that exceeds the trans-

mission limit and is subject to loss through curtailment is only a small percentage of the total amount of energy produced by the additional solar capacity. The model quantifies total combined wind and solar generation as well as the amount of generation in excess of the assumed transmission limit. Since there is no transmission capacity available for excess generation, it will not reach a market, and will not generate any economic value.

Correlation coefficient is a measure that determines the degree to which two variables' movements are associated. It will vary from -1 to +1. A -1 indicates perfect negative correlation, and +1 indicates perfect positive correlation. Table A.1 presents correlation coefficients between hourly wind, solar, and between these variables and the load and the LMP. Wind production is weakly negatively correlated to solar application. Wind is also slightly negatively correlated to the LMP, but the solar application is more positively correlated with the LMP. Load and LMP are positively correlated which follows from the fact that the energy price goes up during periods of high demand.

Table A.1 Correlation of Wind, Solar, LMP and Load at Study Site

	Wind	Solar	LMP	Load
Wind	1			
Solar	-0.187	1		
LMP	-0.285	0.175	1	
Load	-0.469	0.382	0.405	1

Figure A.6 illustrates the complementarity by showing the dispatch of a deployment of the base case. Depending on the transmission capacity, there would more efficient usage as well as curtailment under some scenarios. The hybrid profile in summer show some negative correlation between wind and solar resource - wind is relatively high overnight when there is not solar and the solar peak lags the midday wind peak by few hours. Thus, adding CSP allows for greater transmission usage. However, the hybrid profile in spring shows that due to the extended high generation, the transmission capacity could lead to solar curtailment.

Figure A.6 displays total wind and solar energy production by hour, as well as combined wind and solar energy production, over the course of an entire year. The production data is displayed against a backdrop showing average LMP and SCE (Southern California Edison)

load. For energy price and load data, we used CAISO's marginal price of energy (LMP) data and CAISO's SCE system-wide load corresponding to zone SP-15. LMP or the locational marginal price data has been gathered from the market operator, i.e. CAISO for the balancing energy service prices for the CAISO SP-15 Zone [2].

Most modern electricity power pools use market based location pricing schemes [161], where electric energy prices generally increase during high demand periods. An economic strategy may easily be incorporated which would allow for hybrid plants to maximize profits, and it can be further enhanced by using some energy storage. The fact that the peak electric demand generally corresponds to the peak of solar generation during the mid-hours of a day may help the plant recover its initial investment quicker than independent renewable generation. From Figure A.6, it can be seen that the highest level of energy injected into the electricity grid can occur at times when the cost of the electricity is also high. This will help in early recovery of the high capital intensive installation cost required for such renewable energy generation systems and thus improve future investment opportunities in hybrid renewable generation which is necessary for large scale developments of hybrid plants.

The load data is from CAISO data set for hourly total system load on their entire system. Since the data was only used as a visual reference in graphs and not in any calculation, their exact values has no effect on any of the observations. Output limited by the assumed transmission limit is not displayed here. Some of the observations include:

- The negative correlation between wind and SCE system-wide load, and between wind and LMP, are readily observed.
- The combination of wind and solar thermal output appears to best fill the late afternoon valley in wind production, especially in the late afternoon when energy prices and system-wide loads are at their highest.

Figure A.7 displays similar data shown in Figure A.6, but in average values and also the assumed 375 MW limit (equal to the rated wind capacity (black line at 375 MW), the maximum

[2] Available from http://oasis.caiso.com/mrioasis/logon.do

annual hourly combined production. This figure shows the hours when combined generation exceeds the assumed transmission limit over the course of a year.

Figure A.8 presents the same data sets shown in the previous section, but narrows the display to each of the twelve months of the year. During the summer months (June - August), it shows that wind production tends to be lower than average during the peak month than the annual average while solar production tends to be higher. While some energy is limited in the base case scenario in the afternoon hours, the majority of curtailments occur in the morning (when wind is coming off its peak and solar is still ramping up). This suggests that the value of the energy lost due to curtailment is not as high as it would be if curtailment occurred later in the afternoon.

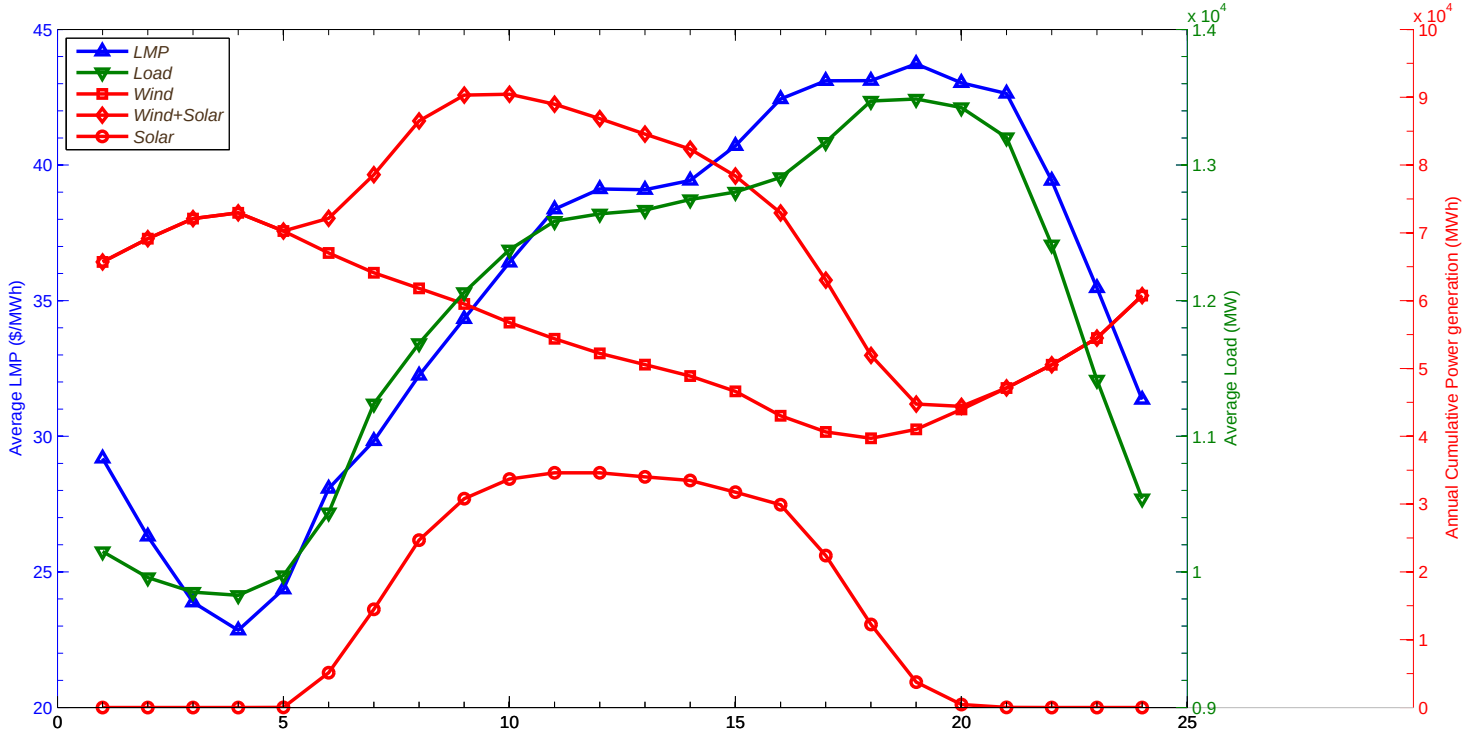

Figure A.6 Cumulative Annual Wind, Concentrated Solar and Combined Production by Hour for Study Site

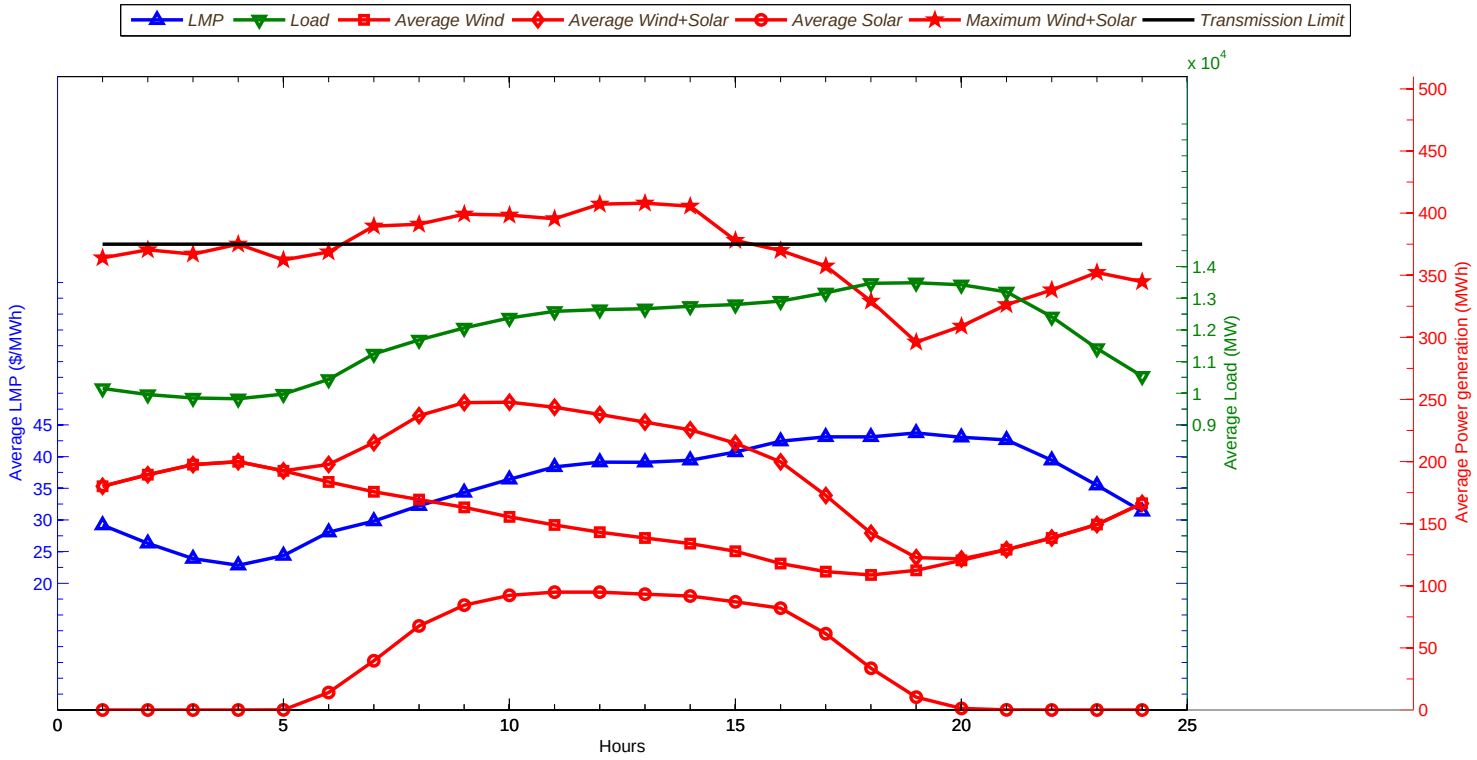

Figure A.7 Average Annual Wind, Concentrated Solar, Combined and Maximum Production by Hour for Study Site

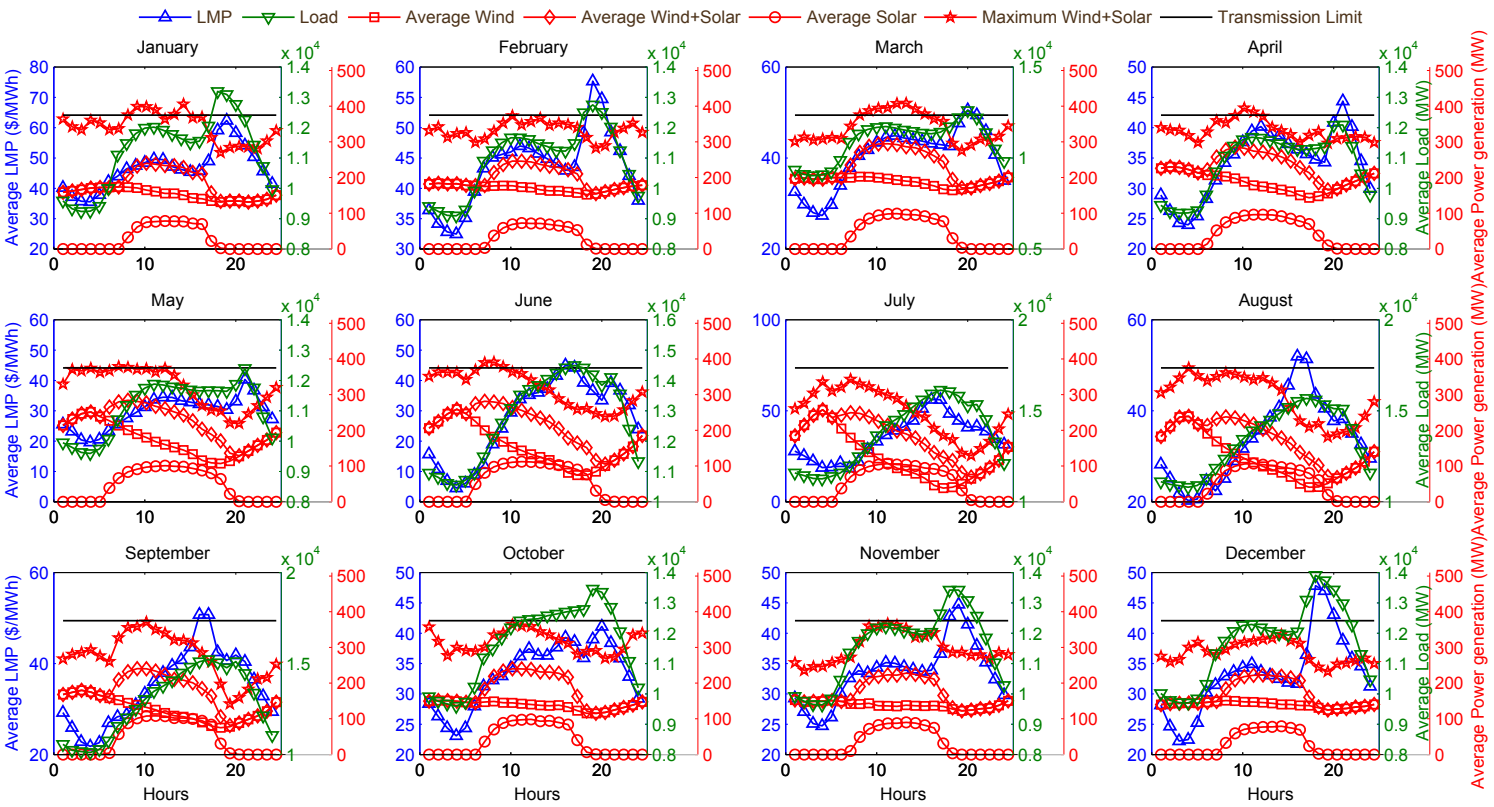

Figure A.8 Average Monthly Wind, Concentrated Solar, Combined and Maximum Production; Base Case: 375 MW Wind, 375 MW Transmission Limit, 125 MW Solar Capacity for Study Site

Capacity duration curves are graphical representations of all hourly data points in the generation data sets, and show the frequency of generation levels throughout the entire year. The time series data values are represented on contour graphs which display the days and hours during which the highest peaks in wind and solar and combined generation occur. Summary duration curves and generation contour maps are displayed and described in Figure A.9. The x-axis in the contour graph denote the 365 days of a year, while the y-axis denote the 24 hours in a day and the pixel color denotes the MW of wind or solar or combined power output.

Wind at the study site spans the full range of possible values during the year, resulting in a smooth distribution of generation values over the full range between 0 and 375 MW. It has a capacity factor of 41%. The peak wind production occurs during late evening and early morning hours which generally do not overlap with intervals with the highest energy prices prices. The modeled solar thermal power plant at the Site produces energy approximately 50% of all hours in the year. Because of the operational characteristics of the modeled plant, the plant is observed to achieve a 32% capacity factor, coming up to maximum production levels starting in the late morning in May through September and continuing to produce at full capacity late into the evening in all but winter months. As shown in the contour graphs, the peak solar production is strongly associated with intervals with the highest energy prices which fall in the late afternoon/early evening of the summer months.

The plots in the extreme right in Figure A.9 summarize the effect of combining wind and solar generation in the base case scenario (375 MW of Wind and 125 MW of Solar). Due to the abundance of wind in the base case, the capacity duration curves and generation contour map remain dominated by the effect of wind. However, several important findings can be observed:

- The low correlation between wind and solar generation can be seen in the capacity duration curves, which show generation levels more evenly spread out among all available hours than for either resource alone.
- There are very few hours in which there is no combined generation: some solar or wind generation is almost always present.
- Combined wind and solar generation exceeds the base case limit of 375 MW approximately

5% of all hours for the wind plus solar thermal combination.

- The hours with excess production appear to be slightly more correlated to peak energy prices when solar thermal and wind generation is combined compared to wind generating alone, as revealed by the combined contour maps.

Having total wind and solar production capacity that exceeds the transmission limit can result in better utilization of available transmission capacity but also means that energy production will occasionally exceed that limit. Table A.2 displays the raw wind, solar, and combined generation and capacity factors associated with the wind plus solar combination analyzed and quantifies losses resulting from exceeding the assumed transmission limit (375 MW) in the base case and also the energy losses due to curtailment as a percentage of the total combined generation. It is seen that the base case build-out result in losses of close to 8% of all raw energy production. This amount can be reduced by further incorporating thermal energy storage for the solar component.

Table A.2 Raw and Limited Energy from Combined Wind and Solar Production Modeled at Study Site

Wind MWh	Wind CF	Solar MWh	Solar CF	Wind+Solar MWh	Constrained MWh	% MWh Lost
1.34E+06	40.59%	3.47E+05	31.6%	1.69E+06	1.55E+06	8.3%

Table A.3 performs the same analysis but substitutes the economic value of energy, based on the LMP during the hour of generation, for the quantity of energy. It is seen that the base case build-out results in economic losses of 8.9% of the total potential value of energy produced.

Table A.3 Raw and Limited Economic Value from Combined Wind and Solar Production Modeled at Study Site

Wind Value ($)	Solar Value ($)	Wind+Solar Value ($)	Constrained Value ($)	% Value Lost
4.53E+07	1.30E+07	5.82E+07	5.30E+07	8.9%

A practical interpretation from Figure A.9 is that expected losses from adding 125 MW of solar thermal generation onto a transmission system with significant wind generation already

present can be very nearly eliminated by increasing available transmission capacity limit by just 50 MW. The reason can be attributed to the fact that solar and wind generation only rarely operate at or near full capacity in unison.

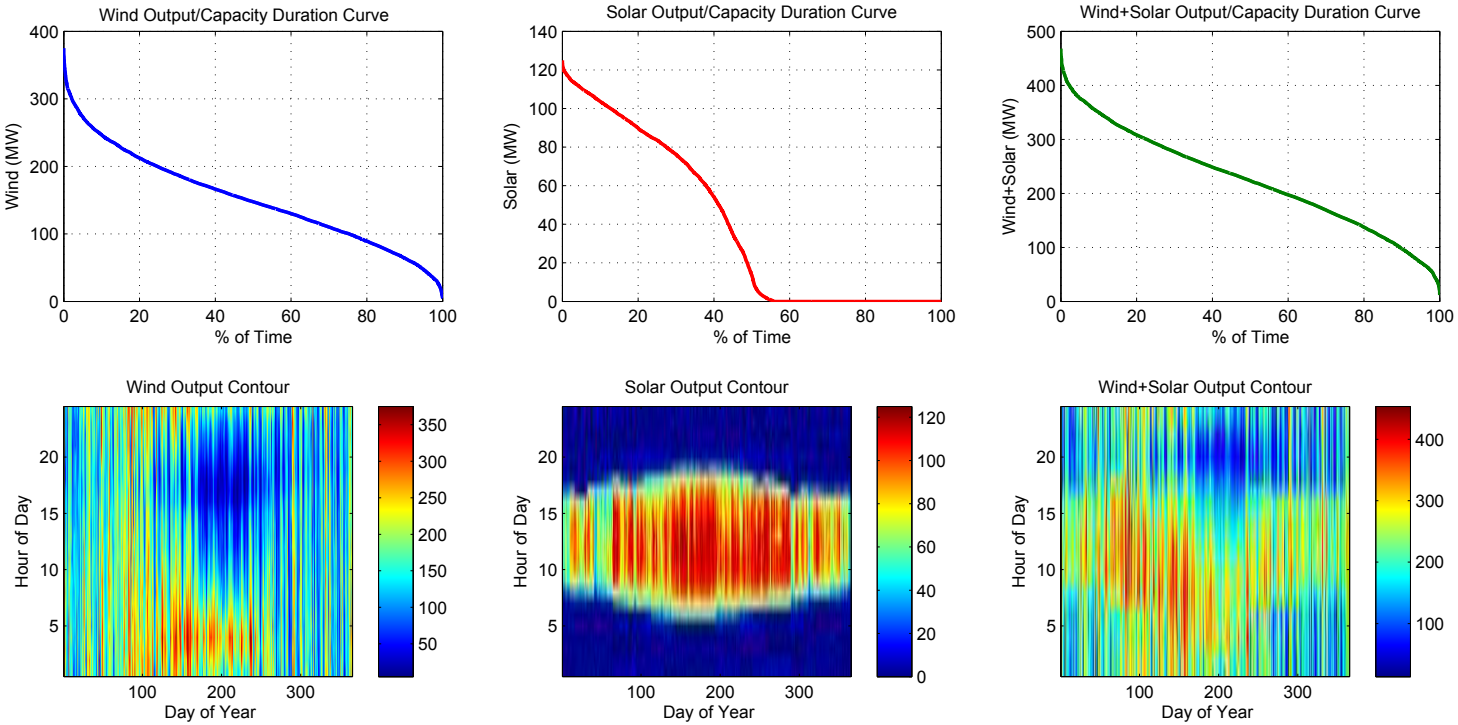

Figure A.9 Capacity Duration Curves and Contour Maps for Wind, Solar and Combined Wind+Solar Energy Production Modeled at Study Site

A Balancing Authority (BA) refers to a reliability entity that is responsible for balancing demand and supply within the metered boundaries of its area to support interconnection frequency. The Western Electric Coordinating Council (WECC) includes several BAs. WECC covers an interconnected power grid. Siting of wind and solar projects is impacted by wind/solar potential of a region. BA boundaries do not always correspond to state boundaries.

The overall variability of intermittent resources is reduced when such resources are aggregated over a wider geographic area. In WECC alone, there are 38 balancing authorities - five of which are generators only - that are each responsible for balancing load and generation within their electrical boundaries (Figure A.10). In addition, balancing authorities schedule interchange transactions on hourly periods, which scheduling procedure itself has a significant effect on balancing reserve capabilities. Operationally speaking, balancing authorities can enhance their ability to provide intermittent resources with balancing service by consolidating balancing operations and pooling their reserve resources. Even with significantly higher penetrations of renewable resources, variability only slightly increases when multiple balancing services are aggregated. In addition, the cost of providing balancing services is reduced when reserves are pooled because balancing authorities have greater access to more and flexible resources.

From Figures A.10 and 6.11, the distribution of different HECS score potential across the different balancing authorities can be determined. For ease of viewing, they are seen side-by-side in Figure A.11, along with the wind and solar DNI resource of WECC. The explanation of the HECS score is given in Table 6.2.

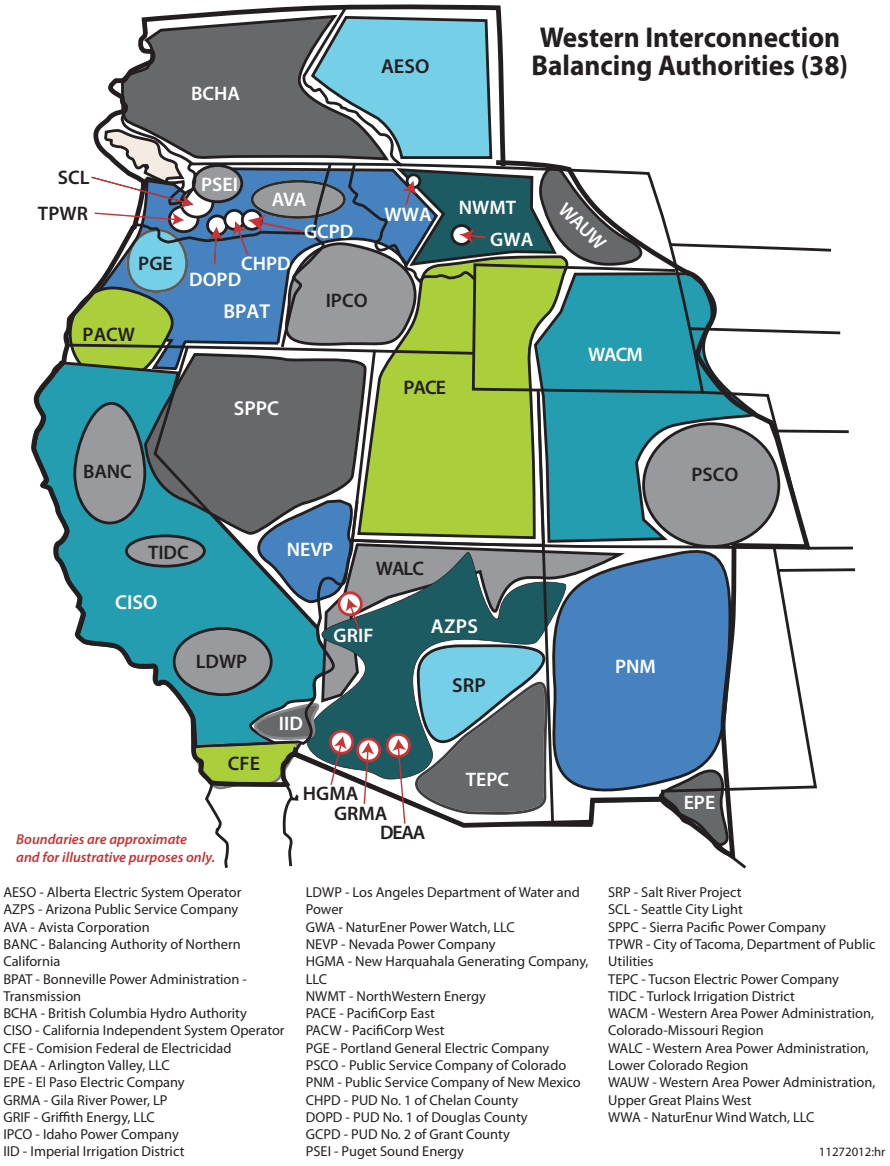

Figure A.10 WECC Balancing Authorities [Source: WECC]

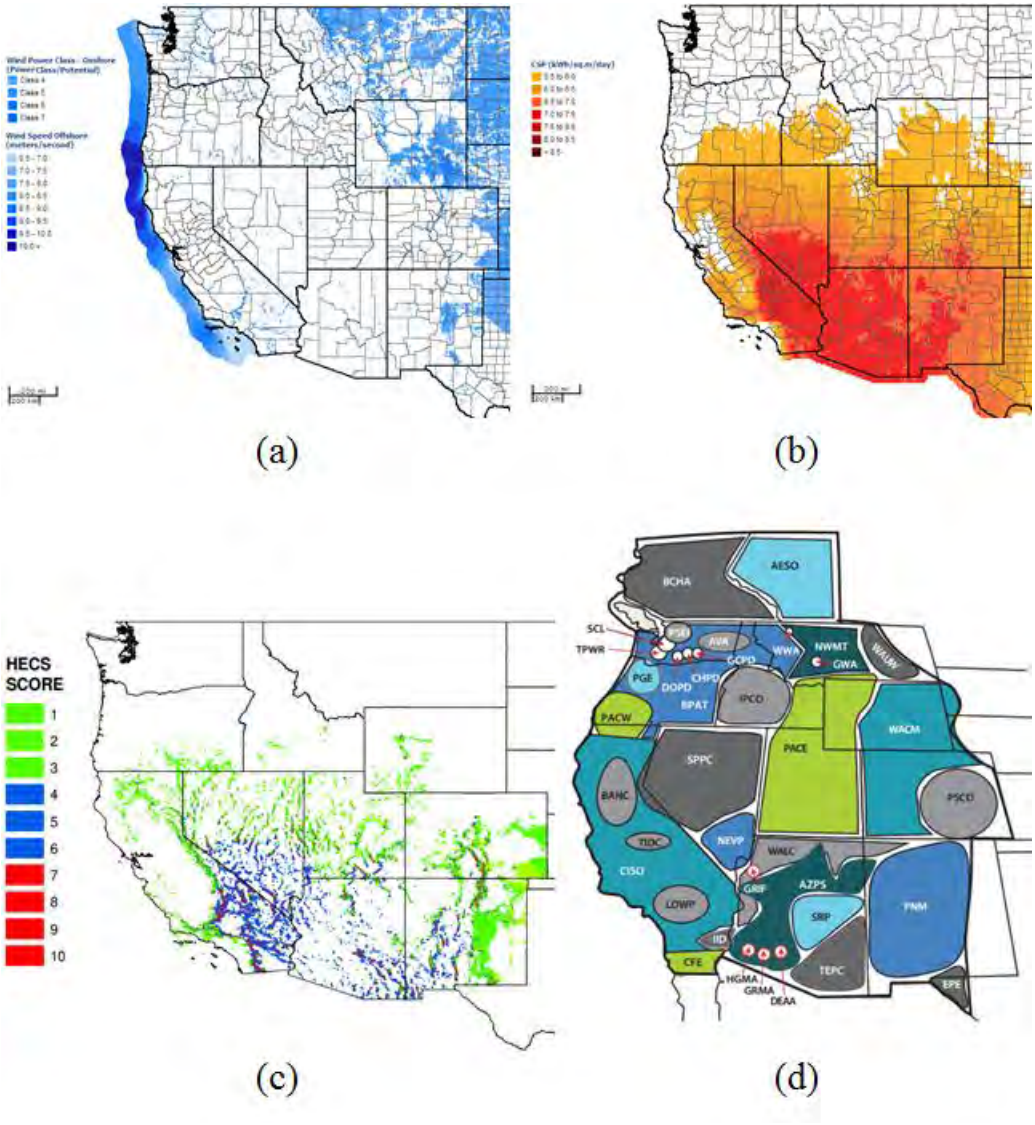

Figure A.11 WECC Wind Resource (a), CSP Resource (b), HECS Resource Score Distribution (c) and Balancing Authorities (d)

In our context, renewable hybridization or combining wind and solar power generation can be considered to be executed on 2 levels - global and local. Global hybridization implies combining the wind resources at say the wind-rich northern part of a BA with the solar resources of the solar-rich southern part of the BA. Considering them as negative load, the net load value can be reduced, the renewable resource output variability can be reduced by employing widespread aggregation of multiple resources. Local hybridization implies the similar combination, except in such a way that they are co-located and can share the same transmission infrastructure in order the supply more amount of renewable generation at each point of interconnection than either single generation technology. The determination of locations is important, the idea is not to compromise the full potential of either wind or solar resource available at a given location, but to identify sites which have favorable resource characteristics of both wind and solar and also close to each other so as to more efficiently use the transmission lines to feed to the grid which are expensive to build and also difficult to get permission for. The benefits that are available in global hybridization by widespread aggregation by using the complementary nature of wind and solar profile are present in local hybridization as well, plus one might get the additional benefit of increased reliability and better use of transmission facilities.

This thesis mainly focuses on siting and sizing of those location in an area where local hybridization following from co-located wind-solar generation can be advantageous.

Comments

Thus, the benefits of co-location wind and solar were explored. The major advantages include increased utilization of existing transmission interconnections, increased system reliability, increase generation during peak demand (summer during the day). Co-location, co-generation and co-ordination leads to smoothing out the local peaks and valleys of energy that individual wind and solar provides; thus wind may be a great base load source and solar may be a great peak load source.

A joint study by the National Renewable Energy Laboratory and Ohio State University [35] has shown that co-locating wind and concentrated solar power (CSP) improves the associated transmission investment. This is due to two synergies between wind and CSP: first, wind

and solar resource availability tends to be slightly negatively correlated. Second, low cost and highly efficient thermal energy storage (TES) can be incorporated into CSP, allowing solar generation to be shifted and used to fill excess capacity not being utilized by wind generation. The resource siting and sizing developed in this thesis can be further coupled with the resource dispatch optimization model developed in [35] to investigate the improved resource profile and the major transmission investment usage.

The resource siting can be executed by using the HECS ID Tool explained in Chapter 3 and the sizing using the optimization model developed in Chapter 4. The annual cost function defined in Eqn (4.28) and the capacity factor function defined in Eqn. (4.43) can be extended to account for the three situations possible with respect to the general layout (Fig. 2.1) explained in Chapter 2, Section 2.3 - namely, (1) when the local/virtual load is absent; (2) when the local/virtual load is present and HECS is grid connected; (3) when the local/virtual load is present and HECS is not connected to the grid i.e., standalone. Each of the individual wind, solar and load demand terms in these equations can be modified to include a binary variable, say F_j ($j = W/S/D$ denoting wind, solar and demand respectively) and $F_j = 0$ or 1 depending on the absence or presence of the corresponding terms. Thus, the terms A_W, A_S and P_D would be modified to $F_W A_W$, $F_S A_S$ and $F_D P_D$ accordingly. This way it will be easy to compare between co-location (F_W=1;F_S=1) or independent siting ((F_W = 1;F_S=0) OR (F_W=0;F_S=1)) of wind and solar resources. The constraints - the power balance constraint (Eqns (4.44), (4.45)) and the design variable constraints (Eqns. (4.49), (4.50)) will need to be modified accordingly to reflect the resource availability and local demand of the site under consideration (meaning either wind alone or solar alone or co-located wind and solar). Also the presence of local/virtual load can be represented by putting $F_D = 0$ or 1; when $F_D = 0$, then Eqn. (4.45) will be removed and the design variables, denoting the land area available for the wind and solar ECSs will be the only binding factor on the sizes.

Since the two objective functions defined are still conflicting with each other, irrespective of the ECS configuration situation, the optimal Pareto front (Figure 4.12) will retain a similar profile curve, however the annual cost and capacity factor values will be different depending on the system configuration.

Also the optimization formulation can be further modified to incorporate the following additional factors - in the cost function: the transmission investment (as a function of the MW capacity and the line length depending on the proximity to existing or future transmission grid) and the revenue generation (as a function of the hourly locational marginal pricing and the hourly combined generation which will be peaking during high load time periods when the prices are relatively higher as well); in the capacity factor function: the inclusion of thermal energy storage to incorporate some dispatchability of solar to store excess energy and fill in during periods of low wind output.

From Table 6.2 and Figures 6.11 and 6.12, we can see that the locations where wind and solar co-location seem feasible are mainly in the south-western USA. Each of the surface cells in Figure 6.11 are of 10 km $\times$ 10 km size or roughly 2470 acres. The cells in Score '10' bin represent the locations which have both very good wind (>800 W/m^2) and solar (>7.5 $kWh/m^2/Day$) resources; followed by the cells in Score bins '7', '8', '9' - which can be classified as demonstrating high potential for HECS. The cells in low score bin, for e.g. Score '4', have either very high wind, low solar or very high solar, low wind - these sites are more suitable for individual wind and solar development rather than focusing on co-location hybridization. If one were to compare the annual costs among say 3 sites - 1 with co-location (score bin 10), and the other 2 being wind standalone and solar standalone (score bin 4), while keeping the energy performance measured by the capacity factor same, then the optimization model developed in Chapter 4 extended with the inclusion of the binary variable F_j as defined above could be used to obtain the optimal Pareto Front. The comparative cost-benefit would however be varying from site to site, depending on the locational resource characteristics.

APPENDIX B. STATISTICAL CONCEPTS

Transformation Theorem

Let x be a random variable following a probability density function $f_x(x)$ and cumulative distribution function $F_x(x)$ such that $f_x(x) = \frac{dF_x(x)}{dx}$. We have another variable y such that $y = g(x)$. Suppose we need to determine the density $f_y(y)$ in terms of the density $f_x(x)$ of x. We assume that x is continuous and $g(x)$ is continuous. To find $f_y(y)$ for a given y, we solve the equation $y = g(x)$ for x in terms of y. Let x_i be all the real roots of $y_i = g(x_i)$, then

$$f_y(y) = \sum_i \frac{f_x(x_i)}{|g'(x_i)|}$$

where

$$g'(x) = \frac{dg(x)}{dx}.$$

Expected Value of a Random Variable

In probability theory, the expected value of a random variable is the weighted average of all possible values that this random variable can take on. The weights used in computing this average correspond to the probabilities in case of a discrete random variable, or densities in case of a continuous random variable [112]. If X is a discrete random variable with probability mass function $p(x)$, then the expected value becomes

$$E(X) = \sum_i x_i p(x_i)$$

If X is a continuous random variable with probability density function $f(x)$, then the expected value becomes

$$E(X) = \int_{-\infty}^{\infty} x f(x) dx$$

Polynomial Least Squares Fitting

Least Squares Fitting (LSF) is a mathematical procedure for finding the best-fitting curve to a given set of points by minimizing the sum of the squares of the offsets ("the residuals") of the points from the curve [120]. For polynomial LSF, generalizing from a straight line (i.e., first degree polynomial) to a k^{th} degree polynomial leads to

$$y = a_0 + a_1 x + \ldots + a_k x^k. \tag{B.1}$$

Vertical LSF proceeds by finding the sum of the squares of the vertical deviations R^2 of a set of n data points.

$$R^2 \equiv \sum_{i=1}^{n} \left[y_i - (a_0 + a_1 x_i + \ldots + a_k x_i^k) \right]^2. \tag{B.2}$$

The condition for R^2 to be a minimum is that

$$\frac{\partial (R^2)}{\partial a_i} = 0 \tag{B.3}$$

for $i = 1 \ldots n$. Taking partial derivatives of (B.2) and equating them to zero gives the following equation in matrix form,

$$\begin{bmatrix} n & \sum_{i=1}^n x_i & \ldots & \sum_{i=1}^n x_i^k \\ \sum_{i=1}^n x_i & \sum_{i=1}^n x_i^2 & \ldots & \sum_{i=1}^n x_i^{k+1} \\ \vdots & \vdots & \ddots & \vdots \\ \sum_{i=1}^n x_i^k & \sum_{i=1}^n x_i^{k+1} & \ldots & \sum_{i=1}^n x_i^{2k} \end{bmatrix} \begin{bmatrix} a_0 \\ a_1 \\ \vdots \\ a_k \end{bmatrix} = \begin{bmatrix} \sum_{i=1}^n y_i \\ \sum_{i=1}^n x_i y_i \\ \vdots \\ \sum_{i=1}^n x_i^k y_i \end{bmatrix} \tag{B.4}$$

This is a Vandermonde matrix. Now, given n points (x_i, y_i) and fitting with polynomial coefficients, $a_0, \ldots, a_k$ gives

$$\begin{bmatrix} y_1 \\ y_2 \\ \vdots \\ y_n \end{bmatrix} = \begin{bmatrix} 1 & x_1 & \ldots & x_1^k \\ 1 & x_2 & \ldots & x_2^k \\ \vdots & \vdots & \ddots & \vdots \\ 1 & x_n & \ldots & x_n^k \end{bmatrix} \begin{bmatrix} a_0 \\ a_1 \\ \vdots \\ 0.1 a_k \end{bmatrix} \tag{B.5}$$

In matrix notation, the equation for a polynomial fit is given by

$$\mathbf{y} = \mathbf{X}\mathbf{a} \tag{B.6}$$

This can be solved by premultiplying by the transpose $\mathbf{X^T}$,

$$\mathbf{X^T}\mathbf{y} = \mathbf{X^T}\mathbf{X}\mathbf{a} \tag{B.7}$$

This matrix equation can be solved numerically, or can be inverted directly if it is well formed, to yield the solution vector

$$\mathbf{a} = (\mathbf{X^T}\mathbf{X})^{-1}\mathbf{X^T}\mathbf{y} \tag{B.8}$$

Coefficient of determination

In statistics, the coefficient of determination R^2 is used in the context of statistical models whose main purpose is the prediction of future outcomes on the basis of other related information. R^2 is most often seen as a number between 0 and 1.0, used to describe how well a regression line fits a set of data. An R^2 near 1.0 indicates that a regression line fits the data well, while an R^2 closer to 0 indicates a regression line does not fit the data very well. It is the proportion of variability in a data set that is accounted for by the statistical model. It provides a measure of how well future outcomes are likely to be predicted by the model.

A data set has values y_i, each of which has an associated modeled value f_i. Here, the values y_i are called the observed values and the modeled values f_i are sometimes called the predicted values. The "variability" of the data set is measured through different sums of squares:

- the total sum of squares (proportional to the sample variance)

$$SS_{tot} = \sum_i (y_i - \overline{y})^2$$

- the regression sum of squares, also called the explained sum of squares

$$SS_{reg} = \sum_i (f_i - \overline{y})^2$$

- the sum of squares of residuals, also called the residual sum of squares

$$SS_{err} = \sum_i (y_i - f_i)^2$$

Here, $\overline{y}$ is the mean of the observed data, i.e. $\overline{y} = \frac{1}{n}\sum_{i=1}^{n} y_i$, where n is the number of observations. the most general definition of the coefficient of determination is

$$R^2 = 1 - \frac{SS_{err}}{SS_{tot}}$$

APPENDIX C. APPLICATION OF GENETIC ALGORITHM IN MULTI-OBJECTIVE OPTIMIZATION

Multi-objective optimization

Multi-objective optimization is concerned with the minimization of a vector of objectives $F(x) = [F_1(x), F_2(x) \dots F_m(x)]$ that can be the subject of a number of constraints or bounds:

$$\begin{aligned} \underset{X \in \Re^n}{\text{minimize}} \quad & F(x) \\ \text{subject to} \quad & G_i(x) = 0, i = 1, \dots k_e; \\ & G_i(x) \leq 0, i = k_e + 1, \dots, k; \\ & l \leq x \leq u. \end{aligned} \tag{C.1}$$

Note that because $F(x)$ is a vector, if any of the components of $F(x)$ are competing, there is no unique solution to this problem. Instead, the concept of non-inferiority [162] (also called Pareto optimality [163] and [164]) must be used to characterize the objectives. A non-inferior solution is one in which an improvement in one objective requires a degradation of another. To define this concept more precisely, consider a feasible region, Ω, in the parameter space. x is an element of the n-dimensional real numbers $x \in \Re^n$ that satisfies all the constraints, i.e.,

$$\Omega = x \in \Re^n, \tag{C.2}$$

subject to the conditions given in (C.1).

This allows definition of the corresponding feasible region for the objective function space Λ :

$$\Lambda = \{y \in \Re^m : y = F(x), x \in \Omega\}. \tag{C.3}$$

The performance vector $F(x)$ maps parameter space into objective function space, as represented in two dimensions in Figure C.1.

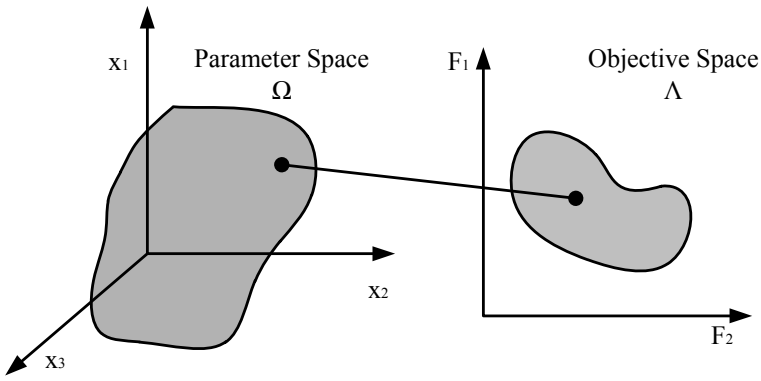

Figure C.1 Mapping from Parameter Space into Objective Function Space

A point $x^* \in \Omega$ can be defined as a non-inferior solution if for some neighborhood of x^*, there does not exist a Δx such that $(x^* + \Delta x) \in \Omega$ and

$$F_i(x^* + \Delta x) \leq F_i(x^*), i = 1, \ldots, m, \text{ and}$$

$$F_j(x^* + \Delta x) < F_j(x^*), \text{ for at least one } j.$$

In Figure C.2, the set of non-inferior solutions lies on the curve between C and D. Points A and B represent specific non-inferior points.

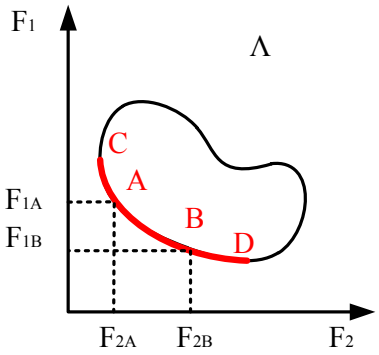

Figure C.2 Set of Non-inferior Solutions

A and B are clearly non-inferior solution points because an improvement in one objective, F_1, requires a degradation in the other objective, F_2, i.e., $F_{1B} < F_{1A}$,$F_{2B} > F_{2A}$. Since any point in Ω that is an inferior point represents a point in which improvement can be attained in all the objectives, it is clear that such a point is of no value. Multi-objective optimization

is, therefore, concerned with the generation and selection of non-inferior solution points. Non-inferior solutions are also called Pareto optima. A general goal in multi-objective optimization is constructing the Pareto optima.

Genetic Algorithm

A genetic algorithm (GA) is an advanced search and optimization technique. It has been developed to imitate the evolutionary principle of natural genetics. Compared with traditional methods (the direct exhaustive search method and the gradient-directed search method) for function optimization, one of the main advantages of the GA is that it is generally robust in finding global optimal solutions, particularly in multi-modal and multi-objective optimization problems.

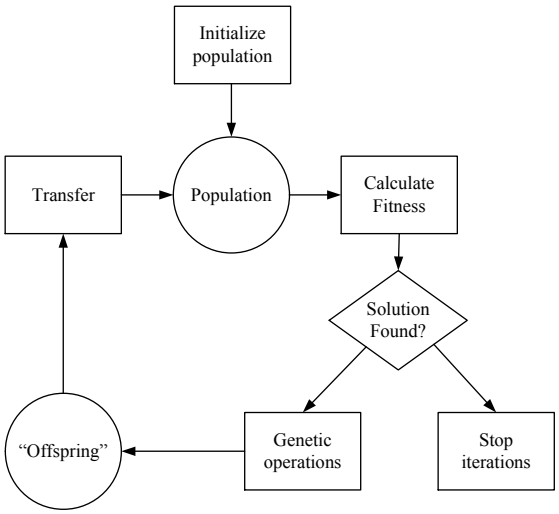

Figure C.3 Basic Steps in a GA

Generally, a GA uses three operators - namely, selection, crossover and mutation to imitate the natural evolution processes. The first step (step $k = 1$) of a genetic evaluation is to determine if the chosen system configuration (called a chromosome) passes the functional evaluation, provides service to the load within the bounds set forth by the expected energy not supplied and the pollutant emissions. If the evaluation qualified chromosome (at step k) has a lower $COST$ function than the lowest value obtained at the previous iterations (step =

$k-1$), this system configuration (chromosome) is considered to be the optimal solution for the minimization problem in this iteration. This optimal solution will be replaced by better solutions, if any, produced in subsequent GA generations during the program evolution. After the selection process, the optimal solution will then be subject to the crossover and mutation operations in order to produce the next generation population until a pre-specified number of generations have been reached or when a criterion that determines the convergence is satisfied.

APPENDIX D. BUS DETAILS OF REDUCED 240-BUS WECC SYSTEM

Researchers at the California ISO (CAISO) developed a 240-bus model from publicly-available data and validated it using the full WECC models [133]. The following table lists the bus details.

Table D.1 Bus Details of Reduced 240-Bus WECC System

Bus #	Bus Name	Base kV	Area Num - Name	Zone Num - Name
1001	FOURCORN	500	10 - SOUTHWST	10 - SOUTHWST
1002	FOURCORN	345	10 - SOUTHWST	10 - SOUTHWST
1003	FOURCORN	230	10 - SOUTHWST	10 - SOUTHWST
1004	SAN JUAN	345	10 - SOUTHWST	10 - SOUTHWST
1032	FCNGN4CC	20	10 - SOUTHWST	10 - SOUTHWST
1034	SJUAN G4	20	10 - SOUTHWST	10 - SOUTHWST
1101	CORONADO	500	10 - SOUTHWST	10 - SOUTHWST
1102	CHOLLA	345	10 - SOUTHWST	10 - SOUTHWST
1131	CORONADO	20	10 - SOUTHWST	10 - SOUTHWST
1201	MOENKOPI	500	10 - SOUTHWST	10 - SOUTHWST
1202	NAVAJO	500	10 - SOUTHWST	10 - SOUTHWST
1232	NAVAJO 2	20	10 - SOUTHWST	10 - SOUTHWST
1301	MEAD	500	10 - SOUTHWST	10 - SOUTHWST
1302	H ALLEN	500	10 - SOUTHWST	10 - SOUTHWST

Continued on next page

Bus #	Bus Name	Base kV	Area Num - Name	Zone Num - Name
1303	H ALLEN	345	10 - SOUTHWST	10 - SOUTHWST
1331	HOOVER	20	10 - SOUTHWST	10 - SOUTHWST
1333	H ALLEN	20	10 - SOUTHWST	10 - SOUTHWST
1401	PALOVRDE	500	10 - SOUTHWST	10 - SOUTHWST
1402	WESTWING	500	10 - SOUTHWST	10 - SOUTHWST
1403	PARKER	230	10 - SOUTHWST	10 - SOUTHWST
1431	PALOVRD2	20	10 - SOUTHWST	10 - SOUTHWST
2000	MEXICO	230	20 - MEXICO	20 - MEXICO
2030	MEXICO	20	20 - MEXICO	20 - MEXICO
2100	IMPERIAL	230	21 - IMPERIAL	21 - IMPERIAL
2130	IMPERIAL	20	21 - IMPERIAL	21 - IMPERIAL
2201	MIGUEL	500	22 - SANDIEGO	22 - SANDIEGO
2202	MIGUEL	230	22 - SANDIEGO	22 - SANDIEGO
2203	MISSION	230	22 - SANDIEGO	22 - SANDIEGO
2233	MISSION	20	22 - SANDIEGO	22 - SANDIEGO
2301	IMPRLVLY	500	22 - SANDIEGO	23 - SDG_MIV
2302	IMPRLVLY	230	22 - SANDIEGO	23 - SDG_MIV
2332	IMPRLVLY	20	22 - SANDIEGO	23 - SDG_MIV
2400	DEVERS	500	24 - SCE_OTHR	24 - SCE_OTHR
2401	LUGO	500	24 - SCE_OTHR	24 - SCE_OTHR
2402	MIRALOMA	500	24 - SCE_OTHR	24 - SCE_OTHR
2403	VALLEY	500	24 - SCE_OTHR	24 - SCE_OTHR
2404	VINCENT	500	24 - SCE_OTHR	24 - SCE_OTHR
2405	SYLMAR S	230	24 - SCE_OTHR	24 - SCE_OTHR
2406	EAGLROCK	230	24 - SCE_OTHR	24 - SCE_OTHR
2407	LITEHIPE	230	24 - SCE_OTHR	24 - SCE_OTHR

Continued on next page

Bus #	Bus Name	Base kV	Area Num - Name	Zone Num - Name
2408	MESA CAL	230	24 - SCE_OTHR	24 - SCE_OTHR
2409	MIRALOMA	230	24 - SCE_OTHR	24 - SCE_OTHR
2410	PARDEE	230	24 - SCE_OTHR	24 - SCE_OTHR
2411	VINCENT	230	24 - SCE_OTHR	24 - SCE_OTHR
2438	MESA CAL	20	24 - SCE_OTHR	24 - SCE_OTHR
2501	SERRANO	500	25 - LAORANGE	25 - LAORANGE
2502	SERRANO	230	25 - LAORANGE	25 - LAORANGE
2503	S.ONOFRE	230	25 - LAORANGE	25 - LAORANGE
2533	S.ONOFRE	20	25 - LAORANGE	25 - LAORANGE
2600	ADELANTO	500	90 - DC TIES	90 - DC TIES
2601	RINALDI	500	26 - LADWP	26 - LADWP
2602	STA E	500	26 - LADWP	26 - LADWP
2603	VICTORVL	500	26 - LADWP	26 - LADWP
2604	INTERMT	345	90 - DC TIES	90 - DC TIES
2605	STA B1	287	26 - LADWP	26 - LADWP
2606	STA B2	287	26 - LADWP	26 - LADWP
2607	VICTORVL	287	26 - LADWP	26 - LADWP
2608	CASTAIC	230	26 - LADWP	26 - LADWP
2609	GLENDAL	230	26 - LADWP	26 - LADWP
2610	HAYNES	230	26 - LADWP	26 - LADWP
2611	OLIVE	230	26 - LADWP	26 - LADWP
2612	RINALDI	230	26 - LADWP	26 - LADWP
2613	RIVER	230	26 - LADWP	26 - LADWP
2614	STA BLD	230	26 - LADWP	26 - LADWP
2615	STA E	230	26 - LADWP	26 - LADWP
2616	STA F	230	26 - LADWP	26 - LADWP

Continued on next page

Bus #	Bus Name	Base kV	Area Num - Name	Zone Num - Name
2617	STA G	230	26 - LADWP	26 - LADWP
2618	STA J	230	26 - LADWP	26 - LADWP
2619	SYLMARLA	230	90 - DC TIES	90 - DC TIES
2620	VALLEY	230	26 - LADWP	26 - LADWP
2621	STA B	138	26 - LADWP	26 - LADWP
2630	HAYNES3G	20	26 - LADWP	26 - LADWP
2631	OLIVE	20	26 - LADWP	26 - LADWP
2634	INTERM1G	20	90 - DC TIES	90 - DC TIES
2637	OWENS G	20	26 - LADWP	26 - LADWP
2638	CASTAI4G	20	26 - LADWP	26 - LADWP
2901	ELDORADO	500	24 - SCE_OTHR	29 - SCE_NV
2902	MOHAVE	500	24 - SCE_OTHR	29 - SCE_NV
3101	EMBRCDRD	230	31 - SNFRNCSC	31 - SNFRNCSC
3102	MARTIN	230	31 - SNFRNCSC	31 - SNFRNCSC
3103	SANMATEO	230	32 - BAYAREA	31 - SNFRNCSC
3104	MARTIN	115	31 - SNFRNCSC	31 - SNFRNCSC
3105	POTRERO	115	31 - SNFRNCSC	31 - SNFRNCSC
3133	SANMATEO	20	32 - BAYAREA	31 - SNFRNCSC
3135	POTRERO	20	31 - SNFRNCSC	31 - SNFRNCSC
3201	C.COSTA	230	32 - BAYAREA	32 - EASTBAY
3202	MORAGA	230	32 - BAYAREA	32 - EASTBAY
3203	NEWARK	230	32 - BAYAREA	32 - EASTBAY
3204	PITSBURG	230	32 - BAYAREA	32 - EASTBAY
3205	SOBRANTE	230	32 - BAYAREA	32 - EASTBAY
3234	PITSBURG	20	32 - BAYAREA	32 - EASTBAY
3301	METCALF	500	32 - BAYAREA	33 - SOUTHBAY

Continued on next page

Bus #	Bus Name	Base kV	Area Num - Name	Zone Num - Name
3302	JEFFERSN	230	32 - BAYAREA	33 - SOUTHBAY
3303	METCALF	230	32 - BAYAREA	33 - SOUTHBAY
3304	MONTAVIS	230	32 - BAYAREA	33 - SOUTHBAY
3305	RAVENSWD	230	32 - BAYAREA	33 - SOUTHBAY
3333	METCALF	20	32 - BAYAREA	33 - SOUTHBAY
3401	GREGG	230	34 - FRESNO	34 - FRESNO
3402	HELMS PP	230	34 - FRESNO	34 - FRESNO
3403	MC CALL	230	34 - FRESNO	34 - FRESNO
3404	PANOCHE	230	34 - FRESNO	34 - FRESNO
3405	WILSON	230	34 - FRESNO	34 - FRESNO
3432	HELMS PP	20	34 - FRESNO	34 - FRESNO
3433	MC CALL	20	34 - FRESNO	34 - FRESNO
3501	FULTON	230	35 - GEYSERS	35 - GEYSERS
3531	FULTON	20	35 - GEYSERS	35 - GEYSERS
3601	HUMBOLDT	115	36 - HUMBOLDT	36 - HUMBOLDT
3631	HUMBOLDT	20	36 - HUMBOLDT	36 - HUMBOLDT
3701	SUMMIT	115	37 - SIERRA	37 - SIERRA
3731	SUMMIT	20	37 - SIERRA	37 - SIERRA
3801	DIABLO	500	38 - CNTCOAST	38 - CNTCOAST
3802	GATES	500	38 - CNTCOAST	38 - CNTCOAST
3803	MIDWAY	500	38 - CNTCOAST	38 - CNTCOAST
3804	GATES	230	38 - CNTCOAST	38 - CNTCOAST
3805	MIDWAY	230	38 - CNTCOAST	38 - CNTCOAST
3806	MORROBAY	230	38 - CNTCOAST	38 - CNTCOAST
3831	DIABLO1	20	38 - CNTCOAST	38 - CNTCOAST
3835	MIDWAY	20	38 - CNTCOAST	38 - CNTCOAST

Continued on next page

Bus #	Bus Name	Base kV	Area Num - Name	Zone Num - Name
3836	MORROBAY	20	38 - CNTCOAST	38 - CNTCOAST
3891	GATES1	500	38 - CNTCOAST	38 - CNTCOAST
3892	MIDWAY1	500	38 - CNTCOAST	38 - CNTCOAST
3893	MIDWAY2	500	38 - CNTCOAST	38 - CNTCOAST
3894	MIDWAY3	500	38 - CNTCOAST	38 - CNTCOAST
3895	MIDWAY4	500	38 - CNTCOAST	38 - CNTCOAST
3896	MIDWAY5	500	38 - CNTCOAST	38 - CNTCOAST
3897	MIDWAY6	500	38 - CNTCOAST	38 - CNTCOAST
3901	LOSBANOS	500	39 - PGE_OTHR	39 - PGE_OTHR
3902	MOSSLAND	500	39 - PGE_OTHR	39 - PGE_OTHR
3903	TESLA	500	39 - PGE_OTHR	39 - PGE_OTHR
3904	VACA - DIX	500	39 - PGE_OTHR	39 - PGE_OTHR
3905	TABLE MT	500	39 - PGE_OTHR	39 - PGE_OTHR
3906	ROUND MT	500	39 - PGE_OTHR	39 - PGE_OTHR
3907	BELLOTA	230	39 - PGE_OTHR	39 - PGE_OTHR
3908	BRIGHTON	230	39 - PGE_OTHR	39 - PGE_OTHR
3909	COLGATE	230	39 - PGE_OTHR	39 - PGE_OTHR
3910	CORTINA	230	39 - PGE_OTHR	39 - PGE_OTHR
3911	COTWDPGE	230	39 - PGE_OTHR	39 - PGE_OTHR
3912	GLENN	230	39 - PGE_OTHR	39 - PGE_OTHR
3913	GOLDHILL	230	39 - PGE_OTHR	39 - PGE_OTHR
3914	IGNACIO	230	39 - PGE_OTHR	39 - PGE_OTHR
3915	LAKEVILE	230	39 - PGE_OTHR	39 - PGE_OTHR
3916	LOGAN CR	230	39 - PGE_OTHR	39 - PGE_OTHR
3917	LOSBANOS	230	39 - PGE_OTHR	39 - PGE_OTHR
3918	MOSSLAND	230	39 - PGE_OTHR	39 - PGE_OTHR

Continued on next page

Bus #	Bus Name	Base kV	Area Num - Name	Zone Num - Name
3919	PALERMO	230	39 - PGE_OTHR	39 - PGE_OTHR
3920	RIO OSO	230	39 - PGE_OTHR	39 - PGE_OTHR
3921	ROUND MT	230	39 - PGE_OTHR	39 - PGE_OTHR
3922	TABLE MT	230	39 - PGE_OTHR	39 - PGE_OTHR
3923	TESLA	230	39 - PGE_OTHR	39 - PGE_OTHR
3924	VACA - DIX	230	39 - PGE_OTHR	39 - PGE_OTHR
3925	COTWDPGE	115	39 - PGE_OTHR	39 - PGE_OTHR
3926	RIO OSO	115	39 - PGE_OTHR	39 - PGE_OTHR
3931	ROUND MT	20	39 - PGE_OTHR	39 - PGE_OTHR
3932	MOSSLAND	20	39 - PGE_OTHR	39 - PGE_OTHR
3933	TESLA	20	39 - PGE_OTHR	39 - PGE_OTHR
4001	MALIN	500	40 - NORTHWST	40 - S_JONDAY
4002	SUMMER L	500	40 - NORTHWST	40 - S_JONDAY
4003	BURNS	500	40 - NORTHWST	40 - S_JONDAY
4004	GRIZZLY	500	40 - NORTHWST	40 - S_JONDAY
4005	JOHN DAY	500	40 - NORTHWST	40 - S_JONDAY
4006	BIG EDDY	500	40 - NORTHWST	40 - S_JONDAY
4007	CELILOCA	500	40 - NORTHWST	40 - S_JONDAY
4008	MALIN	345	40 - NORTHWST	40 - S_JONDAY
4009	BIG EDDY	230	40 - NORTHWST	40 - S_JONDAY
4010	CELILO	230	90 - DC TIES	90 - DC TIES
4031	MALIN	20	40 - NORTHWST	40 - S_JONDAY
4035	JOHN DAY	20	40 - NORTHWST	40 - S_JONDAY
4039	DALLES21	20	40 - NORTHWST	40 - S_JONDAY
4090	MALIN1	500	40 - NORTHWST	40 - S_JONDAY
4091	GRIZZLY1	500	40 - NORTHWST	40 - S_JONDAY

Continued on next page

Bus #	Bus Name	Base kV	Area Num - Name	Zone Num - Name
4092	GRIZZLY2	500	40 - NORTHWST	40 - S_JONDAY
4093	GRIZZLY3	500	40 - NORTHWST	40 - S_JONDAY
4094	GRIZZLY4	500	40 - NORTHWST	40 - S_JONDAY
4095	GRIZZLY5	500	40 - NORTHWST	40 - S_JONDAY
4096	GRIZZLY6	500	40 - NORTHWST	40 - S_JONDAY
4097	GRIZZLY7	500	40 - NORTHWST	40 - S_JONDAY
4101	COULEE	500	40 - NORTHWST	41 - N_JONDAY
4102	HANFORD	500	40 - NORTHWST	41 - N_JONDAY
4103	BELL	500	40 - NORTHWST	41 - N_JONDAY
4104	BELL	230	40 - NORTHWST	41 - N_JONDAY
4131	COULEE	20	40 - NORTHWST	41 - N_JONDAY
4132	HANFORD	20	40 - NORTHWST	41 - N_JONDAY
4201	NORTH	500	40 - NORTHWST	42 - W_CASCAD
4202	WCASCADE	500	40 - NORTHWST	42 - W_CASCAD
4203	WILLAMET	500	40 - NORTHWST	42 - W_CASCAD
4204	MERIDIAN	500	40 - NORTHWST	42 - W_CASCAD
4231	NORTH G3	20	40 - NORTHWST	42 - W_CASCAD
4232	WCASCADE	20	40 - NORTHWST	42 - W_CASCAD
5001	CANADA	500	50 - CANADA	50 - CANADA
5002	CANALB	500	50 - CANADA	50 - CANADA
5003	CA230TO	230	50 - CANADA	50 - CANADA
5004	CA230	230	50 - CANADA	50 - CANADA
5031	CANAD G1	20	50 - CANADA	50 - CANADA
5032	CMAIN GM	20	50 - CANADA	50 - CANADA
6101	MIDPOINT	500	61 - IDAHO	61 - IDAHO
6102	MIDPOINT	345	61 - IDAHO	61 - IDAHO

Continued on next page

Bus #	Bus Name	Base kV	Area Num - Name	Zone Num - Name
6103	BORAH	345	61 - IDAHO	61 - IDAHO
6104	BORAH	230	61 - IDAHO	61 - IDAHO
6132	MIDPOINT	20	61 - IDAHO	61 - IDAHO
6201	COLSTRP	500	60 - ROCKY MT	62 - MONTANA
6202	GARRISON	500	60 - ROCKY MT	62 - MONTANA
6203	COLSTRP	230	60 - ROCKY MT	62 - MONTANA
6204	GARRISON	230	60 - ROCKY MT	62 - MONTANA
6205	MONTANA	230	60 - ROCKY MT	62 - MONTANA
6231	COLSTRP	20	60 - ROCKY MT	62 - MONTANA
6235	MONTA G1	20	60 - ROCKY MT	62 - MONTANA
6301	BRIDGER	345	60 - ROCKY MT	63 - WYOMING
6302	LARAMIE	345	60 - ROCKY MT	63 - WYOMING
6303	BRIDGER2	230	60 - ROCKY MT	63 - WYOMING
6304	LARAMIE	230	60 - ROCKY MT	63 - WYOMING
6305	NAUGHTON	230	60 - ROCKY MT	63 - WYOMING
6333	BRIDGER	20	60 - ROCKY MT	63 - WYOMING
6335	NAUGHT	20	60 - ROCKY MT	63 - WYOMING
6401	TRACYSPP	345	64 - N NEVADA	64 - N NEVADA
6402	SUMITSPP	115	64 - N NEVADA	64 - N NEVADA
6403	VALMY	345	64 - N NEVADA	64 - N NEVADA
6404	GONDER	345	64 - N NEVADA	64 - N NEVADA
6433	VALMY	20	64 - N NEVADA	64 - N NEVADA
6501	BENLOMND	345	60 - ROCKY MT	65 - UTAH
6502	CAMP WIL	345	60 - ROCKY MT	65 - UTAH
6503	EMERY	345	60 - ROCKY MT	65 - UTAH
6504	MONA	345	60 - ROCKY MT	65 - UTAH

Continued on next page

Bus #	Bus Name	Base kV	Area Num - Name	Zone Num - Name
6505	PINTO	345	60 - ROCKY MT	65 - UTAH
6506	PINTO PS	345	60 - ROCKY MT	65 - UTAH
6507	SIGURD	345	60 - ROCKY MT	65 - UTAH
6508	SPAN FRK	345	60 - ROCKY MT	65 - UTAH
6509	TERMINAL	345	60 - ROCKY MT	65 - UTAH
6510	BENLOMND	230	60 - ROCKY MT	65 - UTAH
6533	EMERY	20	60 - ROCKY MT	65 - UTAH
7001	COLOEAST	345	60 - ROCKY MT	70 - COLORADO
7002	CRAIG	345	60 - ROCKY MT	70 - COLORADO
7031	COLOEAST	20	60 - ROCKY MT	70 - COLORADO
7032	CRAIG	20	60 - ROCKY MT	70 - COLORADO
8001	OLINDA	500	80 - SMUD	80 - SMUD
8002	TRACY	500	80 - SMUD	80 - SMUD
8003	COTWDWAP	230	80 - SMUD	80 - SMUD
8004	RNCHSECO	230	80 - SMUD	80 - SMUD
8005	TRACYPMP	230	80 - SMUD	80 - SMUD
8033	COTWDWAP	20	80 - SMUD	80 - SMUD
8034	RNCHSECO	20	80 - SMUD	80 - SMUD

BIBLIOGRAPHY

[1] S. Rahman and A. de Castro. Environmental impacts of electricity generation: a global perspective. *Energy Conversion, IEEE Transactions on*, 10(2):307 –314, Jun 1995.

[2] B. Bose. Global warming: Energy, environmental pollution, and the impact of power electronics. *Industrial Electronics Magazine, IEEE*, 4(1):6 –17, Mar 2010.

[3] Wei Zhou, Chengzhi Lou, Zhongshi Li, Lin Lu, and Hongxing Yang. Current status of research on optimum sizing of stand-alone hybrid solar-wind power generation systems. *Applied Energy*, 87(2):380–389, February 2010.

[4] M.H. Nehrir, C. Wang, K. Strunz, H. Aki, R. Ramakumar, J. Bing, Z. Miao, and Z. Salameh. A Review of Hybrid Renewable/Alternative Energy Systems for Electric Power Generation: Configurations, Control, and Applications. *Sustainable Energy, IEEE Transactions on*, 2(4):392 –403, Oct 2011.

[5] M.K. Deshmukh and S.S. Deshmukh. Modeling of hybrid renewable energy systems. *Renewable and Sustainable Energy Reviews*, 12(1):235 – 249, 2008.

[6] Trent Berry and Mark Jaccard. The renewable portfolio standard:: design considerations and an implementation survey. *Energy Policy*, 29(4):263 – 277, 2001.

[7] Database of state incentives for renewables and efficiency (DSIRE). Website (Last Accessed: March 1, 2013), 2012. http://www.dsireusa.org/.

[8] U.S. Wind Industry Third Quarter Market Report October 2011. Website (Last Accessed: March 1, 2013), Oct 2011. http://www.awea.org/learnabout/publications/reports/upload/3Q-2011-AWEA-Market-Report-for-Public.pdf.

[9] U.S. Solar Market Trends 2010. Website (Last Accessed: March 1, 2013), Jun 2011. http://irecusa.org/wp-content/uploads/2011/06/IREC-Solar-Market-Trends-Report-June-2011-web.pdf.

[10] Caisheng Wang and M.H. Nehrir. Power management of a stand-alone wind/photovoltaic/fuel cell energy system. *Energy Conversion, IEEE Transactions on*, 23(3):957 –967, Sep 2008.

[11] C.I. Aspliden. Hybrid solar-wind energy conversion systems meteorological aspects. In *Meteorology and Energy, 1981. WMO Technical Conference on*, Dec 1981.

[12] Christina E. Hoicka and Ian H. Rowlands. Solar and wind resource complementarity: Advancing options for renewable electricity integration in ontario, canada. *Renewable Energy*, 36(1):97 – 107, 2011.

[13] W. Kellogg, M.H. Nehrir, G. Venkataramanan, and V. Gerez. Optimal unit sizing for a hybrid wind/photovoltaic generating system. *Electric Power Systems Research*, 39(1):35 – 38, 1996.

[14] M. A. Elhadidy and S. M. Shaahid. Parametric study of hybrid (wind + solar + diesel) power generating systems. *Renewable Energy*, 21(2):129 – 139, 2000.

[15] Hongxing Yang, Lin Lu, and Wei Zhou. A novel optimization sizing model for hybrid solar-wind power generation system. *Solar Energy*, 81(1):76 – 84, 2007.

[16] Report: CEC-500-2007-081-APB - Intermittency Analysis Project: Appendix B, Impact of Intermittent Generation on Operation of California Power Grid. Website (Last Accessed: March 1, 2013), Jul 2007. http://www.uwig.org/CEC-500-2007-081-APB.pdf.

[17] R. Chedid, H. Akiki, and S. Rahman. A decision support technique for the design of hybrid solar-wind power systems. *Energy Conversion, IEEE Transactions on*, 13(1):76 –83, Mar 1998.

[18] W.D. Kellogg, M.H. Nehrir, G. Venkataramanan, and V. Gerez. Generation unit sizing and cost analysis for stand-alone wind, photovoltaic, and hybrid wind/PV systems. *Energy Conversion, IEEE Transactions on*, 13(1):70 –75, Mar 1998.

[19] F. Giraud and Z.M. Salameh. Steady-state performance of a grid-connected rooftop hybrid wind-photovoltaic power system with battery storage. *Energy Conversion, IEEE Transactions on*, 16(1):1 –7, Mar 2001.

[20] F. Bonanno, A. Consoli, A. Raciti, B. Morgana, and U. Nocera. Transient analysis of integrated diesel-wind-photovoltaic generation systems. *Energy Conversion, IEEE Transactions on*, 14(2):232 –238, Jun 1999.

[21] Yi Li, V.G. Agelidis, and Y. Shrivastava. Wind-solar resource complementarity and its combined correlation with electricity load demand. In *Industrial Electronics and Applications, 2009. ICIEA 2009. 4th IEEE Conference on*, pages 3623 –3628, May 2009.

[22] G.C Bakos and N.F Tsagas. Technoeconomic assessment of a hybrid solar/wind installation for electrical energy saving. *Energy and Buildings*, 35(2):139 – 145, 2003.

[23] Kyoto protocol. Website (Last Accessed: March 1, 2013), 1998. http://unfccc.int/kyoto_protocol/items/2830.php.

[24] Report: NREL/TP-500-43373 - ERCOT Event on February 26, 2008: Lessons Learned. Website (Last Accessed: March 1, 2013), Jul 2008. http://www.nrel.gov/docs/fy08osti/43373.pdf.

[25] NERC Accommodating High Levels of Variable Generation. Website (Last Accessed: March 1, 2013), Apr. 2009. http://www.nerc.com/files/IVGTF_Report_041609.pdf.

[26] Massachusetts Institute of Technology. MIT Study on the Future of the Electric Grid. Website (Last Accessed: March 1, 2013), 2011. http://web.mit.edu/mitei/research/studies/the-electric-grid-2011.shtml.

[27] Jose L. Bernal-Agustin and Rodolfo Dufo-Lopez. Simulation and optimization of stand-alone hybrid renewable energy systems. *Renewable and Sustainable Energy Reviews*, 13(8):2111 – 2118, 2009.

[28] J.P. Reichling and F.A. Kulacki. Utility scale hybrid wind-solar thermal electrical generation: A Case Study for Minnesota. *Energy*, 33(4):626 – 638, 2008.

[29] M.A. Elhadidy and S.M. Shaahid. Promoting applications of hybrid (wind+photovoltaic+diesel+battery) power systems in hot regions. *Renewable Energy*, 29(4):517 – 528, 2004.

[30] Brian D. Vick and R. Nolan Clark. Large scale deployment of renewable energy by combining wind farms with solar thermal power plants. In *Conference of the American Solar Energy Society*, Jul. 2006.

[31] Brian D. Vick, R. Nolan Clark, and Mark Mehos. Improved electrical load match in california by combining solar thermal power plants with wind farms. In *Conference of the American Solar Energy Society*, May 2008.

[32] Brian Vick, Ken Starcher, Ray Clark, and Jeremy Traurig. Matching wind resource in the southern great plains with utility electrical loading. In *Global Windpower*, Mar. 2004.

[33] Report: NREL/SR-5500-47078 - Eastern Wind Integration and Transmission Study. Website (Last Accessed: March 1, 2013), Feb. 2011. http://www.nrel.gov/docs/fy11osti/47078.pdf.

[34] Report: NREL/SR-550-47434 - Western Wind and Solar Integration Study. Website (Last Accessed: March 1, 2013), May 2010. http://www.nrel.gov/docs/fy10osti/47434.pdf.

[35] Ramteen Sioshansi and Paul Denholm. NREL/TP-6A20-53291 - Transmission Benefits of Co-Locating Concentrating Solar Power and Wind. Website (Last Accessed: March 30, 2013), Mar. 2012. http://www.nrel.gov/docs/fy12osti/53291.pdf.

[36] R. Billinton and R. Karki. Maintaining supply reliability of small isolated power systems using renewable energy. *Generation, Transmission and Distribution, IEE Proceedings-*, 148(6):530 –534, Nov 2001.

[37] R. Billinton and R. Karki. Capacity expansion of small isolated power systems using PV and wind energy. *Power Systems, IEEE Transactions on*, 16(4):892 –897, Nov 2001.

[38] R. Billinton, Bagen, and Y. Cui. Reliability evaluation of small stand-alone wind energy conversion systems using a time series simulation model. *Generation, Transmission and Distribution, IEE Proceedings-*, 150(1):96 – 100, Jan 2003.

[39] R.G. Deshmukh and R. Ramakumar. Reliability analysis of combined wind-electric and conventional generation systems. *Solar Energy*, 28(4):345 – 352, 1982.

[40] P. Giorsetto and K.F. Utsurogi. Development of a new procedure for reliability modeling of wind turbine generators. *Power Apparatus and Systems, IEEE Transactions on*, PAS-102(1):134 –143, Jan 1983.

[41] Xifan Wang, Hui-Zhu Dai, and R.J. Thomas. Reliability modeling of large wind farms and associateed electric utility interface systems. *Power Apparatus and Systems, IEEE Transactions on*, PAS-103(3):569 –575, Mar 1984.

[42] R. Billinton and A.A. Chowdhury. Incorporation of wind energy conversion systems in conventional generating capacity adequacy assessment. *Generation, Transmission and Distribution, IEE Proceedings C*, 139(1):47 –56, Jan 1992.

[43] M. Caramanisember. Analysis of non-dispatchable options in the generation expansion plan. *Power Apparatus and Systems, IEEE Transactions on*, PAS-102(7):2098 –2103, Jul 1983.

[44] C. Singh and Y. Kim. An efficient technique for reliability analysis of power systems including time dependent sources. *Power Systems, IEEE Transactions on*, 3(3):1090 –1096, Aug 1988.

[45] E. Ofry and A. Braunstein. The loss of power supply probability as a technique for designing stand-alone solar electrical (photovoltaic) systems. *Power Apparatus and Systems, IEEE Transactions on*, PAS-102(5):1171 –1175, May 1983.

[46] S.A. Klein and W.A. Beckman. Loss-of-load probabilities for stand-alone photovoltaic systems. *Solar Energy*, 39(6):499 – 512, 1987.

[47] G. Desrochers, M. Blanchard, and S. Sud. A monte-carlo simulation method for the economic assessment of the contribution of wind energy to power systems. *Energy Conversion, IEEE Transactions on*, EC-1(4):50 –56, Dec 1986.

[48] R. Billinton, Hua Chen, and R. Ghajar. A sequential simulation technique for adequacy evaluation of generating systems including wind energy. *Energy Conversion, IEEE Transactions on*, 11(4):728 –734, Dec 1996.

[49] E.S. Gavanidou, A.G. Bakirtzis, and P.S. Dokopoulos. A probabilistic method for the evaluation of the performance and the reliability of wind-diesel energy systems. *Energy Conversion, IEEE Transactions on*, 8(2):197 –206, Jun 1993.

[50] A.C. Saramourtsis, A.G. Bakirtzis, P.S. Dokopoulos, and E.S. Gavanidou. Probabilistic evaluation of the performance of wind-diesel energy systems. *Energy Conversion, IEEE Transactions on*, 9(4):743 –752, Dec 1994.

[51] A.G. Bakirtzis. A probabilistic method for the evaluation of the reliability of stand alone wind energy systems. *Energy Conversion, IEEE Transactions on*, 7(1):99 –107, Mar 1992.

[52] Z.M. Salameh, B.S. Borowy, and A.R.A. Amin. Photovoltaic module-site matching based on the capacity factors. *Energy Conversion, IEEE Transactions on*, 10(2):326 –332, Jun 1995.

[53] I. Abouzahr and R. Ramakumar. Loss of power supply probability of stand-alone wind electric conversion systems: a closed form solution approach. *Energy Conversion, IEEE Transactions on*, 5(3):445 –452, Sep 1990.

[54] I. Abouzahr and R. Ramakumar. Loss of power supply probability of stand-alone photovoltaic systems: a closed form solution approach. *Energy Conversion, IEEE Transactions on*, 6(1):1 –11, Mar 1991.

[55] I. Abouzahr and R. Ramakumar. An approach to assess the performance of utility-interactive wind electric conversion systems. *Energy Conversion, IEEE Transactions on*, 6(4):627 –638, Dec 1991.

[56] I. Abouzahr and R. Ramakumar. An approach to assess the performance of utility-interactive photovoltaic systems. *Energy Conversion, IEEE Transactions on*, 8(2):145 –153, Jun 1993.

[57] G. Tina, S. Gagliano, and S. Raiti. Hybrid solar/wind power system probabilistic modelling for long-term performance assessment. *Solar Energy*, 80(5):578 – 588, 2006.

[58] S.H. Karaki, R.B. Chedid, and R. Ramadan. Probabilistic performance assessment of autonomous solar-wind energy conversion systems. *Energy Conversion, IEEE Transactions on*, 14(3):766 –772, Sep 1999.

[59] D.A. Halamay, T.K.A. Brekken, A. Simmons, and S. McArthur. Reserve requirement impacts of large-scale integration of wind, solar, and ocean wave power generation. *Sustainable Energy, IEEE Transactions on*, 2(3):321 –328, Jul 2011.

[60] R. Chedid and S. Rahman. Unit sizing and control of hybrid wind-solar power systems. *Energy Conversion, IEEE Transactions on*, 12(1):79 –85, Mar 1997.

[61] B.S. Borowy and Z.M. Salameh. Methodology for optimally sizing the combination of a battery bank and PV array in a wind/PV hybrid system. *Energy Conversion, IEEE Transactions on*, 11(2):367 –375, Jun 1996.

[62] Tomas and Markvart. Sizing of hybrid photovoltaic-wind energy systems. *Solar Energy*, 57(4):277 – 281, 1996.

[63] A.D. Bagul, Z.M. Salameh, and B. Borowy. Sizing of a stand-alone hybrid wind-photovoltaic system using a three-event probability density approximation. *Solar Energy*, 56(4):323 – 335, 1996.

[64] Eftichios Koutroulis, Dionissia Kolokotsa, Antonis Potirakis, and Kostas Kalaitzakis. Methodology for optimal sizing of stand-alone photovoltaic/wind-generator systems using genetic algorithms. *Solar Energy*, 80(9):1072 – 1088, 2006.

[65] G.C. and Seeling-Hochmuth. A combined optimisation concet for the design and operation strategy of hybrid-PV energy systems. *Solar Energy*, 61(2):77 – 87, 1997.

[66] José L. Bernal-Agustín, Rodolfo Dufo-López, and David M. Rivas-Ascaso. Design of isolated hybrid systems minimizing costs and pollutant emissions. *Renewable Energy*, 31(14):2227 – 2244, 2006.

[67] Rodolfo Dufo-López and José L. Bernal-Agustín. Multi-objective design of PV-wind-diesel-hydrogen-battery systems. *Renewable Energy*, 33(12):2559 – 2572, 2008.

[68] Lingfeng Wang and C. Singh. Multicriteria design of hybrid power generation systems based on a modified particle swarm optimization algorithm. *Energy Conversion, IEEE Transactions on*, 24(1):163 –172, Mar 2009.

[69] J.A. Castle. Thirteenth ieee photovoltaic specialists conference. In *(442) European Power and Energy Systems*, pages 738 – 742, 1981.

[70] W.J. Burke, H.M. Merrill, F.C. Schweppe, B.E. Lovell, M.F. McCoy, and S.A. Monohon. Trade off methods in system planning. *Power Systems, IEEE Transactions on*, 3(3):1284 –1290, Aug 1988.

[71] D. Connolly, H. Lund, B.V. Mathiesen, and M. Leahy. A review of computer tools for analysing the integration of renewable energy into various energy systems. *Applied Energy*, 87(4):1059 – 1082, 2010.

[72] Federal Energy Regulatory Commission. Standard Interconnection Agreements and Procedures for Large Generators. Website (Last Accessed: March 1, 2013), Jun. 2010. http://www.ferc.gov/legal/maj-ord-reg/land-docs/order2003.asp.

[73] Federal Energy Regulatory Commission. Standard Interconnection Agreements for Wind Energy and Other Alternative Technologies. Website (Last Accessed: March 1, 2013), Jun. 2008. http://www.ferc.gov/industries/electric/indus-act/gi/wind.asp.

[74] IEEE. IEEE Application Guide for IEEE Std 1547, IEEE Standard for Interconnecting Distributed Resources with Electric Power Systems. *IEEE Std 1547.2-2008*, pages 1–207, 2009.

[75] Shangyou Hao and A. Papalexopoulos. Reactive power pricing and management. *Power Systems, IEEE Transactions on*, 12(1):95 –104, Feb 1997.

[76] K. Bhattacharya and Jin Zhong. Reactive power as an ancillary service. *Power Systems, IEEE Transactions on*, 16(2):294 –300, May 2001.

[77] K. Zou, A. P. Agalgaonkar, K. M. Muttaqi, and S. Perera. Distribution system planning with incorporating DG reactive capability and system uncertainties. *Sustainable Energy, IEEE Transactions on*, 3(1):112 –123, Jan 2012.

[78] R.J. Konopinski, P. Vijayan, and V. Ajjarapu. Extended Reactive Capability of DFIG Wind Parks for Enhanced System Performance. *Power Systems, IEEE Transactions on*, 24(3):1346 –1355, Aug 2009.

[79] J.M. Carrasco, L.G. Franquelo, J.T. Bialasiewicz, E. Galvan, R.C.P. Guisado, Ma.A.M. Prats, J.I. Leon, and N. Moreno-Alfonso. Power-Electronic Systems for the Grid Integration of Renewable Energy Sources: A Survey. *Industrial Electronics, IEEE Transactions on*, 53(4):1002 –1016, Jun 2006.

[80] Zhe Chen, J.M. Guerrero, and F. Blaabjerg. A Review of the State of the Art of Power Electronics for Wind Turbines. *Power Electronics, IEEE Transactions on*, 24(8):1859 –1875, Aug 2009.

[81] S. Huseinbegovic and B. Perunicic. New reactive power control concept for converter based renewable energy sources. In *Control Automation (MED), 2011 19th Mediterranean Conference on*, pages 850 –855, Jun 2011.

[82] V.H.M. Quezada, J.R. Abbad, and T.G.S. Roman. Assessment of energy distribution losses for increasing penetration of distributed generation. *Power Systems, IEEE Transactions on*, 21(2):533 – 540, May 2006.

[83] V. C. Ganti, B. Singh, S. K. Aggarwal, and T. C. Kandpal. DFIG-Based Wind Power Conversion with Grid Power Leveling for Reduced Gusts. *Sustainable Energy, IEEE Transactions on*, 3(1):12 –20, Jan 2012.

[84] Yifan Tang and Longya Xu. A flexible active and reactive power control strategy for a variable speed constant frequency generating system. *Power Electronics, IEEE Transactions on*, 10(4):472 –478, Jul 1995.

[85] Nayeem Rahmat Ullah and Torbjrn Thiringer. Variable Speed Wind Turbines for Power System Stability Enhancement. *Energy Conversion, IEEE Transactions on*, 22(1):52 –60, Mar 2007.

[86] N.R. Ullah, T. Thiringer, and D. Karlsson. Voltage and Transient Stability Support by Wind Farms complying with the E.ON Netz Grid Code. *Power Systems, IEEE Transactions on*, 22(4):1647 –1656, Nov 2007.

[87] Prabha Kundur. *Power System Stability and Control*. McGraw-Hill Professional, 2006.

[88] P. Vijayan, S. Sarkar, and V. Ajjarapu. A novel voltage stability assessment tool to incorporate wind variability. In *Power Energy Society General Meeting, 2009. PES '09. IEEE*, pages 1 –8, Jul 2009.

[89] Wind energy resource atlas of the united states: Table 1-1. Website (Last Accessed: March 1, 2013), 2009. http://rredc.nrel.gov/wind/pubs/atlas/tables/1-1T.html.

[90] Aabakken J. *Power Technologies Energy Data Book*. US Department of Energy - National Renewable Energy Laboratory, 2005.

[91] M. Wittmann, H. Breitkreuz, M. Schroedter-Homscheidt, and M. Eck. Case studies on the use of solar irradiance forecast for optimized operation strategies of solar thermal power plants. *Selected Topics in Applied Earth Observations and Remote Sensing, IEEE Journal of*, 1(1):18 –27, Mar 2008.

[92] The Solar Prospector. Website (Last Accessed: March 1, 2013), Jan 2010. http://maps.nrel.gov/node/10.

[93] Richard Perez, Pierre Ineichen, Kathy Moore, Marek Kmiecik, Cyril Chain, Ray George, and Frank Vignola. A new operational model for satellite-derived irradiances: Description and Validation. *Solar Energy*, 73(5):307 – 317, 2002.

[94] National Solar Radiation Data Base: 1991- 2010 Update. Website (Last Accessed: March 1, 2013), 2010. http://rredc.nrel.gov/solar/old_data/nsrdb/1991-2010/.

[95] Report: NREL/SR-550-47676 - Development of Regional Wind Resource and Wind Plant Output Datasets. Website (Last Accessed: March 1, 2013), Mar 2010. http://www.nrel.gov/docs/fy10osti/47676.pdf.

[96] Report: NREL/SR-550-46764 - Development of Eastern Regional Wind Resource and Wind Plant Output Datasets. Website (Last Accessed: March 1, 2013), Dec 2009. http://www.nrel.gov/docs/fy10osti/46764.pdf.

[97] Renewable Portfolio Standard Policies Summary Map. Website (Last Accessed: March 1, 2013), Feb. 2013. http://www.dsireusa.org/documents/summarymaps/RPS_map.pdf.

[98] Andrew Prince et al. Visualizing the U.S. Electric Grid. Website (Last Accessed: March 1, 2013), May 2009. http://www.npr.org/templates/story/story.php?storyId=110997398.

[99] G.E.P. Box and G.M. Jenkins. *Time Series Analysis, Forecasting, and Control*. Oakland, CA: Holden-Day, 1970.

[100] G.M. Jenkins Box, G.E.P. and G.C. Reinsel. *Time Series Analysis, Forecasting, and Control, 3rd ed.* Englewood Cliffs, NJ: Prentice Hall, 1994.

[101] Robert H. Shumway and David S. Stoffer. *Time Series Analysis and Its Applications: With R Examples, 2nd ed.* Springer, 2006.

[102] H. Lund. Large-scale integration of optimal combinations of PV, wind and wave power into the electricity supply. *Renewable Energy*, 31(4):503 – 515, 2006.

[103] Dominik Heide, Lueder von Bremen, Martin Greiner, Clemens Hoffmann, Markus Speckmann, and Stefan Bofinger. Seasonal optimal mix of wind and solar power in a future, highly renewable Europe. *Renewable Energy*, 35(11):2483 – 2489, 2010.

[104] J. Widen. Correlations between large-scale solar and wind power in a future scenario for Sweden. *Sustainable Energy, IEEE Transactions on*, 2(2):177 –184, Apr 2011.

[105] S.H. Karaki, B.A. Salim, and R.B. Chedid. Probabilistic model of a two-site wind energy conversion system. *Energy Conversion, IEEE Transactions on*, 17(4):530 – 536, Dec 2002.

[106] Adrian Ilinca, Ed McCarthy, Jean-Louis Chaumel, and Jean-Louis Rétiveau. Wind potential assessment of quebec province. *Renewable Energy*, 28(12):1881 – 1897, 2003.

[107] Report: NREL/CP-500-38109 - Towards a Wind Energy Climatology at Advanced Turbine Hub Heights. Website (Last Accessed: March 1, 2013), May 2005. http://www.nrel.gov/docs/fy05osti/38109.pdf.

[108] M. R. Patel. *Wind and Solar Power Systems*. Boca Raton, FL: CRC Press, 1999.

[109] Melih Yaramoglu, Russel B. Brinsfield, and Robert E. Muller Jr. Estimation of solar radiation using stochastically generated cloud cover data. *Energy in Agriculture*, 4:227 – 242, 1985.

[110] Sathyajith Mathew. *Wind Energy: Fundamentals, Resource Analysis and Economics*. Springer, 2006.

[111] Harold J. Larson. *Introduction to Probability Theory and Statistical Inference*. Wiley, Third edition, 1982.

[112] Athanasios Papoulis. *Probability, Random Variables and Stochastic Processes, 3rd Edition*. McGraw-Hill Companies, 1991.

[113] Christina Jennings. Modules of Photovoltaic Module Performance. Technical Report Report: EPRI AP-6006, Project 1607-2, Palo Alto, Calif.: The Institute, Sep. 1988.

[114] OASIS - California ISO - System Load Reports. Website (Last Accessed: March 1, 2013), 2010. http://oasishis.caiso.com/.

[115] ERCOT - Hourly Load Data Archives. Website (Last Accessed: March 1, 2013), 2010. http://www.ercot.com/gridinfo/load/load_hist/.

[116] R. Billington and R.N. Allan. *Reliability Evaluation of Power Systems*. New York: Plenum Press, 1996.

[117] Le Xie, P.M.S. Carvalho, L.A.F.M. Ferreira, Juhua Liu, B.H. Krogh, N. Popli, and M.D. Ilicť and. Wind integration in power systems: Operational challenges and possible solutions. *Proceedings of the IEEE*, 99(1):214 –232, Jan 2011.

[118] Lynn E. Bussey and Ted G. Eschenbach. *The Economic Analysis of Industrial Projects*. Prentice Hall, 1992.

[119] Torsten Lund, Poul Sørensen, and Jarle Eek. Reactive power capability of a wind turbine with doubly fed induction generator. *Wind Energy*, 10(4):379–394, 2007.

[120] Eric Weisstein. Least squares fitting–polynomial. Website (Last Accessed: March 1, 2013), 2011. http://mathworld.wolfram.com/LeastSquaresFittingPolynomial.html.

[121] Siemens Power Technologies International. PSS/E 32.0 Program Application Guide, Jun 2009.

[122] R.D. Zimmerman, C.E. Murillo-Sať andnchez, and R.J. Thomas. MATPOWER: Steady-State Operations, Planning, and Analysis Tools for Power Systems Research and Education. *Power Systems, IEEE Transactions on*, 26(1):12 –19, Feb 2011.

[123] R. Piwko, R. DeMello, R. Gramlich, W. Lasher, D. Osborn, C. Dombek, and K. Porter. What Comes First? *Power and Energy Magazine, IEEE*, 5(6):68 –77, Nov-Dec 2007.

[124] H.W. Dommel and W.F. Tinney. Optimal Power Flow Solutions. *Power Apparatus and Systems, IEEE Transactions on*, PAS-87(10):1866 –1876, Oct 1968.

[125] Hongye Wang, C.E. Murillo-Sanchez, R.D. Zimmerman, and R.J. Thomas. On Computational Issues of Market-Based Optimal Power Flow. *Power Systems, IEEE Transactions on*, 22(3):1185 –1193, Aug 2007.

[126] P. Pinson, C. Chevallier, and G.N. Kariniotakis. Trading Wind Generation rom Short-Term Probabilistic Forecasts of Wind Power. *Power Systems, IEEE Transactions on*, 22(3):1148 –1156, Aug 2007.

[127] A. Fabbri, T. GomezSanRoman, J. RivierAbbad, and V.H. MendezQuezada. Assessment of the Cost Associated with Wind Generation Prediction Errors in a Liberalized Electricity Market. *Power Systems, IEEE Transactions on*, 20(3):1440 – 1446, Aug 2005.

[128] V. Ajjarapu and C. Christy. The continuation power flow: a tool for steady state voltage stability analysis. *Power Systems, IEEE Transactions on*, 7(1):416 –423, Feb 1992.

[129] Guide to WECC/NERC Planning Standards I.D: Voltage Support and Reactive Power. Website (Last Accessed: March 1, 2013), Mar 2006. http://www.wecc.biz/committees/StandingCommittees/PCC/TSS/Shared%20Documents/Voltage%20Stability%20Guide.pdf.

[130] S. Sarkar and V. Ajjarapu. MW Resource Assessment Model for a Hybrid Energy Conversion System with Wind and Solar Resources. *Sustainable Energy, IEEE Transactions on*, 2(4):383 –391, Oct 2011.

[131] B Parsons, M Milligan, J C Smith, E DeMeo, B Oakleaf, K Wolf, M Schuerger, R Zavadil, M Ahlstrom, and D Y Nakafuji. Grid impacts of wind power variability: Recent assessments from a variety of utilities in the united states. *European Wind Energy Conference*, pages 1–16, 2006.

[132] A.A. Chowdhury and D.O. Koval. Modeling non-dispatchable wind energy sources in generating capacity reliability planning. In *(442) European Power and Energy Systems*, Jun 2004.

[133] J.E. Price and J. Goodin. Reduced network modeling of WECC as a market design prototype. In *Power and Energy Society General Meeting, 2011 IEEE*, pages 1 –6, Jul. 2011.

[134] J. Jung, Chen-Ching Liu, S.L. Tanimoto, and V. Vittal. Adaptation in load shedding under vulnerable operating conditions. *Power Systems, IEEE Transactions on*, 17(4):1199 – 1205, Nov. 2002.

[135] Nan-Peng Yu, Chen-Ching Liu, and J. Price. Evaluation of Market Rules Using a Multi-Agent System Method. *Power Systems, IEEE Transactions on*, 25(1):470 –479, Feb. 2010.

[136] California ISO 2007 Transmission Plan - 2007 through 2016. Website (Last Accessed: March 1, 2013), Jan. 2007. http://www.caiso.com/1b6b/1b6bb4d51db0.pdf.

[137] J.E. Price and A. Sheffrin. Adapting California's energy markets to growth in renewable resources. In *Power and Energy Society General Meeting, 2010 IEEE*, pages 1 –8, Jul. 2010.

[138] Reduced Network Modeling of WECC as a Market Design Prototype. Website (Last Accessed: March 1, 2013), Mar. 2012. http://www.pserc.wisc.edu/documents/publications/reports/2010_reports/WECC240%20data%20for%20IEEE%20PES%202011GM0942.zip.

[139] WECC 10-Year Regional Transmission Plan. Website (Last Accessed: March 1, 2013), Sep. 2011. http://www.wecc.biz/library/StudyReport/Wiki%20Pages/Home.aspx.

[140] NREL Renewable Energy Atlas. Website (Last Accessed: March 1, 2013), Nov. 2012. http://maps.nrel.gov/re_atlas.

[141] Report: DOE/GO-102008-2567 - 20% Wind Energy by 2030: Increasing Wind Energy's Contribution to U.S. Electricity Supply. Website (Last Accessed: March 1, 2013), Jul 2008. http://www.nrel.gov/docs/fy08osti/41869.pdf.

[142] WECC Maps of the Western Interconnection. Website (Last Accessed: March 1, 2013), Nov. 2012. http://www.wecc.biz/library/Pages/Interconnection%20Maps.aspx/.

[143] ArcMap. *version 10.1*. ESRI (Environmental Systems Resource Institute), Redlands, California, 2012.

[144] MATLAB. *version 8 (R2012b)*. The MathWorks Inc., Natick, Massachusetts, 2012.

[145] NREL Dynamic Maps, GIS Data, & Analysis Tools: Wind Data. Website (Last Accessed: March 1, 2013), Nov. 2012. http://www.nrel.gov/gis/data_wind.html.

[146] NREL Dynamic Maps, GIS Data, & Analysis Tools: Solar Data. Website (Last Accessed: March 1, 2013), Nov. 2012. http://www.nrel.gov/gis/data_solar.html.

[147] MATLAB. Mapping Toolbox User's Guide Version 3.6, Sep. 2012.

[148] Western Wind Resources Dataset. Website (Last Accessed: March 1, 2013), Oct. 2012. http://wind.nrel.gov/Web_nrel/.

[149] Siemens Power Technologies International. PSS/E 33.2 Program Application Guide Volume 1 and 2, Jul. 2012.

[150] Siemens Power Technologies International. PSS/E 33.2 program operation manual, Jul. 2012.

[151] America's Energy Future Panel on Electricity from Renewable Resources; National Research Council. *Electricity from Renewable Resources: Status, Prospects, and Impediments*. The National Academies Press, 2010.

[152] Report RETI-1000-2008-003-F: Renewable Energy Transmission Initiative Phase 1B Final Report. Website (Last Accessed: March 31, 2013), Jan. 2009. http://www.energy.ca.gov/2008publications/RETI-1000-2008-003/RETI-1000-2008-003-F.PDF.

[153] NREL: Western Wind and Solar Integration Study. Website (Last Accessed: March 1, 2013), 2010. http://www.nrel.gov/wind/systemsintegration/wwsis.html.

[154] Changling Luo and Boon-Teck Ooi. Frequency deviation of thermal power plants due to wind farms. *Energy Conversion, IEEE Transactions on*, 21(3):708–716, 2006.

[155] Sompop Pattanariyankool and Lester B. Lave. Optimizing transmission from distant wind farms. *Energy Policy*, 38(6):2806 – 2815, 2010.

[156] Friedrich Koch, Istvan Erlich, Fekadu Shewarega, and Udo Bachmann. The effect of large offshore and onshore wind farms on the frequency of a national power supply system; simulation modelled on Germany. *Wind Engineering*, 27(5):393–404, 2003.

[157] EDF Renewable Energy dedicates the Pacific Wind Project and Catalina Solar Project. Website (Last Accessed: March 31, 2013), Oct. 2012. http://www.edf-re.com/about/press/edf_renewable_energy_dedicates_the_pacific_wind_project_and_catalina_solar/.

[158] Slayton Solar Project - Final Milestone Report. Website (Last Accessed: March 31, 2013), Mar. 2013. http://www.xcelenergy.com/staticfiles/xe/Corporate/Corporate%20PDFs/SlaytonSolar-RDF_Final_Milestone_Report.pdf.

[159] Ben Ryan Steven M. Wiese, Elisabeth Long. Assessment of Wind/Solar Co-Located Generation in Texas. Website (Last Accessed: March 30, 2013), Jul. 2009. http://www.cleanenergyassociates.com/wp-content/uploads/2013/03/AE-Colocated-Solar-Wind-Study-20090923.pdf.

[160] Report: Wires - Integrating Locationally-Constrained Resources into Transmission Systems: A Survey of U.S. Practices. Website (Last Accessed: March 31, 2013), Oct. 2008. http://www.wiresgroup.com/images/WIRES_Report_LCR.pdf.

[161] A.J. Conejo, E. Castillo, R. Minguez, and F. Milano. Locational marginal price sensitivities. *Power Systems, IEEE Transactions on*, 20(4):2026 – 2033, Nov. 2005.

[162] L. Zadeh. Optimality and non-scalar-valued performance criteria. *Automatic Control, IEEE Transactions on*, 8(1):59 – 60, Jan 1963.

[163] Yair Censor. Pareto optimality in multiobjective problems. *Applied Mathematics & Optimization*, 4:41–59, 1977. 10.1007/BF01442131.

[164] N.O Da Cunha and E Polak. Constrained minimization under vector-valued criteria in finite dimensional spaces. *Journal of Mathematical Analysis and Applications*, 19(1):103 – 124, 1967.